

<http://researchcommons.waikato.ac.nz/>

## Research Commons at the University of Waikato

### Copyright Statement:

The digital copy of this thesis is protected by the Copyright Act 1994 (New Zealand).

The thesis may be consulted by you, provided you comply with the provisions of the Act and the following conditions of use:

- Any use you make of these documents or images must be for research or private study purposes only, and you may not make them available to any other person.
- Authors control the copyright of their thesis. You will recognise the author's right to be identified as the author of the thesis, and due acknowledgement will be made to the author where appropriate.
- You will obtain the author's permission before publishing any material from the thesis.

# **Felsic volcanism in the eastern Waihi area; process origins of the Corbett and Ratarua ignimbrites and the Hikurangi Rhyolite**

A thesis submitted in partial fulfilment  
of the requirements for the degree  
of  
**Masters of Science (Research)**  
in Earth Sciences  
at  
**The University of Waikato**  
by  
**Elizabeth Teresa Cook**

---

The University of Waikato  
2016



THE UNIVERSITY OF  
**WAIKATO**  
*Te Whare Wānanga o Waikato*



# Abstract

---

Volcanic activity began in the north Coromandel Volcanic Zone (CVZ) at 18 Ma, migrated southward during the Miocene to Pliocene, and continued until the Pleistocene (1.9 Ma). The Waihi Caldera was active during the Pliocene and has been infilled with lake sediments (Romanga Formation) and three rhyolitic ignimbrites of the Whitianga Group, the Corbett, Waikino and Owharoa ignimbrites. This study constrains the volcanic history and processes involved in the formation of three volcanic units in eastern Waihi; the Corbett Ignimbrite, Ratarua Ignimbrite and Hikurangi Rhyolite. Detailed stratigraphic logs, petrographic studies, geochemical analyses and U-Pb dating of zircons are presented for each unit.

The Corbett Ignimbrite is a widespread deposit which is constrained to eastern Waihi. It has a maximum exposed thickness of 18 m at its type section, and is a creamy-buff, pumice-rich, crystal-rich, moderately-welded ignimbrite. The basal zone of the ignimbrite is pumice-rich (40-50%), crystal-rich (20-30%) and contains two distinct lithic concentration zones. At one locality the ignimbrite consists of a 9 m thick densely welded zone with abundant fiamme. The matrix is composed of fine ash with shard textures only visible under the scanning electron microscope. Crystals comprise plagioclase, quartz, hornblende, orthopyroxene, augite, titanomagnetite, ilmenite and zircon. Lithics are predominantly andesite with minor rhyolite, dacite and greywacke. Lithic concentration zones suggest that collapse and erosion of the vent occurred several times during the eruption, and these were emplaced by rapid depositional pulses. The upper half of the outcrop represents a more steady flow. Pumice and glass shard composition shows a transition from andesitic to rhyolitic. The source of the Corbett Ignimbrite was thought to have been from either a silicic centre in the vicinity of the Bowentown Rhyolite or from the Waihi Caldera. However, the U-Pb age  $6.09 \pm 0.34$  Ma is consistent with older source vents located elsewhere, with two other possible vent locations assessed.

The Corbett Ignimbrite pyroclastic flow was constrained by the welded, fiamme and crystal-rich, dacitic Ratarua Ignimbrite which has been dated at  $6.79 \pm 0.42$  Ma. The Ratarua Ignimbrite is exposed on hillsides as angular blocks ranging

from 30 cm to several metres in size. Crystals comprise plagioclase, hornblende, orthopyroxene, augite, titanomagnetite, ilmenite and zircon. Lithics are andesite, dacite, rhyolite and rare sandstone.

The spherulitic Hikurangi Rhyolite dome belongs to the Homunga Rhyolite formation and overlies the Corbett Ignimbrite in southeastern Waihi. This rhyolite dome contains quartz, plagioclase, biotite, titanomagnetite and ilmenite phenocrysts. Petrographical analysis of granophyric intergrowth crystals indicates the presence of a granite body below this dome, which is the first evidence of granite present in southern CVZ. U-Pb dating of zircons determined an age of  $4.53 \pm 0.13$  Ma for this dome showing a younging in age of the Homunga Rhyolite formation southwards.

The units included in this study show a progression in volcanism with a transition from andesite dominant to rhyolitic. The Ratarua Ignimbrite formed during an earlier period dominated by andesite volcanism. This ignimbrite pre-dates the Corbett Ignimbrite, which formed during later andesitic volcanism in the eastern Waihi area, predating the Waihi Caldera. The youngest unit in this study, the Hikurangi Rhyolite, shows younger rhyolitic volcanism in southeastern Waihi.

# Acknowledgements

---

This project would not have been possible without the encouragement, assistance and support I received from so many people. I am grateful to have the opportunity to acknowledge and thank them.

I am indebted to my supervisor Adrian Pittari for his guidance, support and hours spent editing chapters. His ongoing enthusiasm for volcanology made my time spent on this project highly enjoyable. I am also thankful for the help received from Roger Briggs who provided endless knowledge and insight into the study area, as well as the hands on help received in the field (including flooded boots).

This research would not have been possible without the expertise and guidance from the Department of Earth Sciences technical staff; Renat Radosinsky, Ganqing Xu, Kirsty Vincent, Annette Rodgers and Helen Turner. As well as the help from Ian Schipper (Victoria the University of Wellington).

I would like to acknowledge the land owners Donna and Greg and the owners of the Tomsett farm who allowed me to run around their land with a sledgehammer collecting rocks.

Thank you to my fellow earth scientists who made my time at the University of Waikato unforgettable. The endless discussions and procrastination made a stressful time enjoyable. Thanks to Hannah Julian for field assistance, providing a scale in photos and the baking which kept me going.

I would like to acknowledge the funding received from the University of Waikato Masters Research Scholarship and the Broad Memorial Fund.

A special thank you to my friends and family for listening to my endless talking about this topic. To my parents for their encouragement, love and support. My time throughout my studies gave me a deep appreciation of the time and financial support you have provided. To Steph who answered numerous stressed out calls and gave me advice and a second home when I needed a break. Thanks to Andy for providing the delicious food and many laughs. Lastly I would like to thank Peter Oliver for his help in every aspect of my study. Your determination to get every sample (even if that included swimming in some questionable water), positivity and support made all this possible. Thank you for putting up with me.



# Table of Contents

---

Abstract .....	i
Acknowledgements .....	iii
Table of Contents .....	v
List of Figures .....	x
List of Tables.....	xvii
Chapter One: Introduction.....	1
1.1 Research Objectives.....	2
1.2 Location of Study.....	2
1.3 Tectonic Setting .....	3
1.4 Regional Geology of the Coromandel Volcanic Zone.....	5
1.5 Geology of the Waihi area .....	6
1.6 Structure of the Waihi area .....	8
1.7 Previous Work .....	9
1.8 Structure of thesis .....	9
Chapter Two: Methodology .....	11
2.1 Field work.....	11
2.2 Thin section preparation .....	12
2.3 Microscope Petrography .....	12
2.4 Scanning Electron Microscope (SEM) .....	13
2.5 Electron Microprobe .....	14
2.6 X-Ray Diffraction .....	14
2.7 X-Ray Fluorescence.....	14
2.8 Separation for dating.....	15
2.9 Dating using Laser Ablation Inductively Coupled Plasma Spectrometry .....	16

Chapter Three: Corbett Ignimbrite .....	19
3.1 Introduction .....	19
3.2 Location and distribution .....	20
3.3 Facies.....	22
3.4 Facies architecture.....	25
3.5 Petrography and Mineralogy .....	30
3.5.1 Introduction.....	30
3.5.2 Crystals .....	31
3.5.3 Juvenile clasts .....	34
3.5.4 Lithics .....	39
3.5.5 Interstitial matrix .....	40
3.6 Pumice and Glass Shard Geochemistry .....	41
3.6.1 Introduction.....	41
3.6.2 Rock classification.....	41
3.6.3 Major element chemistry .....	44
3.6.4 Trace element chemistry .....	46
3.6.5 Glass shard chemistry .....	48
3.7 Dating.....	49
3.7.1 Introduction.....	49
3.7.2 Zircon age results.....	49
3.8 Petrographic, mineralogical and geochemical characteristics of the Bowentown Rhyolite .....	52
3.8.1 Introduction.....	52
3.8.2 Petrography and mineralogy.....	52
3.8.3 Geochemistry .....	57
3.8.4 Dating .....	58
3.9 Discussion .....	60
3.9.1 Introduction.....	60

3.9.2 Components.....	60
3.9.3 Process interpretations of Corbett Ignimbrite facies .....	61
3.9.4 Mechanisms causing vertical and lateral variations .....	64
3.9.5 Magma generation.....	67
3.9.6 Relationship with Bowentown Rhyolite .....	69
Chapter Four: Ratarua Ignimbrite .....	71
4.1 Introduction.....	71
4.2 Location and distribution .....	72
4.3 Facies .....	73
4.4 Facies architecture .....	73
4.5 Petrography and mineralogy .....	75
4.5.1 Introduction .....	75
4.5.2 Crystals.....	76
4.5.3 Fiamme.....	77
4.5.4 Lithics.....	80
4.6 Fiamme geochemistry.....	81
4.6.1 Introduction .....	81
4.6.2 Rock classification .....	81
4.6.3 Major element chemistry.....	82
4.6.4 Trace element chemistry .....	84
4.7 Dating.....	86
4.7.1 Introduction .....	86
4.7.2 Zircon age results .....	86
4.8 Discussion.....	88
4.8.1 Introduction .....	88
4.8.2 Components.....	88
4.8.3 Welding .....	89
4.8.4 Eruption processes.....	90

4.8.5 Ratarua Ignimbrite relationship with andesites and dacites of the Coromandel Group .....	90
Chapter Five: Hikurangi Rhyolite .....	93
5.1 Introduction .....	93
5.2 Location and distribution .....	94
5.3 Facies.....	95
5.4 Petrography and mineralogy .....	96
5.4.1 Introduction.....	96
5.4.2 Phenocrysts .....	96
5.4.3 Groundmass .....	103
5.5 Geochemistry .....	104
5.5.1 Introduction.....	104
5.5.2 Rock classification.....	104
5.5.3 Major element chemistry .....	105
5.5.4 Trace element chemistry .....	107
5.6 Dating .....	109
5.6.1 Introduction.....	109
5.6.2 Zircon age results.....	109
5.7 Discussion .....	111
5.7.1 Spherulite growth.....	111
5.7.2 Evidence of deep basement geology.....	112
5.7.3 Mineralogical and geochemical relationship with other related rhyolite domes in the CVZ .....	113
Chapter Six: Discussion .....	115
6.1 Introduction .....	115
6.2 Possible vent locations for the Corbett Ignimbrite.....	115
6.2.1 A southern source near the Bowentown Rhyolite .....	115
6.2.2 Waihi Caldera .....	116
6.2.3 Tunaiti Caldera .....	117

6.2.4 Volcanic source east of Waihi.....	119
6.3 Ages of CVZ volcanics.....	120
6.3.1 Origin of inherited zircons .....	121
6.4 Geological history of eastern Waihi area.....	122
6.4.1 Volcanic sequence in eastern Waihi.....	123
Chapter Seven: Conclusions .....	129
References .....	131
Appendix I: Sample Catalogue .....	137
Appendix II: Stratigraphic logs .....	149
Appendix III: Point counting results .....	157
Appendix IV: XRD results.....	161
Appendix V: Electron microprobe results .....	169
Appendix VI: XRF results .....	189
Appendix VII: LA-ICP-MS specifications .....	195
Appendix VIII: Dating results.....	197

# List of Figures

---

Figure 1.1 Map showing the study location (red box). Maps sourced from Google Maps (October, 2015). .....	3
Figure 1.2 The major volcanic regions in the North Island of New Zealand including the HVR which contains the Coromandel Volcanic Zone, Hauraki Rift and the Kiwitahi Volcanic Zone (after Malengreau <i>et al.</i> , 2000). .....	4
Figure 1.3 Simplified geology of the Waihi region extending to the southern Coromandel Peninsula, (after Smith <i>et al.</i> , 2006). .....	7
Figure 3.1 Simplified geological map for the Waihi region. The Corbett Ignimbrite localities are labelled. Based on Braithwaite and Christie (1996) 1:50,000 geological map of Waihi. ....	19
Figure 3.2 Corbett Ignimbrite type section of 18 m thickness .....	21
Figure 3.3 1.5 m thick exposure of Corbett Ignimbrite along Ananui Falls track in Katikati .....	21
Figure 3.4 Outcrop of Corbett Ignimbrite at the base of the type section (locality 1, Figure 3.1) showing facies hc-f1 with lapilli-sized andesite lithics and abundant pumice lapilli .....	22
Figure 3.5 Corbett Ignimbrite facies hc-f2 lithic concentration zone, at the type section (locality 1, Figure 3.1) with lithics up to block-size. Lithic concentration zone is outlined in red. ....	23
Figure 3.6 Corbett Ignimbrite hc-f3 pumice-rich facies with angular pumice at Ngatitangata Road (locality 7, Figure 3.1). ....	24
Figure 3.7 (A) Shows hc-f4 in the field with abundant fiamme. (B) Shows hc-f4 with a higher abundance of lithics.....	24
Figure 3.8 Stratigraphic log at the Corbett Ignimbrite type section (locality 1, Figure 3.1). The position of facies hc-f1, hc-f2 and hc-f3 are shown. Maximum pumice and lithic sizes with abundances (%) are shown on graphs aligned at measured heights.....	26
Figure 3.9 (A) Corbett Ignimbrite type section (locality 2, Figure 3.1) and (B) distribution of the different facies across the exposed face.....	27
Figure 3.10 Stratigraphic log of the Corbett Ignimbrite at locality 7 with facies hc-f1, hc-f2 and hc-f3 shown .....	28
Figure 3.11 Stratigraphic log of the Corbett Ignimbrite at locality 3 (Figure 3.1). Facies hc-f1, hc-f2 and hc-f3 are shown. A burnt tree log found in hc-f1 is shown at 0.7 m height. ....	28

Figure 3.12 (A) Stratigraphic log of the welded Corbett Ignimbrite locality 11 (Figure 3.1) with facies hc-f4 (B) Outcrop distribution of facies.....	29
Figure 3.13 Free crystals in the matrix. All images are under cross polarized light except for images C and F which are plane polarized light. (A) Plagioclase crystal displaying twinning and oscillatory zoning under XP. (B) An embayed quartz crystal under XP. (C) Two augite crystals. (D) Two orthopyroxene crystals. (E) Shows two elongated hornblende crystals with green/brown colouration. (F) Magneite crystal with a prismatic shape. ....	32
Figure 3.14 (A) Backscatter image of an opaque crystal found in the Corbett Ignimbrite. (B) The blue points represent Si, green represents Fe and pink represents Ti showing a titanomagnetite and ilmenite crystal joined together. ....	33
Figure 3.15 (A) Shows Pumice found within the Corbett Ignimbrite with a wavy texture. (B) Shows a thin section sample under SEM. The arrow is pointing to a bubble with thin glass walls. ....	34
Figure 3.16 Albite - anorthite- orthoclase ternary diagram for plagioclase crystals in pumice in the Corbett Ignimbrite. Classification according to Deer et al. (1992).....	36
Figure 3.17 Wollastonite - enstatite - ferrosilite ternary diagram for pyroxene crystals found in Corbett Ignimbrite pumice. Classification from Deer et al., 1992.....	38
Figure 3.18 Fiamme in the Corbett Ignimbrite at site 11 with a glassy groundmass.....	39
Figure 3.19 Different lithics found within the Corbett Ignimbrite. (A) Crystal rich rhyolite lithic with a crystalline groundmass. (B) Two pyroxene andesite lithic with aligned crystals and a glassy, hyalopilitic groundmass. (C) Dacite lithic which is rich in quartz phenocrysts. (D) Greywacke lithic with a granular texture. ....	40
Figure 3.20 glass shards at different magnifications in the Corbett Ignimbrite showing the different shapes observed.....	41
Figure 3.21 Plot of Na <sub>2</sub> O + K <sub>2</sub> O vs SiO <sub>2</sub> wt. % of Corbett Ignimbrite bulk pumice and glass shard analysis (based on Deer <i>et al.</i> , 1992). ....	42
Figure 3.22 Plot of K <sub>2</sub> O vs. SiO <sub>2</sub> wt. % of Corbett Ignimbrite bulk pumice and glass shard analysis (based on Le Maitre <i>et al.</i> , 2002).....	42
Figure 3.23 Corbett Ignimbrite type section (locality 1) with compositions of bulk pumice samples determined by XRF analysis. ....	43

Figure 3.24 Harker diagrams of selected major elements found in pumice samples (blue circles) and glass shards (red triangles) vs SiO <sub>2</sub> wt. %.....	45
Figure 3.25 Harker variation plots of trace element geochemistry from XRF results of whole pumice clasts. ....	47
Figure 3.26 Ternary plot showing the relationship between FeO, CaO and K <sub>2</sub> O in glass shards found within the Corbett Ignimbrite.....	48
Figure 3.27 The distribution of ages of Corbett Ignimbrite zircon crystals that were ablated by LA-ICP-MS excluding the oldest zircons analysed. ....	50
Figure 3.28 The full distribution of ages of Corbett Ignimbrite zircon crystals that were ablated by LA-CIP-MS.....	51
Figure 3.29 (A) Shows radiating structure of spherulites with crystalline groundmass infilling gaps. (B) Shows a fan shaped spherulite. (C) Shows quartz and plagioclase phenocrysts. (D) Shows a prismatic augite crystal. (E) Shows an elongated orthopyroxene crystal.....	54
Figure 3.30 Albite - anorthite- orthoclase ternary diagram for plagioclase in sample 10.1.2 in the Bowentown Rhyolite. Classification according to Deer et al., (1992) .....	55
Figure 3.31 Wollastonite - enstatite - ferrosilite ternary diagram for pyroxene crystals found in Bowentown Rhyolite. Classification from Morimoto et al., 1988 (Deer et al., 1992). ....	56
Figure 3.32 Plot of K <sub>2</sub> O vs. SiO <sub>2</sub> wt. % of Corbett Ignimbrite XRF and glass shard analysis and Bowentown Rhyolite XRF analysis (based on Le Maitre <i>et al.</i> , 2002).....	57
Figure 3.33 The distribution of ages of Bowentown Rhyolite zircon crystals that were ablated by LA-ICP-MS excluding the oldest zircons analysed. ....	58
Figure 3.34 The full distribution of ages of Bowentown Rhyolite zircon crystals that were ablated by LA-ICP-MS.....	59
Figure 3.35 Pyroclastic flow model (Sparks <i>et al.</i> , 1973) showing characteristics in one flow unit and the flow pulses observed at the Corbett Ignimbrite type section .....	66
Figure 4.1 Simplified geological map for the Waihi region. Localities studied for the Ratarua Ignimbrite are included in this map. Based on Braithwaite and Christie (1996)'s 1:50,000 geological map of Waihi. ....	71
Figure 4.2 Ratarua sample collection sites at locality 13 .....	72

Figure 4.3 Sample 3 taken of Ratarua Ignimbrite at locality 13. Sample shows hard welded material with dark colouration.....	73
Figure 4.4 Stratigraphic log of the Ratarua Ignimbrite constructed based on field observations at locality 13. The position of facies Ir-f1 and Ir-f2 are shown. Maximum fiamme and lithic sizes with abundances (%) are shown on graphs aligned at measured heights. ....	74
Figure 4.5 Crystals in the Ratarua Ignimbrite matrix, all images are in plane polarised light except B which is in cross polarized. (A) Plagioclase crystal with a sieve texture and showing corrosion. (B) Crystal with oscillatory zoning and partial resorption. (C) Two types of pyroxene crystals found in the Ratarua Ignimbrite. (D) Hornblende under plane light with a prismatic shape. ....	76
Figure 4.6 Fiamme found within the Ratarua Ignimbrite. (A) Plagioclase and augite crystals contained in the fiamme. (B) Wavy nature of the fiamme with a dark glassy matrix. ....	77
Figure 4.7 Albite – anorthite - orthoclase ternary diagram for plagioclase crystals in fiamme in the Ratarua Ignimbrite. Classification according to Deer et al. (1992).....	78
Figure 4.8 Wollastonite - enstatite - ferrosilite ternary diagram for pyroxene crystals found in Corbett Ignimbrite pumice. Classification from Deer et al., (1992).....	79
Figure 4.9 The different lithic types in the Ratarua Ignimbrite all under cross polarized light. (A) Andesite lithic taking up the entire photo, this lithic is crystal rich with mafic crystals. (B) Dacite lithic with a high abundance of quartz and plagioclase. (C) Rounded rhyolite lithic. (D) Poorly sorted argillite lithic.....	80
Figure 4.10 Plot of Na <sub>2</sub> O + K <sub>2</sub> O vs SiO <sub>2</sub> wt. % of the Ratarua Ignimbrite XRF analysis of bulk fiamme (based on Deer <i>et al.</i> , 1992). ....	81
Figure 4.11 Plot of K <sub>2</sub> O vs. SiO <sub>2</sub> wt. % of the Ratarua Ignimbrite bulk fiamme XRF analysis (based on Le Maitre <i>et al.</i> , 2002). ....	82
Figure 4.12 Harker diagrams of selected major elements found in fiamme samples, versus SiO <sub>2</sub> wt. %.....	83
Figure 4.13 Harker variation plots of trace element geochemistry from XRF results of whole fiamme. ....	85
Figure 4.14 The distribution of ages of Ratarua Ignimbrite zircon crystals that were ablated by LA-ICP-MS excluding the oldest zircons analysed.....	86
Figure 4.15 The full distribution of ages of Ratarua Ignimbrite zircon crystals that were ablated by LA-ICP-MS .....	87
Figure 4.16 Ignimbrite welding zones (McPhie <i>et al.</i> , 1993). ....	89

Figure 4.17 Plot of K <sub>2</sub> O vs. SiO <sub>2</sub> wt.% of the Ratarua Ignimbrite bulk fiamme XRF analysis compared with results of Coromandel Group rocks analysed by Booden <i>et al.</i> , (2012). (Based on Le Maitre <i>et al.</i> , 2002). .....	91
Figure 5.1 Geological map of the different formations around Waihi. Localities studied is included in this map. Based from Braithwaite and Christies (1996) 1:50,000 geological map of Waihi.....	94
Figure 5.2 (A) Stratigraphic log of the Hikurangi Rhyolite showing no variation vertically throughout a 10 m high section. (B) Outcrop of the Hikurangi Rhyolite at locality 2. (C) A close up image of a section showing the creamy white facies.....	95
Figure 5.3 (A) Shows spherulitic groundmass with average size spherulites. (B) Shows a plagioclase crystal displaying polysynthetic twinning. (C) Shows a larger biotite flake with an elongated shape. (D) Shows a quartz phenocryst with an embayment in the upper left hand corner of the crystal. ....	97
Figure 5.4 Albite - anorthite- orthoclase ternary diagram for plagioclase in sample 2.1.1 in the Hikurangi Rhyolite. Classification according to Deer <i>et al.</i> (1992).....	98
Figure 5.5 The composition of biotite phenocrysts found within the Hikurangi Rhyolite in relation to the principle components of biotite compositions and the field in which most natural biotite lie (shaded grey) after Deer <i>et al.</i> , (1992).....	99
Figure 5.6 Granophyric intergrowth crystal found within the Hikurangi Rhyolite. (A) Shows the crystal under cross polarized light with the orthoclase being visible and the quartz dark, appearing in triangle shapes. (B) Shows the crystal when the quartz is visible....	101
Figure 5.7 Granophyric intergrowth crystal under the electron microscope with analysis points.....	102
Figure 5.8 Albite - anorthite- orthoclase ternary diagram for plagioclase in a granophyric intergrowth crystal in the Hikurangi Rhyolite. Classification according to Deer <i>et al.</i> , (1992). ....	102
Figure 5.9 Spherulite, in a sample of the Hikurangi Rhyolite.....	103
Figure 5.10 halloysite aggregates within the Hikurangi Rhyolite groundmass...	103
Figure 5.11 Plot of + K <sub>2</sub> O vs SiO <sub>2</sub> wt. % of the Hikurangi Rhyolite (based on Deer <i>et al.</i> , 1992). ....	104
Figure 5.12 Plot of K <sub>2</sub> O vs. SiO <sub>2</sub> wt. % of the Hikurangi Rhyolite XRF analysis (based on Le Maitre <i>et al.</i> , 2002).....	105
Figure 5.13 Harker variation diagrams of selected major elements in the Hikurangi Rhyolite. ....	106

Figure 5.14 Harker variation plots of trace element geochemistry from XRF results of the Hikurangi Rhyolite. ....	108
Figure 5.15 The distribution of ages of Hikurangi Rhyolite zircon crystals that were ablated by LA-ICP-MS.....	110
Figure 5.16 Nucleation (N) and growth rate (G) curves of variation with increasing undercooling showing the general trend in grainsizes and shapes produced at each stage (Vernon, 2004). ....	111
Figure 5.17 Plot of K <sub>2</sub> O vs. SiO <sub>2</sub> wt. % of the Homunga Rhyolite domes and Bowentown Rhyolite. Data for Shark Bay Dome and Whale Bay Dome from Vincent (2012). ....	114
Figure 6.1 Cross section of the Waihi Caldera showing the relationship between the different units found in the Waihi area (Smith <i>et al.</i> , 2006).....	116
Figure 6.2 Map of the Coromandel Volcanic Zone showing the Whitianga Group distribution and associate calderas (Briggs & Fulton, 1990).....	118
Figure 6.3 Map of previously dated igneous rocks of the CVZ showing age ranges from Early-Miocene to Late Pliocene-Early Pleistocene (Vincent, 2012).....	120
Figure 6.4 Key geological units of the Waihi area with the locations of dated samples and U-Pb ages obtained for the units included in this study (geology based on Brathwaite & Christie, 1996). ....	122
Figure 6.5 Volcanic stratigraphy of the Waihi area. Based on Smith <i>et al.</i> (2006), Brathwaite and Christie (1996), Vincent (2012) and Julian (2016).....	124
Figure 6.6 North to south profile of the Waihi Caldera showing the elevation of the different stratigraphic units contained within the caldera.....	126



# List of Tables

---

Table 3.1 Results obtained from point counting four thin sections of the matrix of the Corbett Ignimbrite* .....	30
Table 3.2 Percentage proportions of the components within pumice obtained from point counting thin sections of pumice clasts from the Corbett Ignimbrite* .....	35
Table 3.3 Different zoning observed in samples analysed under the electron microprobe based on CaO and Na <sub>2</sub> O values. ....	37
Table 3.4 Results obtained from point counting 2 thin sections of the Bowentown rhyolite .....	53
Table 3.5 Simplified description of the four facies found within the Corbett Ignimbrite .....	62
Table 3.6 A summary of the key similarities and differences for the Corbett Ignimbrite and Bowentown Rhyolite .....	70
Table 4.1 Percentage proportions of the components obtained from point counting four thin sections of the Ratarua Ignimbrite* .....	75
Table 4.2 Percentage proportions of the components within fiamme obtained from point counting thin sections after fiamme within the Ratarua Ignimbrite* .....	77
Table 4.3 Zoning observed in samples analysed under the electron microprobe based on CaO and Na <sub>2</sub> O values. ....	79
Table 5.1 Results obtained from point counting 4 thin sections of the Hikurangi Rhyolite* .....	96
Table 5.2 Zoning observed in samples analysed under the electron microprobe based on CaO and Na <sub>2</sub> O values. ....	99



# Chapter One

## Introduction

---

The Waihi Region was an area of active volcanism located at the southern end of the extinct Coromandel Volcanic Zone (CVZ), North Island, New Zealand. The CVZ was active from c. 18 to 1.9 Ma and was the precursor to the presently-active Taupo Volcanic Zone (TVZ) (Booden *et al.*, 2012). Although the area has been mapped at a 1:50,000 scale by Brathwaite and Christie (1996), showing the distribution of the volcanic deposits, the volcanic processes and eruption histories of volcanic centres in the Waihi region have not been studied in detail. Silicic volcanism occurred predominantly along the central axis and eastern side of the CVZ where there are abundant ignimbrites, rhyolite domes and lava flows. The Waihi Basin is a fault-angle depression with basin-infill up to 1.5 m thickness, consisting of lake sediments and ignimbrite sheets. The semi-rectangular shape and locally-derived ignimbrite infill are consistent with a caldera structure (Brathwaite & Christie, 1996) that has been confirmed by geophysical studies (Smith *et al.*, 2006). This study determines the volcanic processes and eruption history of several spatially-related ignimbrite deposits and rhyolite domes within the eastern side of Waihi. The volcanic units included in this study are the Corbett Ignimbrite, Ratarua Ignimbrite and Hikurangi Rhyolite, which are all derived from local sources. The Corbett Ignimbrite is the oldest member of the Ohinemuri Subgroup with an estimated age of Late Pliocene. The Bowentown Rhyolite has been suggested as a potential source for the Corbett Ignimbrite by Brathwaite and Christie (1996) and is therefore included in this study, in less detail, to determine the probability of this as a source. Overlying the Corbett Ignimbrite in the northeastern region of Waihi is the dacitic Ratarua Ignimbrite with an approximate age of 5 Ma (Brathwaite & Christie, 1996). Southern extents of the Corbett Ignimbrite are overlain by the Hikurangi Rhyolite which is the largest feature in southern Waihi. The Hikurangi Rhyolite is a dome with no age determined, it is thought to be approximately 5 Ma (Brathwaite & Christie, 1996).

The study aims to determine the volcanic history and processes of felsic volcanism at the eastern side of the Waihi area.

## **1.1 Research Objectives**

This study is focused on providing a better understanding of the volcanic history in the eastern Waihi area through detailed study of the Corbett Ignimbrite, Ratarua Ignimbrite and Hikurangi Rhyolite. The objectives of the study were:

- To describe the facies characteristics and internal structures of the Hikurangi Rhyolite, Corbett Ignimbrite and Ratarua Ignimbrite,
- To determine the petrographical and mineralogical characteristics of each of these units by microscopic petrography, scanning electron microscopy and X-ray diffractometry,
- To investigate geochemical characteristics of each of these units through whole rock geochemistry by X-ray fluorescence spectrometry and glass chemistry by electron microprobe analysis, and
- To determine the maximum eruption ages for each of these units using U-Pb dating methods on zircons

## **1.2 Location of Study**

In this study the Hikurangi Rhyolite, Ratarua Ignimbrite and Corbett Ignimbrite were studied in detail. The Bowentown Rhyolite was included in lesser detail, with two samples collected from one site at Bowentown Heads to allow analysis, to determine its potential association with the Corbett Ignimbrite. These units occur in the eastern Waihi area (Figure 1.1) where they are found in the landscape as rolling hills, bluffs and boulder fields with exposures along streams. The Corbett Ignimbrite is the most extensive unit in the study. The northernmost location examined in this study is an outcrop on Landlyst Road (approximately 8 km northeast of Waihi township). The southernmost outcrop is found along Waitengaue Stream accessed through the Department of Conservation Ananui Falls track (approximately 11.5 km south of Waihi township). The Ratarua Ignimbrite is examined at two sites in this study in the northern region of the Waihi area, with the exposures along Waihi Whangamata Road. As the CVZ contains a significant amount of rhyolite deposits, including several rhyolite

domes, the Hikurangi Rhyolite dome was included in this study to determine its age and internal stratigraphy. As the majority of the rhyolite dome is now covered by forestry only one exposure was accessible as an outcrop along Woodlands Road.

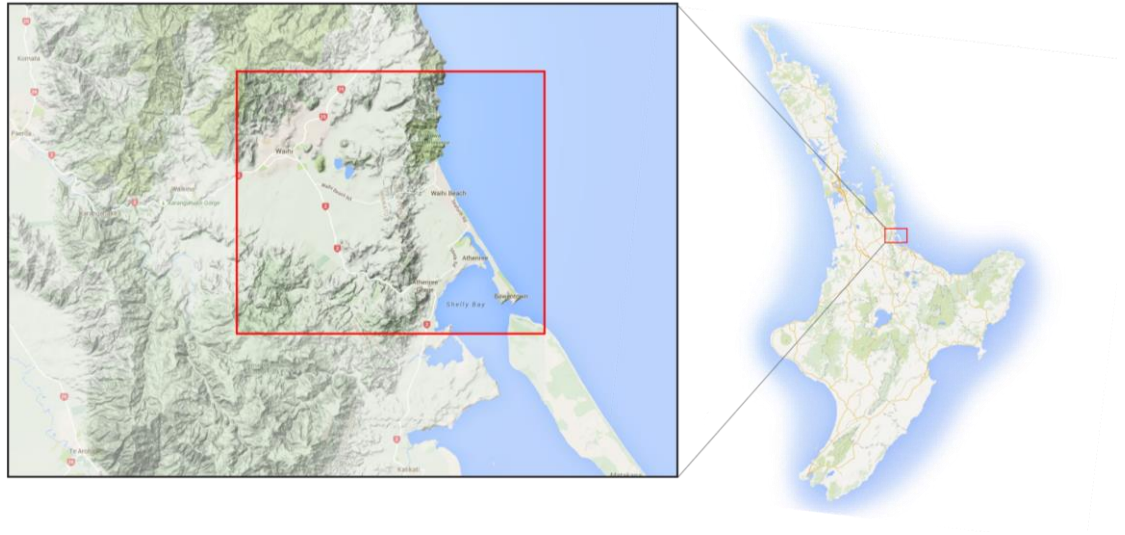


**Figure 1.1 Map showing the study location (red box). Maps sourced from Google Maps (October, 2015).**

### **1.3 Tectonic Setting**

The geology of New Zealand is largely influenced by the changing position of the Indian-Pacific plate boundary where the Pacific plate is currently subducting under the Australian plate (Cole, 1986).

The CVZ is a 200 km-long by 35 km-wide continental volcanic arc within the Hauraki Volcanic Region, which is the largest and longest-lived area of andesite-dacite volcanism in New Zealand (Figure 1.2). This arc also encompasses the Kiwitahi Volcanic Zone and the central Hauraki Rift. The Hauraki Volcanic Region has a NNW trend which is due to episodic Neogene arc volcanism over an older horst-graben structure in the Mesozoic basement (Skinner, 1986).

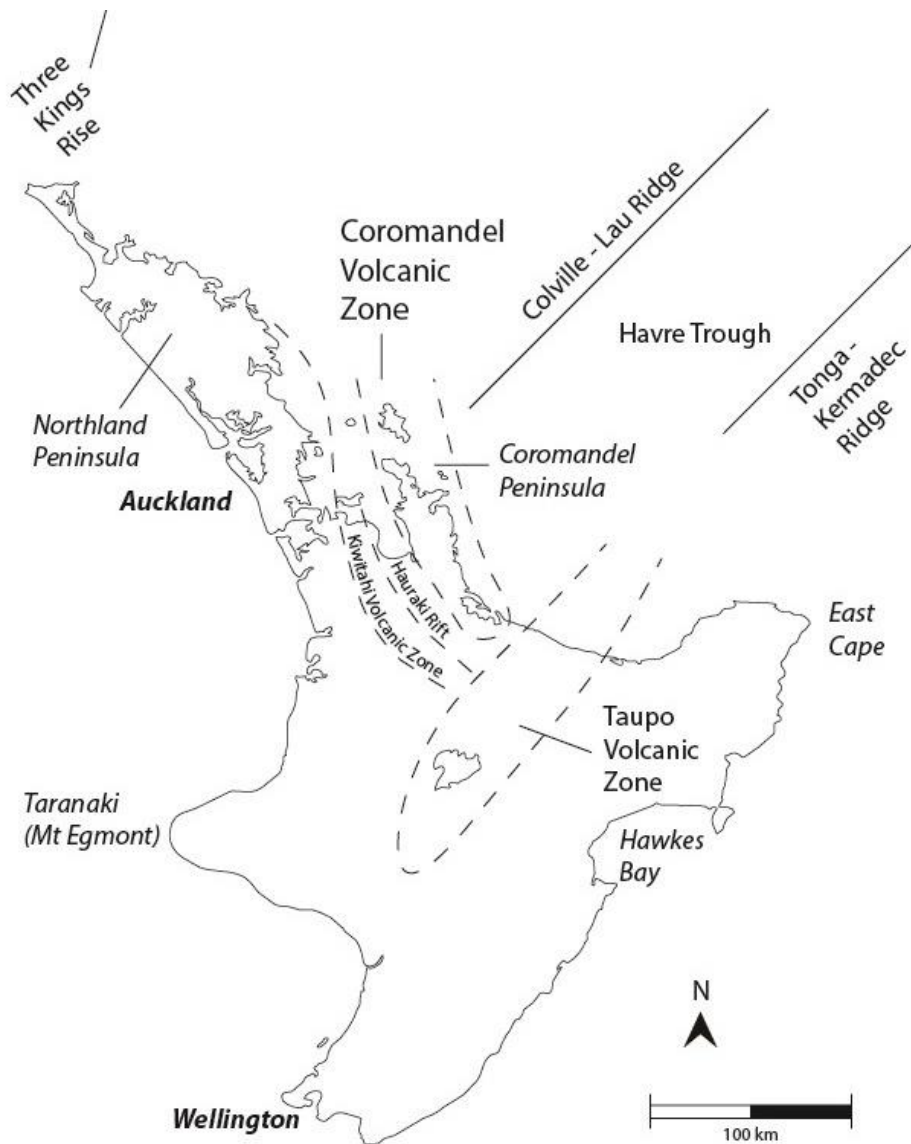


**Figure 1.2 The major volcanic regions in the North Island of New Zealand including the HVR which contains the Coromandel Volcanic Zone, Hauraki Rift and the Kivityahi Volcanic Zone (after Malengreau *et al.*, 2000).**

Southeast migration of volcanic arcs began to occur 25 Ma representing the southward trending movement through the plates (Adams *et al.*, 1994). In the North Island there are three distinct volcanic arcs which represent southeast migration through time: the southward trending Three Kings – Northland – Coromandel arc, the Colville Lau arc, and the Taupo Volcanic Zone – White Island – Kermadec arc (Malengreau *et al.*, 2000). Movement has transitioned from the southerly direction in the Northland Volcanic Arc to a northeast-southwest direction at the CVZ and finally subparallel to the orientation of the active TVZ (Nicholson *et al.*, 2003).

Subduction-related andesitic volcanism occurred within the Northland Volcanic Zone (NVZ) during the early Miocene and by the late Miocene to early Pliocene rhyolitic volcanism dominated the central and southern parts of the CVZ, extending to Tauranga (Malengreau *et al.*, 2000). Silicic volcanism is significant throughout the CVZ and is thought to be due to extension across the CVZ back arc throughout the time of southwards migration of the Australian-Pacific plate boundary to its current position parallel to the TVZ (Nicholson *et al.*, 2003).

#### **1.4 Regional Geology of the Coromandel Volcanic Zone**

The CVZ has been the subject of much previous study and is regarded as the precursor to the active TVZ to the southeast. The mid to late nineteenth century saw significant exploration of mineralised volcanic zones around Thames, Coromandel and Waihi due to the discovery of gold (Adams *et al.*, 1994). The CVZ is found within the larger Hauraki Volcanic Region (HVR) which is the longest lived region of andesite-dacite volcanism within New Zealand, with dacite deposits tending to follow andesite at any one locality (Ballance, 1975). The HVR also encompasses the Kiwitahi Volcanic Zone (KVZ) and the central Hauraki Rift. The Coromandel Peninsula is comprised of Miocene to Quaternary volcanics, comprised of a wide range of igneous rocks from basalt to rhyolite in composition (Skinner, 1986), which have developed on top of Mesozoic greywacke basement. The Hauraki Rift bounds the Coromandel Peninsula to the west; this is a large graben infilled with Quaternary and Tertiary sediments. The southern extent of the peninsula overlaps with the TVZ, which is presently still active (Smith *et al.*, 2006).

The structure of the CVZ is constrained by two fault sets; one dominantly oriented NW-NNW, the other oriented NE-ESE. These faults extend into the Neogene rocks and are thought to be controlled by pre-existing horst and graben faults in the greywacke basement (Haworth, 1993). These graben blocks are derived from late Jurassic greywacke that are overlain by minor Oligocene and Miocene marine sediments covered by a thick sequence of Miocene and Pleistocene volcanics which vary in composition from basalts to rhyolites (Skinner, 1986).

Volcanic activity began at approximately 18 Ma and transitioned southwards (Smith *et al.*, 2006) where it was joined, from 12 Ma, by rhyolitic volcanism which has since dominated the structure of volcanism in the North Island (Booden *et al.*, 2012). Volcanism in the CVZ from 7-2 Ma was dominated by rhyolite domes, ignimbrites, pumice breccia and associated breccias which form the subgroups of the Whitianga group within the Waihi area. Silicic volcanic centres throughout the CVZ have been identified using negative gravity anomalies (Malengreau *et al.*, 2000; Smith *et al.*, 2006) as well as the identification of arcuate or circular structures and spatially-related thick intracaldera ignimbrites and silicic dome complexes (Briggs and Fulton, 1990).

Active volcanism ended approximately 1.5 Ma, with volcanism transitioning into the TVZ (Smith *et al.*, 2006). The transition from the CVZ to the currently active TVZ is considered to have occurred without any significant interval in volcanic activity or major change in major element geochemistry. This suggests there is either a continuation or an overlapping interval when the CVZ and TVZ were both active (Carter *et al.*, 2004).

## **1.5 Geology of the Waihi area**

Waihi makes up the southern portion of the CVZ with younger volcanics occurring (Figure 1.3). The basement geology of Waihi is estimated at depths of 0.2 to 3 km (Hochstein & Nixon, 1979) and comprised of volcanic greywacke, sandstone and argillite belonging to the Late Jurassic rocks of the undifferentiated Manaia Hill Group. Unconformably overlying this greywacke basement is the Early Miocene to Early Pleistocene volcanic rocks belonging to the Coromandel Group and Whitianga Group. The Coromandel Group consists of pyroxene or pyroxene-hornblende andesite, with lesser dacite and rhyodacite (Skinner, 1986) and contains three subgroups: Waiwawa, Omahine and Kaimai subgroups. The Waiwawa Subgroup predominantly crops out to the west and north of the Mangakino and Waihi faults, whereas to the east and south of these faults the Uretara formation of the Kaimai subgroup dominates the area. The Mangakino fault makes a distinct boundary between these units. The location of the Waihi Fault is not clear as it has been covered by sheets of younger ignimbrites which belong to the Whitianga Group (Smith *et al.*, 2006) which is Late Miocene to

Pliocene in age. The Whitianga Group contains three subgroups: Minden Rhyolite, Coroglen and Ohinemuri subgroups. In the northeast of the CVZ minor basalts are related to Whitianga Group rhyolites. The southern extent consists of Pliocene andesite to dacite belonging to both Omahine and Kaimai subgroups. Marine sediments of the Oligocene Te Kuiti Group and Early Miocene Waitemata Group may have been deposited and eroded before the later deposition of the Coromandel Group (Braithwaite & Christie, 1996).

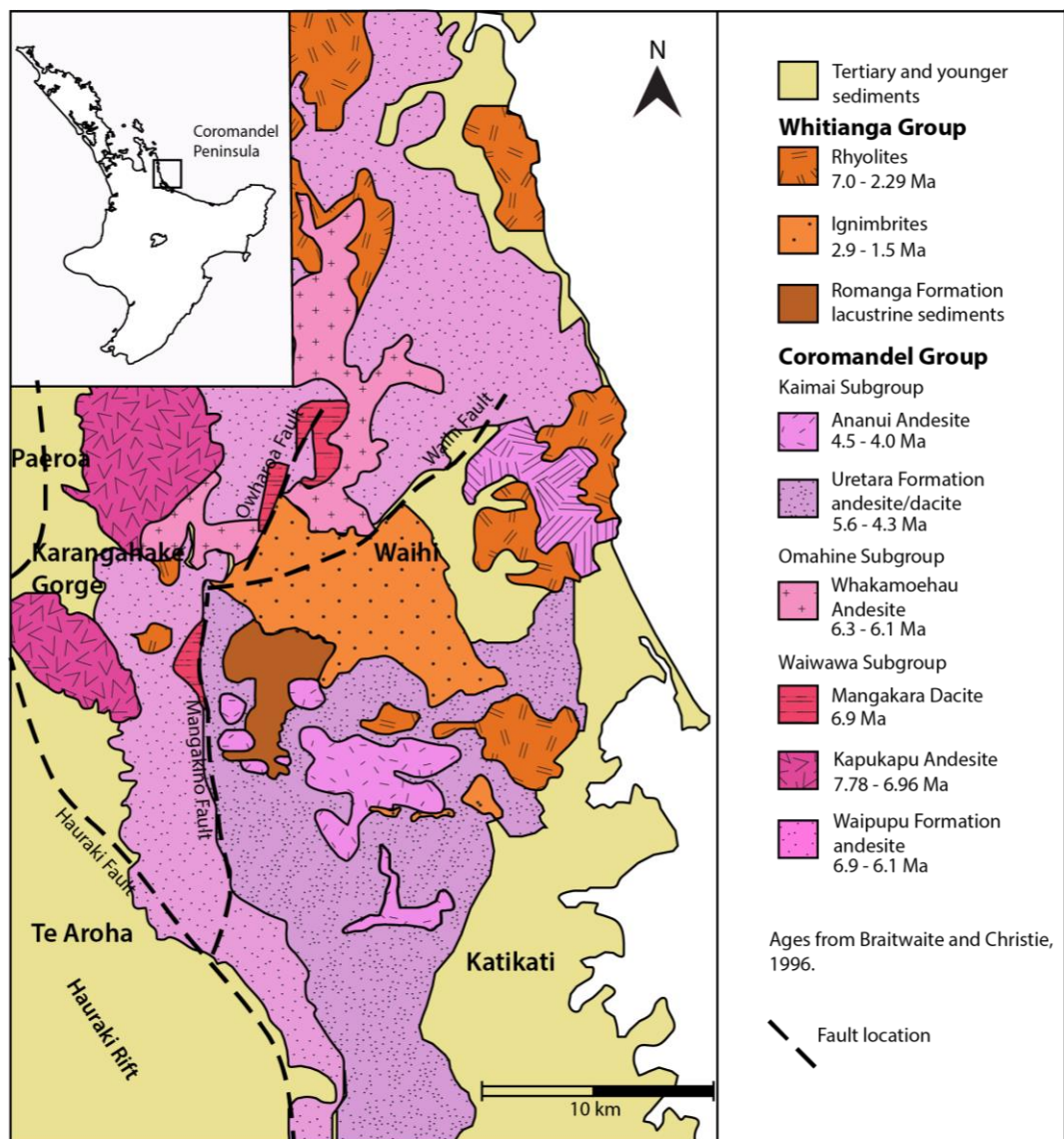


**Figure 1.3** Simplified geology of the Waihi region extending to the southern Coromandel Peninsula, (after Smith et al., 2006).

Late Pleistocene sedimentary deposits of the Tauranga Group, which are also found in the Waihi area, consist of alluvial and estuarine deposits, ignimbrite, tephra as well as postglacial sand dunes and alluvial fans which fill the nearby Tauranga Basin. The Matua and Piako subgroups make up the Tauranga Group (Braithwaite & Christie, 1996). These are the youngest formations found in Waihi and mark the end of active volcanism in the CVZ.

## **1.6 Structure of the Waihi area**

Within the local Waihi area the volcanic succession is predominantly basal Coromandel Group andesites which are unconformably overlain by the Whitianga Group rhyolites, ignimbrites and lesser dacites. The structure within the region is dominated by NNE-NE trending faults, with a potential caldera feature within the Waihi area (Haworth, 1993). In the Coromandel Peninsula there are four significant anomalies which mark calderas and graben structures. The calderas identified in the northern Coromandel are characterised by similar physical depths and sizes as the Waihi Basin. These features are filled with rhyolitic and ignimbrite deposits with low density compositions (Malengreau *et al.*, 2000). The Waihi Basin has been interpreted to be a fault-angled depression through gravity and resistivity data. The northern and western boundaries of this depression are bounded by the Ohinemuri and Mangakino faults which provided a structural weakness in the crust that formed the caldera (Cole *et al.*, 2005). The southern and eastern boundaries are shallow-dipping and are not fault bound (Braithwaite & Christie, 1996). The influence of local faults caused the collapse to form a polygonal-shaped trapdoor caldera, with faults controlling the steep northern and western margins. The trapdoor shape was formed due to the collapse of having less impact in the southern and eastern sectors causing shallow dips in this region (Smith *et al.*, 2006). The basin infill reaches 1.5 km thickness and consists of sediments of low resistivity and low density as well as ignimbrite sheets of the Waikino, Owaharoa and Corbett ignimbrites (Braithwaite & Christie, 1996).

## **1.7 Previous Work**

The Hikurangi Rhyolite dome, Corbett Ignimbrite and Ratarua Ignimbrite have not been dated, nor studied in detail; only their distribution has been mapped (Hunt, 1991; Brathwaite and Christie, 1996). Hunt (1991) identified the Corbett Ignimbrite and mapped its extent throughout the Waihi district. Hunt (1991)'s mapping data was included in Brathwaite and Christie (1996)'s 1:50,000 map of the Geology of the Waihi area along with basic descriptions of the units. This map was largely based on previous work as well as air photograph interpretation. Hunt (1991) also identified the Ratarua Ignimbrite as welded ignimbrite unit two, and further detail was included in Brathwaite and Christie (1996)'s publication. Vincent (2012) studied 16 rhyolitic lavas and 5 rhyolitic ignimbrites from the eastern CVZ to generate new U-Pb zircon ages. This study excluded the Hikurangi Rhyolite, Corbett Ignimbrite and Ratarua Ignimbrite. Vincent (2012) and Brathwaite and Christie (1996) also dated the other rhyolites belonging to the Homunga formation, as well as the related Owharoa Ignimbrite. The study area is also covered by Smith *et al* (2006) which focuses on the potential presence of a trapdoor caldera in Waihi. This study included both the Hikurangi Rhyolite and Corbett Ignimbrite but did not contain any detail on their internal stratigraphy.

## **1.8 Structure of thesis**

In Chapter 2 the different methods used throughout this research are described. Chapters 3, 4 and 5 are focused on each unit (the Corbett Ignimbrite, Ratarua Ignimbrite and Hikurangi Rhyolite respectively) as this study included three distinct volcanic units. Chapter 3 also includes research on the Bowentown Rhyolite to allow further analysis on the potential relationship between this rhyolite and the Corbett Ignimbrite. These chapters present results from studying these units to better understand the volcanic history. These results include; facies characteristics, petrography and mineralogy, geochemical properties and ages obtained through U-Pb dating of zircons. A detailed discussion is included at the end of each of these chapters providing interpretations on key findings. Chapter 6 discusses; the potential sources for the Corbett Ignimbrite, the age of the CVZ volcanics, sources of inherited zircons and the geological history of the eastern Waihi area in relation to the volcanic units studied. Chapter 7 synthesis key findings to present the conclusions of this study.



# Chapter Two

## Methodology

---

### 2.1 Field work

Field work to determine the stratigraphy and facies variations of the Corbett Ignimbrite, Ratarua Ignimbrite and Hikurangi Rhyolite was completed over 3 months. Samples were also collected of the Bowentown Rhyolite. Each unit were identified through the field descriptions and localities identified in Brathwaite and Christie (1996)'s 1:50,000 geological map of the Waihi area. After an initial sample was taken of each unit type the diagnostic characteristics of the sample was used to find more occurrences.

At each site that was studied GPS coordinates were recorded, and photographs were taken to record the characteristics of the outcrops. The locations studied were selected based on the amount of exposure and accessibility. These key locations were used to determine the different facies occurrences and thicknesses of each unit, as well as their distribution throughout Waihi. At sites where there was significant, well preserved exposure, detailed stratigraphic logs were constructed; four of Corbett Ignimbrite, one of the Ratarua Ignimbrite and one of the Hikurangi Rhyolite. Only one stratigraphic log was constructed of both the Ratarua Ignimbrite and Hikurangi Rhyolite due to limited access to well exposed sites. These stratigraphic logs included the maximum pumice and lithic sizes throughout the outcrop, based on the average of the five largest pumice and lithic clasts visible. Component proportions are visual field estimates and are generally recorded as volume percentage of that locations bulk rock. Grainsize, textural variations, component descriptions and any other notable features were also recorded. At each site where stratigraphic logs were constructed samples were collected from different representative heights. Samples were also taken from the studied units at seven other field sites, but no logging was done at these sites due to lack of exposure. There were restrictions to samples which could be taken due to accessibility and height restrictions. The full list of samples are included in the sample catalogue presented in Appendix I and stratigraphic logs including descriptions are presented in Appendix II.

## **2.2 Thin section preparation**

50 thin sections were made to be analysed. The samples were cut using a diamond saw to produce a block which would cover a glass slide, leaving margins of 1-2 mm. The side to be mounted to the glass was ground, using a diamond grinder, to ensure a flat surface. Once dry the rock surface was impregnated with Araldite K39 two-part resin with a predetermined ratio of 2 g resin to 1 g of hardener. The sample was left to absorb this mixture and when absorption was complete the excess of this mixture was removed by scrapping the surface with a tongue depressor. These samples were then left to set overnight. The impregnated surface was then ground using a #600 polish powder on a frosted glass plate until the excess of the mixture was removed and the initial rock surface was again exposed, leaving only depressions infilled. Glass sides (4.5 x 2.7 cm) were frosted on one side using a diamond discoplan to ensure a flat surface. The dried polished samples were mounted onto the frosted side of the glass slide with Hillquest thin section epoxy using a ratio of 2.3 g resin to 1 g hardener. Bubbles were removed by circulating the frosted slide along the surface. The samples were left to dry overnight. The mounted blocks were then cut to ~1 mm thickness using the Struerd Discoplan-TS. The ~1mm on the samples were trimmed to ~30  $\mu$ m through the same method. Cover slips were applied to seal the sample using a petropoxy at a ratio of 1 ml resin to 0.1 ml hardener. The samples were then left to dry overnight. Thin sections were labelled with the in-field locality number and an additional suffix representing sample number from that locality.

## **2.3 Microscope Petrography**

All thin sections that were made were analysed under the microscope however samples representative of the bulk rock, pumice and lithic clasts were selected for point counting.

Thin sections were observed under a transmitted light microscope in both plane and cross polarised light. Quantitative data on mineral and groundmass abundances was obtained by point counting. For each sample the stage interval was set at 0.3mm and the number of counts per slide were recorded (minimum of 400 counts) to ensure a fair representation of the sample. Only components that

were less than 2mm were counted to ensure proportions of minerals were not skewed. The thin sections that were point counted were selected based on their representative properties. Both the Corbett Ignimbrite and Ratarua Ignimbrite counts included interstitial matrix, crystals, pumice, vesicles in pumice, fiamme, phenocrysts in pumice/fiamme and lithics. Groundmass and phenocrysts in the rhyolite samples were counted. When there was uncertainty on the identity of a crystal it was recorded based on best estimations and petrographical knowledge and it was noted each time this occurred. The total of uncertain minerals was calculated for each thin section counted and this was used to gain an estimated margin of error to account for any small inconsistencies.

## **2.4 Scanning Electron Microscope (SEM)**

Two different types of samples were prepared for scanning electron microscopy (SEM) analysis; samples of matrix, pumice and fiamme for high magnification images of different microtextures, as well as polished thin sections for backscatter and elemental analysis. Small matrix and pumice samples were analysed under the microscope to allow for high resolution images of the different features. These samples were obtained by extracting a fresh surface of the selected specimen which were under 1 cm x 1 cm in size. These samples were mounted onto a specimen stub by placing it on a tapes surface and then lining any gaps against the tape with a carbon paint to ensure conductivity. These specimen stubs were placed into the Hitachi E1030 Ion Sputter Coater and where the sample was covered in a coating of platinum to increase conductivity. Once this was complete the sample was able to be processed in the SEM. Polished thin sections were prepared for both the SEM and electron microprobe analysis. These thin sections followed the same initial steps as the samples with cover slips with cutting, grinding, impregnation, mounting to glass and the initial cut to remove the block from the glass. These samples were then ground back in the discoplan until the majority of quartz crystals were at a dark yellow colour. #500 grit paper was used to grind the sample back further until the majority of crystals were at the right colouration. The thin section was then polished until there was a flat, reflective surface.

## **2.5 Electron Microprobe**

Electron microprobe analysis was used to gain geochemical data on five polished thin sections; two Corbett Ignimbrite thin sections and one for each of the Ratarua Ignimbrite, Hikurangi Rhyolite and Bowentown Rhyolite (refer to section 2.4 for polished thin section methods). This was done using the JEOL JXA-8230 SuperProbe Electron Probe Microanalyser at the School of Geography, Environment and Earth Sciences, Victoria the University of Wellington, with the assistance of Ian Schipper. The geochemistry of individual crystals were investigated in all samples and glass shard composition was also analysed for the two Corbett Ignimbrite thin sections. Each polished thin section was carbon coated to ensure conductivity. Glass shards were analysed with an electron gun accelerating voltage of 8 kV, a 1000 pA beam current, and an probe diameter of 3µm as glass shard were under 10µm in size. 30 glass shards were analysed in total, 15 points on both Corbett Ignimbrite thin sections. Crystals were analysed with an electron gun accelerating voltage of 12 kV, a 1000 pA beam current and an electron spot. Standardisation used a set of previously analysed glass shards and crystals.

## **2.6 X-Ray Diffraction**

Matrix samples of each rock was used for XRD analysis. These matrix samples were dried in an oven at 50°C for 24 hours and then crushed into a fine powder using a tungsten carbide ring mill. Samples were analysed using the Panalytical Empyrean XRD machine in the Faculty of Science and Engineering, University of Waikato. Bulk samples were run for 2-80 °2θ at 50 seconds per step. 21 Samples were analysed with XRD; one for the Bowentown Rhyolite; eight for the Corbett Ignimbrite; six for the Hikurangi Rhyolite; and six for the Ratarua Ignimbrite.

## **2.7 X-Ray Fluorescence**

Each sample studied had different features extracted for XRF preparation; pumice from Corbett Ignimbrite, fiamme from Ratarua Ignimbrite and matrix from both the Hikurangi Rhyolite and Bowentown rhyolite. Pumice and fiamme clasts were extracted from the matrix using a diamond blade dremel. Wherever possible

pumice and fiamme greater than 4 cm in size were used as smaller clasts may no longer be truly representative of magmatic composition, having lost crystals during fragmentation during eruption (Wolff, 1985). The pumice and fiamme samples were then grinded, using a diamond grinder, to remove any remaining matrix. To remove any foreign material that may cause contamination all samples were washed using distilled water twice and then were left to soak overnight before drying in an oven at 50°C for 24 hours. The dried samples were then crushed into a fine powder using a tungsten carbide mill in order to homogenise them. The parts of the mill used were carefully cleaned to ensure no contamination between samples. Aluminium cups were then used to make 40 mm pressed pellets. These required 8-9 grams of sample mixed with 25 drops of PVA binder in a paper cup using a wonder spatula, to ensure no contamination as the XRF does not detect carbon. Once well mixed a hydraulic press was used to compress the sample into the aluminium cups. The samples were then analysed using the Bruker S8 Tiger XRF in the Faculty of Science and Engineering, the University of Waikato.

## **2.8 Separation for dating**

The first major component to U-Pb dating is to complete mineral separation. The bulk rock collected was crushed through a jaw crusher and then ground in a bico pulverisator which was set at a 0.50 mm clearance to a sand of 0.500 mm. A Gemini table otherwise known as a 'shaking' table was then used, with the sample tray at 55 Hz and the table at 22 Hz, used to wash away the very fine, dust sized particles from each sample. As the sample was processed through the Gemini table the particles were crudely separated by density with different density material being collected in the appropriate container. The densest mineral fractions were then oven dried and the remaining samples were stored. The oven dried heavy mineral fraction was further processed through a Frantz Isodynamic magnetic separator, at 1.0 A, to remove any material which has magnetic properties. The non-magnetic proportion of sample was processed through sodium polytungstate (SPT) heavy liquid with heavy minerals which sank in the liquid with a specific gravity between 2.85 and 3.01 g.cm were collected and stored in a paper filter cone. This sample was then put through the inclined Frantz magnetic separator (15° front-to-back, 10° side-to-side, 0.5 A) to produce a final non-magnetic, heavy mineral fraction. The best 50-100 zircons (where possible), that

were free of inclusions and/or cracks and wider than 60  $\mu\text{m}$ , were selected. These zircons were then mounted on double sided tape on a glass slide to be made into a polished block. Using a camera mounted on a stereo microscope, image(s) were taken of the sample to ensure the highest quality grains could be pre-selected and mapped for dating.

## **2.9 Dating using Laser Ablation Inductively Coupled Plasma Spectrometry**

U-Pb isotopes  $^{204}\text{Pb}$ ,  $^{206}\text{Pb}$ ,  $^{207}\text{Pb}$ ,  $^{208}\text{Pb}$ ,  $^{232}\text{Th}$ ,  $^{235}\text{U}$ ,  $^{238}\text{U}$  were measured using a resolution SE series excimer laser (193 nm) and an Elan 6100 DRCII Inductively Coupled Plasma Mass Spectrometer in the Faculty of Science and Engineering, the University of Waikato. LA-ICP-MS specifications are presented in Appendix VII and all raw data collected from this testing is included in Appendix VIII.

Data was acquired using laser software Geostar v8.50 and ICPMS software Elan v3.4. A zircon of a known age and two analytical standards were used to check against the data for samples with an unknown age included in this study. The NIST610 is a glass standard which is homogeneous in 61 trace elements. This was used to check the concentration of elements in unknown samples. The second standard used was the GJ1 which is a large homogeneous zircon which is of gem quality (Jackson et al., 2004) that has been obtained from the School of Earth and Planetary Sciences at Macquarie University in Australia. The GJ1 has TIMS age of  $608 \pm 0.4$  Ma (Jackson et al., 2004) and is used for calibration to ensure corrections are made for any mass discrimination by the ICP-MS. Temora2 zircon crystals were also used as they have a known zircon age of  $4.16.78 \pm 0.33$  Ma and are able to be used as a method check These zircon crystals are derived from the eastern Australia from the Middledale Gabbroic Diorite of the Paleozoic Lachlan Orogen (Black et al., 2004).

The NIST610 is a glass standard and was analysed twice at the start and at the end of the session. GJ1 was analysed at start and end as well as twice between every 9-12 unknowns. Temora2 was analysed twice at the start and twice at the end of each session.

Zircons were dated based on the method of Solari et al. (2009) where 30µm was used for spot sizes for standards and unknowns (60µm was used for NIST610). Laser firing was set at 5 Hz (with the energy on spot being approximately 0.042 mJ ) at 25% power to achieve an energy density on the sample of approximately 6 J.cm<sup>2</sup>. Data was then reduced using lolite v3.1 with the 'U-Pb Geochronology 4' data reductions scheme. Histograms were plotted with KDE (Kernel Density Estimation) using 'DensityPlotter' (Vermeesch, 2012).



# Chapter Three

## Corbett Ignimbrite

### 3.1 Introduction

The Corbett Ignimbrite is a widespread deposit found at multiple outcrops within the eastern Waihi area, however, as it is the oldest known ignimbrite from the Ohinemuri Subgroup a large amount of this unit has been buried and/or eroded since its deposition. The Corbett Ignimbrite was examined at nine localities (Figure 3.1) in this study ensuring a fair representation of variations that occurred from the northern to southern limits of the mapped deposit, as mapped by Brathwaite and Christie (1996).

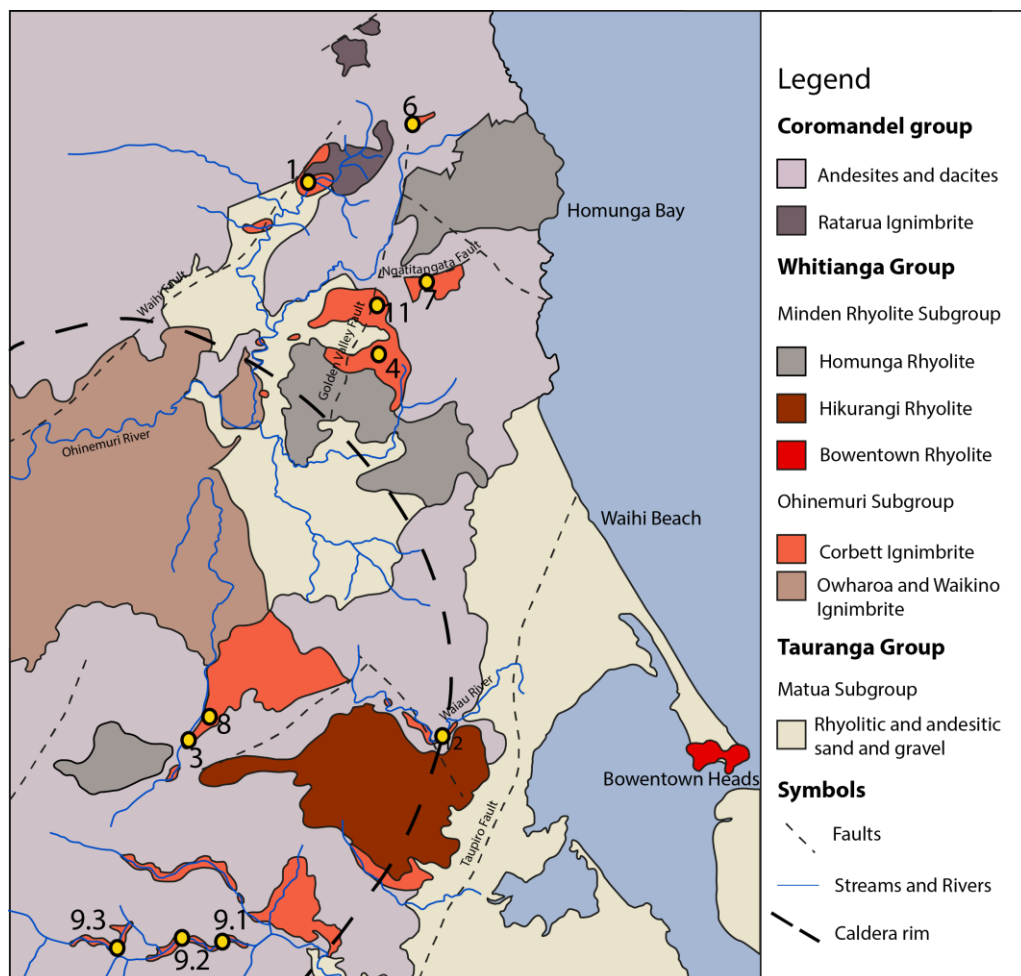


**Figure 3.1 Simplified geological map for the Waihi region. The Corbett Ignimbrite localities are labelled. Based on Braithwaite and Christie (1996) 1:50,000 geological map of Waihi.**

Analysis of the Bowentown Rhyolite is included within this chapter as two samples were collected to gain petrography, mineralogy, geochemistry analyses and an age. This is to assess the genetic relationship, if any, with the Corbett Ignimbrite as suggested by Brathwaite and Christie (1996). Spatially related units Ratarua Ignimbrite and Hikurangi Rhyolite are also being explored in separate chapters, as they are significantly larger units.

This chapter documents the distribution and facies architecture, petrography, mineralogy, and whole pumice and glass geochemistry of the Corbett Ignimbrite. A new U-Pb age is also presented.

### **3.2 Location and distribution**

Brathwaite and Christie (1996)'s geological map of the Waihi area showed the Corbett Ignimbrites exposure is confined to the eastern region. This distribution shows the Corbett Ignimbrite is found within the approximated boundaries of the inferred caldera (Figure 3.1) as well as further north.

The type section (locality 13, Figure 3.1) is a cliff face at Corbett Road, approximately 5 km north of Waihi, which has the maximum exposed thickness of 18 m (Figure 3.2). Exposures of Corbett Ignimbrite occur further south, as far as Woodlands Road along the Department of Conservation Ananui Falls track near Katikati, approximately 11.5 km south of Waihi (locality 9, Figure 3.1). This site provided the minimum exposed thickness of 1.5 m (Figure 3.3) showing a 16.5 m variation in thickness between the northern and southern limits. Locality 12, found at Athenree gorge, was proven to be an andesite sample and is not part of the Corbett Ignimbrite. This sample is included in the sample catalogue and thin sections but is not discussed further in this study. Locality 4, found at Trig Road North (6418895.938N, 2767509.228E) is highly altered so no sample was collected for further analysis.

The Corbett Ignimbrite overlies the Romanga Formation, which is composed of lake sediments, and underlies the younger widespread Owharoa and Waikino

ignimbrites (Brathwaite & Christie, 1996). Corbett Ignimbrite outcrops vary from road cuttings to flow sheets to boulder fields. Correlation between outcrops was based on characteristics that were consistent throughout each site which were identified in Brathwaite and Christie (1996). These diagnostic characteristics were the creamy white buff colour, poor sorting, fine grainsize, pumice-rich zones as well as the crystal rich matrix.



**Figure 3.2 Corbett Ignimbrite type section of 18 m thickness**

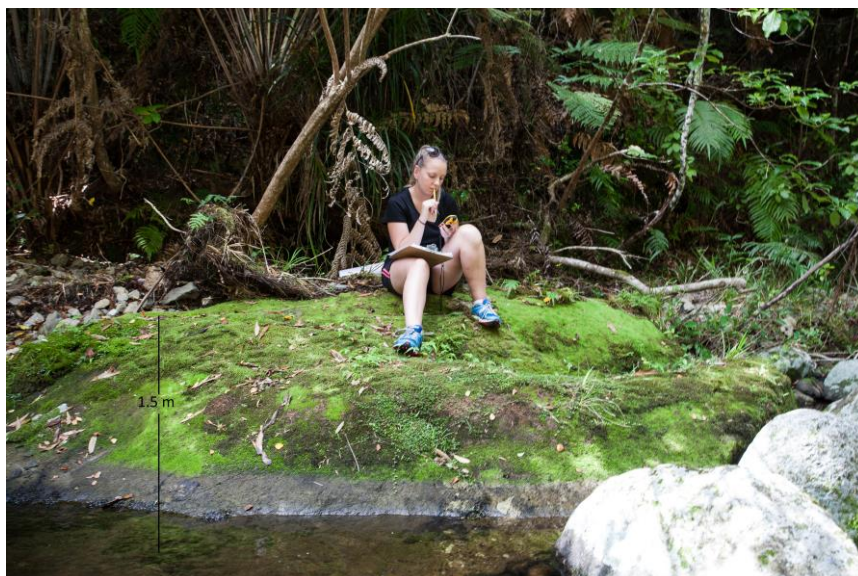


**Figure 3.3 1.5 m thick exposure of Corbett Ignimbrite along Ananui Falls track in Katikati**

### 3.3 Facies

Four distinct facies, hc-f1 to hc-f4, were identified in the Corbett Ignimbrite based on variations in pumice and lithic abundance, degree of welding and the presence of fiamme.

Facies hc-f1 is characterised as a non-welded, massive, poorly sorted, pumice and crystal-rich, coarse ash ignimbrite. Pumice is typically medium lapilli-sized, subangular, white/cream coloured, porphyritic with fine spherical vesicles. Pumice makes up to 50% of the bulk rock and are equidimensional not flat, with a maximum size range of 6 - 140 mm. Subangular, fine lapilli-sized lithics of andesite are abundant. Lithics are typically subangular and make up 5 - 10% of the bulk rock (Figure 3.4) with a maximum size range of 4 - 125 mm. The matrix is crystal-rich with plagioclase, quartz, hornblende, orthopyroxene, augite and opaques. This facies was found to contain a burnt tree log at locality 3 (Figure 3.1) which is 700 mm in length and 140 mm in width and relatively intact.



**Figure 3.4 Outcrop of Corbett Ignimbrite at the base of the type section (locality 1, Figure 3.1) showing facies hc-f1 with lapilli-sized andesite lithics and abundant pumice lapilli**

Facies hc-f2 is characterised as a dark grey andesite lithic concentration zone with a coarse-ash, massive matrix (Figure 3.5). This is a pumice-poor (10%) facies with a maximum pumice size range of 20 - 70 mm. Lithics vary in size laterally from very coarse lapilli to block-size. Lithic concentrations increase in pockets reaching up to 50% of the bulk rock with a maximum size range of 9 - 120 mm. The matrix is crystal-rich with plagioclase, quartz, hornblende, orthopyroxene, augite and opaques.



**Figure 3.5 Corbett Ignimbrite facies hc-f2 lithic concentration zone, at the type section (locality 1, Figure 3.1) with lithics up to block-size. Lithic concentration zone is outlined in red.**

Facies hc-f3 is characterised as pumice-rich with a low abundance of lithics. This facies shows grading with lithics decreasing in percentage vertically. Pumice is porphyritic with fine spherical vesicles. Pumice reaches 50% of the bulk rock with maximum sizes ranging from 8 - 100 mm. Pumice varies in shape at different localities with rounded pumice at the type section (locality 1, Figure 3.1) and subrounded to angular pumice at Ngatitangata Road (locality 7, Figure 3.1) (Figure 3.6). Lithics decrease to concentrations of less than 1% of the bulk rock with maximum sizes ranging from 8 - 48 mm. The matrix is the same texture and composition to previous facies.



**Figure 3.6 Corbett Ignimbrite hc-f3 pumice-rich facies with angular pumice at Ngatitangata Road (locality 7, Figure 3.1).**

Facies hc-f4 is only found at one locality (locality 11, Figure 3.1) and is characterised as fiamme (25%) and crystal-rich (7%) (Figure 3.7). This facies is massive, poorly sorted and moderately welded. Fiamme is elongate, containing feldspar crystals, which is both rectangular and cusped in form. Matrix is crystal rich with angular quartz, plagioclase, augite, orthopyroxene hornblende and opaques. This facies is lithic poor (5%) with grey, subrounded lithics of andesite.

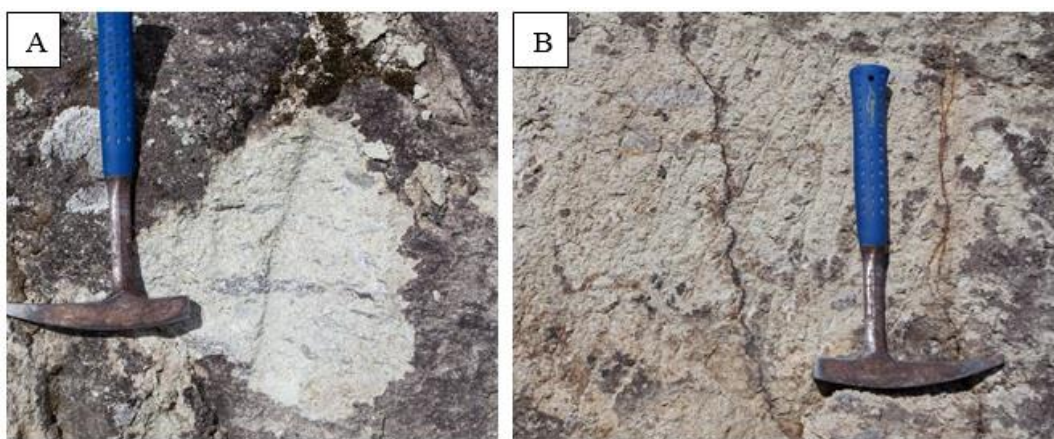


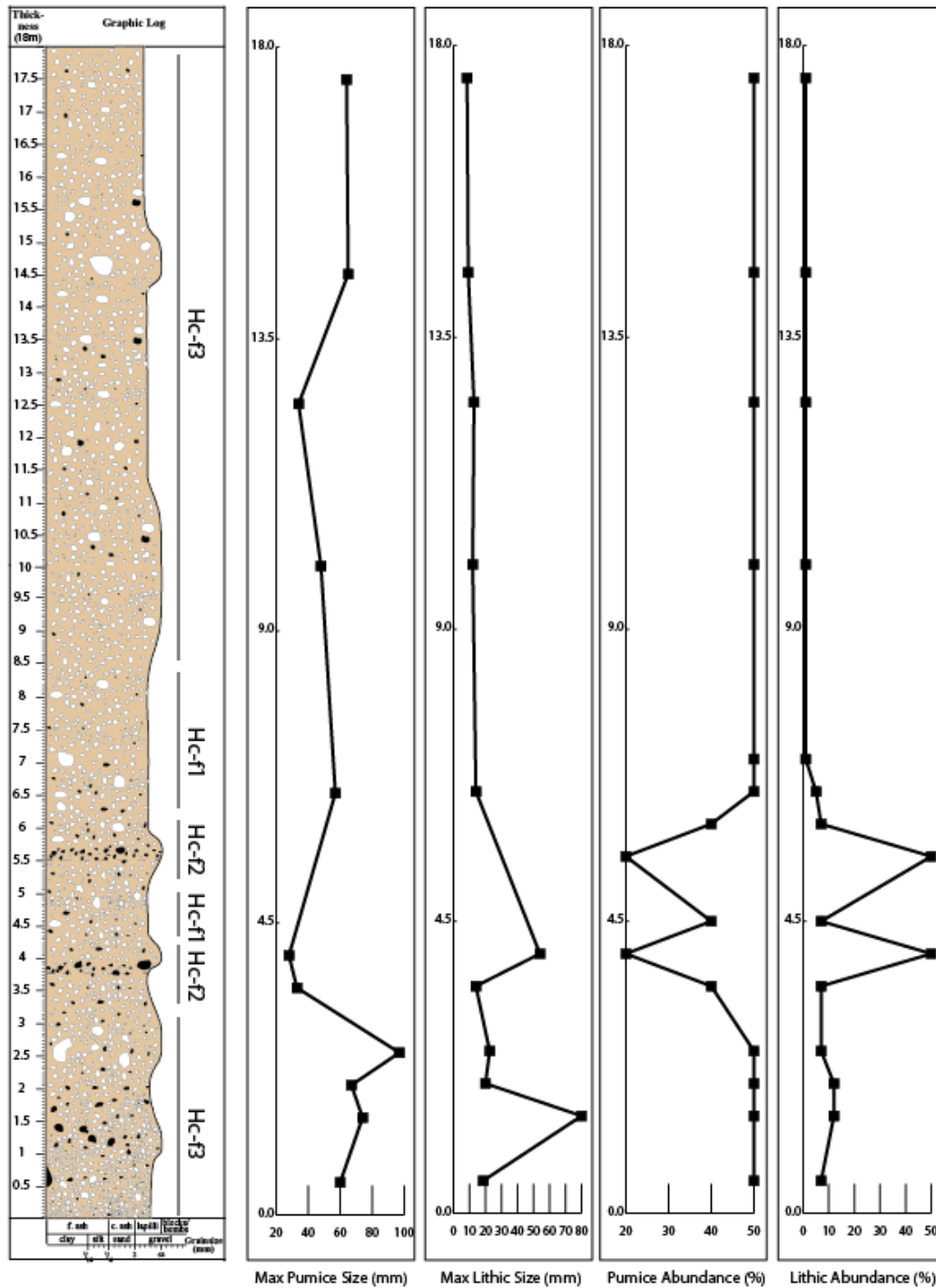
**Figure 3.7 (A) Shows hc-f4 in the field with abundant fiamme. (B) Shows hc-f4 with a higher abundance of lithics**

### 3.4 Facies architecture

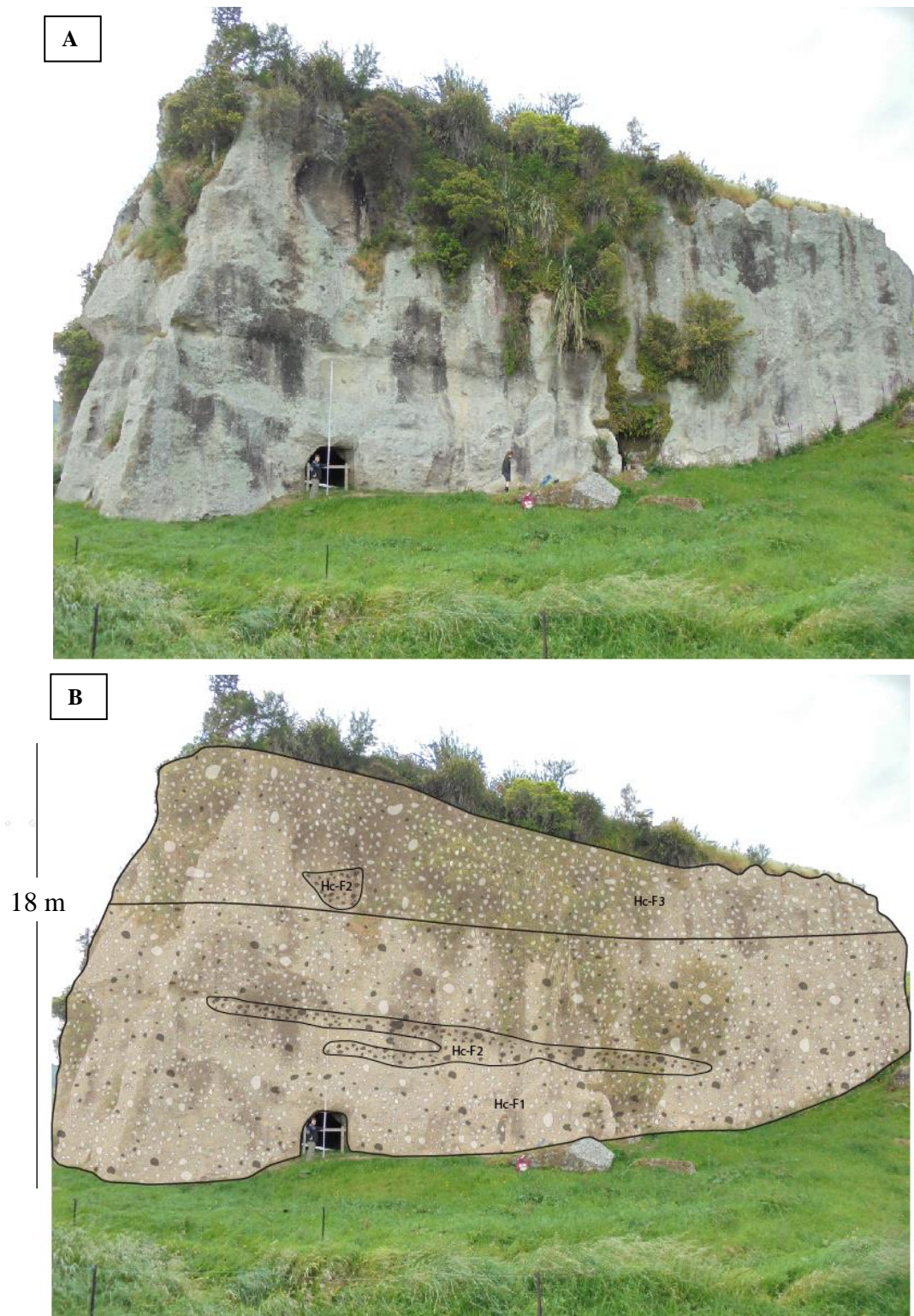
Facies hc-f1, hc-f2 and hc-f3 dominate all the localities of Corbett Ignimbrite with one exception at locality 11 (Figure 3.1). The lower extent of the Corbett Ignimbrite at the type section is dominated by pumice, which totals 50% of the bulk rock, and contains andesite lithics which make up 5-10 % of the bulk rock (facies hc-f1), as shown in Figure 3.8. The strongly defined concentration zones of lithics that are facies hc-f2 is found at both 3.6 m and 5.5 m above ground level. The upper 10.5 m of the type section consists of the pumice rich, lithic poor hc-f3 with pumice concentration increasing towards the final 5 m, with a small lithic concentration zone confined within this facies (Figure 3.9).

Similar relationships between facies hc-f1, hc-f2 and hc-f3 are also visible at locality 7 (Figure 3.10) and locality 3 (Figure 3.11). Locality 3 is a 3 m road cutting found at Woodlands Road by the Walls Road intersection. The lower portion of this road cutting is dominated by the pumice and crystal rich facies hc-f1 with approximately 10 % lithics. At 0.5 m there is a lithic concentration zone found within hc-f1. The upper 1.6 m of this road cutting is pumice-rich with a very low abundance of lithics, consistent with hc-f3. The southernmost exposure of Corbett Ignimbrite along the Ananui Falls track in Katikati (localities 9.1-9.3, Figure 3.1) also consists of hc-f3 which is the only facies found within the minimum exposure of Corbett Ignimbrite seen in the field (Figure 3.3). Locality 4 is a highly altered road cutting, however, lithic concentration zones were observed in a pumice rich matrix (no sample was collected for analysis due to its high alteration). Localities 6 and 8 were boulder outcrops and therefore did not show relationships between different facies as there is limited exposure.

Locality 11 (Figure 3.1) differs from all other Corbett Ignimbrite sites included in this study as fiamme is present. This locality, at Golden Valley Road, comprises a 10 m exposure of the Corbett Ignimbrite in a small quarry (Figure 3.12). Facies hc-f4 is observed only at this location. The entire 10 m outcrop consists of facies hc-f4 with minimal variations in fiamme abundances.



**Figure 3.8** Stratigraphic log at the Corbett Ignimbrite type section (locality 1, Figure 3.1). The position of facies hc-f1, hc-f2 and hc-f3 are shown. Maximum pumice and lithic sizes with abundances (%) are shown on graphs aligned at measured heights.



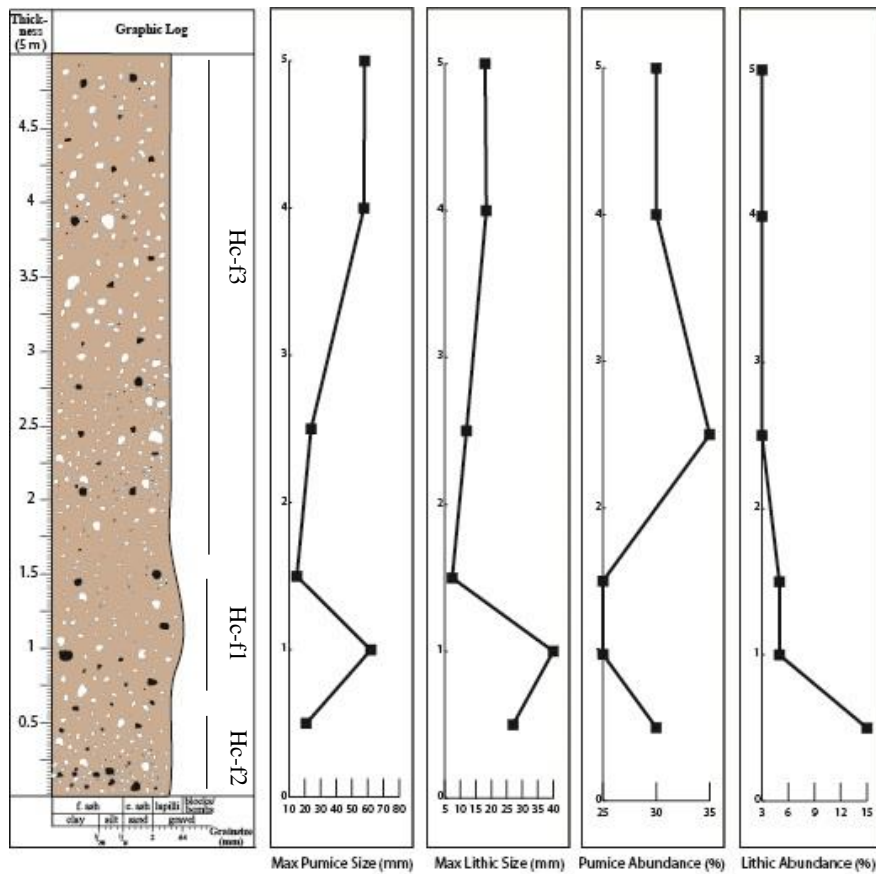


**Figure 3.10** Stratigraphic log of the Corbett Ignimbrite at locality 7 with facies hc-f1, hc-f2 and hc-f3 shown

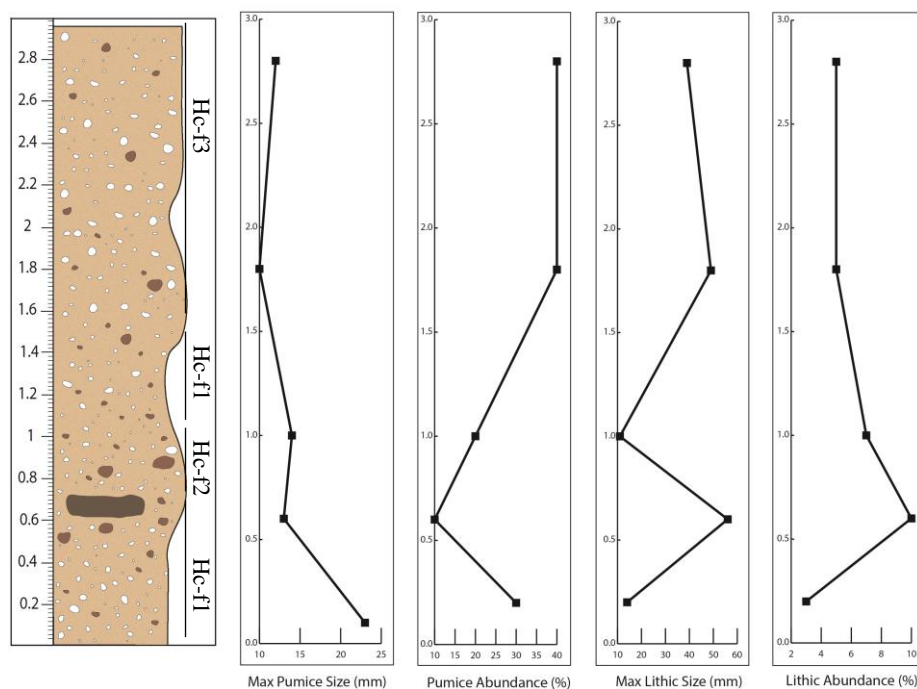


**Figure 3.11** Stratigraphic log of the Corbett Ignimbrite at locality 3 (Figure 3.1). Facies hc-f1, hc-f2 and hc-f3 are shown. A burnt tree log found in hc-f1 is shown at 0.7 m height.

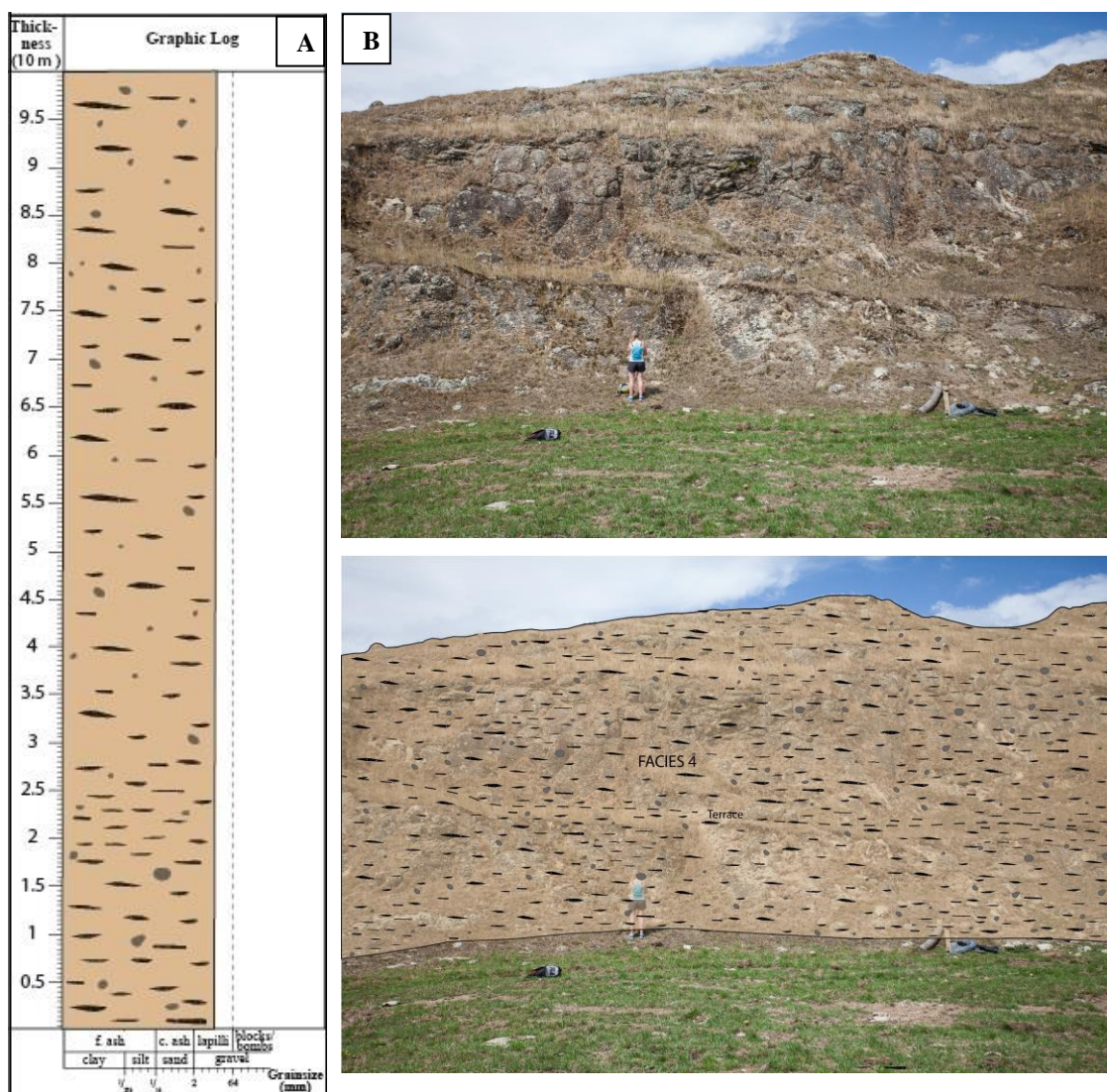


**Figure 3.12 (A) Stratigraphic log of the welded Corbett Ignimbrite locality 11 (Figure 3.1) with facies hc-f4 (B) Outcrop distribution of facies.**

## 3.5 Petrography and Mineralogy

### 3.5.1 Introduction

26 thin sections were created for optical microscope analysis, 1 polished thin section for SEM, 2 polished thin sections for electron microprobe and 7 crushed powder groundmass samples for XRD analysis. Raw point counting results are included in Appendix III, graphs for XRD analysis are presented in Appendix IV and raw data from the electron microprobe presented in Appendix V. Point counting focused on matrix rich samples to determine free crystal percentages (Table 3.1).

**Table 3.1 Results obtained from point counting four thin sections of the matrix of the Corbett Ignimbrite\***

Sample	1.1.1	3.1.1	9.3.1	9.2.1	Average
Interstitial matrix	57.2	57.6	54.3	62	57.8
Pumice**	7	-	22	6.5	8.9
Plagioclase	27.2	24.5	10	14.3	19
Hornblende	1.3	2.4	1.5	3.7	2.2
Orthopyroxene	1.2	3	2	2.3	2.1
Augite	2.3	2.2	2.4	1	1.9
Quartz	2.5	2.8	3.3	9.3	4.5
Opakes	1	0.6	0.5	0.9	0.8
Lithics**	0.3	6.9	4.1	0	2.8
Total	100%	100%	100%	100%	100%
Margin of Error***	1.2%	1.5%	1.1%	1.5%	1.3%
Total crystals	35.5%	35.5%	19.6%	31.5%	30.5%

\*All samples were analysed to 800 counts, except sample 1.1.1 which had 600, with a stage interval of 0.3 mm)

\*\* Pumice and lithic percentages are lower due to samples selected for point counting being matrix rich

\*\*\* Margin of error determined by recording number of uncertain counts

### 3.5.2 Crystals

The Corbett Ignimbrite is crystal rich with quartz and plagioclase, as well as anorthite and albite members found in XRD, graphs for these results are presented in Appendix IV. Other crystals found are hornblende, orthopyroxene, augite and opaques, (Table 3.1). Cristobalite is identified in XRD analysis with a strong presence at locality 3 and locality 11 (Figure 3.1). Crystals often have sharp jagged points. Glass shards are unable to be resolved under the transmitted light microscope.

Plagioclase is highly abundant with percentage proportions of the matrix ranging from 10% - 27.2% and sizes of 0.2 - 2 mm. Intragranular fractures are seen in many of these crystals due to stress during crystallisation or eruption processes. Oscillatory zoning (Figure 3.13 A) and sieve-texture occur throughout the plagioclase crystals indicating disequilibrium during crystallisation.

Quartz is also found throughout the Corbett Ignimbrite with a varying matrix abundance of 2.5% - 9.3% (Table 3.1). Quartz varies in shape from rounded to rectangular, and less commonly embayed and resorbed crystals (Figure 3.13 B). The embayments found in these quartz crystals represent unstable growth or dissolution in the melt. The sizes of the quartz crystals range from 0.05 - 1.5 mm.

Augite crystals are prismatic with sizes ranging from 0.2 - 0.8 mm. These crystals often have torn or ragged edges with abundances ranging from 1 - 2.4%. Orthopyroxene is present as elongate crystals with sizes ranging from 0.15 - 1 mm and abundances of 1.2% - 3%.

Prismatic and elongated crystals of hornblende have abundances ranging from 1.3 - 3.7%. These crystals vary in sizes from 0.12 - 1.3 mm.

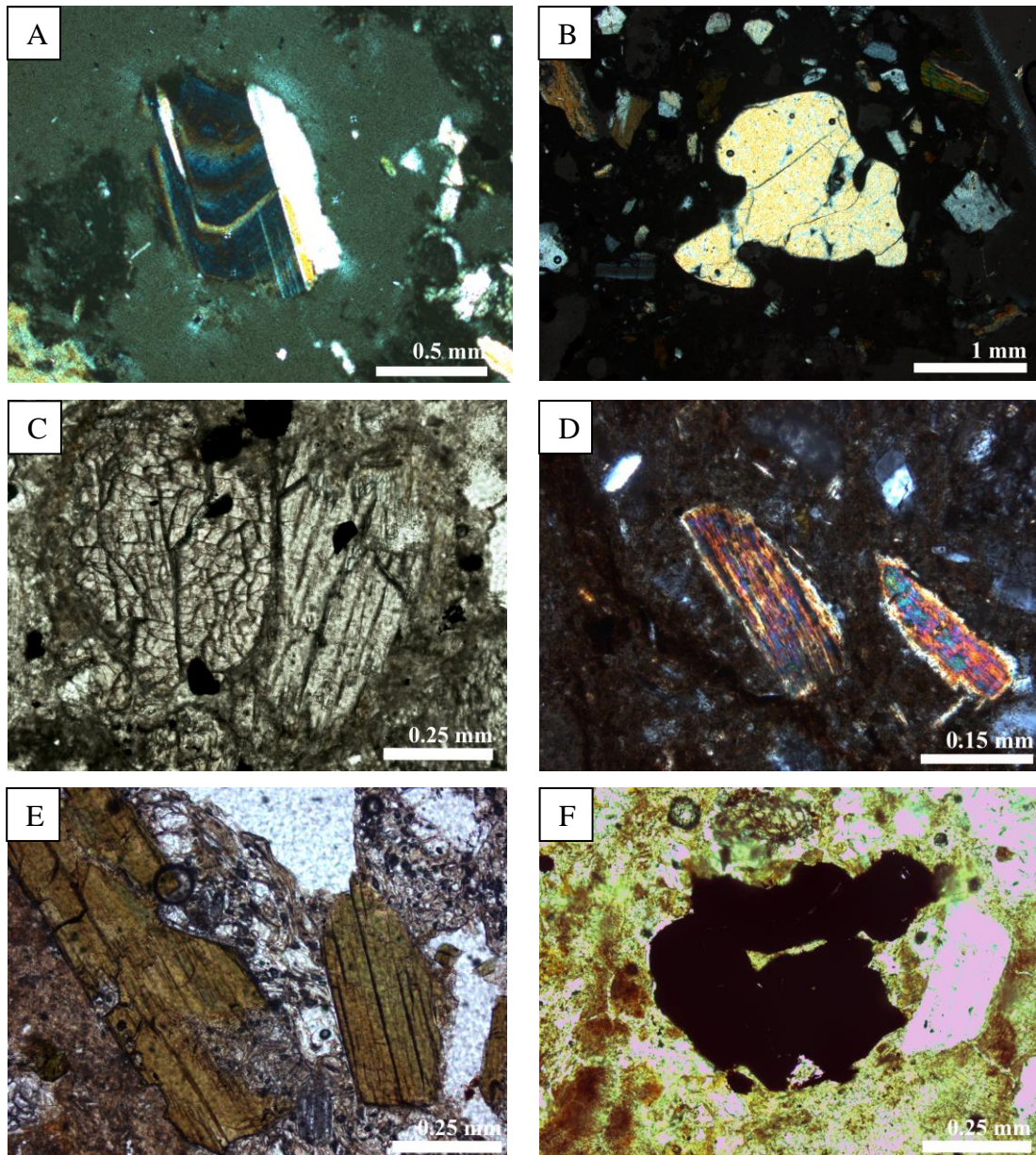


**Figure 3.13 Free crystals in the matrix. All images are under cross polarized light except for images C and F which are plane polarized light. (A) Plagioclase crystal displaying twinning and oscillatory zoning under XP. (B) An embayed quartz crystal under XP. (C) Two augite crystals. (D) Two orthopyroxene crystals. (E) Shows two elongated hornblende crystals with green/brown colouration. (F) Magnetite crystal with a prismatic shape.**

Opaques are low in abundance throughout these deposits with an average abundance of less than 1% (Figure 3.13). The different opaque crystals were identified through SEM EDS analysis; both titanomagnetite and ilmenite are present (Figure 3.14). Titanomagnetite is the most common and is observed as an isometrical anhedral square crystal. Ilmenite is found rarely throughout the Corbett Ignimbrite as hexagonal and elongated crystals.

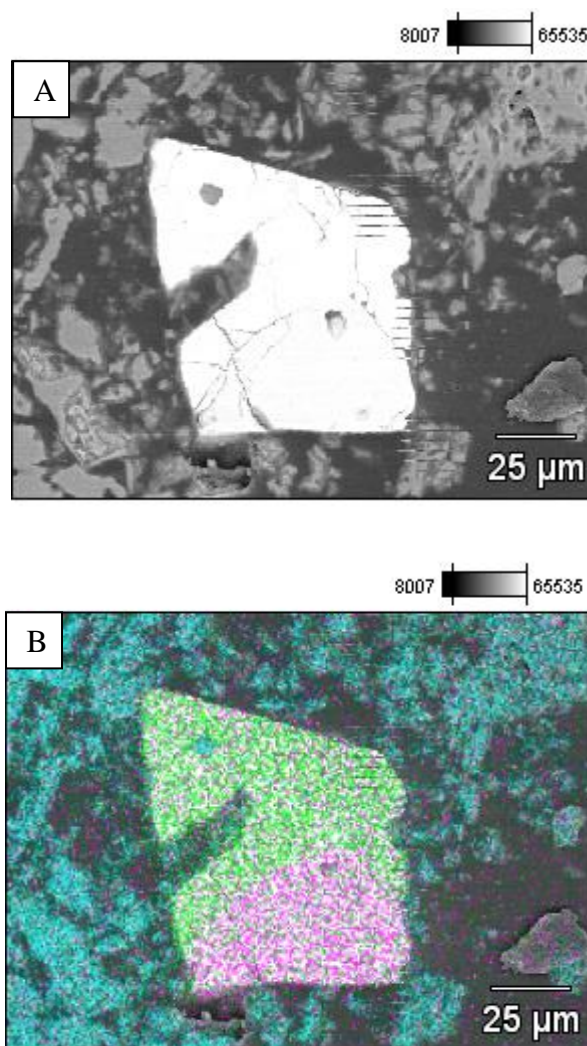


**Figure 3.14 (A) Backscatter image of an opaque crystal found in the Corbett Ignimbrite. (B) The blue points represent Si, green represents Fe and pink represents Ti showing a titanomagnetite and ilmenite crystal joined together.**

### 3.5.3 Juvenile clasts

Pumice displays a characteristic wavy texture (Figure 3.15) and varies with some pumice being slightly devitrified and not uniformly isotropic. Observations under SEM showed the pumice to be finely vesicular with relatively small vesicles that average 100 $\mu$ m in diameter. These vesicles are separated by thin walls (Figure 3.15 B) with glass filaments around vesicles. The vesicles vary with them displaying a heterogeneous texture as well as there being shear zones where vesicles are more stretched out and appear more wavy. Pumice is moderate to highly vesicular with vesicles averaging 60.9% (Table 3.2).

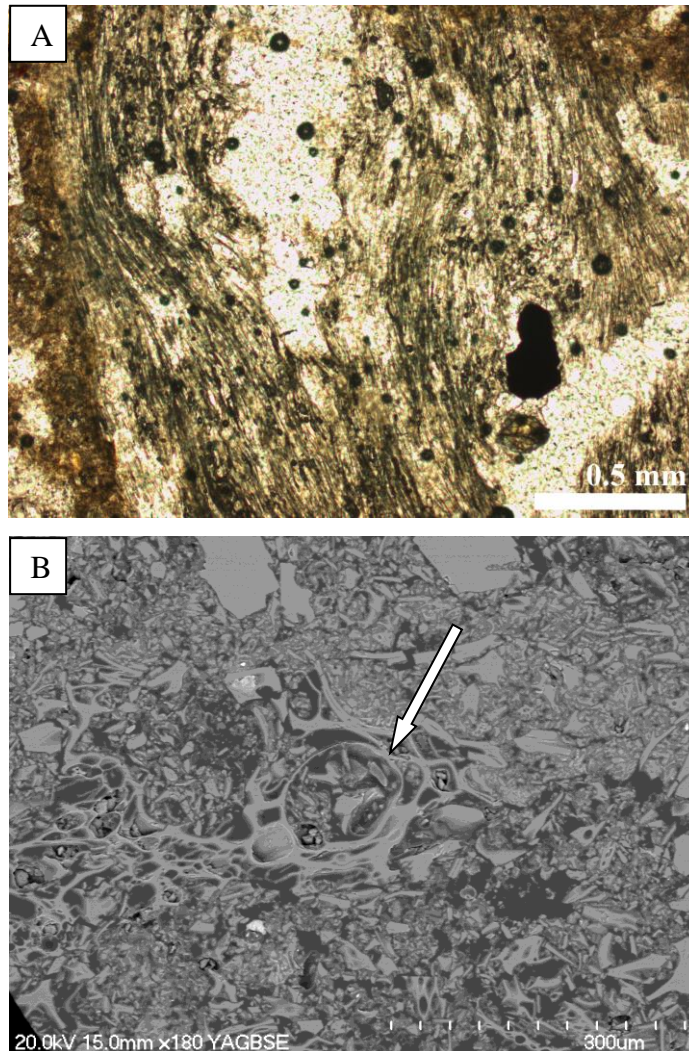


**Figure 3.15 (A) Shows Pumice found within the Corbett Ignimbrite with a wavy texture. (B) Shows a thin section sample under SEM. The arrow is pointing to a bubble with thin glass walls.**

Plagioclase (An<sub>60-43</sub>, Figure 3.16) and quartz phenocrysts dominate the pumice crystal content with an average of 4.3% and 4.2% respectively. Normal, reverse and oscillatory zoning is present in phenocrysts analysed under the electron microprobe. Both normal and reverse geochemical zoning is observed in plagioclase phenocrysts. Reverse zoning was the most dominant type of zoning found in the limited data set of the two samples (Table 3.3). A large portion of quartz phenocrysts show resorption. Ferromagnesian minerals of augite, Wo<sub>45-36</sub>, En<sub>43-40</sub>, Fs<sub>21-14</sub> (Figure 3.17), hornblende and orthopyroxene (En<sub>69-51</sub>) are also present within the pumice. Orthopyroxene has an average abundance of 1.3 % in the pumice and has the highest abundance of the ferromagnesium minerals. Within the pumice there are opaques of titanomagnetite and ilmenite with an overall average abundance of 1.2%. Microprobe analysis of two thin sections confirmed only the presence of titanomagnetite with compositions of TiO<sub>2</sub> 10-11 wt. % and FeO 70-78%, no ilmenite crystals were probed.

**Table 3.2 Percentage proportions of the components within pumice obtained from point counting thin sections of pumice clasts from the Corbett Ignimbrite\***

Sample	1.1.1	1.3.1	1.4.1	1.5.2	6.1.2	8.1.2	9.3.2	Average
Vesicles	68.0	73.5	52.2	57.7	62.8	59.7	52.2	60.9
Glass	20.7	17.2	31.0	32.0	27.3	22.7	31.0	25.9
Plagioclase	4.5	5.2	4.5	4.0	3.5	3.7	4.5	4.3
Quartz	3.2	2.0	5.2	2.5	3.3	7.7	5.2	4.2
Orthopyroxene	1.2	0.2	2.7	1.0	0.2	1.0	2.7	1.3
Augite	1.0	-	1.7	0.7	1.0	0.7	1.7	1.0
Hornblende	0.5	-	2.0	0.2	0.2	3.7	2.0	1.2
Opaques	0.7	1.7	0.5	1.7	1.7	0.5	0.5	1.1
Total	100%	100%	100%	100%	100%	100%	100%	100%
Margin of error**	1.8%	0.5%	1.7%	4.0%	1.5%	1.0%	1.7%	2.2%
Total crystals***	26.8%	33.0%	30.1%	24.3%	9.9%	43.8%	35.1%	29%

\*All samples were analysed to 400 counts with a stage interval of 0.3 mm

\*\* Margin of error determined by recording number of uncertain counts

\*\*\* Total crystals calculated without vesicles included to represent magma composition

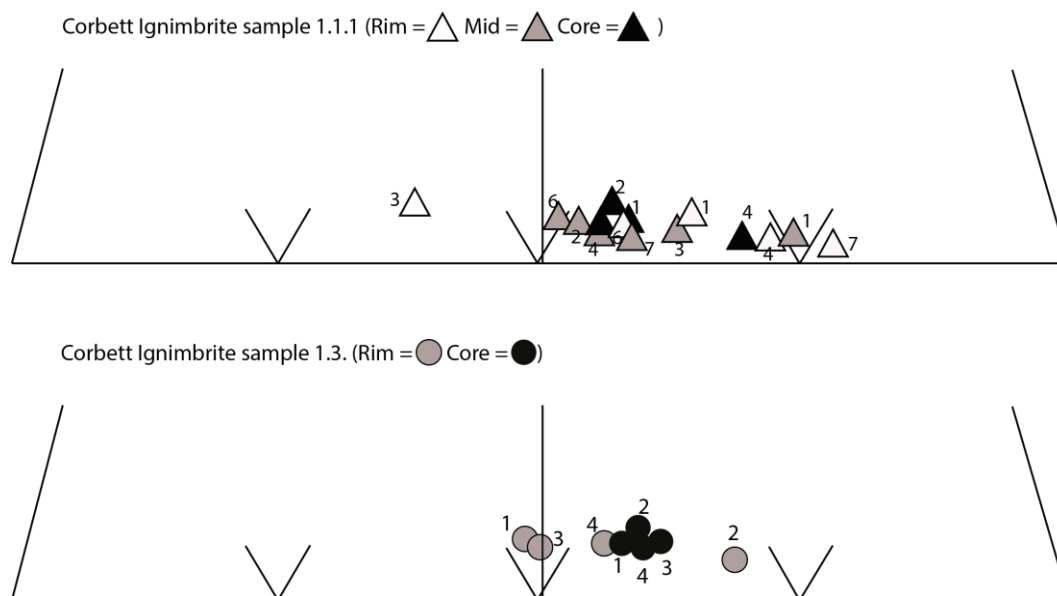
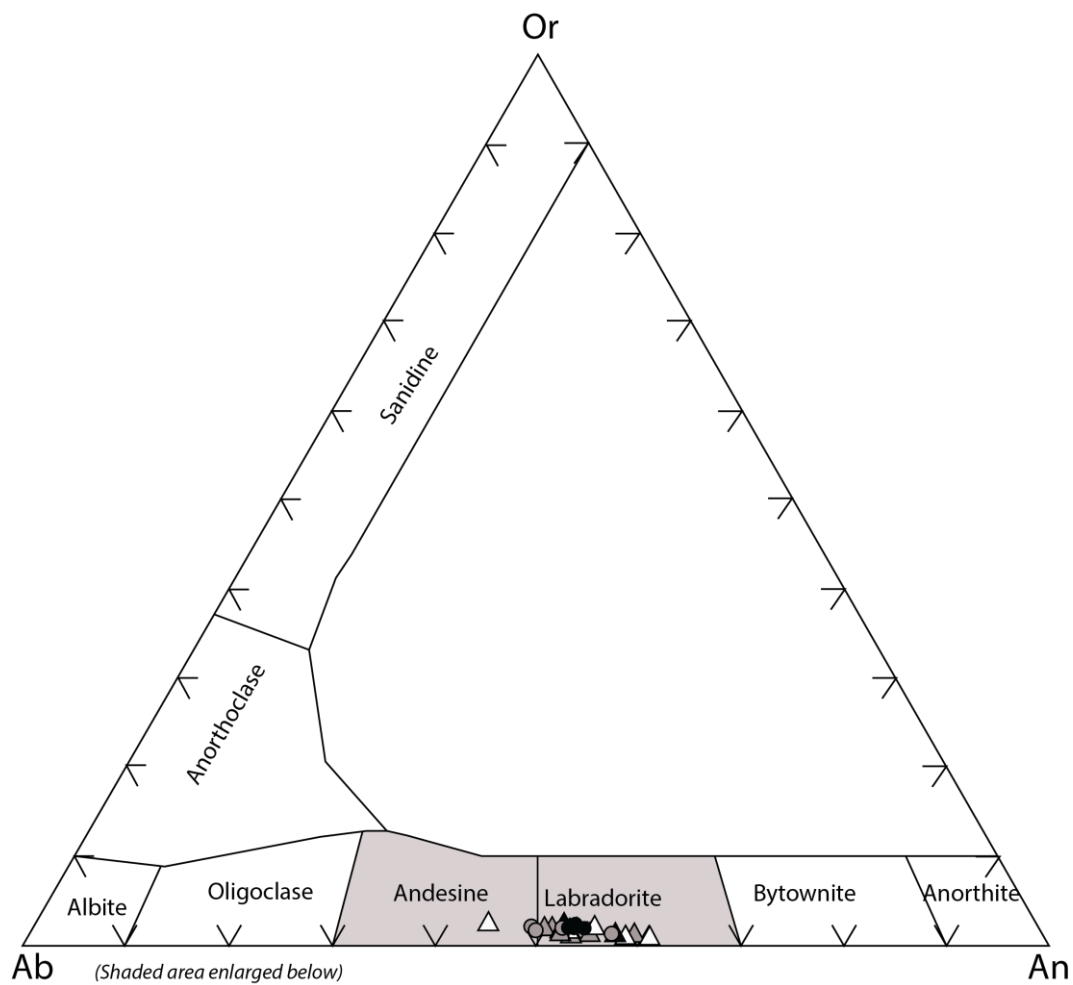


**Figure 3.16 Albite - anorthite- orthoclase ternary diagram for plagioclase crystals in pumice in the Corbett Ignimbrite. Classification according to Deer et al. (1992).**

**Table 3.3 Different zoning observed in samples analysed under the electron microprobe based on CaO and Na<sub>2</sub>O values.**

<b>Sample</b>	<b>CaO</b>	<b>Na<sub>2</sub>O</b>	<b>Zoning</b>
1.1.1 – 1 – core	10.202	4.966	Oscillatory zoning
1.1.1 – 1 - mid	11.561	4.287	
1.1.1 – 1 – rim	10.689	4.749	
1.1.1 – 2 – mid	9.946	5.195	Reverse zoning
1.1.1 – 2 – core	10.321	5.059	
1.1.1 – 3 – mid	10.196	4.617	Normal zoning
1.1.1 – 3 – rim	8.536	5.759	
1.1.1 – 4 – core	11.271	4.539	Oscillatory zoning
1.1.1 – 4 – mid	10.132	5.081	
1.1.1 – 4 – rim	11.533	4.471	
1.1.1 – 6 – mid	9.843	5.278	Reverse zoning
1.1.1 – 6 – rim	10.203	4.963	
1.1.1 – 7 – mid	10.345	4.976	Reverse zoning
1.1.1 – 7 – rim	11.977	4.207	
1.3.2 – 1 – mid	9.623	5.381	Reverse zoning
1.3.2 - 1 – rim	10.426	5.037	
1.3.2 – 2 – mid	11.201	4.652	Normal zoning
1.3.2 – 2 – rim	10.544	4.952	
1.3.2 – 3 – mid	9.727	5.462	Reverse zoning
1.3.2 – 3 – rim	10.596	4.827	
1.3.2 – 4 – mid	10.369	5.114	Reverse zoning
1.3.2 – 4 – rim	10.527	4.948	

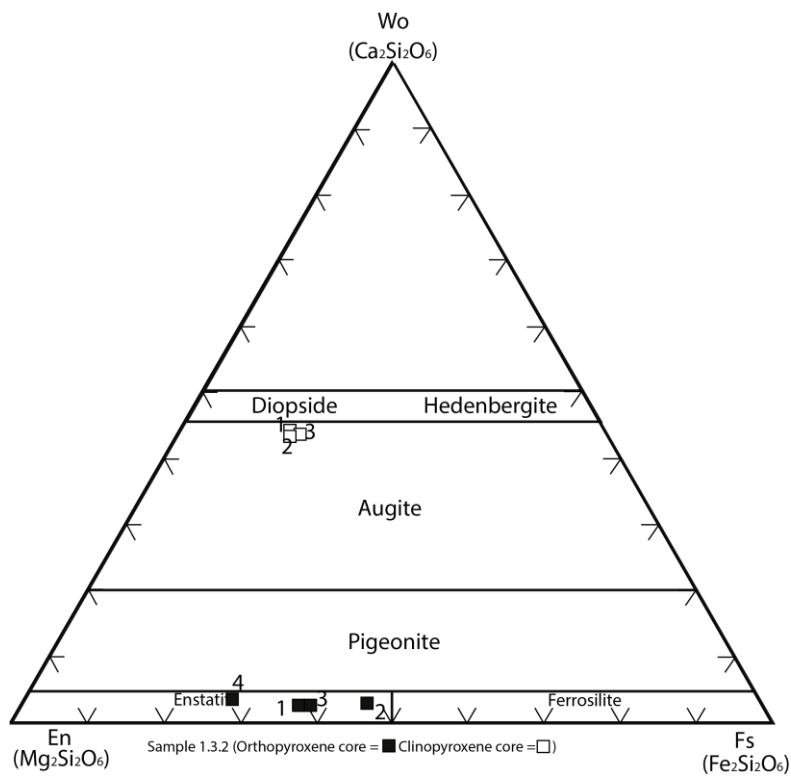
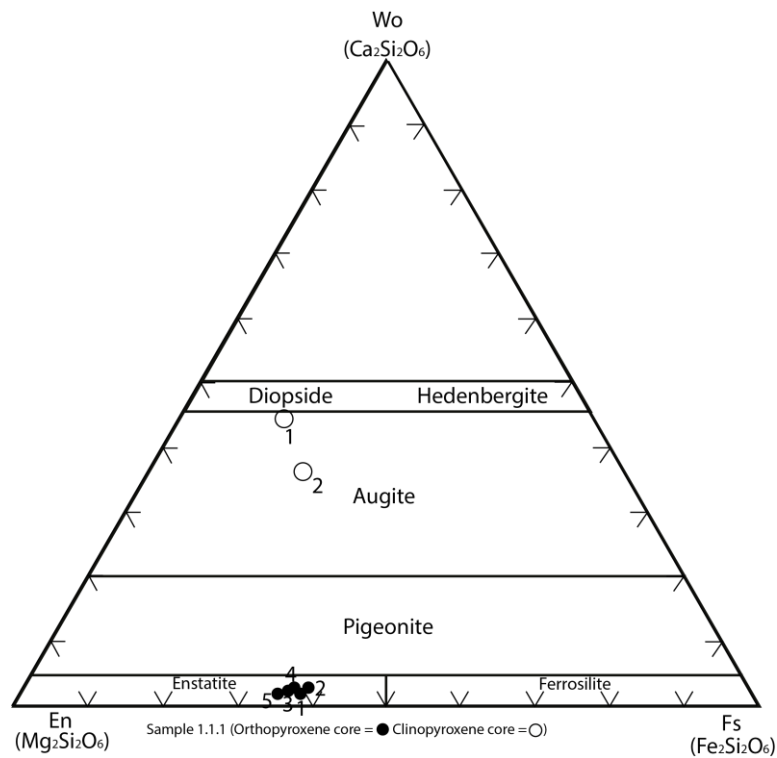


**Figure 3.17 Wollastonite - enstatite - ferrosilite ternary diagram for pyroxene crystals found in Corbett Ignimbrite pumice. Classification from Deer et al., 1992.**

At site 11 (Figure 3.1) the Corbett Ignimbrite was found to have elongate lenses of fiamme. Under thin section the fiamme has a dark brown glassy groundmass (Figure 3.18) with phenocrysts of quartz, plagioclase, augite, orthopyroxene, hornblende and opaques. The fiamme has ragged, wispy ends that wrap around phenocrysts.

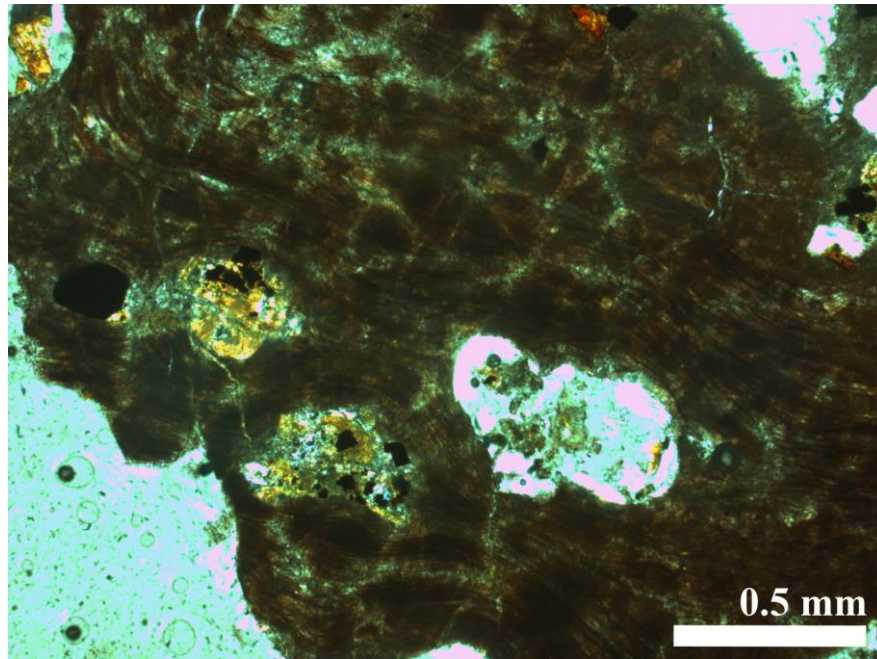


**Figure 3.18 Fiamme in the Corbett Ignimbrite at site 11 with a glassy groundmass**

#### **3.5.4 Lithics**

There are four lithic types that occur throughout the thin sections analysed for the Corbett Ignimbrite; rhyolite, andesite, dacite and greywacke (Figure 3.19). The rhyolite lithics are crystal-rich with a high abundance of plagioclase, orthopyroxene and augite phenocrysts, and minor opaques held within a slightly crystalline groundmass. Vesicular rhyolite lithics also occur with coalesced vesicles and phenocrysts of plagioclase, hornblende and quartz. Andesite lithics are the most common lithic type occurring throughout the Corbett Ignimbrite. These andesite lithics are two pyroxene andesite with augite and orthopyroxene phenocrysts showing alignment with lesser plagioclase. Phenocrysts are held in a glassy, hyalopilitic groundmass. Dacite lithics are less common and have a high crystal abundance with quartz being a significant phenocryst found. These lithics also contain a lower abundance of plagioclase. Rare greywacke lithics contain quartz and plagioclase phenocrysts held within a granular groundmass.

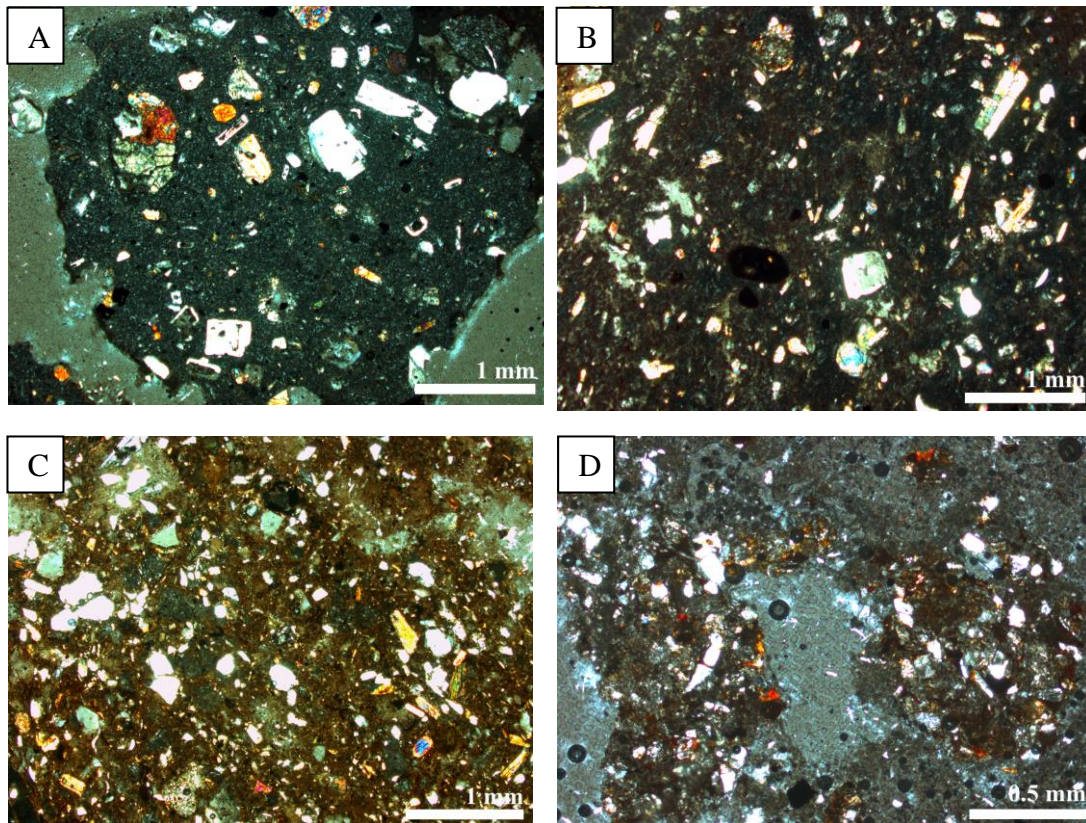


**Figure 3.19** Different lithics found within the Corbett Ignimbrite. (A) Crystal rich rhyolite lithic with a crystalline groundmass. (B) Two pyroxene andesite lithic with aligned crystals and a glassy, hyalopilitic groundmass. (C) Dacite lithic which is rich in quartz phenocrysts. (D) Greywacke lithic with a granular texture.

### 3.5.5 Interstitial matrix

Under transmitted light microscopy glass shards could not be resolved. However, they were observable by SEM analysis. These glass shards are poorly sorted with 10 to 20  $\mu\text{m}$  shards as well as sand-sized showing this ignimbrite contains a large volume percent of fine broken glass shards as a vitriclastic matrix. There is no alignment orientation with the glass shards being held together by finer-grained submicron-sized material. Cuspate, lunate, y-shaped and platy shards are found in the Corbett Ignimbrites matrix (Figure 3.20).

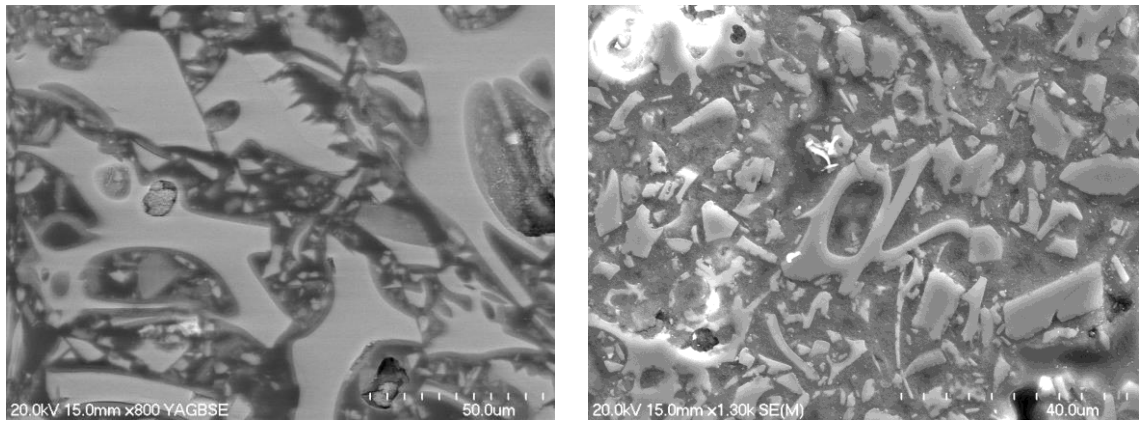


**Figure 3.20 glass shards at different magnifications in the Corbett Ignimbrite showing the different shapes observed**

### **3.6 Pumice and Glass Shard Geochemistry**

#### **3.6.1 Introduction**

Eight pumice and two fiamme samples from the Corbett Ignimbrite were analysed by X-ray fluorescence spectrometry. Five of the pumice samples were sourced from the type section (locality 1, Figure 3.1) and the remaining three were derived from localities 7, 8 and 9. The two fiamme samples were from locality 11. Pumice and fiamme were analysed to avoid problems of contamination by non-juvenile components that occur with whole rock samples. Analysing pumice allows for the geochemical data to be used as an indicator for magmatic processes. All pumice samples show some degree of secondary hydration (1-11.81 wt. % LOI), but pumices had a glassy and fresh appearance. Major and trace element data are included in Appendix VI. Glass shard geochemical data was obtained by electron microprobe analysis of 24 shards across two samples with the raw data in Appendix V.

#### **3.6.2 Rock classification**

The classification of a rock can be determined through the subdivision of subalkalic rocks by observing the total Na<sub>2</sub>O and K<sub>2</sub>O wt. % value against SiO<sub>2</sub> wt. % (Rollinson, 1993). Geochemical results from XRF analysis showed that the Corbett Ignimbrite ranges from rhyolitic to andesitic in composition (Figure 3.21) with the majority of pumice samples being dacitic. The two fiamme samples analysed were andesitic and dacitic in composition and the eight pumice samples

ranged from andesitic (less than that of the fiamme sample) to rhyolitic in composition.

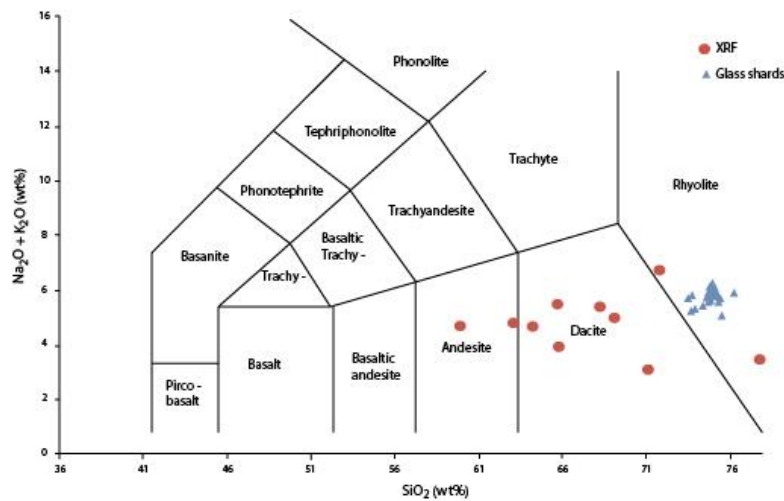


**Figure 3.21** Plot of  $\text{Na}_2\text{O} + \text{K}_2\text{O}$  vs  $\text{SiO}_2$  wt. % of Corbett Ignimbrite bulk pumice and glass shard analysis (based on Deer *et al.*, 1992).

A  $\text{K}_2\text{O}$  vs  $\text{SiO}_2$  diagram was also produced (Figure 3.22).  $\text{SiO}_2$  values (normalised to 100%, volatile free) range in the Corbett Ignimbrite from 56-71 wt. % (with the type section showing variations between 58-70 wt. %) showing a change in composition from rhyolitic to andesitic. At the type section the samples range between dacitic and rhyolitic throughout the thickness of the outcrop with dacite being the dominant composition (Figure 3.23).

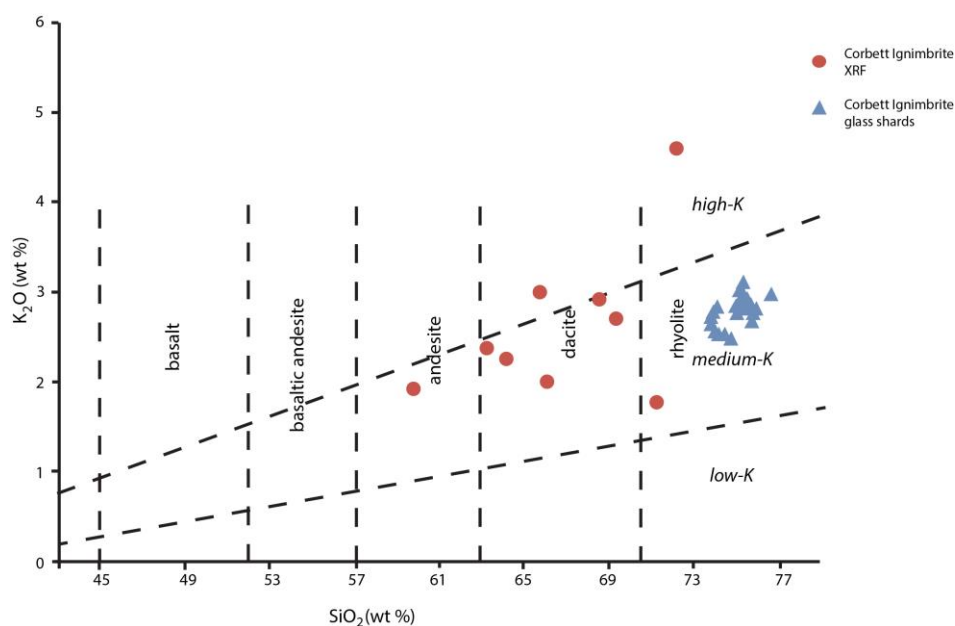
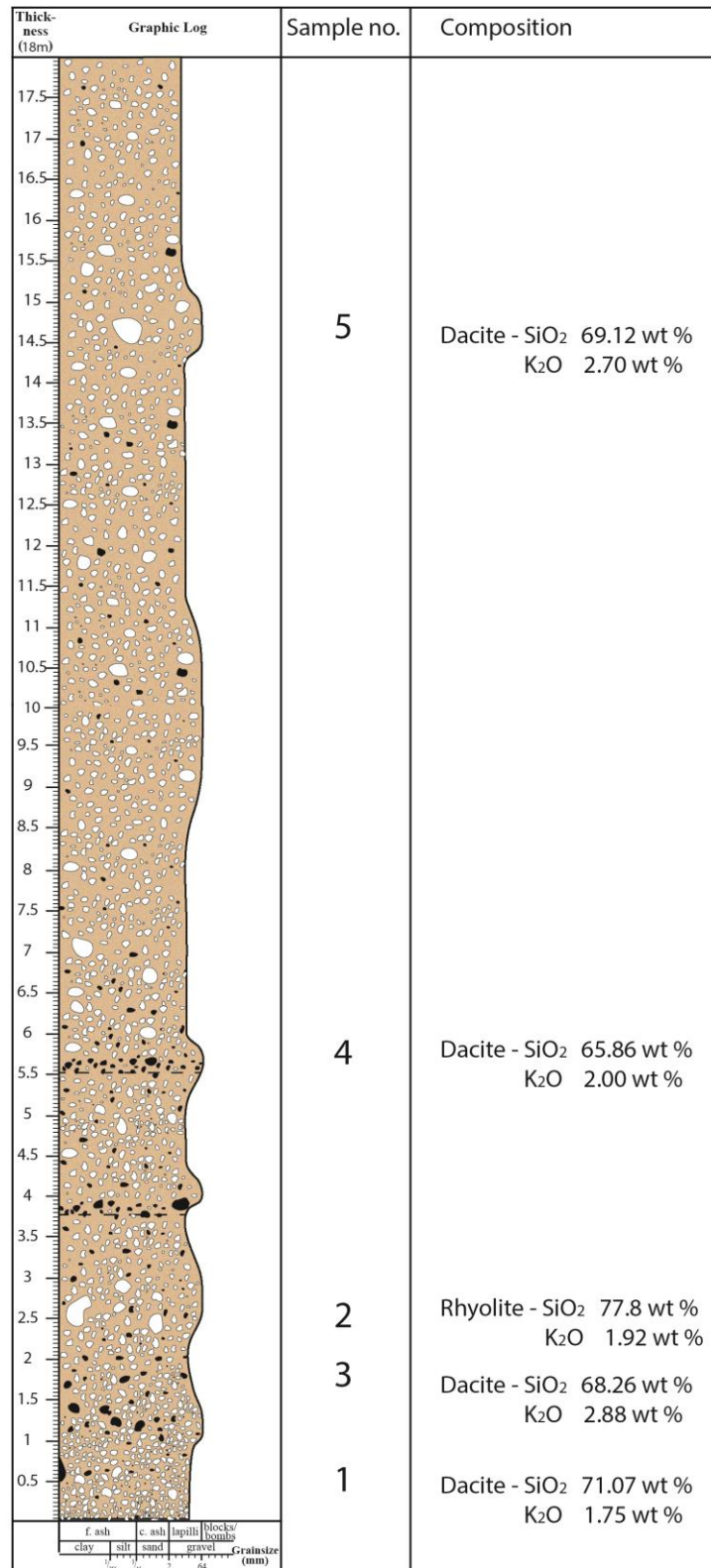


**Figure 3.22** Plot of  $\text{K}_2\text{O}$  vs.  $\text{SiO}_2$  wt. % of Corbett Ignimbrite bulk pumice and glass shard analysis (based on Le Maitre *et al.*, 2002).



### 3.6.3 Major element chemistry

Harker variation plots are used to plot the weight percentages of major and trace elements against  $\text{SiO}_2$  to determine relationships between individual rocks. The major elements from XRF analysis of bulk pumice are plotted against glass shard composition (determined by electron microprobe analysis) to assess any relationships (Figure 3.24). For each major element chosen the compositions of pumice are more variable than the compositions of glass, which show little variation. Glass shards are expected to show less variation in  $\text{SiO}_2$  content due to their high  $\text{SiO}_2$  composition. Pumice samples are expected to show more variation as their compositions include a range of phenocrysts.

In each of the plots in Figure 3.24 there is a bulk pumice outlier which is more silica-rich than the glass compositions. As XRD analysis determined the presence of cristobalite in this sample (as discussed in section 3.5.2) it is thought that many of these samples have had vapour phase alteration. Vapour-phase alteration causes silica to be added due to the crystallisation of quartz inside vesicles causing an increase in silica content.

Harker plots of whole pumice major element compositions  $\text{Al}_2\text{O}_3$ ,  $\text{CaO}$ ,  $\text{Fe}_2\text{O}$ ,  $\text{NaO}$ , and  $\text{MgO}$  with respect to  $\text{SiO}_2$  wt. % showed negative trends (Figure 3.24). These negative trends are traditionally interpreted as fractional crystallisation with fractionation of plagioclase ( $\text{Al}_2\text{O}_3$ ,  $\text{CaO}$ ), iron oxides, clinopyroxene, orthopyroxene and hornblende ( $\text{Fe}_2\text{O}$ ).  $\text{K}_2\text{O}$  shows a positive correlation with  $\text{SiO}_2$  indicating it is an incompatible element and is not involved in crystal fractionation. However recent work by Cooper (2014) shows that compositional variations can be attributed to varying crystal content. Point count component analysis on different pumice samples in the Corbett Ignimbrite shows variation in crystal content (Table 3.2) which may control the trends seen in major elements. There is a much larger range of compositions in pumice samples compared to glass (Figure 3.24) which indicates the compositions of pumice are controlled by their crystal rich nature and are a reflection of the crystal assemblage and crystallinity of each pumice sample (Cooper, 2014). Samples rich in  $\text{SiO}_2$  correspond to a higher abundance of glass, and therefore less crystals, indicated by the negative trends of most major elements against  $\text{SiO}_2$ .  $\text{Fe}_2\text{O}$  shows high

values in Figure 3.24 due to mafics and opaques in the pumice.  $K_2O$  shows a stable relationship with outliers being due to vapour phase alteration.

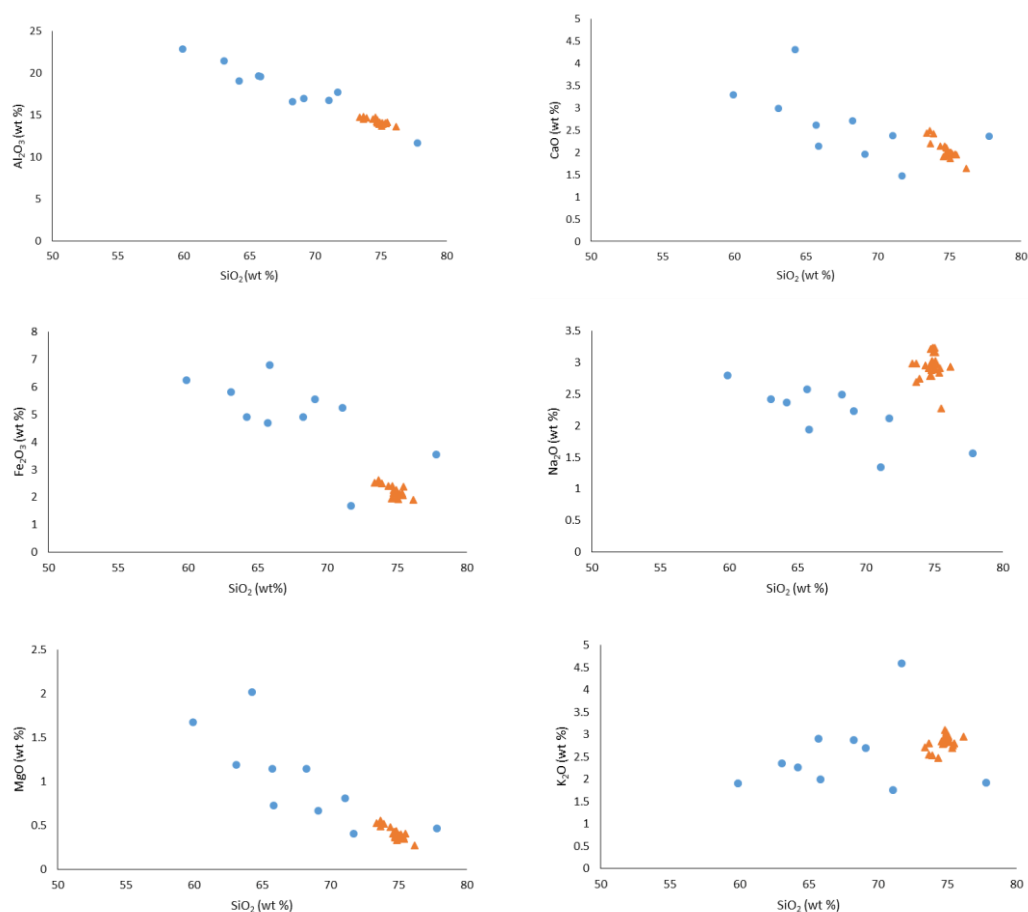


**Figure 3.24 Harker diagrams of selected major elements found in pumice samples (blue circles) and glass shards (red triangles) vs  $SiO_2$  wt. %.**

### 3.6.4 Trace element chemistry

Compositions of trace elements were determined through XRF for 10 samples (the same as those analysed for major elements). 29 trace elements (in ppm) were analysed (Appendix VI). Trace element Harker plots can be used to help determine the geochemical processes that may have occurred within the chamber. Trace elements were plotted against  $\text{SiO}_2$  to determine any trends as well as incompatible elements (Figure 3.25)

Rb vs  $\text{SiO}_2$  shows a similar trend to  $\text{K}_2\text{O}$  vs  $\text{SiO}_2$  as Rb substitutes for  $\text{K}_2\text{O}$  in silicates, especially feldspar. Both show a varied trend with outliers due to vapour phase alteration within the pumice. Zr and Sr are controlled by plagioclase content and show a reasonably steady composition as  $\text{SiO}_2$  increases (Figure 3.25). Ba vs  $\text{SiO}_2$  shows a steady trend with one outlier at 1136 ppm being vapour phase altered. Rb vs Sr show a negative correlation with Rb decreasing as Sr increases, this trend is also present in Ba vs Zr. Positive correlation is present with Ba vs Rb and Rb vs Zr, however the trend observed in Rb vs Zr is weak with more scatter.

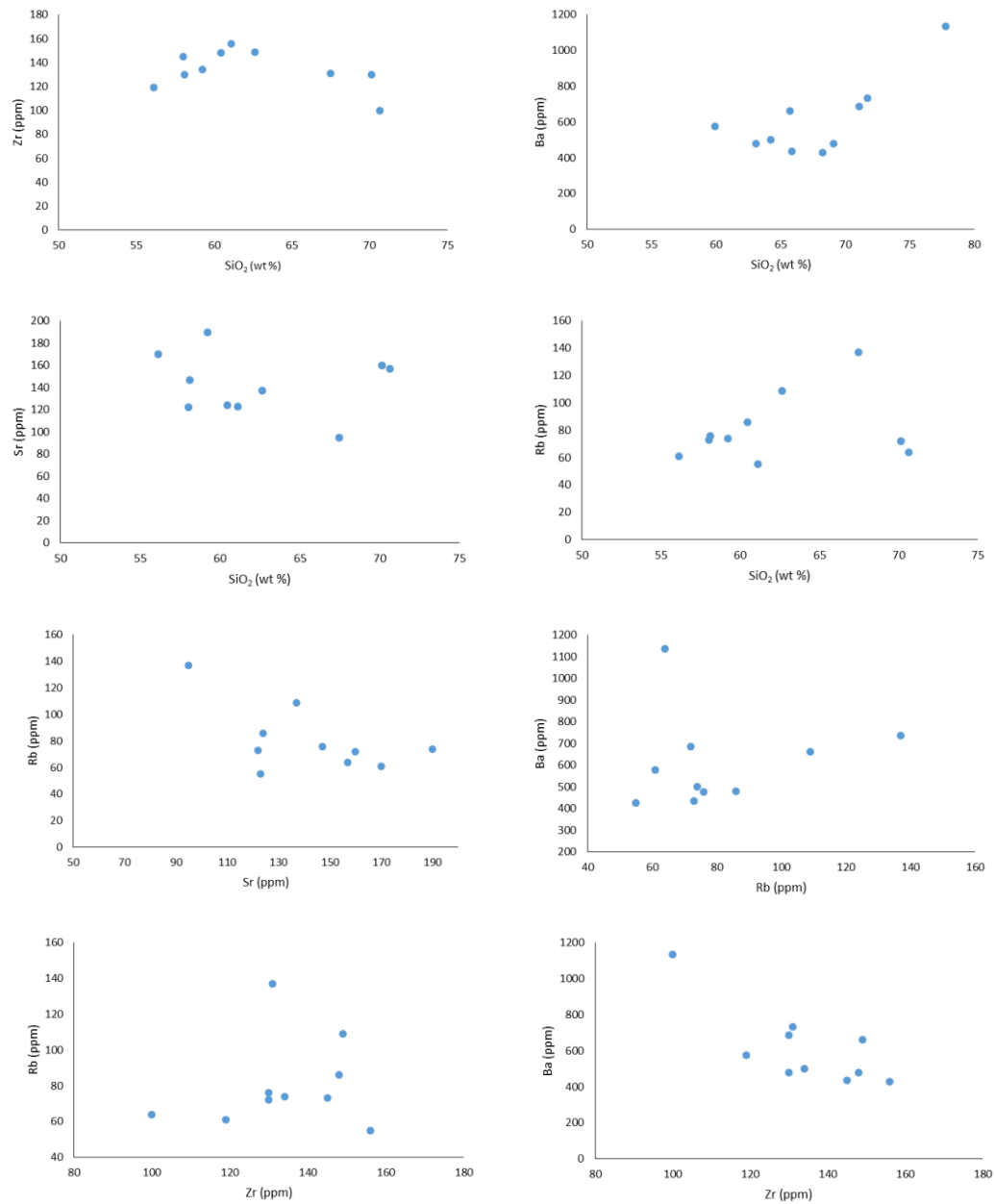


**Figure 3.25 Harker variation plots of trace element geochemistry from XRF results of whole pumice clasts.**

### 3.6.5 Glass shard chemistry

Glass shard compositions for two Corbett Ignimbrite samples (1.1.1p and 1.3.2p) were analysed using the electron microprobe at Victoria University. The glass shards in these samples were medium in potassium (2.48-3.10 wt. %) and high in silica (73-76% wt. %) and were rhyolitic in composition as shown in Figure 3.22. This is consistent with previous interpretations of the Corbett Ignimbrite as a rhyolitic ignimbrite however it contrasts with the varying compositions obtained through major element analysis of pumice samples.

Comparisons of glass shard FeO, CaO and K<sub>2</sub>O compositions show that all glass shards have a similar composition (Figure 3.26). There is little variation observed in these samples.

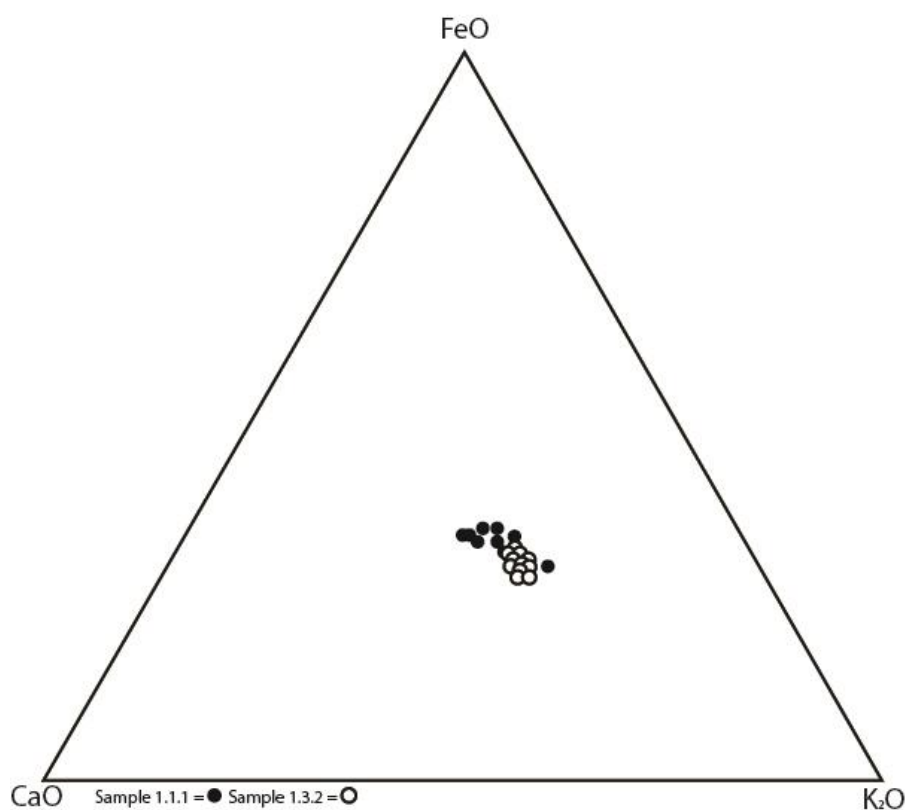


**Figure 3.26 Ternary plot showing the relationship between FeO, CaO and K<sub>2</sub>O in glass shards found within the Corbett Ignimbrite**

## **3.7 Dating**

### **3.7.1 Introduction**

The Corbett Ignimbrite was inferred by Brathwaite and Christie (1996) to stratigraphically underlie the Owharoa Ignimbrite based on a 56 m thick pumice lapilli tuff, proposed to be the Corbett Ignimbrite, which is overlain by Owharoa Ignimbrite in drill core. The Owharoa and Waikino ignimbrites have fission track ages determined by Kohn (1973) of  $2.89 \pm 0.38$  and  $1.53 \pm 0.23$  respectively. Early fission track ages are not consistent with modern dating techniques. Vincent (2012) redated the Owharoa Ignimbrite using U-Pb methods, providing a more reliable age of  $3.76 \pm 0.05$ . The Corbett Ignimbrite has not been previously dated so a U-Pb age is determined. The application of U-Pb dating of zircons provides a crystallisation age and places a maximum age limit on the eruption concerned. The full list of zircon ages analysed in the Corbett Ignimbrite is included in Appendix VIII.

### **3.7.2 Zircon age results**

47 spots on zircons were initially dated, however 21 spots on zircons were considerably older than the general cluster and were excluded from the age calculation. The remaining 26 spots were used to determine the age. The Corbett Ignimbrite showed a range of zircon ages with an average around 6 Ma (Figure 3.27). Ablation of zircons through LA-ICP-MS provided an age of  $6.09 \pm 0.34$  Ma.

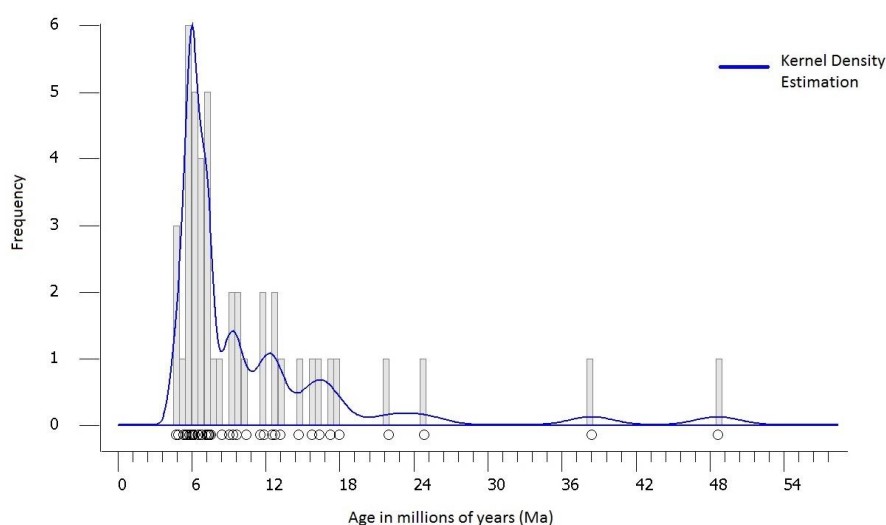


**Figure 3.27 The distribution of ages of Corbett Ignimbrite zircon crystals that were ablated by LA-ICP-MS excluding the oldest zircons analysed.**

A large proportion of zircons pre-date the age determined for crystallisation. The range of these ages are shown in Table VIII.1 in Appendix VIII. The full age range of zircons analysed is 4.7 to 173 Ma (Figure 3.28). Zircons that were not included in the age determination of the Corbett Ignimbrite were dominantly Miocene (9 – 21.9 Ma), with lesser Oligocene (24.8 Ma), Eocene (38.4 – 48.6 Ma), Early Cretaceous (119 Ma) and Mid Jurassic (173 Ma). Zircons that were less than 10 Ma may be antecrysts which are crystals derived from the same magma chamber but were crystallised prior to the most recent eruption, or alternatively in a previous eruption cycle (Vincent, 2012). The oldest of these zircons (Mid Jurassic) are derived from the underlying Jurassic basement. The potential origin of the zircons older than the Corbett Ignimbrite but younger than the basement are assessed in Chapter Six.

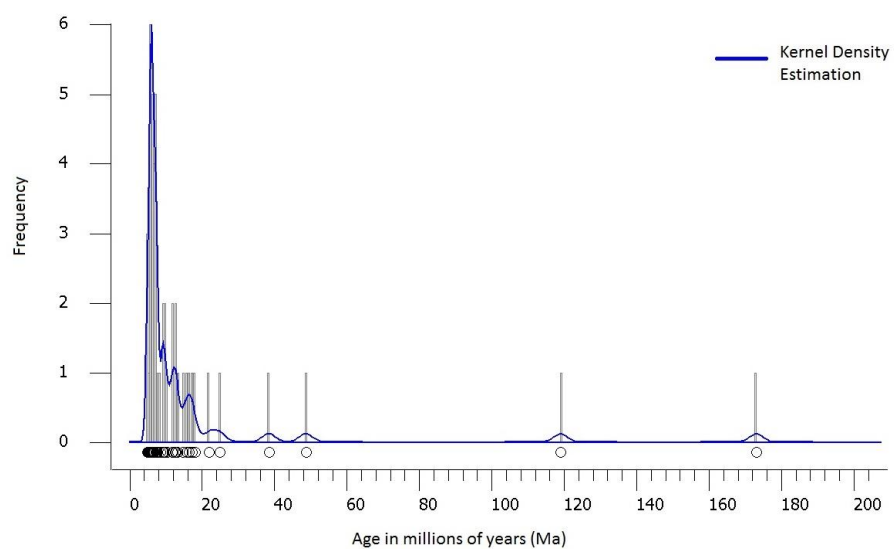


**Figure 3.28 The full distribution of ages of Corbett Ignimbrite zircon crystals that were ablated by LA-CIP-MS**

## **3.8 Petrographic, mineralogical and geochemical characteristics of the Bowentown Rhyolite**

### **3.8.1 Introduction**

In the field 2 samples of the Bowentown Rhyolite was taken. Brathwaite and Christie (1996) described the Bowentown Rhyolite as a lava dome complex of perilitic and spherulitic plagioclase-orthopyroxene rhyolite which was found to have minor flanking breccias of glassy rhyolite. The samples for this study were collected to gain an age to assess the genetic relationship, if any, with the Corbett Ignimbrite as suggested by Brathwaite and Christie (1996). Previous ages have been obtained by K-Ar ( $2.89 \pm 0.07$  Ma, Brathwaite & Christie, 1996) and fission track ( $2.29 \pm 0.21$  Ma, Rutherford, 1978). These ages are thought to be accurate, however to be consistent with the dating of the Corbett Ignimbrite in this study U-Pb zircon ages is determined.

### **3.8.2 Petrography and mineralogy**

2 thin sections were created for optical microscope analysis, 1 polished thin sections for electron microprobe and 1 crushed powder groundmass sample for XRD analysis (graphs for XRD analysis are presented in Appendix IV). These methods were used to enable comparisons to the petrography and mineralogy of the Corbett Ignimbrite.

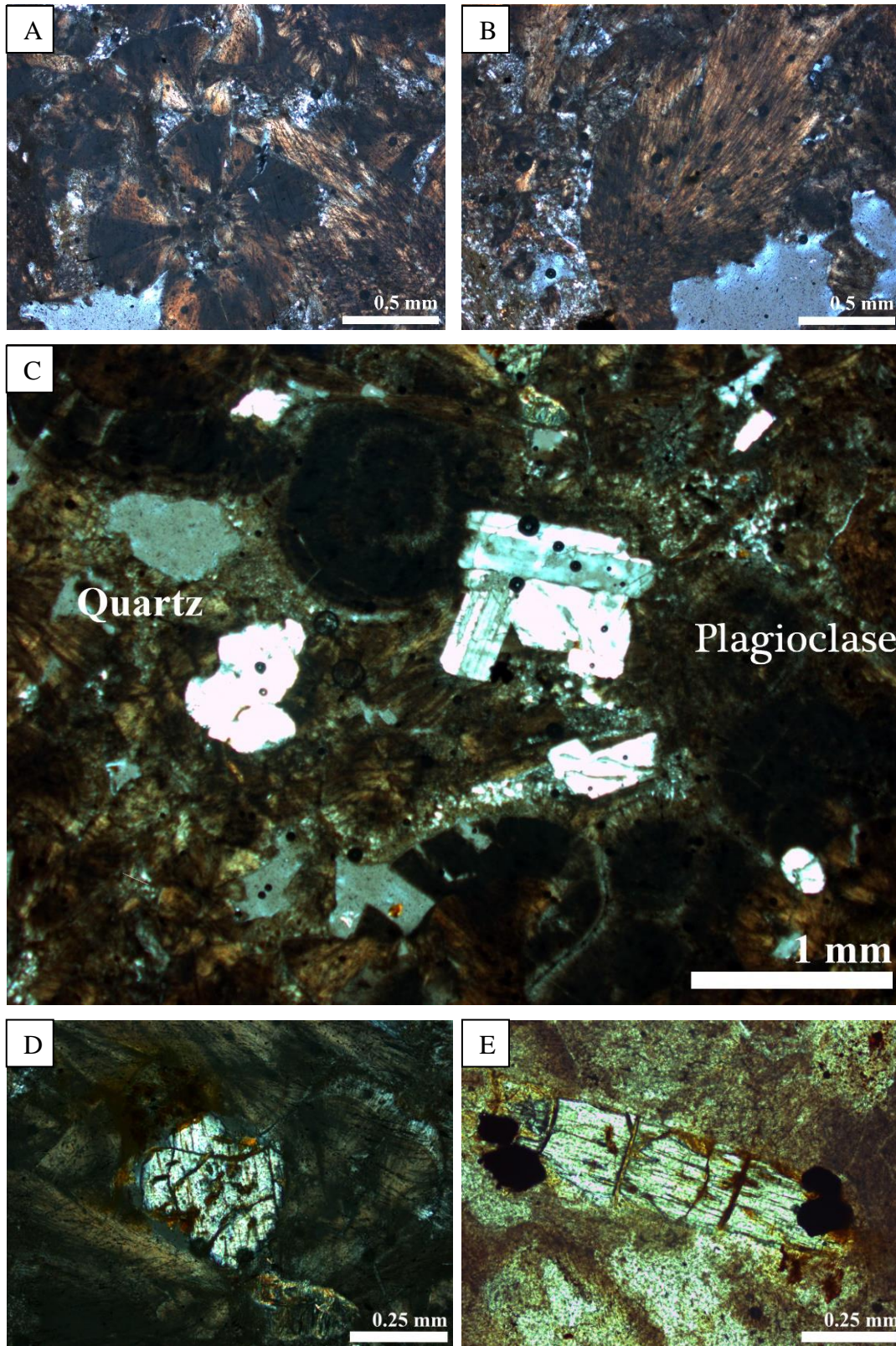
Analysis of these thin sections showed the Bowentown rhyolite as a spherulitic rhyolite with quartz and plagioclase as well as rare orthopyroxene, biotite, and opaques. Microprobe analysis of one thin section confirmed the presence of titanomagnetite and ilmenite. The titanomagnetite had compositions of  $\text{TiO}_2$  10 wt. % and FeO 78-79 wt. % and ilmenite with compositions of  $\text{TiO}_2$  46-47 wt. % and FeO 46-47 wt. %. This rhyolite has a low mineral abundance with the groundmass averaging 94% (Table 3.4). XRD analysis of one sample shows the Bowentown Rhyolite groundmass contains cristobalite.

**Table 3.4 Results obtained from point counting 2 thin sections of the Bowentown rhyolite**

<b>Sample</b>	<b>10.1.1</b>	<b>10.1.2</b>	<b>Average</b>
Groundmass	94.1	93.9	94
Quartz	2	1.6	1.8
Plagioclase	2.9	3.4	3.15
Orthopyroxene	0.1	0.63	0.37
Biotite	0.25	0.38	0.32
Opaques	0.5	0.5	0.5
Total	100%	100%	100%
Margin of error	0.38%	0.5%	0.44%

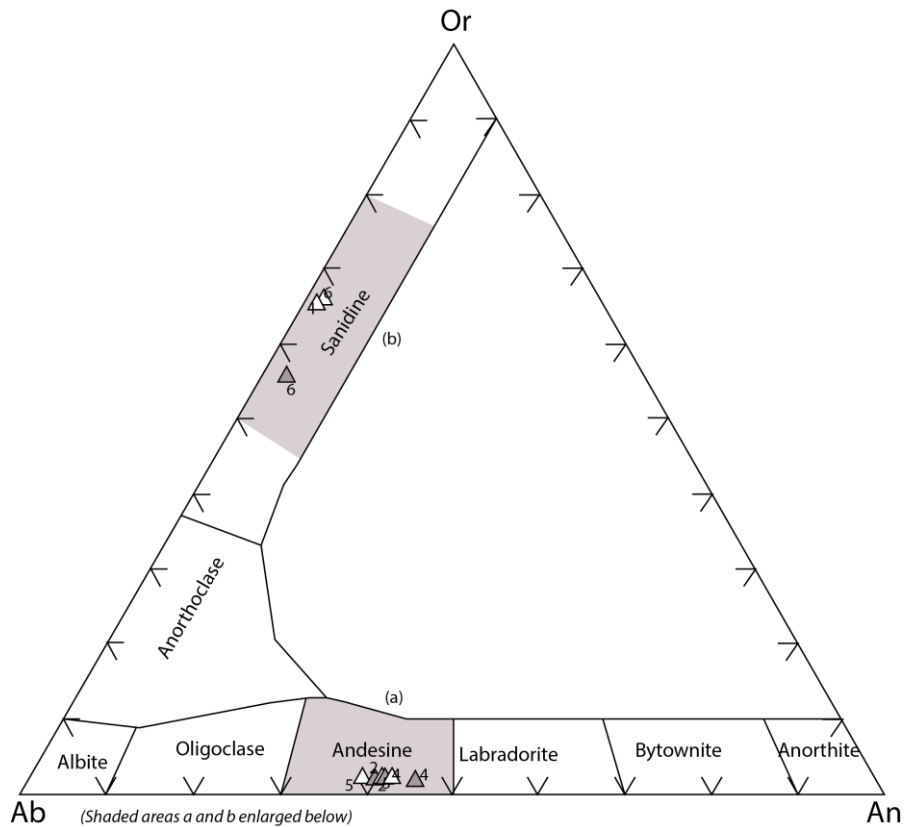
\*All samples were analysed to 800 counts with a stage interval of 0.3 mm



The groundmass of this lava deposit consists of glassy spherulites which vary from spherical to fan shaped (Figure 3.29). These spherulites are comprised of radiating fibres. Spherulites do not infill the entire groundmass as the gaps between spherulites are a devitrified microcrystalline groundmass. These spherulites range from 0.3 - 1.2mm in size with an average of 0.5 mm.

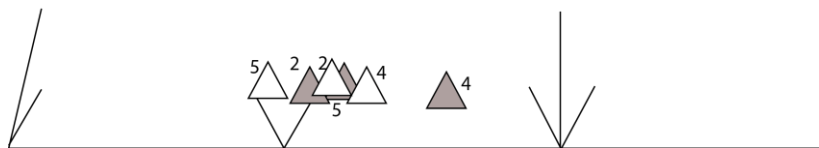


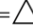
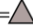
**Figure 3.29** (A) Shows radiating structure of spherulites with crystalline groundmass infilling gaps. (B) Shows a fan shaped spherulite. (C) Shows quartz and plagioclase phenocrysts. (D) Shows a prismatic augite crystal. (E) Shows an elongated orthopyroxene crystal.

Plagioclase and quartz are the two most common minerals found within the Bowentown Rhyolite with an average of 3.15% and 1.8% respectively (Figure 3.29). Plagioclase (An<sub>45-2</sub>, Figure 3.30) often appears as prismatic phenocrysts which show twinning. Quartz commonly appears with embayments.



Bowentown Rhyolite sample 10.1.2 (a) (Rim =  Mid = )



Bowentown Rhyolite sample 10.1.2 (b) (Rim =  Mid = )

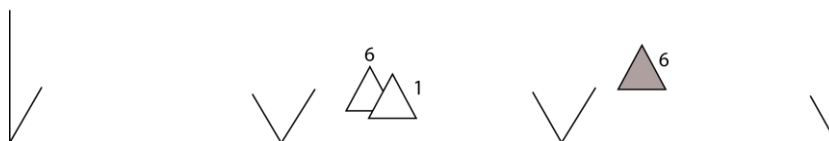


**Figure 3.30 Albite - anorthite- orthoclase ternary diagram for plagioclase in sample 10.1.2 in the Bowentown Rhyolite. Classification according to Deer et al., (1992)**

The Bowentown Rhyolite contains orthopyroxene (En<sub>49-54</sub>, Figure 3.31) which is low in abundance with an average of 0.37%, (Figure 3.29). Orthopyroxene crystals vary in shape with prisms and elongate crystals present with sizes of 0.2 - 1.2 mm.

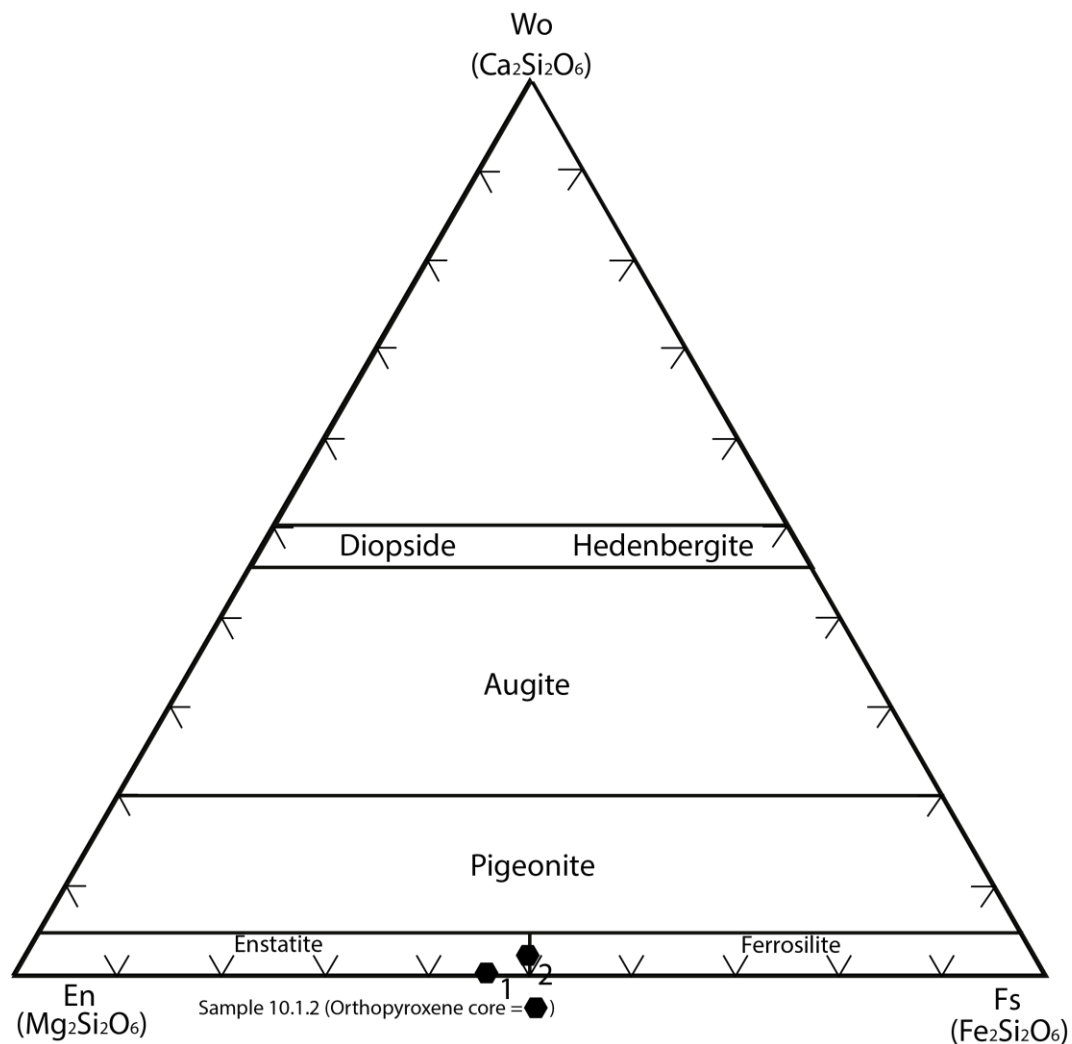


**Figure 3.31 Wollastonite - enstatite - ferrosilite ternary diagram for pyroxene crystals found in Bowentown Rhyolite. Classification from Morimoto et al., 1988 (Deer et al., 1992).**

### 3.8.3 Geochemistry

To enable comparison to the Corbett Ignimbrites geochemical results one sample of Bowentown Rhyolite was analysed. Only one sample was analysed as it is only being used to determine if there is any genetic relationship with the Corbett Ignimbrite. Geochemical processes occurring within this magma chamber are not being assessed. Major and trace element data are included in Appendix VI.

Classification of this rock is shown in a  $K_2O$  vs  $SiO_2$  plot (Figure 3.32) as this method of classification plots eliminate problems associated with loss/gain of  $Na_2O$  during secondary processes. This plot shows the Bowentown Rhyolite is close in composition to the Corbett Ignimbrites glass shards with a medium-K value of  $SiO_2$  75.78 wt. % and  $K_2O$  value of 2.72 wt. %. The composition of the Bowentown Rhyolite does not correlate well with the XRF analysis of Corbett Ignimbrite bulk pumice samples. The Bowentown Rhyolite is a glass rich spherulitic rhyolite and therefore has a higher  $SiO_2$  content.

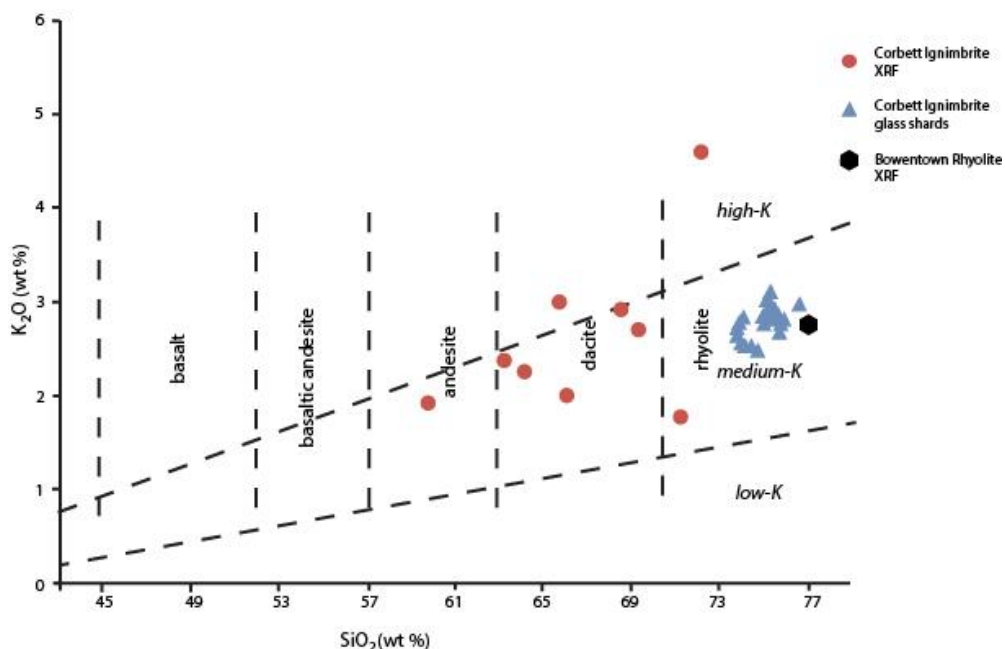


**Figure 3.32** Plot of  $K_2O$  vs.  $SiO_2$  wt. % of Corbett Ignimbrite XRF and glass shard analysis and Bowentown Rhyolite XRF analysis (based on Le Maitre *et al.*, 2002).

### 3.8.4 Dating

The Bowentown Rhyolite has been previously dated by Brathwaite and Christie (1996) with a K-Ar age of  $2.89 \pm 0.07$  Ma which is slightly older than an early fission track age of  $2.29 \pm 0.21$  Ma on obsidian from Bowentown (Rutherford 1978). To be consistent with other ages determined in this study a U-Pb age was obtained using zircons in the Bowentown Rhyolite. The full list of zircon ages obtained is included in Appendix VIII.

68 spots on zircons were initially dated, however 18 spots on zircons were considerably older than the general cluster. The remaining 50 spots were used to determine the age. U-Pb dating showed the average zircon age to approximately 2 Ma (Figure 3.33) with the determined age for the Bowentown Rhyolite being  $2.09 \pm 0.39$  Ma. This is younger than both of the previously determined ages obtained through K-Ar and fission track dating methods, however, it is within error with Rutherford (1978)'s  $2.29 \pm 0.21$  Ma age.

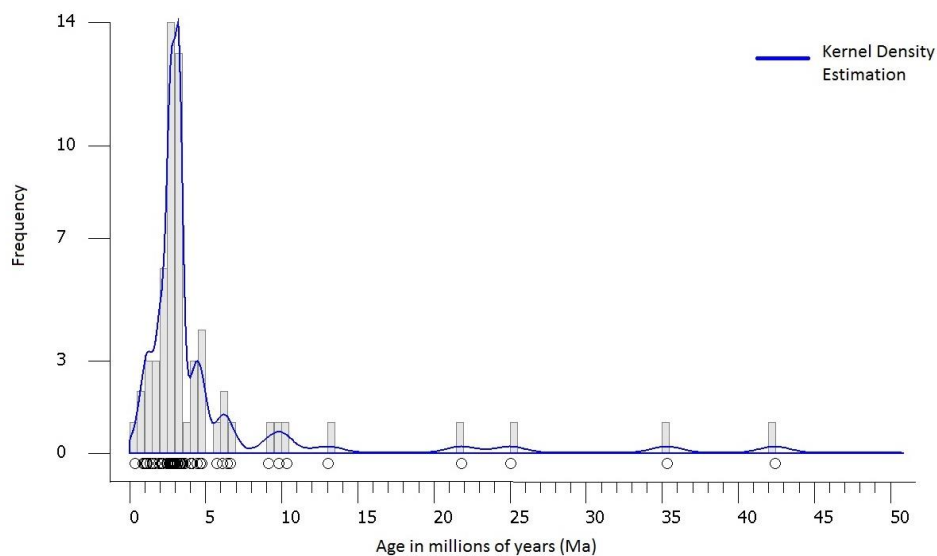


**Figure 3.33** The distribution of ages of Bowentown Rhyolite zircon crystals that were ablated by LA-ICP-MS excluding the oldest zircons analysed.

Within the whole data set of zircons analysed there was a range of older zircons from 5.1 Ma to 250.4 Ma. Several provided a Jurassic age, with the oldest being 250 Ma, which significantly predate the age of crystallisation (Figure 3.34). These older Jurassic zircons are likely to be derived from the underlying basement.

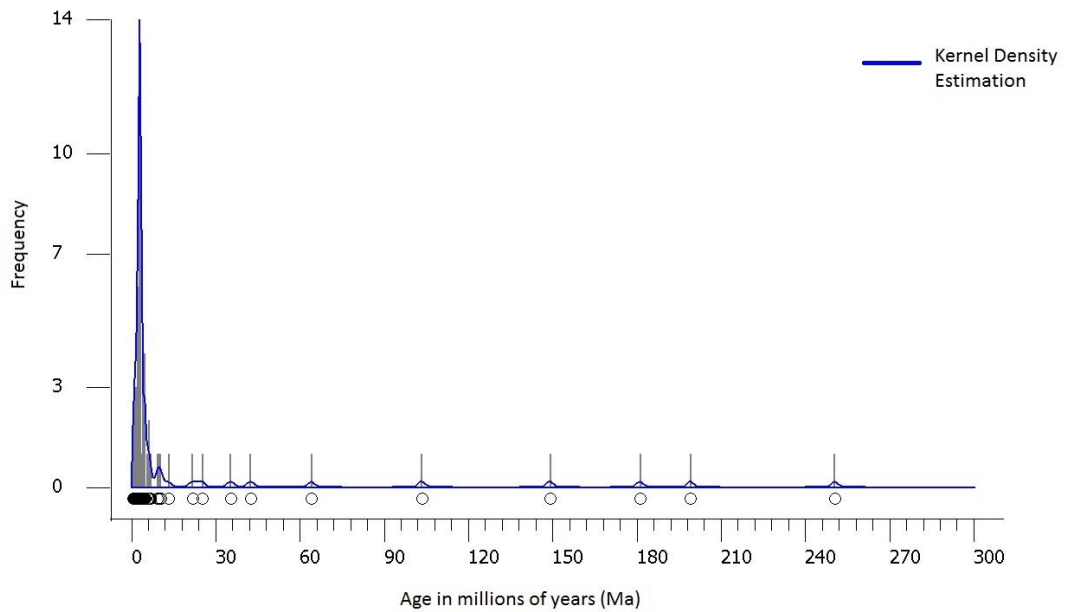


**Figure 3.34** The full distribution of ages of Bowentown Rhyolite zircon crystals that were ablated by LA-ICP-MS.

## **3.9 Discussion**

### **3.9.1 Introduction**

The Corbett Ignimbrite extends from 5 km northeast of Waihi and 11.5 km south and is confined to the eastern side of the Waihi area. This discussion presents an understanding of the components, process interpretations of facies, mechanisms causing vertical and lateral variations and magma generation. The relationship between the Corbett Ignimbrite and spatially related Bowentown Rhyolite is also evaluated as this rhyolite dome has been proposed as a source for the Corbett Ignimbrite (Brathwaite & Christie, 1996).

### **3.9.2 Components**

Throughout all facies lithics are predominantly andesite with lesser rhyolite, dacite and greywacke. These lithics are derived from the underlying geology. The presence of multiple lithic types within the Corbett Ignimbrite matrix shows a significant vertical section of the conduit stratigraphy contributed to the lithic population. Greywacke lithics are derived from the basement stratigraphy of the surrounding wall rock around the magma chamber and conduit. The Waipupu Formation is the basement rock in this area and has been estimated to reach 3 km depth within the caldera (Smith *et al.*, 2006). If the Corbett Ignimbrite is derived from the caldera then the greywacke may be derived from depths greater than 3 km.

Crystals found in the Corbett Ignimbrite matrix and pumice are plagioclase, quartz, augite, orthopyroxene, hornblende and opaques (in order of abundance). These mafic minerals reflect the dacitic composition in this ignimbrite, however they are not found (with the exception of orthopyroxene) in the younger overlying Owaharoa and Waikino ignimbrites (Brathwaite & Christie, 1996). Crystals often have sharp jagged points.

Free crystals total to an average of 30.5% of the matrix whereas crystals account for approximately 29% of pumice (on a vesicle free basis). Pumice is non-homogeneous with a range (9-44%) of crystal contents recorded in the four

samples point counted (Table 3.2). The close averages of free crystals compared to those in pumice show there was little elutriation during transportation. Pumice has a characteristic wavy texture which is due to high shear during fragmentation of the magma causing the pumice to stretch. Shear zones show localised vesicle elongation which vary between straight and curved. Regions of slightly elongate vesicles occur on either side of shear zones.

Glass shards were observed under SEM analysis as the vitriclastic matrix was not visible under the optical microscope due to their fine scale. Glass shards were cusped, Y shaped, fragments of broken bubbles as well as flat plates from the glass walls separating large flattened vesicles. There are many variables that affect the shape of glass shards, however evidence shows bubble wall and junction shards tend to form in lower viscosity rhyolitic magmas at temperatures less than 850°C (Izett, 1981). Glass shards are the dominant component of the ash which forms the binding material for larger juvenile clasts and lithic fragments. These glass shards are poorly sorted with 10 to 20 µm shards as well as sand-sized. The fine scale of these glass shards, and absence of orientation or alignment, indicate an explosive eruption where larger glass shards were destroyed. Ash portions in ignimbrites are expected to rise to significant heights in convective plumes which are dispersed by winds, producing extensive, vitric-enriched ash-fall deposits (Sparks & Walker, 1977). However, the presence of these fine glass shards indicates a significant proportion of fines were not elutriated as common in other ignimbrites.

The fiamme present in the Corbett Ignimbrite typically have ragged ends which often wrap around crystals and are aligned parallel to bedding. Within the fiamme crystals of plagioclase and quartz can be seen in hand sample with sizes reaching 1 mm. The lithics entrained in outcrop are consistent with previous facies. Fiamme is also found in the overlying younger Owaharoa Ignimbrite (Brathwaite & Christie, 1996).

### **3.9.3 Process interpretations of Corbett Ignimbrite facies**

Pyroclastic flows are high-concentration density currents of pyroclasts dispersed in gas that are high in temperature and generated by explosive volcanic eruptions

(Giordano, 1998). The Corbett Ignimbrite consists of a range of facies types which are either regionally extensive (lithic and pumice rich ignimbrite; lithic concentration zone; and matrix-supported pumice concentration zones) or only localised occurrences (fiamme and lithic rich). The Corbett Ignimbrite has four distinct facies which were determined based on variations in pumice and lithic abundance, degree of welding and the presence of fiamme. A simplified description of each facies is contained in Table 3.5. The facies identified provide a record of the processes and different stages that occurred within this pyroclastic flow.

**Table 3.5 Simplified description of the four facies found within the Corbett Ignimbrite**

<b>Facies</b>	<b>Description</b>
<b>Hc-f1</b>	Non-welded, massive, poorly sorted, pumice and crystal-rich, coarse ash ignimbrite.
<b>Hc-f2</b>	Dark grey andesite lithic concentration zone with a coarse-ash, massive matrix.
<b>Hc-f3</b>	Pumice and crystal-rich with a low abundance of lithics which are predominantly andesite
<b>Hc-f4</b>	Moderately welded, massive, poorly sorted, fiamme and crystal-rich matrix with lithics predominantly andesite.

#### **Facies Hc-f1**

Facies hc-f1 is a pumice, lithic and crystal rich deposit which comprises the bulk of the ignimbrite. Several larger lithic clasts occur scattered evenly throughout parts of facies along with smaller sized lithics and pumice. The presence of this unit indicates a non-uniform deposition due to the discontinuous nature of this facies (Branney & Kokelaar, 2002). The presence of a burnt tree log in this facies at locality 3 (Figure 3.1) suggests a dry eruption (Milner *et al.*, 2002) that would have been greater than 250°C in temperature, as this is the minimum temperature required to produce charcoal (Efford *et al.*, 2014). Temperature ranges between 200 to 900°C have been measured in charcoalified wood in other pyroclastic flows (Scott & Glasspool, 2005).

### **Facies Hc-f2**

Facies hc-f2 is a lithic concentration zone of predominantly sub-angular, block sized andesite lithics. This shows large-scale conduit erosion as represented by the coarse maximum lithic clast size (ranging from 9 to 120 mm) and high lithic content (up to 50%) of vent-derived andesite lithic clasts (Pittari *et al.*, 2008). The larger lithic clasts are concentrated in a zone at the base of a flow layer. Matrix-supported lithic concentration zones found in several outcrops were deposited in valleys during intervals of relatively high flow energy. Controls on these zones are generally related to variations in supply from the vent as well as a response to specific topographic situations (Bryan *et al.*, 1998). These lithics concentrations represent flow pulsing, where caldera collapse events have caused more lithics to be entrained within the flow and occur near the base, as well as higher stratigraphic levels. Lithic concentrations are higher at the base of the flow where they continue to flow until resistance forces overpass the driving ones.

### **Hc-f3**

Facies hc-f3 shows a more steady flow where there is a low abundance of lithics and a high proportion of pumice. This suggests that the matrix behaved as a homogeneous fluid phase in which the larger pumice clasts floated to the top (Sparks *et al.*, 1973). This ignimbrite flow unit shows a reverse grading of large pumice clasts and a normal grading of lithic clasts.

### **Hc-f4**

Facies hc-f4 is characterised as a fiamme and crystal rich deposit. Fiamme occurs when there is great enough temperature and loading causing pumice to flatten forming elongated lenses (Bull & McPhie, 2007). This facies was found at one locality (locality 11, Figure 3.1) and is either the result of an air fall or flow deposit. Welded air-fall tuffs are common and indicate post-emplacement compaction and welding over a wide area. Flattening of fiamme in welded air-fall tuffs occurs by the momentum of the falling pyroclasts (Cas & Wright, 1987), however welded air fall deposits typically occur around the vent as they decrease in temperature quickly. As the vent is unknown the distance from the vent is not able to be assessed. Poor sorting in this facies is a strong indicator that it was sourced from a pyroclastic flow (Fisher & Schmincke, 1984). The fiamme present

wrap around crystals and are aligned parallel to bedding which is also indicative of a flow.

#### **3.9.4 Mechanisms causing vertical and lateral variations**

Ignimbrites are formed by explosive volcanic activity and are deposited by transport processes resulting directly from this activity (Cas & Wright, 1987). Characteristics of deposits reflect the local pyroclastic flow transport and depositional dynamics which are controlled by variations in eruption dynamics at the vent, as well as the interaction of the pyroclastic flow with the local topography (Pittari *et al.*, 2006). Facies hc-f4 has only one occurrence meaning its timing within the eruption is difficult to constrain, however, the other facies show three main stages that occurred throughout the eruption; (1) pyroclastic flow rich in lithics, crystals and pumice (hc-f1); (2) caldera collapse events showing flow pulsing causing lithic concentration zones (hc-f2); and (3) waning eruption, shown by crystal and pumice-rich, lithic poor ignimbrite deposits (hc-f3). However ignimbrite depositional processes are not fully understood with several different theories being produced. To determine what has happened during the time of deposition for the Corbett Ignimbrite all theories must be examined.

#### **Topography controls**

The Corbett Ignimbrite is only visible in the eastern Waihi area with the northernmost and southernmost exposures found 7.5 km north east and 12.5 km south of Waihi town respectively. The full exposure of the Corbett Ignimbrite may not be observable as it is believed to be the oldest ignimbrite in the Ohinemuri Subgroup and may be buried by younger deposits including the younger Owharoa and Waikino ignimbrites.

The topography in the Waihi area prior to the deposition of this ignimbrite was highly irregular, dominated by andesite stratovolcanoes. This resulted in the flows of younger ignimbrites flow direction being directed, with the Corbett Ignimbrite being largely constrained to valleys or other topographic lows. The type section at Corbett Road, locality 1, approximately 5km northeast of Waihi town is an 18 m thick deposit which infills a valley bound by surrounding hills of andesitic and dacitic volcanic units. Drill cores in northern Waihi found a 57 m thick

hornblende-bearing pumice lapilli tuff which overlies lake and fluvial sediments (McKay, 1985), as well as a 56 m thick pumice lapilli tuff overlain by 3 m of andesite boulder alluvium and 2 m of Owharoa Ignimbrite (Rabone & Keall, 1985). These lapilli tuffs are likely to be the Corbett Ignimbrite due to the presence of hornblende as well as its location below the younger Owharoa Ignimbrite. These are significantly thick deposits which infilled a large paleovalley.

Many of the exposures of the Corbett Ignimbrite are found following rivers (with the southernmost deposits of the Corbett Ignimbrite found following Waitengaue Stream 12.5 km south of Waihi) or at road cuttings. Only two occurrences, localities 6 and 8, have boulders of this ignimbrite found on hills. This distribution of the Corbett Ignimbrite suggests that either flow did not have enough velocity to flow over elevated land causing the pyroclastic flow to be channelized into lower lying valleys, or alternatively, the flow had covered elevated land but has since been eroded leaving few exposures. As fiamme is resultant from high temperature and loading it may be closer to the start of the flow, indicating a vent location northeast of the Waihi township. Alternatively fiamme may have been due to the pyroclastic flow infilling a large valley causing an increase in welding.

### **Changes in eruption intensity**

Emplacement mechanisms of ignimbrites is widely debated with the controversy about the distinction between surge and flow mechanisms needing to be considered (Capaccioni *et al.*, 2001). Some ignimbrites are thought to be generated from a highly concentrated, non-fluidized density current that moves as a laminar mass which stop 'en masse' due to the forces of friction. As a response to this movement the deposit at the outcrop is a fair representation of the moving flow before deposition (Capaccioni *et al.*, 2001). These deposits are controlled by shear-induced processes with inverse size grading at the base and density-induced normal grading at the top (Sparks, 1976). However this does not account for the lithic concentration zones and interaction between the different facies present in the Corbett Ignimbrite which are likely to be a result of layer-by-layer deposition. The virtriclastic matrix of this ignimbrite is not visible under the optical microscope (only observable under SEM analysis) indicating an explosive eruption where larger glass shards were destroyed.

The interaction of facies hc-f1, hc-f2 and hc-f3 reflect changes that occurred throughout the eruption and at the time of deposition. The relationship between these different facies shows variations which are zonal showing a pattern of transitions both vertically and horizontally. Pumice and lithic-rich facies hc-f1 is seen alternating with lithic concentration zones (hc-f2) and is overlain by a pumice-rich, lithic-poor facies (hc-f3) indicating an unsteady deposition which was emplaced layer-by-layer from much thicker flows (Branney & Kokelaar, 2002).

The main body of this pyroclastic density current may have been moving in segments of different pulses that run very close to each other (Gottsmann & Marti, 2008). These pulses are created during collapse events at the vent and show the variations between lithic concentration zones and lithic and pumice-rich facies grading into pumice-rich, lithic-poor facies (Figure 3.35).

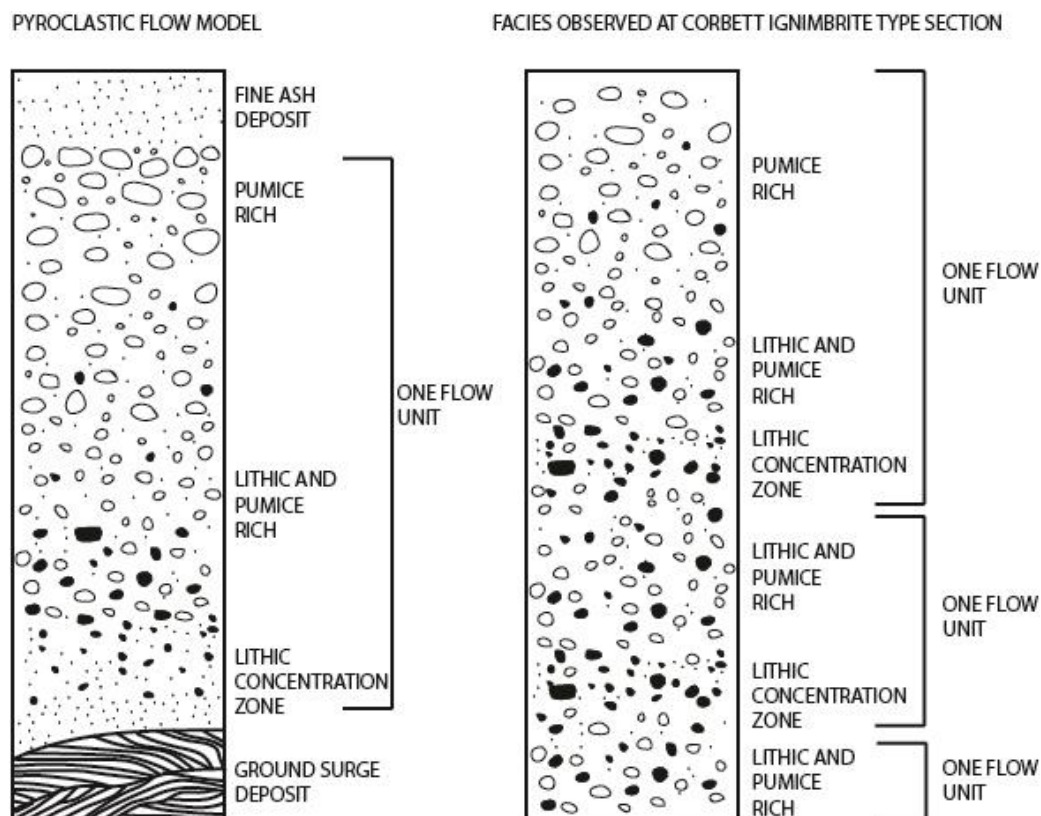


**Figure 3.35 Pyroclastic flow model (Sparks *et al.*, 1973) showing characteristics in one flow unit and the flow pulses observed at the Corbett Ignimbrite type section**

The abundance and maximum clast size of pumice increases with stratigraphic elevation in the Corbett Ignimbrite, suggesting that degassing, abrasion of the vent and the magma ascent rate, and therefore, the degree of fragmentation decreased throughout the course of the eruption (Brink, 2012). The presence of fiamme rich facies hc-f4 shows an area of high temperature and loading causing pumice to compact and become flattened. However, as much of the Corbett Ignimbrite has been buried and/or eroded it is difficult to understand the full extent of the interaction and distribution of the different facies.

### **3.9.5 Magma generation**

The petrographic, mineralogical and geochemical analyses undertaken on the Corbett Ignimbrite provide insight into the magma chamber processes. Magma chamber processes often modify the composition of the primary magma caused by partial melting of the source, fractional crystallisation, magma mixing, contamination, or due to the interaction of a mixture of these processes (Rollinson, 1993).

#### **Plagioclase zonation**

Plagioclase crystals are an important tool in understanding magma generation as they are thought to record the chemical properties of magmatic liquids in their growth patterns.

Changes in composition occurs in the melt with falling temperature. The zoning shown by differences in composition throughout plagioclase crystals indicates that there was insufficient time for the earlier crystals to react with the liquid and interchange material (Deer *et al.*, 1992). The plagioclase crystals analysed under the electron microprobe in this study are predominantly labradorite with lesser andesine.

Reverse zoning is the dominant geochemical zoning present in these crystals, where Na-rich cores become more Ca-rich outwards from the core. Reverse zoning is often found in plagioclase crystals that have sieve texture, which were observed under the optical microscope. This increase in Ca represents a gradual

rise in temperature and/or an increase in water content of the melt (Cooper, 2014).  $An_{60-43}$  is present in the Corbett Ignimbrite which helps constrain the temperature and water content within the melt. Crystallisation experiments of an A-type granite by Klimm *et al.* (2003) show that at  $An_{47}$  temperatures are approximately 850°C with melt  $H_2O$  contents of around 4-5 wt. %. Zones with higher An content form in hotter parts of the magma chamber, while lower An contents indicate a cooler part of the chamber (Shcherbakov *et al.*, 2011). Normal zoning is observed where the plagioclase crystal changes from calcic to less calcic as one moves outwards from the core, oscillatory zoning is also present where there is alternations of thin zones of different calcic content. The cores are generally calcic with a more sodic rim (Figure 3.16). Along with compositional zoning the presence of sieve textures in plagioclase show disequilibrium during crystallisation which may have occurred during ascent due to decreasing temperature (Cooper, 2014). This shows that the dominant amount of plagioclase crystals formed in the lower, higher temperature parts of the magma chamber with resorption occurring as they ascended through the chamber to shallower depths. However, oscillatory zoning in other plagioclase crystals indicates convection movements of these crystals in the magma (Shcherbakov *et al.*, 2011).

### **Changes in composition**

Geochemical analysis of the Corbett Ignimbrite shows a transition in composition throughout the time of eruption. This ignimbrite shows an evolutionary trend in composition varying from andesitic to rhyolitic, with most samples analysed being dacitic in composition. This geochemical zonation may reflect a zonation in the source magma chamber (Willcock *et al.*, 2013). Magma columns become hotter with increasing depth causing them to become chemically more mafic and more phenocryst rich (Fisher & Schmincke, 1984). Zonations are seen at the type section (locality 1, Figure 3.1) where pumice analysed show variations in composition between dacitic and rhyolitic (Figure 3.23). Zonations are also seen at locality 11 (Figure 3.1) where the lower 2 m is andesite and transitions into dacitic. The sharp variations in pumice composition may represent mixing of discrete magma compositions immediately prior to and during the eruption (McPhie *et al.*, 1993). However, Cooper (2014) suggested compositional variations can be attributed to varying crystal content variations in pumice. Pumice samples from the Corbett Ignimbrite are nonhomogeneous with changes

in crystal content and ranges in major elements and silica, however the glass analysed showed a homogeneous composition and represent the liquid composition at the eutectic. This shows melt is staying constant in the magma chamber, however the magma chamber was not zoned in chemistry but instead was physically zoned in crystal content controlling compositional changes.

Magma viscosity is also dependent on the crystal content, as well as the content of bubbles. At approximately 30 vol. % crystals (as seen in the Corbett Ignimbrite, vesicle free) the magma viscosity is generally 5 to 10 times higher than the equivalent melt viscosity (Pittari, 2004). Many silicic eruptions end with withdrawal of a crystal-rich mush, indicating magma viscosity is an important part in slowing and ending such an event (Hildreth, 2004).

### **3.9.6 Relationship with Bowentown Rhyolite**

The Bowentown Rhyolite has been included in this study to test the hypothesis proposed by Brathwaite and Christie (1996) that the Corbett Ignimbrite may be sourced from a silicic centre in the vicinity of this rhyolite dome. The distribution of the Corbett Ignimbrite may suggest the source vent lay to the southeast, and both the Corbett Ignimbrite and Bowentown Rhyolite contain orthopyroxene. The similarities and differences between the Corbett Ignimbrite and Bowentown Rhyolite for each type of analysis are summarised in Table 3.6. The most conclusive evidence in determining the relationship between the Bowentown Rhyolite and Corbett Ignimbrite is the comparison in age determined through U-Pb dating of zircons. The Bowentown Rhyolite was found to have an age of  $2.09 \pm 0.34$  Ma, where the Corbett Ignimbrite is substantially older with an age of  $6.04 \pm .032$  Ma. This large age variation shows the Corbett Ignimbrite could not have been sourced from a volcanic centre in the vicinity of the Bowentown Rhyolite as it was deposited before this rhyolite dome.

**Table 3.6 A summary of the key similarities and differences for the Corbett Ignimbrite and Bowentown Rhyolite**

<b>Results</b>	<b>Similarities</b>	<b>Differences</b>
<b>Petrography results</b>	Both contain quartz, plagioclase, orthopyroxene and opaques	The Corbett Ignimbrite also contains hornblende and augite. The Bowentown Rhyolite also contains biotite
<b>Mineralogy results</b>	Both contain andesine, labradorite and enstatite. augite	The Corbett Ignimbrite contains augite. The Bowentown Rhyolite contains sanidine
<b>Geochemistry results</b>	Both have samples with a rhyolitic composition	The Corbett Ignimbrite shows a range in composition from andesitic to rhyolitic
<b>U-Pb age of zircons</b>	No relationship	The Corbett Ignimbrite is $6.04 \pm 0.32$ Ma, whereas the Bowentown Rhyolite is $2.09 \pm 0.34$ Ma

# Chapter Four

## Ratarua Ignimbrite

### 4.1 Introduction

The Ratarua Ignimbrite is a confined deposit which was studied at two locations, locality 5 and 13 (Figure 4.1). This chapter comprises field descriptions, facies characteristics, petrography, mineralogy, geochemistry and U-Pb zircon ages of the Ratarua Ignimbrite. Both Hunt (1991) and Brathwaite and Christie (1996) identified this formation but no further analysis had been conducted. The Ratarua Ignimbrite is located on the hills surrounding the Corbett Ignimbrite type section and belongs to the Kaimai subgroup of andesites.

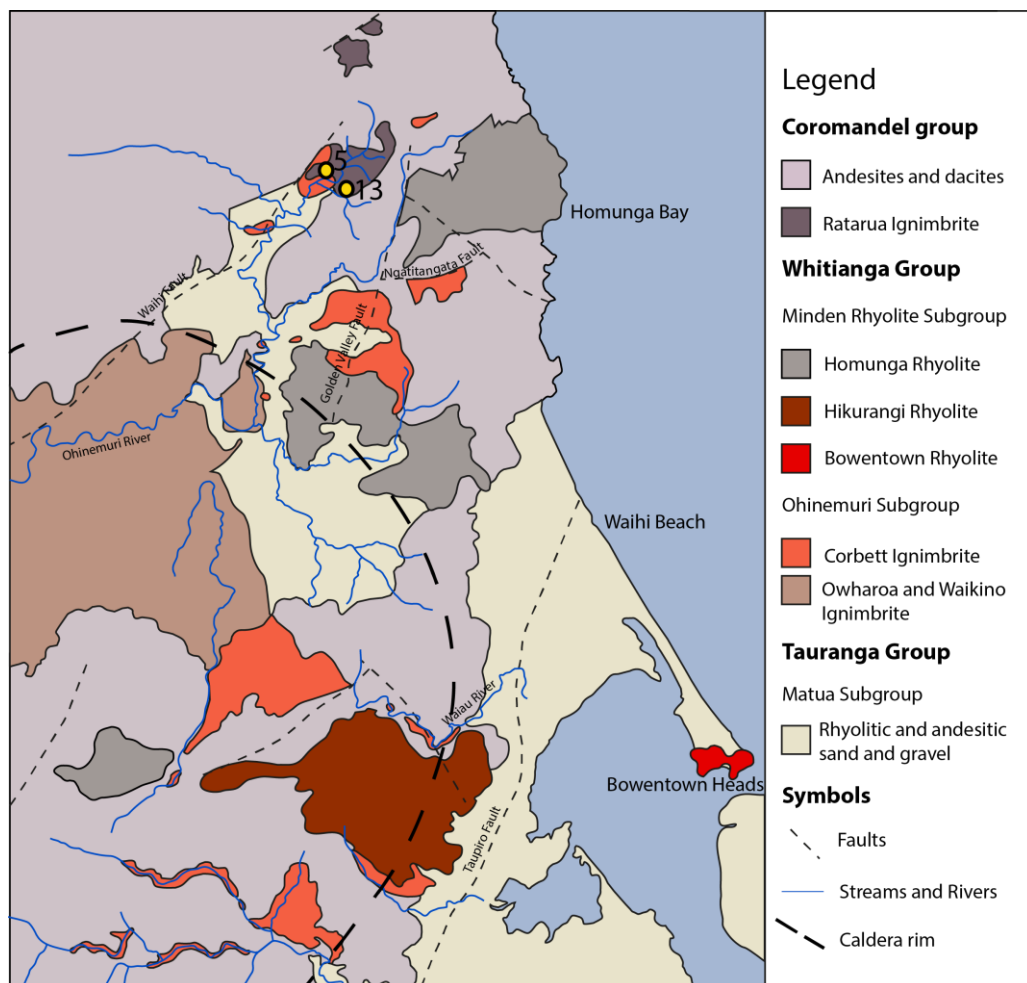


**Figure 4.1** Simplified geological map for the Waihi region. Localities studied for the Ratarua Ignimbrite are included in this map. Based on Braithwaite and Christie (1996)'s 1:50,000 geological map of Waihi.

The Ratarua Ignimbrite is classified as a welded, dacitic ignimbrite which is found within the Waihi area. This ignimbrite is exposed as angular blocks ranging from 30 cm to several metres in size. The name of this formation originated from the Ratarua Stream which is in the northern region of Waihi. Due to the outcrop occurrence of this ignimbrite as individual blocks, studying differences in facies was conducted by studying the characteristics at different elevations in the land; sample locations collected at locality 13 are shown in Figure 4.2.

## 4.2 Location and distribution

The type section for the Ratarua Ignimbrite is located along the Ratarua Stream with a thickness of 60 m (Brathwaite & Christie, 1996). Due to heavy forestry now restricting access to the site the type section was unable to be included in this study. The Ratarua Ignimbrite was instead studied at an alternative location, in the same farmland containing the Corbett Ignimbrite type section, at both locality 5 and 13. Ratarua Ignimbrite is exposed along the tops of the rolling hills on both sides of Waihi-Whangamata Road where it intersects Corbett Road, extending north to Golden Valley Road on the other side of the road. As this formation is exposed as individual blocks on a hillslope, a stratigraphic log was constructed by observing variations in the deposit at different elevations. This resulted in a 10 m stratigraphic log which identified two different facies.



**Figure 4.2 Ratarua sample collection sites at locality 13**

### 4.3 Facies

Ir-f1 is a welded fiamme and crystal-rich dacitic ignimbrite. A high abundance of elongated fiamme is evident in this facies (20-25%) with a maximum size range of 1.5 - 5.6 mm, and contain white and clear crystals. Grey, subangular to angular lithics are also evident with a maximum size of 10 mm.

Ir-f2 also has a dark crystal-rich matrix (Figure 4.3) but has a lower fiamme abundance (10%) with maximum size range of 0.2 - 4.1 mm. Grey lithics are greater in both size and number, with a maximum size of 22 mm, and remain subrounded. Crystals have decreased in concentration (4%).



**Figure 4.3 Sample 3 taken of Ratarua Ignimbrite at locality 13. Sample shows hard welded material with dark colouration**

### 4.4 Facies architecture

At each studied elevation in the landscape the characteristics of the Ratarua Ignimbrite varied between two major facies which are clearly illustrated in Figure 4.4. At the lowest elevation observed facies Ir-f1 is present with a high abundance of fiamme and small grey lithics. This transitions into facies Ir-f2 with fiamme decreasing and lithic size increasing. The highest observable section studied showed facies Ir-f1 dominant again, directly overlying facies Ir-f2.

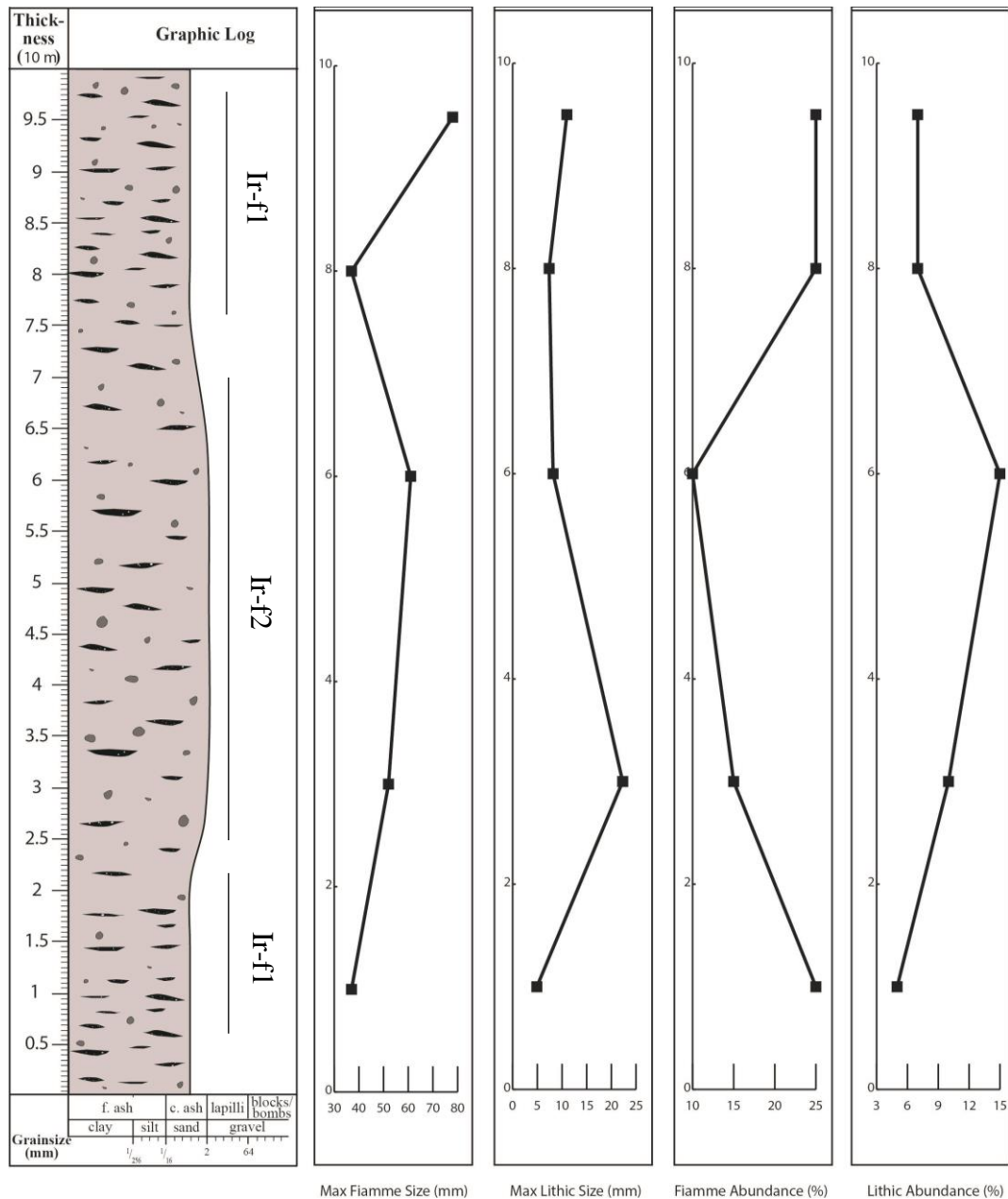


**Figure 4.4** Stratigraphic log of the Ratarua Ignimbrite constructed based on field observations at locality 13. The position of facies Ir-f1 and Ir-f2 are shown. Maximum fiamme and lithic sizes with abundances (%) are shown on graphs aligned at measured heights.

## 4.5 Petrography and mineralogy

### 4.5.1 Introduction

17 thin sections were created for optical microscope analysis, 1 polished thin section for electron microprobe and 6 crushed powder groundmass samples for XRD analysis. Raw data from point counting is included in Appendix III and graphs for XRD analysis are presented in Appendix IV.

Ratarua Ignimbrite is a crystal-rich ignimbrite with a mineral assemblage of plagioclase, hornblende, orthopyroxene, augite and opaques (Table 4.1) held within a glassy devitrified matrix that has evident polygonal cracks. Albite and anorthite were identified through XRD analysis. The crystal-rich matrix contains crystal concentration zones with laths of rectangular plagioclase.

**Table 4.1 Percentage proportions of the components obtained from point counting four thin sections of the Ratarua Ignimbrite\***

Sample	13.1.2	13.1.1	13.3.1	5.1.1	Average
Groundmass	49.1	51.9	56.8	49.4	51.8
Fiamme**	2.8	1	0	1.6	1.35
Plagioclase	32.5	38.1	33.5	36.6	35.2
Orthopyroxene	4.5	2.9	3.5	4	3.8
Hornblende	2.1	1.8	1.4	1.1	1.6
Augite	6.4	3.3	4.4	4.4	4.6
Opaques	0.8	0.4	0	0.3	0.4
Lithics**	1.8	0.8	0.4	2.6	1.4
Total	100%	100%	100%	100%	100%
Crystal content	46.3%	46.3%	42.8%	46.4%	45.45%
Margin of error***	1.6%	1.1%	0.8%	1.1%	1.15%

\*All samples were analysed to 800 counts with a stage interval of 0.3 mm

\*\* Fiamme and lithic percentages are lower due to samples selected for point counting being matrix rich

\*\*\* Margin of error determined by recording number of uncertain counts

#### 4.5.2 Crystals

Plagioclase is the most abundant crystal in this ignimbrite with an average of 35.2% (Table 4.1). Plagioclase displaying sieve texture is common throughout this ignimbrite with crystals showing corroded, partially resorbed textures. Oscillatory zoning is also found in these plagioclase (Figure 4.5).

This is a two-pyroxene ignimbrite with augite and orthopyroxene averaging 4.6% and 3.8% respectively (Figure 4.5). Augite is present as elongated crystals with sizes ranging from 0.15 - 1 mm. Orthopyroxene crystals in this ignimbrite show no pleochroism and is identifiable by its high relief and straight extinction. These crystals range from 0.15 - 0.6 mm.

Hornblende is present with an average of 1.6% with sizes ranging from 0.2 - 0.7 mm. Hornblende is prismatic and elongated with strong green to brown pleochroism (Figure 4.5).

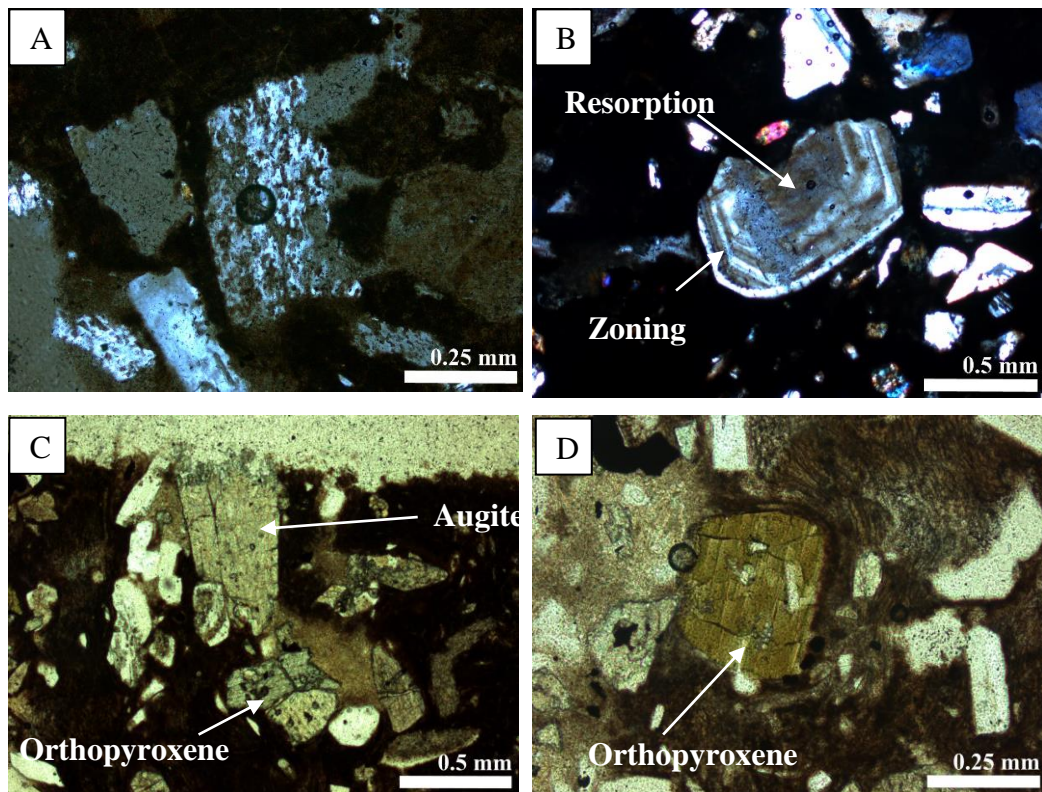


**Figure 4.5 Crystals in the Ratarua Ignimbrite matrix, all images are in plane polarised light except B which is in cross polarized. (A) Plagioclase crystal with a sieve texture and showing corrosion. (B) Crystal with oscillatory zoning and partial resorption. (C) Two types of pyroxene crystals found in the Ratarua Ignimbrite. (D) Hornblende under plane light with a prismatic shape.**

### 4.5.3 Fiamme

The Ratarua Ignimbrite has abundant fiamme with an average of 60.8% of the matrix (Table 4.2). These glassy lenses are crystal-rich.

**Table 4.2 Percentage proportions of the components within fiamme obtained from point counting thin sections after fiamme within the Ratarua Ignimbrite\***

Sample	13.3.2	13.2.1	13.4.2	13.1.3	Average
Fiamme	63.3	61.25	62.75	55.75	60.8
Plagioclase	27.5	25.75	22.75	29.75	26.4
Hornblende	0.5	1	0.5	1.75	0.9
Orthopyroxene	2	3	3.75	4	3.2
Augite	4.5	5.5	6.5	6.75	5.8
Opakes	2.2	3.5	3.75	2	2.9
Total	100%	100%	100%	100%	100%
Margin of error**	1%	0.5%	2.75%	3.25%	0.9%
Crystal content	36.7%	38.75%	37.25%	44.25%	39.2%

\*All samples were analysed to 400 counts with a stage interval of 0.3 mm

\*\* Margin of error determined by recording number of uncertain counts

Fiamme has a glassy brown wavy groundmass with wispy, flame like ends. Fiamme contains crystals of plagioclase, hornblende, orthopyroxene, augite and opaques (Figure 4.6). Microprobe analysis of one thin section showed the presence of titanomagnetite with composition of  $\text{TiO}_2$  7-10 wt. % and FeO 75-78 wt. % as well as ilmenite with  $\text{TiO}_2$  43-44 wt. % and FeO 48-49 wt. %.

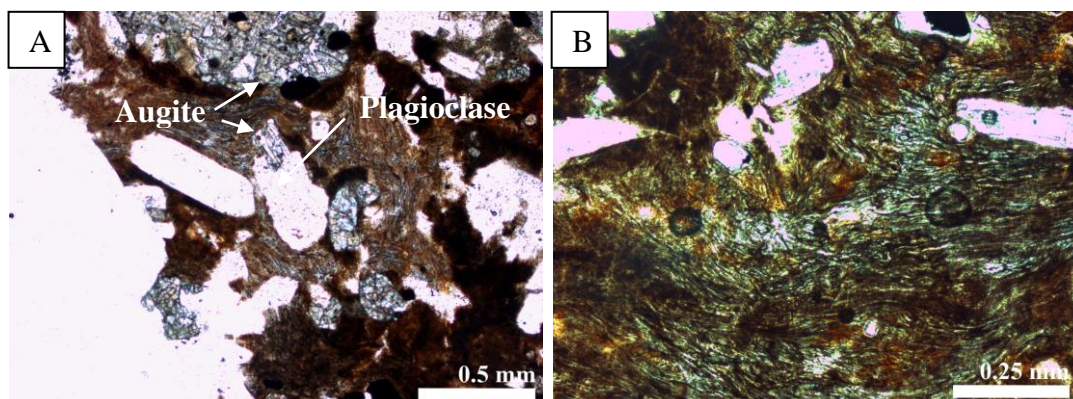


**Figure 4.6 Fiamme found within the Ratarua Ignimbrite. (A) Plagioclase and augite crystals contained in the fiamme. (B) Wavy nature of the fiamme with a dark glassy matrix.**

Plagioclase (An<sub>75-4</sub>, Figure 4.7) is the dominant crystal with an average occurrence of 26.4% as shown in Table 4.2 (raw data is presented in Appendix V). These appear as laths ranging from 0.4 - 1.2 mm in size. Electron microprobe analysis of these plagioclase crystals showed normal zoning where crystals composition changed from calcic to less calcic outwards from the core (Table 4.3).

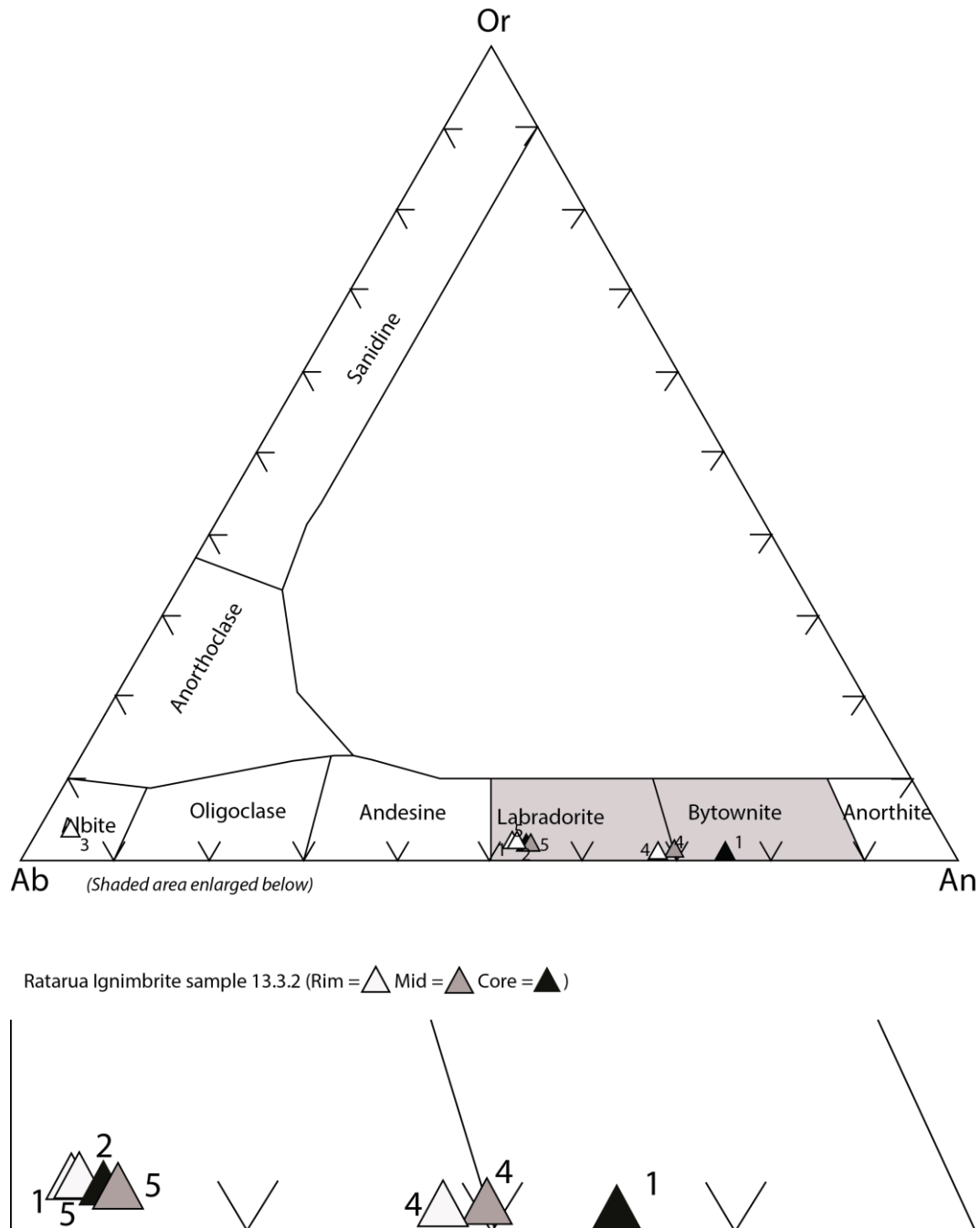


**Figure 4.7 Albite – anorthite - orthoclase ternary diagram for plagioclase crystals in fiamme in the Ratarua Ignimbrite. Classification according to Deer et al. (1992)**

**Table 4.3 Zoning observed in samples analysed under the electron microprobe based on CaO and Na<sub>2</sub>O values.**

Sample	CaO	Na <sub>2</sub> O	Zoning
13.3.2 – 1 – core	14.802	2.687	
13.3.1 – 1 – rim	9.773	4.617	Normal zoning
13.3.2 – 4 – mid	13.627	3.267	
13.3.2 – 4 – rim	12.646	3.815	Normal zoning
13.3.2 – 5 – mid	10.525	4.88	
13.3.2 – 5 – rim	10.015	4.907	Normal zoning

Two pyroxenes are present in the fiamme (Figure 4.6). Augite (Wo<sub>44</sub>, En<sub>41</sub>, Fs<sub>15</sub> and Wo<sub>43</sub>, En<sub>40</sub>, Fs<sub>17</sub>), with an average of 5.8%, is more abundant than orthopyroxene (En<sub>75-57</sub>), averaging 3.2% (Figure 4.8).

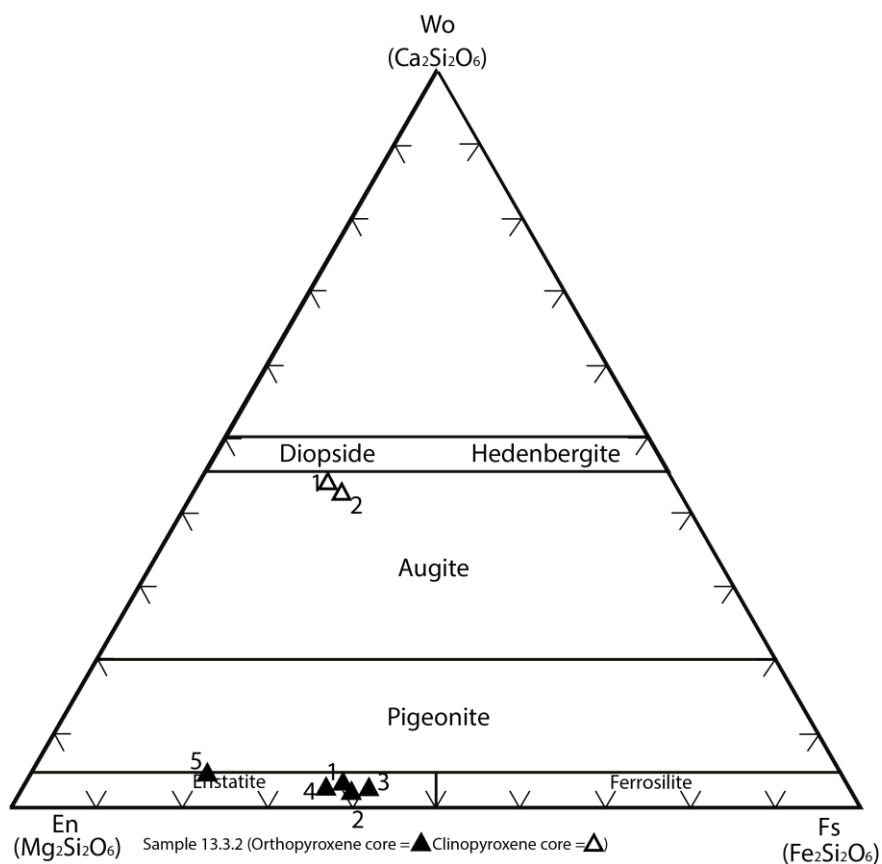


**Figure 4.8 Wollastonite - enstatite - ferrosilite ternary diagram for pyroxene crystals found in Corbett Ignimbrite pumice. Classification from Deer et al., (1992).**

#### 4.5.4 Lithics

The Ratarua Ignimbrite contains andesite, dacite, rhyolite and rare sandstone lithics (Figure 4.9). The andesite lithics are considerably crystal-rich with abundant mafic minerals and a distinct absence of quartz. Dacite lithics have a high abundance of plagioclase and quartz held within a light grey crystal-rich matrix. Mafic crystals are found within these lithics at a low abundance. Rhyolite lithics found within the Ratarua Ignimbrite have a low crystal abundance with a dark brown glassy matrix. One sedimentary lithic was found in these samples. Brathwaite and Christie (1996) identified argillite lithics in this ignimbrite indicating it is likely to be argillite. This lithic is comprised of quartz and plagioclase phenocrysts ranging in size and shape held within a poorly sorted matrix.

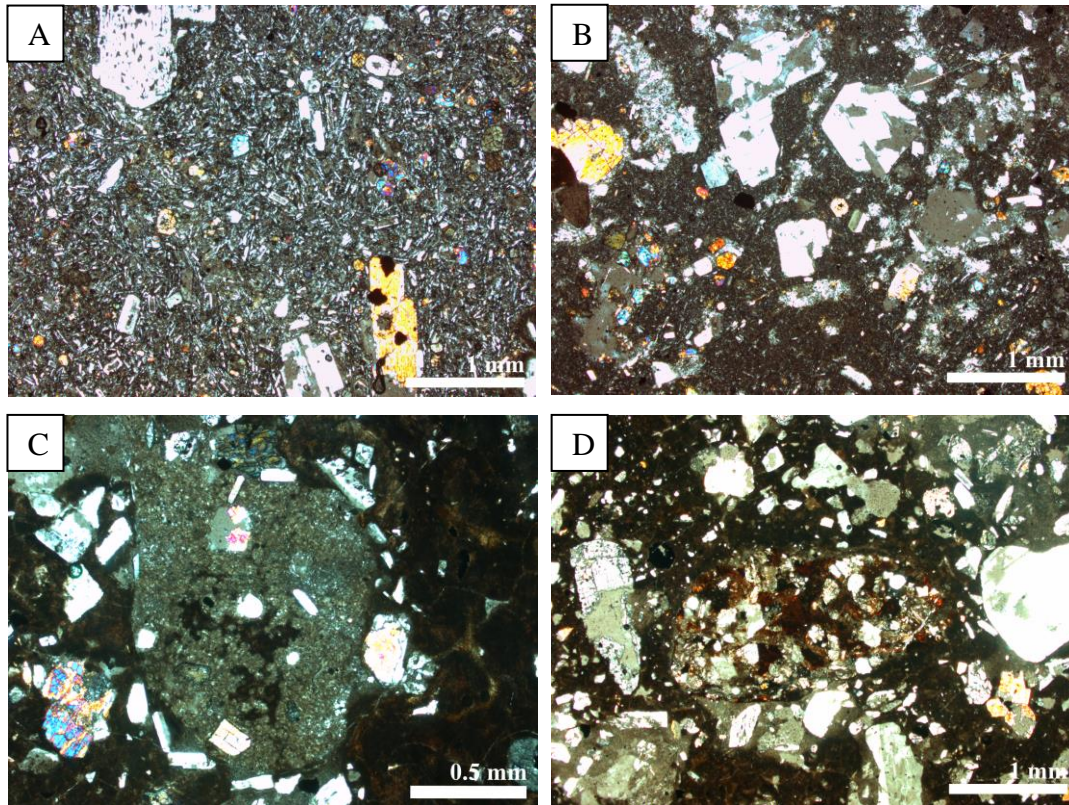


**Figure 4.9** The different lithic types in the Ratarua Ignimbrite all under cross polarized light. (A) Andesite lithic taking up the entire photo, this lithic is crystal rich with mafic crystals. (B) Dacite lithic with a high abundance of quartz and plagioclase. (C) Rounded rhyolite lithic. (D) Poorly sorted argillite lithic.

## 4.6 Fiamme geochemistry

### 4.6.1 Introduction

Six samples of fiamme from the Ratarua Ignimbrite were analysed through XRF methods, five of these fiamme samples were sourced from locality 13. Major and trace data are included in Appendix VI. Fiamme was used instead of bulk rock samples as it is a better indicator of magma composition with less contamination from non-juvenile components.

### 4.6.2 Rock classification

Geochemical analysis using XRF results show that the fiamme in the Ratarua Ignimbrite are dacitic in composition (Figure 4.10) ranging from 63 - 68% wt. %  $\text{SiO}_2$ .

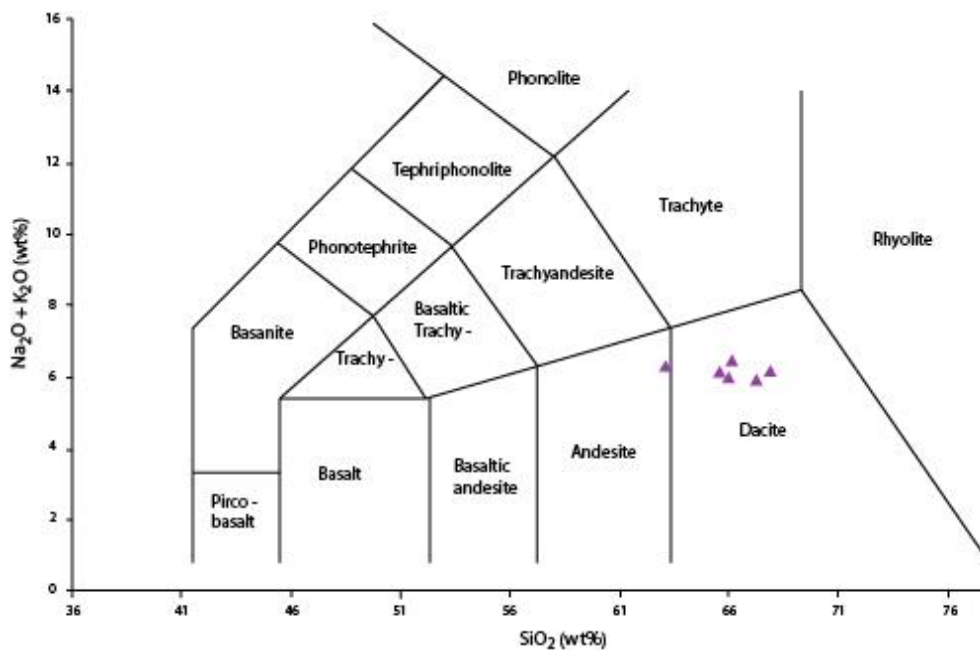
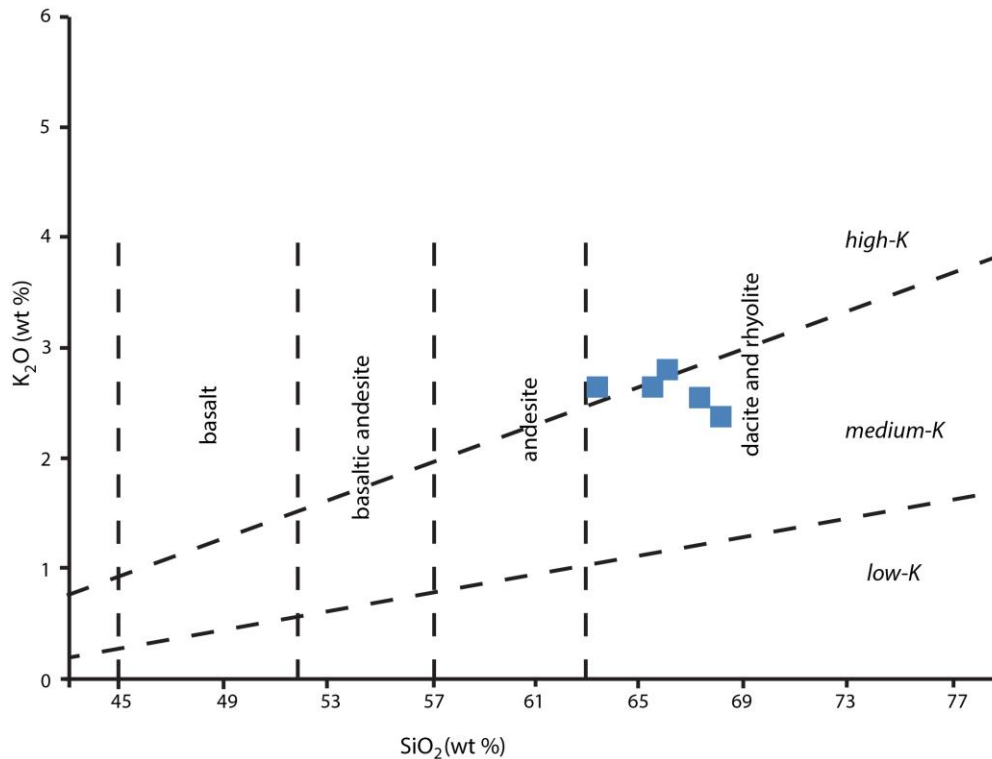


Figure 4.10 Plot of  $\text{Na}_2\text{O} + \text{K}_2\text{O}$  vs  $\text{SiO}_2$  wt. % of the Ratarua Ignimbrite XRF analysis of bulk fiamme (based on Deer *et al.*, 1992).

To further classify this rock a plot of  $K_2O$  vs  $SiO_2$  shows the  $K_2O$  range for this dacitic ignimbrite. It is determined to be a medium-K ignimbrite with  $K_2O$  values ranging from 2.4 - 2.8 wt. % (Figure 4.11).



**Figure 4.11** Plot of  $K_2O$  vs.  $SiO_2$  wt. % of the Ratarua Ignimbrite bulk fiamme XRF analysis (based on Le Maitre *et al.*, 2002).

#### 4.6.3 Major element chemistry

Harker variation plots are used to plot the weight of major and trace elements against  $SiO_2$  to determine relationships between individual rocks.  $SiO_2$  content has a small range (63 - 68 wt. %) causing data points for elements to plot closely to each other. Harker plots of the major element compositions of  $Al_2O_3$ ,  $CaO$ ,  $Fe_2O$ , and  $MgO$  with respect to  $SiO_2$  wt. % showed negative trends (Figure 4.12). These negative trends are generally interpreted as being a result of fractional crystallisation with fractionation of plagioclase ( $Al_2O_3$ ,  $CaO$ ), iron oxides, clinopyroxene, orthopyroxene and hornblende ( $Fe_2O$ ). This does not consider the influence of the variations of crystal content within each sample (Cooper, 2014). The fiamme is crystal rich with a crystal range of 36 - 44%, determined from point count analysis. The abundance of particular crystals within different samples may show an increase in major elements.  $Na_2O$  and  $K_2O$  in respect to  $SiO_2$  wt. % show no relationship.

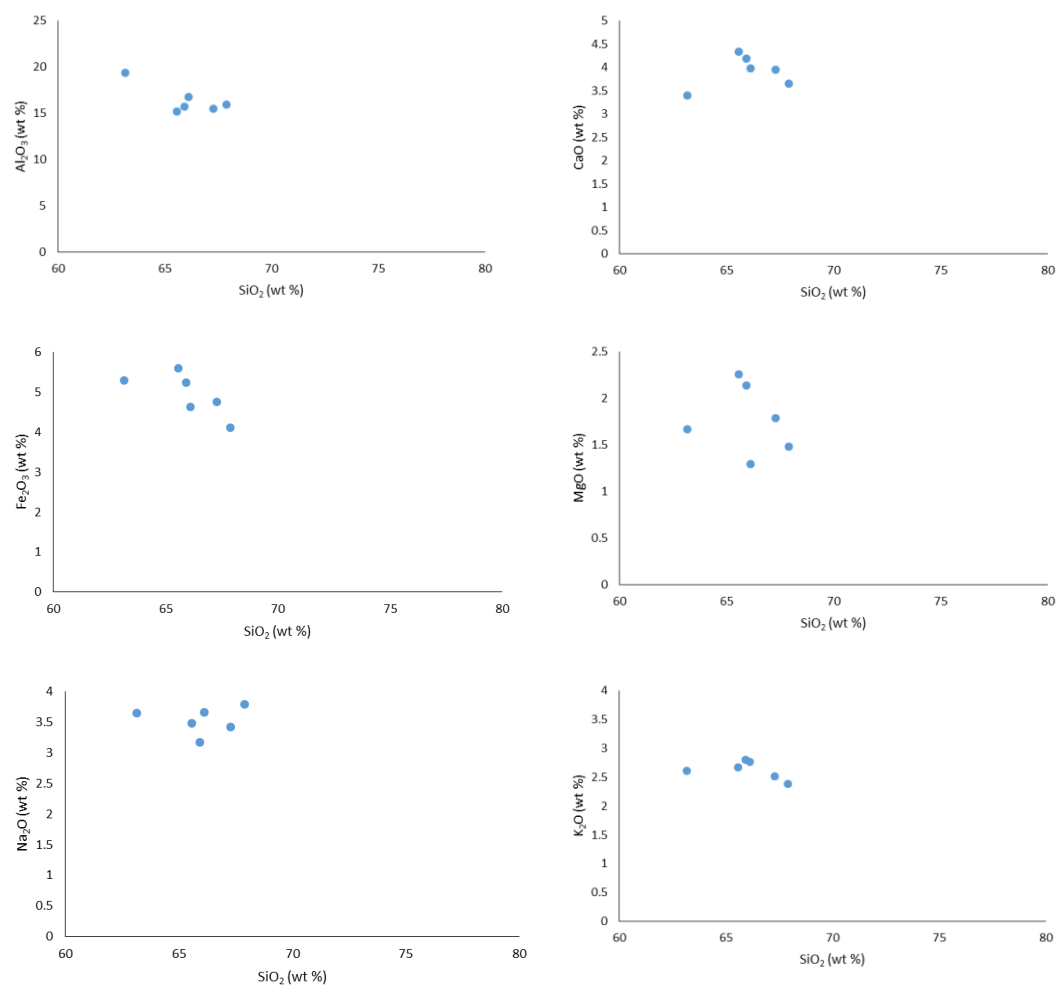


**Figure 4.12** Harker diagrams of selected major elements found in fiamme samples, versus  $\text{SiO}_2$  wt. %.

#### **4.6.4 Trace element chemistry**

Compositions of trace elements were determined through XRF for 6 samples (the same as those analysed for major elements). 29 trace elements (in ppm) were analysed (Appendix VI). Trace element Harker plots can be used to help determine the geochemical processes that may have occurred within the chamber. Trace elements were plotted against  $\text{SiO}_2$  to determine any trends as well as incompatible elements (Figure 4.13).

Trace elements in the Ratarua Ignimbrite show more scattered trends compared to major elemental analysis however trends can still be observed. Rb, Sr and Ba have a weakly negative relationship with  $\text{SiO}_2$  wt. %. Zr shows a similar trend to the major elements  $\text{Al}_2\text{O}_3$  and  $\text{K}_2\text{O}$ , as Zr is controlled by plagioclase content. Incompatible elements plotted against each other show stronger relationships than those plotted against  $\text{SiO}_2$ . Rb vs Sr, Ba vs Rb, Rb vs Zr and Ba vs Zr all show positive relationship trends. Both Rb and Sr are elements that are strongly controlled by plagioclase content. They show a strong relationship when Sr levels are between 150-200 ppm and Rb 80-100 ppm.

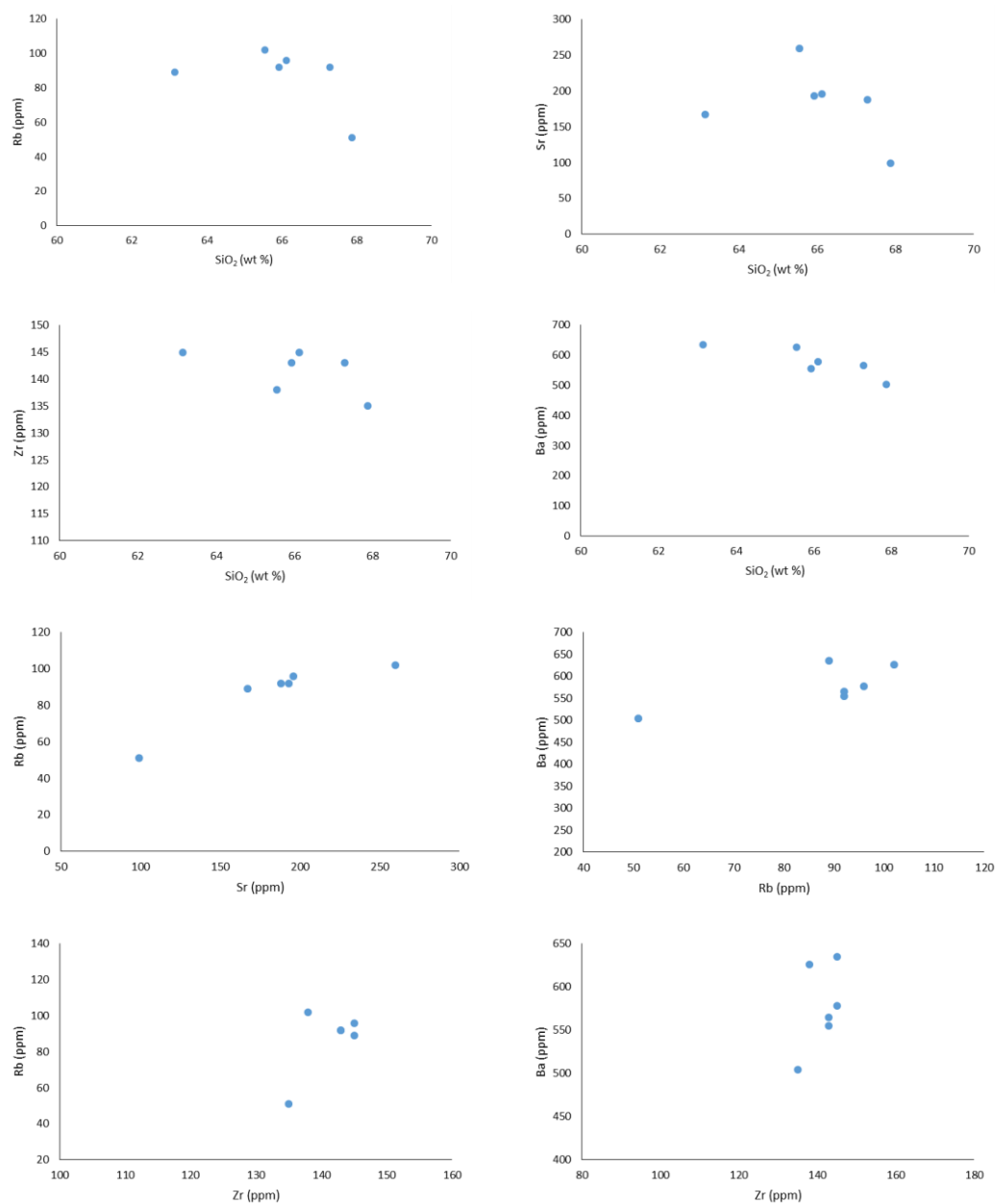


**Figure 4.13 Harker variation plots of trace element geochemistry from XRF results of whole fiamme.**

## 4.7 Dating

### 4.7.1 Introduction

The Ratarua Ignimbrite was previously assumed to be less than 5 Ma old (Brathwaite & Christie, 1996) due its stratigraphic relationship with andesite units in Waihi area. However no age has previously been determined. U-Pb dating of zircons provide an age and margin of error for the Ratarua Ignimbrite.

### 4.7.2 Zircon age results

35 spots on zircons were initially dated, however 8 spots on zircons were considerably older than the general cluster and were excluded from the age calculation (full data set is presented in Appendix VIII). The remaining 27 spots were used to determine the age. The Ratarua Ignimbrite showed a range of zircon ages with an approximate average around 7 Ma (Figure 4.14). Ablation of zircons through LA-ICP-MS provided an age of  $6.79 \pm 0.42$  Ma

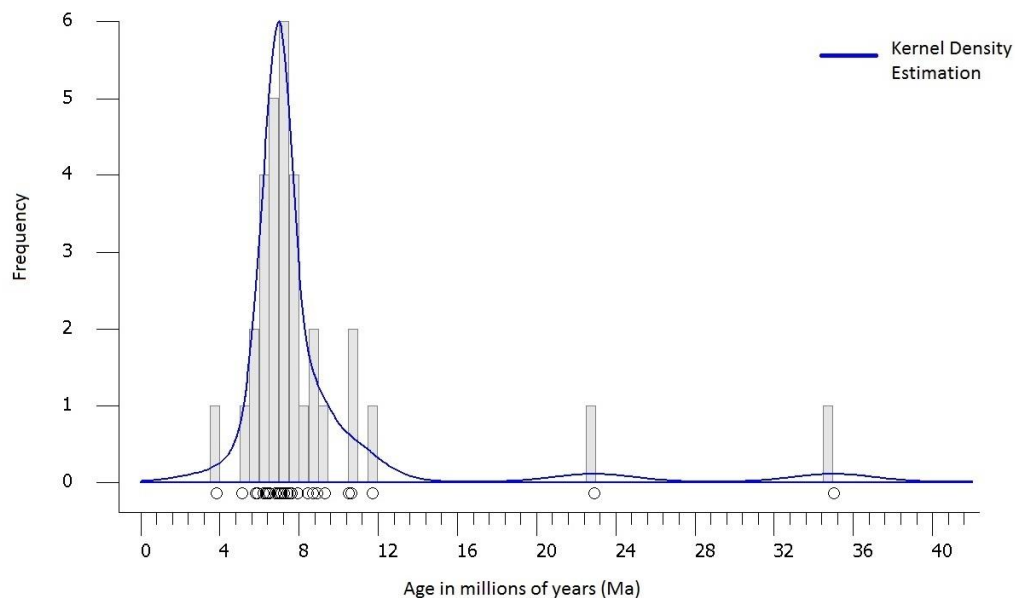


**Figure 4.14** The distribution of ages of Ratarua Ignimbrite zircon crystals that were ablated by LA-ICP-MS excluding the oldest zircons analysed.

Although the majority of zircons provided age ranges close to 7 Ma, 8 zircons showed a wider range of ages (Figure 4.15) grouped into; Early to Mid Miocene (10.5 Ma, 10.6 Ma, 11.7 Ma, 11.8 Ma, 22.9 Ma); Late Eocene (35 Ma); Early Jurassic (187 Ma); and Late Triassic (210 Ma). Those close to 7 Ma are likely to be antecrysts (see Chapter 3 section 3.7.2). The Early Jurassic zircons is derived from the basement of the CVZ which has previously been determined to be Jurassic in age (Brathwaite & Christie, 1996). The Late Triassic zircons are older than the basement showing they are sourced from deeper basement geology. The origin of the zircons which are older than the CVZ but younger than the underlying basement are discussed in Chapter Six.

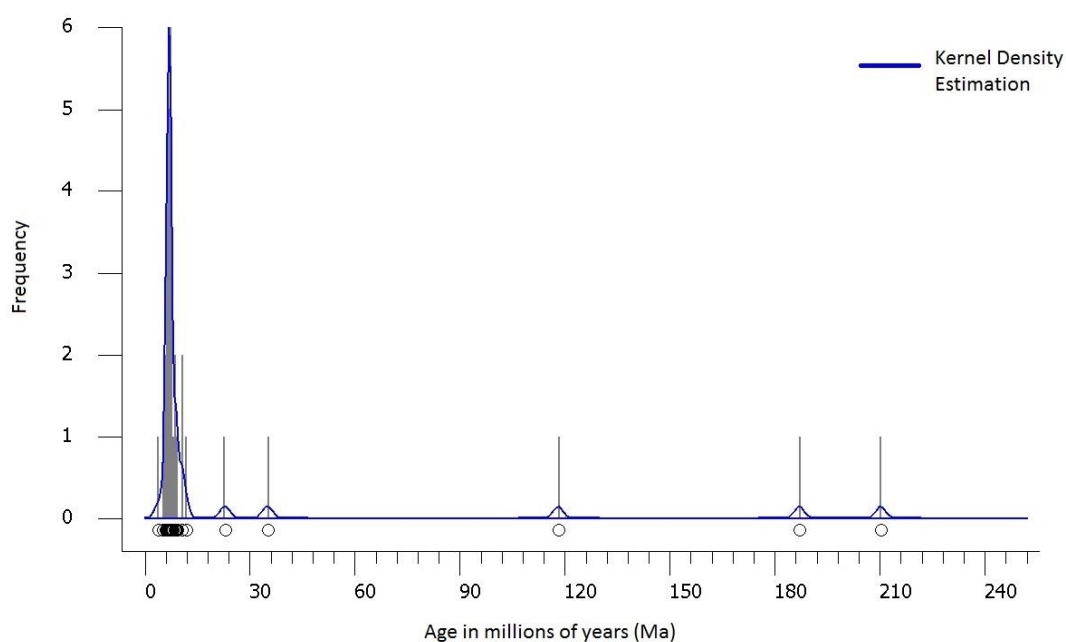


**Figure 4.15 The full distribution of ages of Ratarua Ignimbrite zircon crystals that were ablated by LA-ICP-MS**

## **4.8 Discussion**

### **4.8.1 Introduction**

Dacites are more abundant as pyroclastic rocks rather than lava flows (Fisher & Schmincke, 1984). The Ratarua Ignimbrite is a welded dacitic ignimbrite which outcrops in northern Waihi area. This discussion presents an understanding of the components, welding and eruption processes, and the association between the Ratarua Ignimbrite and the andesites and dacites of the Coromandel Group.

### **4.8.2 Components**

#### **Lithics**

The Ratarua Ignimbrite contains andesite, dacite, rhyolite and rare sandstone lithics. The abundance and subangular to angular shape of andesite lithics indicates these are predominantly derived from the vent, with some being accessory lithics due to the high abundance of andesite in northern Waihi. The sedimentary lithic, thought to be argillite, may be derived from the Mataora Formation which is found throughout the headwaters of the Mataora Stream. This formation is intercalated with the Whiritoa Andesite which underlies the Ratarua Ignimbrite, indicating this lithic was entrained during the pyroclastic flow. Dacite and rhyolite lithics are also accessory lithics that were incorporated into the flow after eruption.

#### **Fiamme**

Fiamme is abundant throughout both facies studied. Crystals found in fiamme are plagioclase, hornblende, orthopyroxene, augite and opaques with an average of 39.2% (on a vesicle free basis). The wavy groundmass of the fiamme indicates a flow formation under high temperatures. The key difference between Ir-f1 and Ir-f2 is the abundance and size of fiamme. Ir-f1 has 20-25% fiamme which range in size from 1.5 – 5.6 mm, where Ir-f2 has 10% fiamme which range in size from 0.2 - 4.1 mm.

## Crystals

The Ratarua Ignimbrite is crystal rich, with an average of 45.5%, and contains plagioclase, hornblende, orthopyroxene, augite and opaques. Crystals are generally more abundant in the matrix than in the pumice showing evidence of preferential concentration in the matrix due to significant elutriation of the fine crystals during flow transport (Montero-Lopez *et al.*, 2015).

### 4.8.3 Welding

The strong presence of fiamme throughout the Ratarua Ignimbrite shows welding. Welding involves the sintering together of hot pumice and glass shards under compositional loading. It is controlled by glass viscosity, which is dependent on temperature and composition, as well as loading which is controlled by the thickness of the deposit (Cas & Wright, 1987). In this dacitic ignimbrite bulk density is at a maximum with low porosity, corresponding to a zone of dense welding which is likely to be close to the vent source (Figure 4.16). The exposures studied were densely welded and covered hillslopes. It is likely the partial to non-welded sections of this ignimbrite have been eroded since its deposition 6.79 Ma.

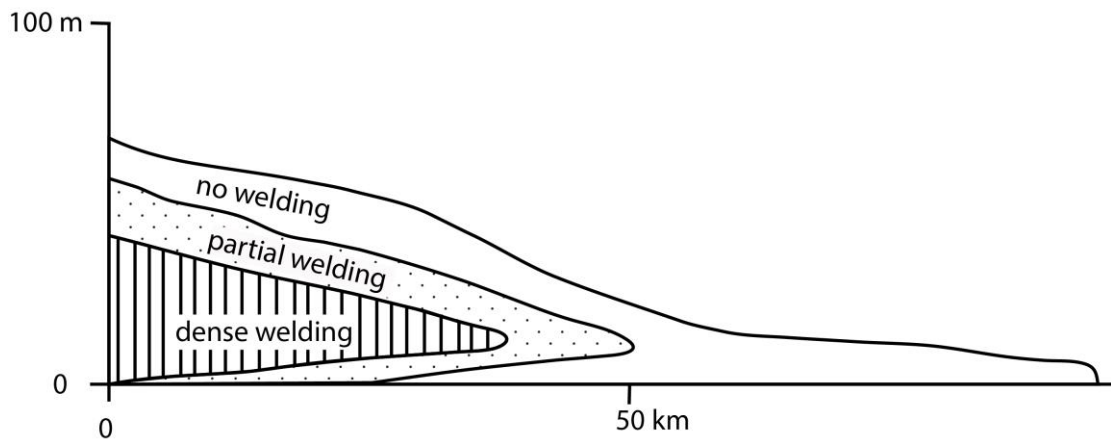


**Figure 4.16 Ignimbrite welding zones (McPhie *et al.*, 1993).**

The type section of the Ratarua Ignimbrite is located in the headwaters of Mataora Stream (not included in this study) which has also been recorded as being welded with fiamme (Brathwaite & Christie, 1996). The presence of this fiamme classifies it as a pyroclastic deposit instead of a lava flow.

#### **4.8.4 Eruption processes**

The degree of welding also provides insight into what was occurring at the time of deposition. The temperature at the time of emplacement for ignimbrites is variable which was explained by Sparks and Pinkerton (1978) through an eruptive column collapse model. Eruptions with low gas content and velocity result in low collapse heights with little loss of heat during collapse often producing densely welded ignimbrites. The Ratarua Ignimbrite shows variation in welding which may be due to widening of the vent with a decrease in gas content during eruption and column collapse causing increases in emplacement temperature and welding (Cas & Wright, 1987).

#### **4.8.5 Ratarua Ignimbrite relationship with andesites and dacites of the Coromandel Group**

The Ratarua Ignimbrite formed during a period dominated by andesite and dacite volcanism. Within the Waihi area the Coromandel Group andesites of Late Miocene are the oldest recorded in Waihi area with the Waiwawa Subgroup containing units with K-Ar ages of 7.94 to 6.31 Ma (Brathwaite & Christie, 1996). The youngest andesite in the Coromandel Group is the Ananui Andesite which belongs to the Kaimai Subgroup and was found to have a K-Ar age of  $3.78 \pm 0.06$  Ma (Brathwaite & Christie, 1996).

The Ratarua Ignimbrite belongs to the younger Kaimai Subgroup. The age of the Ratarua Ignimbrite is determined to be  $6.79 \pm 0.45$  through U-Pb dating, which is considerably older than suggested by Brathwaite and Christie (1996) who predicted its age to be less than c. 5 Ma. The age was originally thought to be younger than c. 5 Ma as it stratigraphically overlies the Matangia Andesite which has had a single K-Ar age of 5.47 Ma (Brathwaite & Christie, 1996). The inconsistencies between the ages of the Ratarua Ignimbrite and Matangia Andesite may be due to K-Ar dating providing inconsistent ages and therefore may be incorrect. Also it is unclear in Brathwaite and Christie (1996) if there is a direct contact between the two units or if it is inferred to overlie the Matangia Andesite.

This andesitic succession occurs as massive flows, autoclastic breccias, lahars, tuffs and dikes (Skinner, 1986) which overlie the basement in Waihi. They form

the hills throughout the landscape and are likely to be remnants of stratovolcanoes which have since been heavily eroded. The Ratarua Ignimbrite erupted contemporaneously with other andesitic and dacitic members of the Coromandel Group.

The Coromandel Group formed north of Waihi and showed variation over time. A key feature of the andesitic Coromandel Group is that the rocks of most of the formations have similar geochemical properties. Booden *et al.*, (2012) studied an andesite and a dacite of the Waipupu formation and found both contain plagioclase crystals with sodic bytownite compositions. These two units also contain plagioclase crystals with cores that differ in composition; the andesite contains plagioclase with anorthitic cores, whereas the dacite contains a plagioclase with labradoritic core. The composition found for this Waipupu formation dacite is consistent with results obtained for the Ratarua Ignimbrite. The Ratarua Ignimbrite shows a predominantly medium potassic calc-alkaline relationship which shows a positive relationship with other Coromandel Group rocks analysed by Booden *et al.*, (2012) which were also found to be medium potassic (Figure 4.17). The consistency in composition of the Coromandel Group rocks indicates that similar processes formed magmas with similar source materials (Booden *et al.*, 2012).

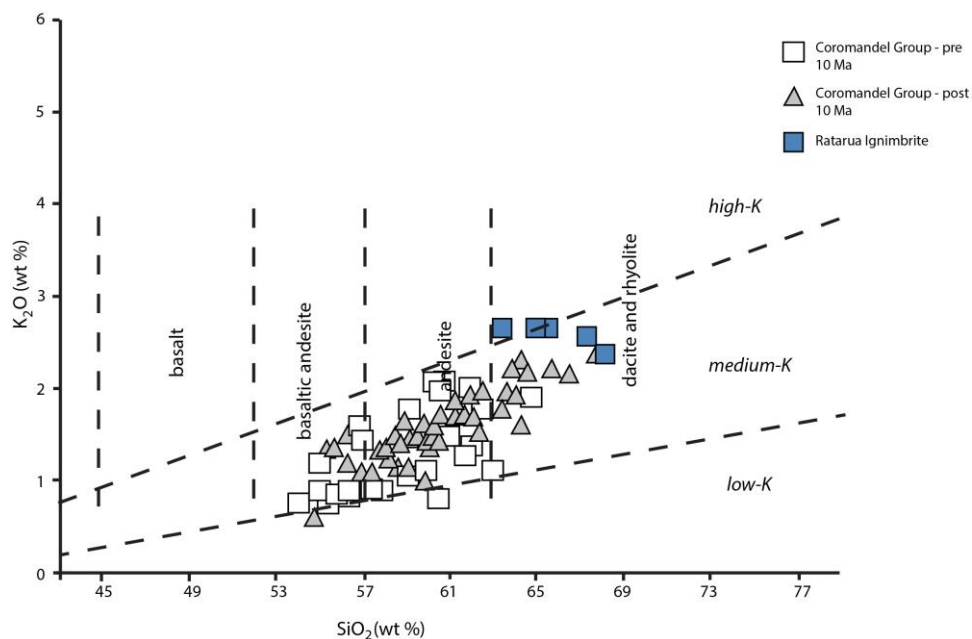


**Figure 4.17** Plot of K<sub>2</sub>O vs. SiO<sub>2</sub> wt.% of the Ratarua Ignimbrite bulk fiamme XRF analysis compared with results of Coromandel Group rocks analysed by Booden *et al.*, (2012). (Based on Le Maitre *et al.*, 2002).



# Chapter Five

## Hikurangi Rhyolite

---

### 5.1 Introduction

The Hikurangi Rhyolite is only exposed in one location, locality 2, as it is a confined rhyolite dome and is the most prominent feature in southern Waihi. The Hikurangi Rhyolite belongs to the Homunga Rhyolite formation which contains three other rhyolite domes; Whale Bone Bay, Shark Bay and Ruahorehore. The Hikurangi Rhyolite is the southernmost dome belonging to the Homunga Rhyolite formation.

This rhyolite is creamy beige, spherulitic, crystal-rich with abundant plagioclase, quartz, biotite and opaque crystals (Figure 5.1). Although variations in crystal abundance occurs the deposit is massive with little differences in matrix. This rhyolite dome is spatially related to the Corbett Ignimbrite and is being explored for any genetic relationships, if any, it may share with this widespread ignimbrite.

This chapter documents the facies, petrography, mineralogy, geochemistry and U-Pb age of the Hikurangi Rhyolite.

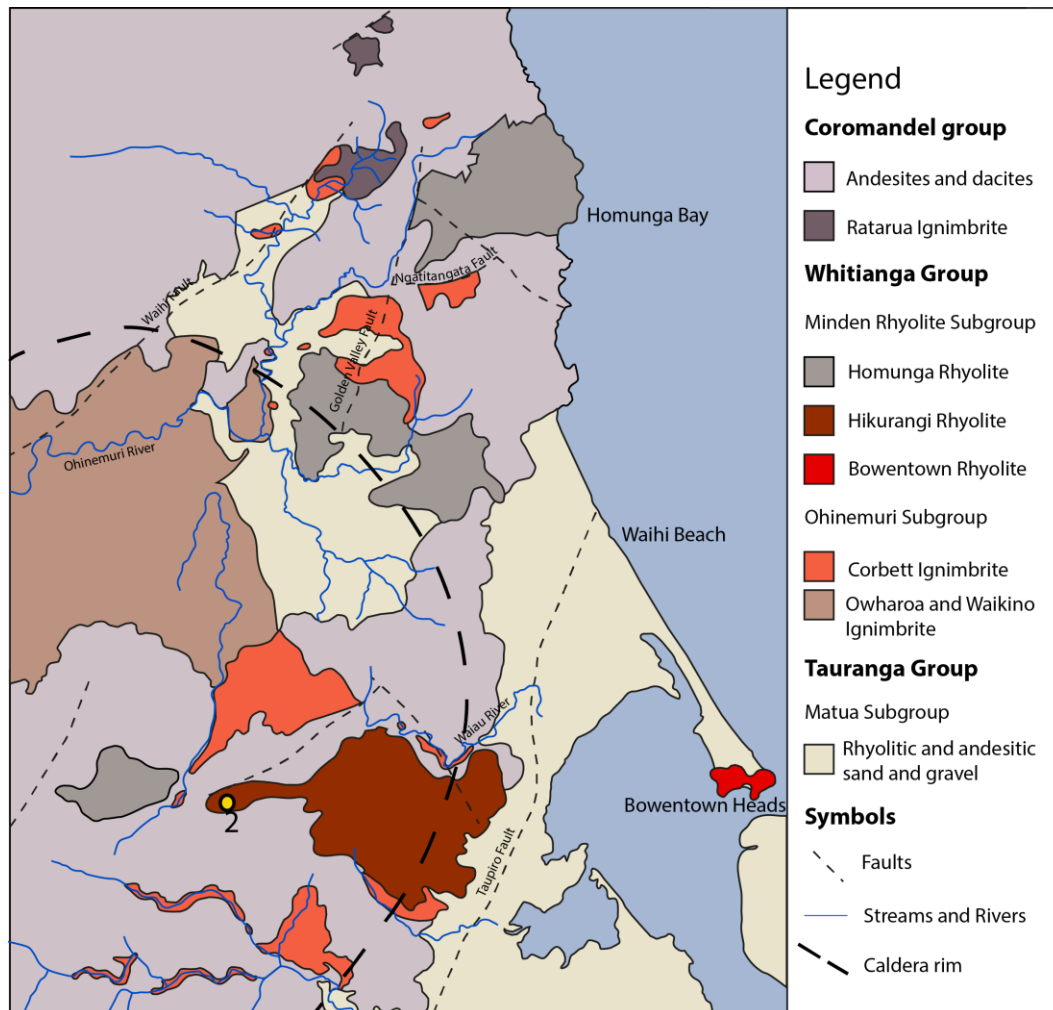


**Figure 5.1 Geological map of the different formations around Waihi. Localities studied is included in this map. Based from Braithwaite and Christies (1996) 1:50,000 geological map of Waihi.**

## 5.2 Location and distribution

Due to extensive forest cover and inaccessibility only one outcrop of the Hikurangi Rhyolite was able to be included in this study. Hikurangi Rhyolite was exposed along Woodlands Road in south Waihi (locality 2, Figure 5.1). This is a 10 m high, massive deposit which shows the internal structure of this part of the rhyolite. Samples were collected along the horizontal extent of this outcrop to determine any compositional variations. The Hikurangi Rhyolite overlies the extensive Uretara Formation.

### 5.3 Facies

Only one facies was identified for the Hikurangi Rhyolite. This is a massive, creamy white, porphyritic, spherulitic, crystalline facies (Figure 5.2) which contains biotite, quartz and plagioclase phenocrysts of typically 1-2 mm in size. As it is a massive deposit this is the only facies that characterises the rhyolite at Woodlands Road.

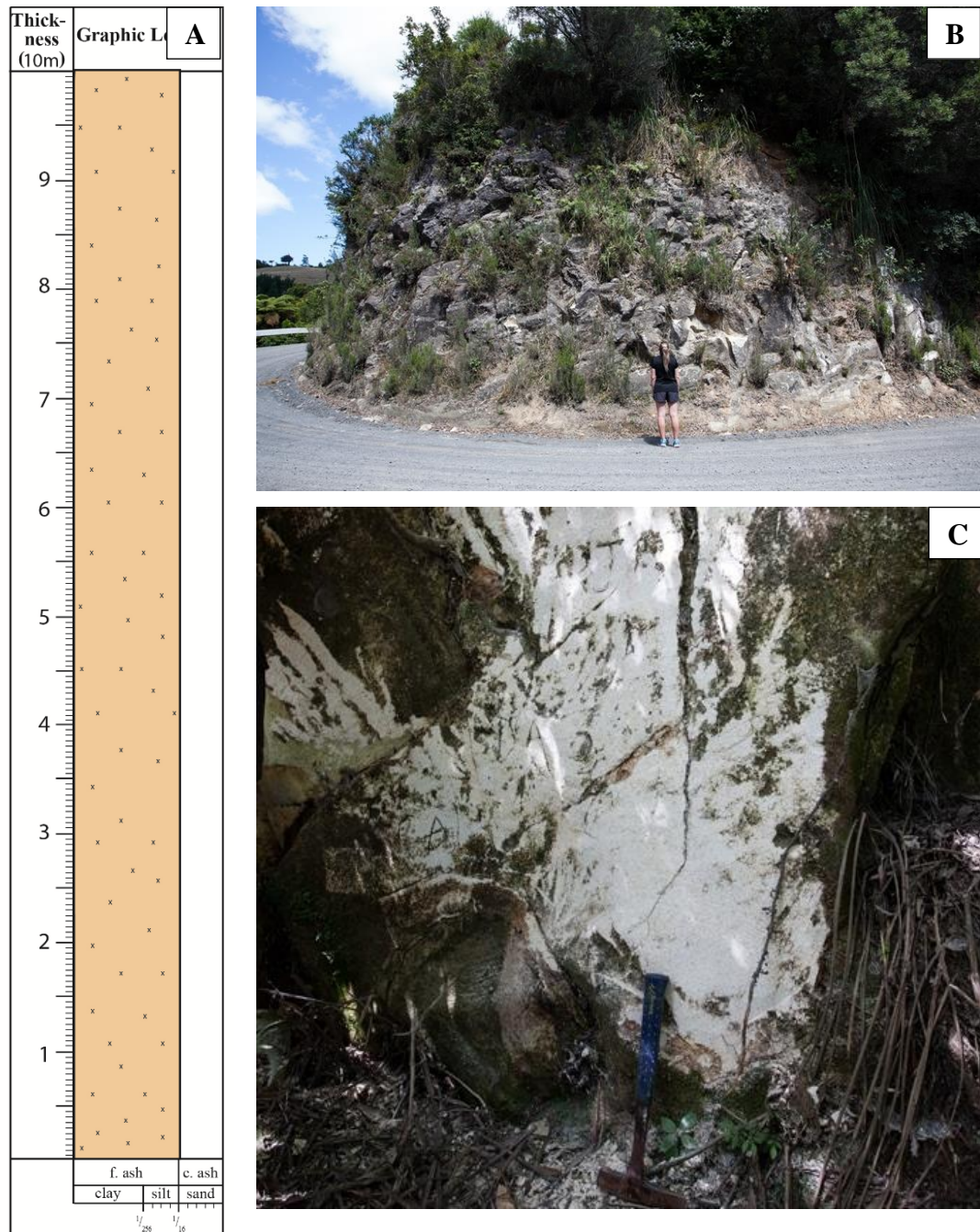


**Figure 5.2 (A) Stratigraphic log of the Hikurangi Rhyolite showing no variation vertically throughout a 10 m high section. (B) Outcrop of the Hikurangi Rhyolite at locality 2. (C) A close up image of a section showing the creamy white facies.**

## 5.4 Petrography and mineralogy

### 5.4.1 Introduction

5 thin sections were created for optical microscope analysis, 1 polished thin section for SEM, 1 polished thin sections for electron microprobe and 6 crushed powder groundmass samples for XRD analysis. Raw point counting results are included in Appendix III and XRD analysis graphs are presented in Appendix IV. These techniques were used to gain and understanding of the petrography and mineralogy of the Hikurangi Rhyolite.

### 5.4.2 Phenocrysts

As the abundance of minerals and groundmass was consistent throughout each thin section four of these were point counted to gain quantitative data. This rhyolite has a low mineral abundance with groundmass averaging 82.4% of points counted under a microscope (Table 5.1).

**Table 5.1 Results obtained from point counting 4 thin sections of the Hikurangi Rhyolite\***

Sample	2.1.1	2.2.1	2.5.1	2.6.1	Average
Groundmass	80	84.5	82.3	82.9	82.4
Quartz	4.9	2.5	5.9	6.6	4.8
Plagioclase	10.8	8.5	7.1	8.1	8.6
Biotite	3.8	4.2	4.1	2.3	3.6
Opakes	0.5	0.3	0.5	0.1	0.33
Total	100%	100%	100%	100%	100%
Margin of error**	0.4%	1%	0.8%	0.4%	0.65%
Total crystals	20%	15.5%	17.7%	17.1%	17.6%

\*All samples were analysed to 800 counts with a stage interval of 0.3 mm

\*\* Margin of error determined by recording number of uncertain counts

The mineral assemblage of the Hikurangi Rhyolite is biotite, plagioclase, quartz and rare opaques held within a dark to light brown spherulitic ground mass (spherulites averaging 5 mm) of devitrified glass (Figure 5.3). XRD analysis of the groundmass of six samples shows the Hikurangi Rhyolite contains cristobalite, resulting from hydrothermal alteration, and also identified the presence of albite and anorthite in each sample analysed. Microprobe analysis of one thin section confirmed the presence of two titanomagnetite crystals with compositions of  $\text{TiO}_2$  7 wt. % and FeO 76-77 wt. %. Other readings collected were disregarded due to low totals. One occurrence of a granophyric intergrowth was observed in sample 2.5.1 with quartz found within a plagioclase crystal.

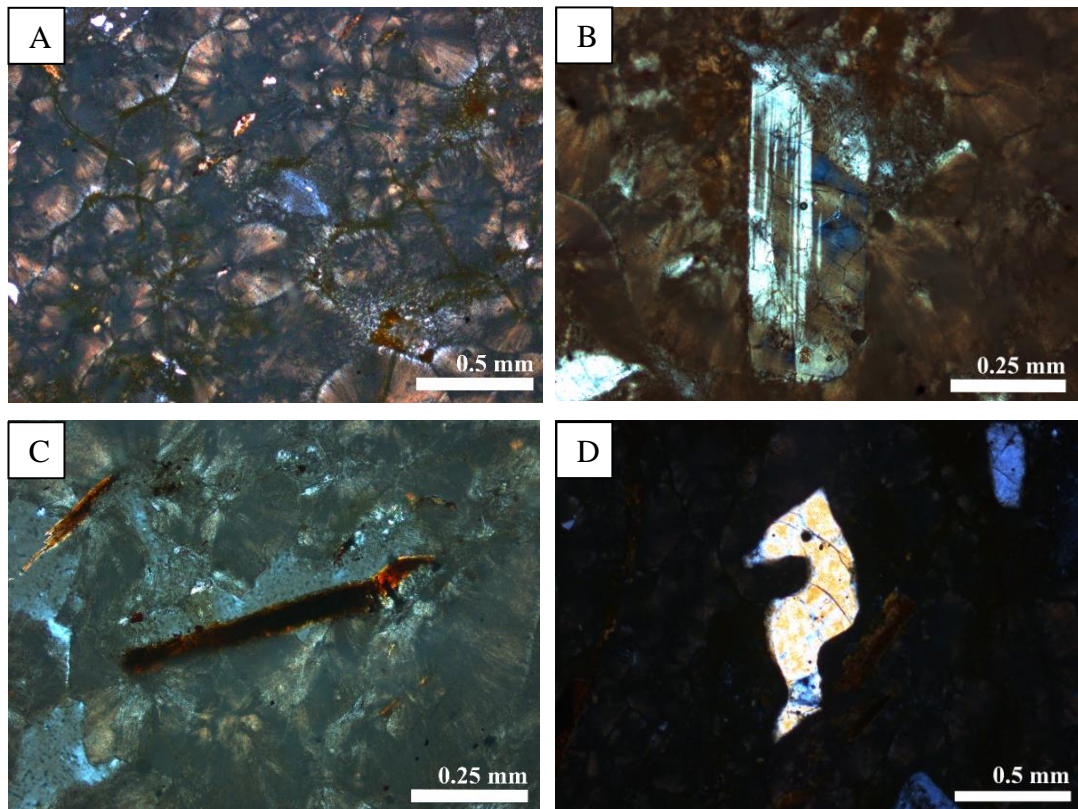


**Figure 5.3 (A) Shows spherulitic groundmass with average size spherulites. (B) Shows a plagioclase crystal displaying polysynthetic twinning. (C) Shows a larger biotite flake with an elongated shape. (D) Shows a quartz phenocryst with an embayment in the upper left hand corner of the crystal.**

Plagioclase (An<sub>33-1</sub>, Figure 5.4) was the most common phenocryst found within the Hikurangi Rhyolite with an average of 8.6% (Table 5.1). These crystals range from 0.15 - 2 mm in size with majority displaying distinct polysynthetic twinning. Analysis of one thin section under electron microprobe (Appendix V) showed both reverse and normal zoning present in plagioclase crystals (Table 5.2).

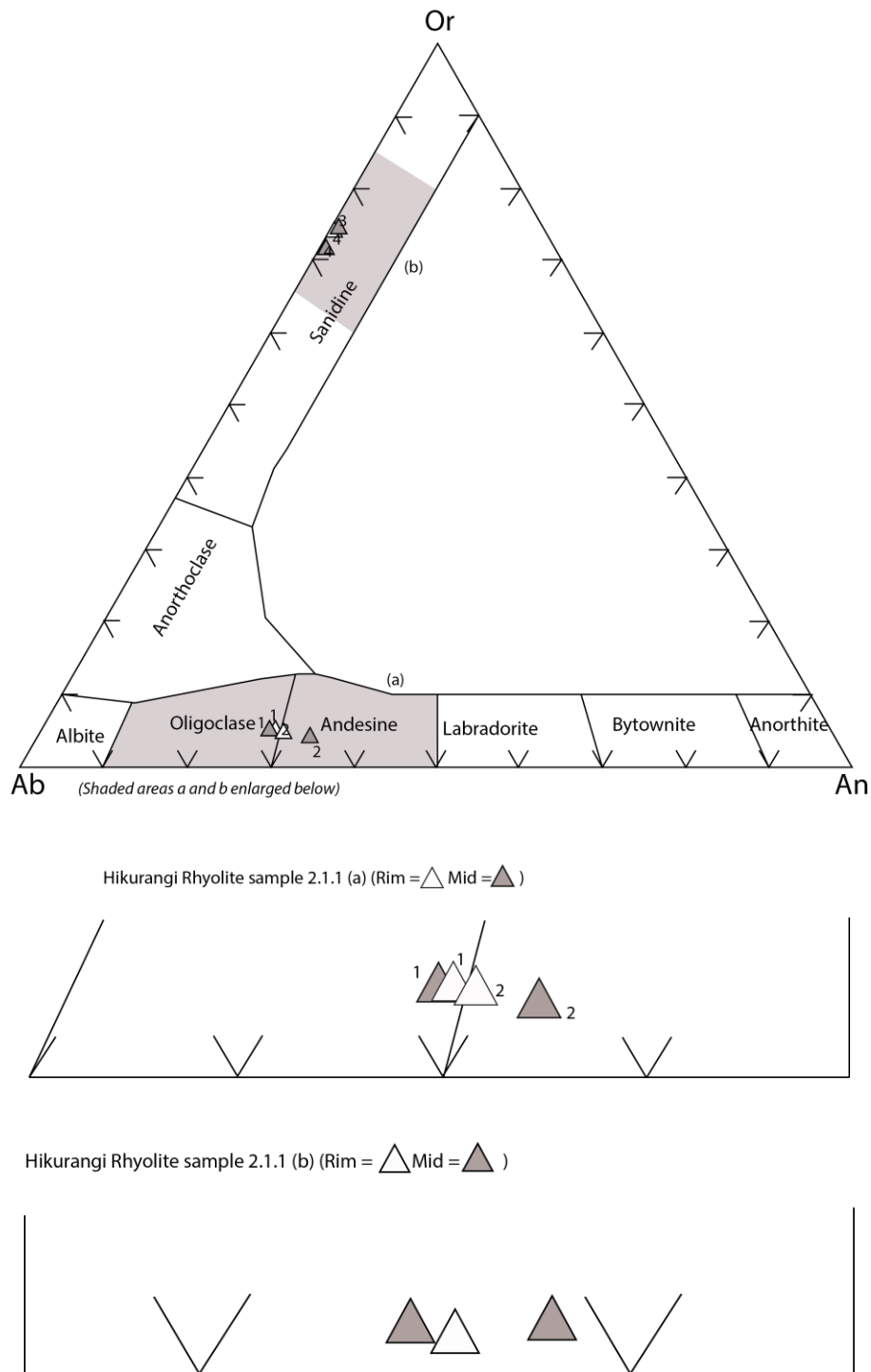


**Figure 5.4 Albite - anorthite- orthoclase ternary diagram for plagioclase in sample 2.1.1 in the Hikurangi Rhyolite. Classification according to Deer et al. (1992)**

**Table 5.2 Zoning observed in samples analysed under the electron microprobe based on CaO and Na2O values.**

Sample	CaO	Na2O	Zoning
2.1.1 – 1 – mid	5.356	7.268	Reverse zoning
2.1.1 – 1 – rim	5.525	7.211	
2.1.1 – 2 – mid	6.388	6.839	Normal zoning
2.1.1 – 2 – rim	5.721	7.137	
2.1.1 – 4 – mid	0.153	2.576	Normal zoning
2.1.1 – 4 – rim	0.136	2.671	

Biotite is consistently found throughout the Hikurangi Rhyolite and is best viewed under plan light. The biotite is elongated and appears as flakes (Figure 5.3) which are dark brown changing to a lighter brown under non cross polarized light. Less commonly biotite is present as hexagonal black crystals. The biotite is aligned and is often weathered causing an alteration in colour with red and orange colours common at the outer edges. Electron microprobe results show biotite is iron rich with a composition close to the siderophyllite composition (Figure 5.5).

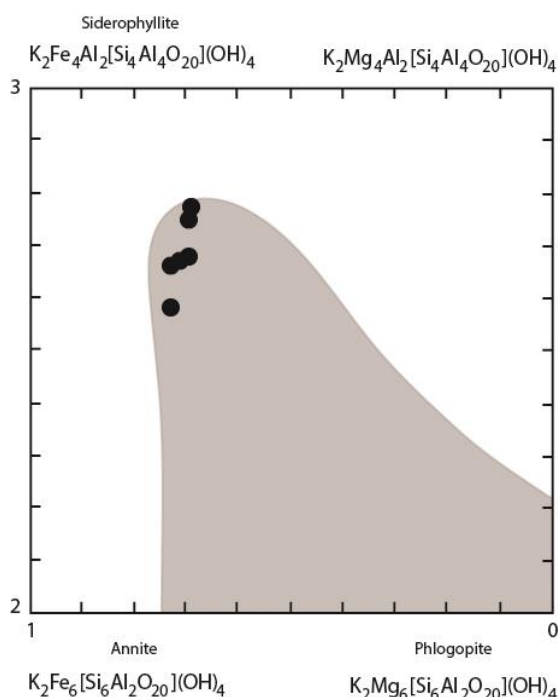


**Figure 5.5 The composition of biotite phenocrysts found within the Hikurangi Rhyolite in relation to the principle components of biotite compositions and the field in which most natural biotite lie (shaded grey) after Deer *et al.*, (1992).**

Quartz was not a common mineral in the Hikurangi Rhyolite with a lower percentage than biotite. Quartz crystals are rectangular in shape and often showed embayment surfaces with large portions of the quartz missing (Figure 5.3). The embayments are infilled by the spherulitic groundmass as well as circular inclusions which often occur where there is embayments. Quartz appeared as intact phenocrysts as well as broken fragments.

In slide 2.5.1 and 2.1.1p two granophyric intergrowth xenocrysts were found (Figure 5.6 and Figure 5.7). These types of xenocrysts are derived from granite bodies, indicating the presence of one below this rhyolite dome. These xenocrysts show an intergrowth relationship between an orthoclase (Figure 5.8) and quartz crystal. Crystals probed were determined to be orthoclase due to the granite origin and the higher formation temperatures associated with granites. These crystals are approximately 3 mm in size and are the only occurrence found within the thin sections made. The texture of this crystal has produced triangular shaped quartz which is being held within a large feldspar crystal and can be described as a graphic texture. This granophyric intergrowth shows two crystals which have crystallised at the same time. A biotite flake intrudes this crystal.

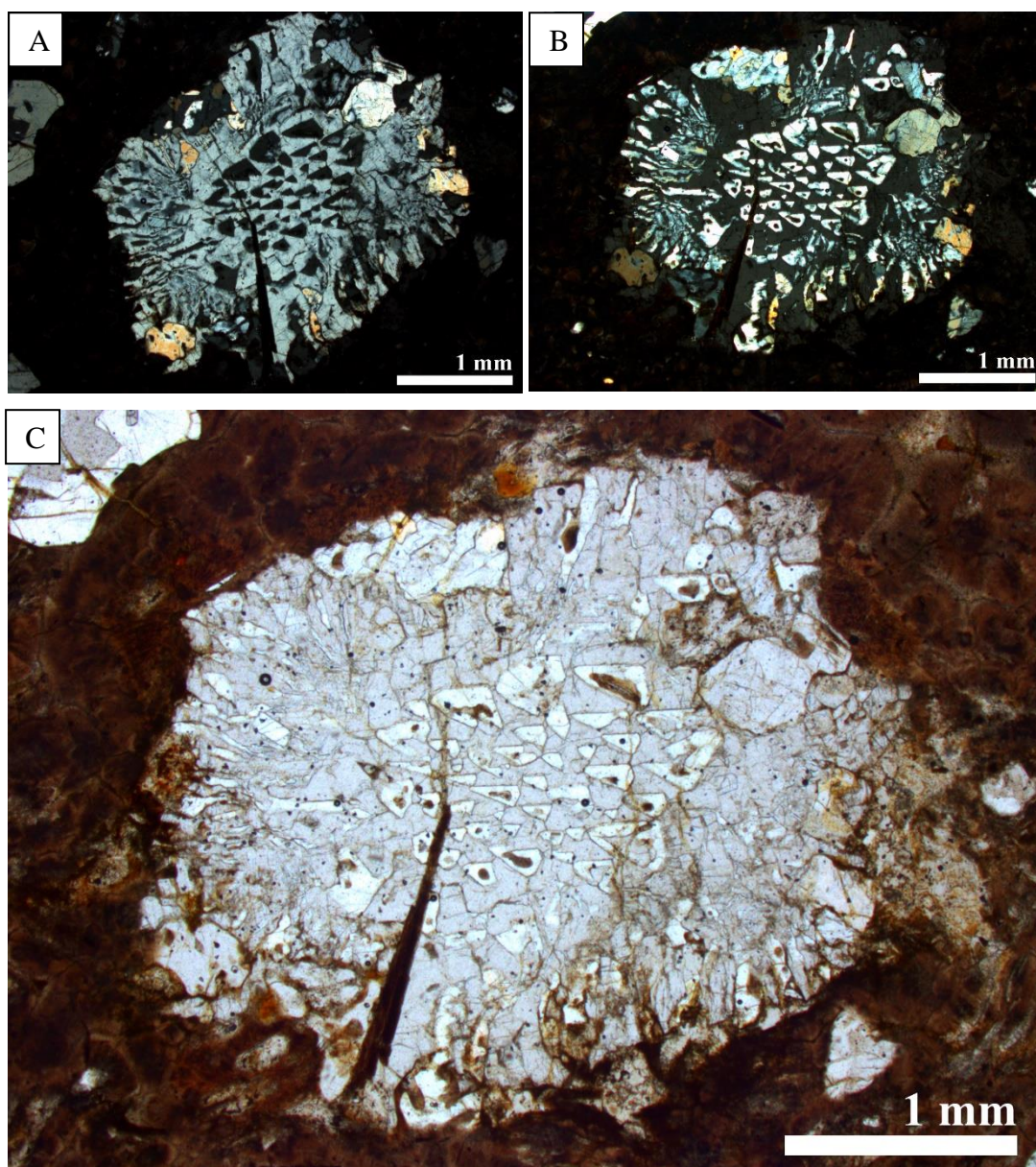


**Figure 5.6 Granophyric intergrowth crystal found within the Hikurangi Rhyolite. (A) Shows the crystal under cross polarized light with the orthoclase being visible and the quartz dark, appearing in triangle shapes. (B) Shows the crystal when the quartz is visible**

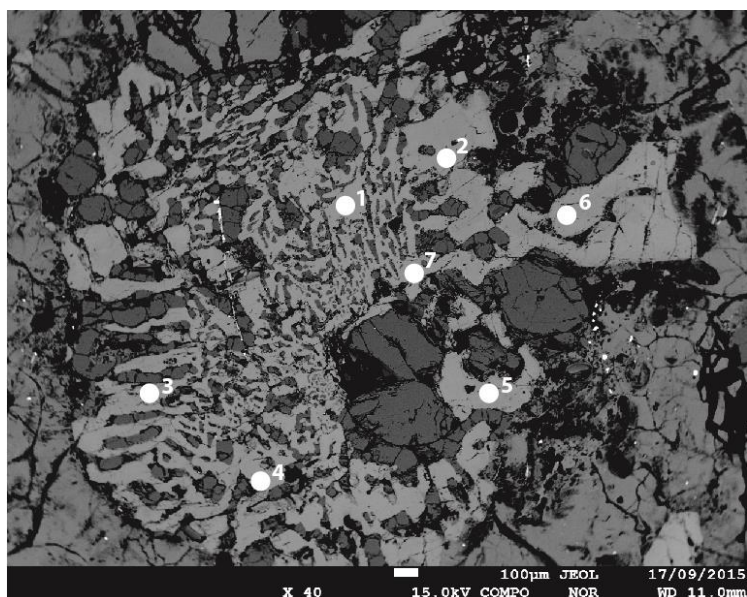


**Figure 5.7** Granophyric intergrowth crystal under the electron microscope with analysis points

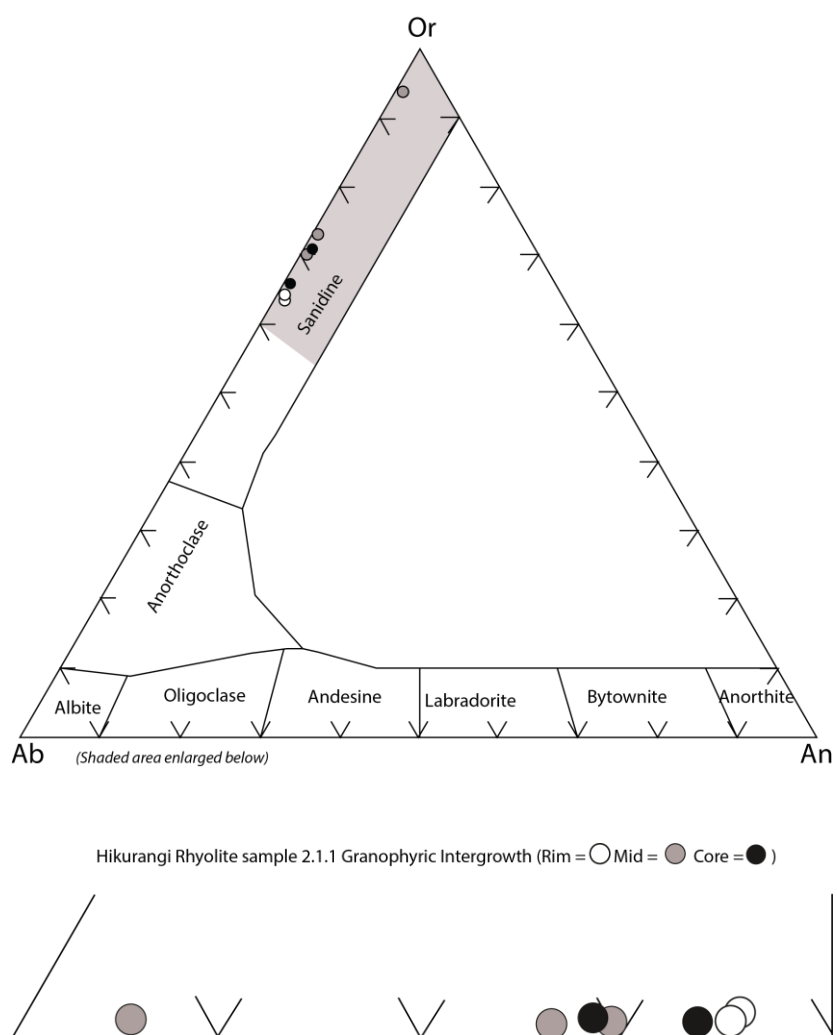


**Figure 5.8** Albite - anorthite- orthoclase ternary diagram for plagioclase in a granophyric intergrowth crystal in the Hikurangi Rhyolite. Classification according to Deer et al., (1992).

### 5.4.3 Groundmass

The groundmass of the Hikurangi Rhyolite consists of a spherulitic texture which shows the devitrification of glass. The spherulite bodies are coalesced and are comprised of aggregates of needles which appear as very fine radiating fibres. Spherulites have open clusters of widely spaced crystal fibres and are consistently present throughout each slide examined. The spherulite features are only visible under a microscope and are unable to be seen in hand sample. The SEM shows the topography of these spherulites as individual rounded masses (Figure 5.9). The spherulitic texture of the rhyolite, due to crystallisation of the volcanic glass, is observed throughout the entirety of samples on scales of 200 to 500um.

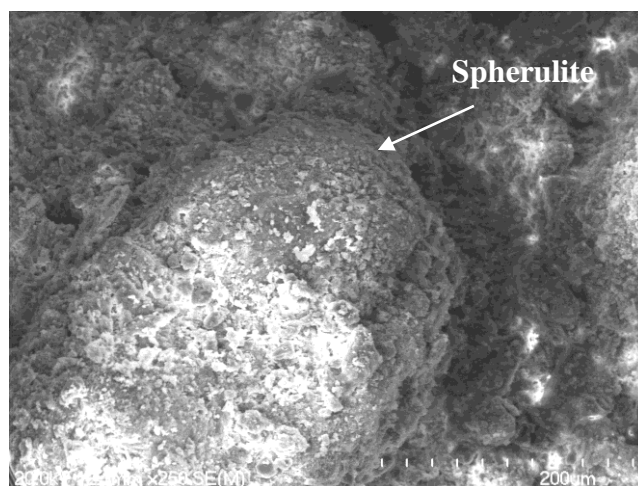


**Figure 5.9 Spherulite, in a sample of the Hikurangi Rhyolite**

Throughout the rhyolite the porous structure of the spherulites contains halloysite aggregates which have tubular and spherical geomorphologies (Figure 5.10).

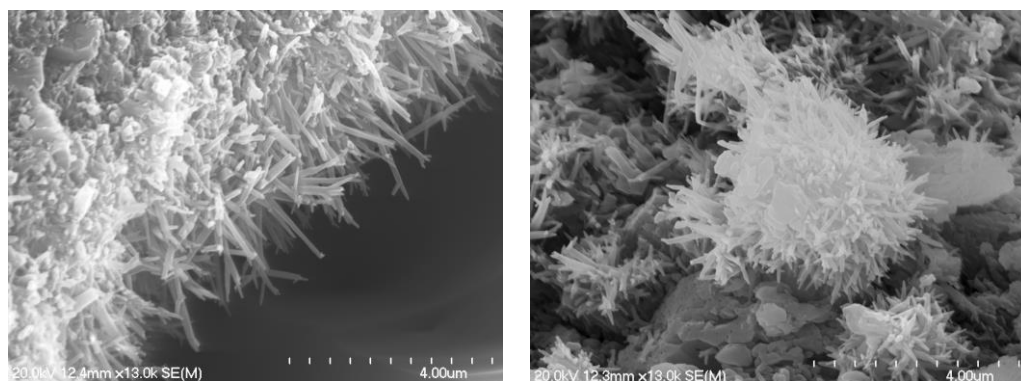


**Figure 5.10 halloysite aggregates within the Hikurangi Rhyolite groundmass**

## 5.5 Geochemistry

### 5.5.1 Introduction

Geochemical analysis was conducted on six samples across the width of the outcrop studied. These results only represent one site of the lava dome. This means trends and interpretations are limited.

### 5.5.2 Rock classification

Geochemical results allow the classification of rocks by determining the relationship between  $\text{Na}_2\text{O}$  and  $\text{K}_2\text{O}$  value against  $\text{SiO}_2$  wt. %. Analysis of the Hikurangi Rhyolite show it is strongly rhyolitic in composition (Figure 5.11).

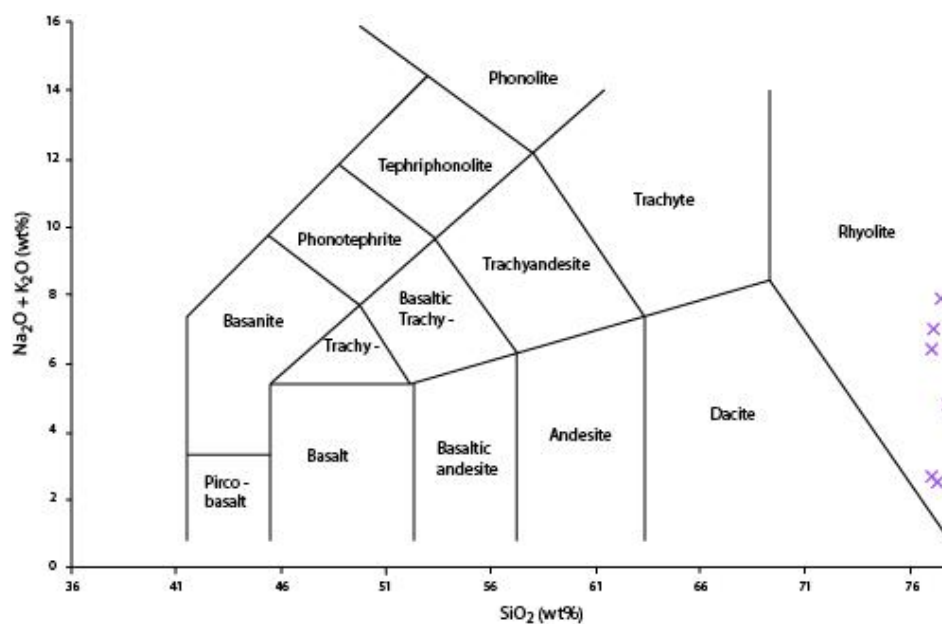
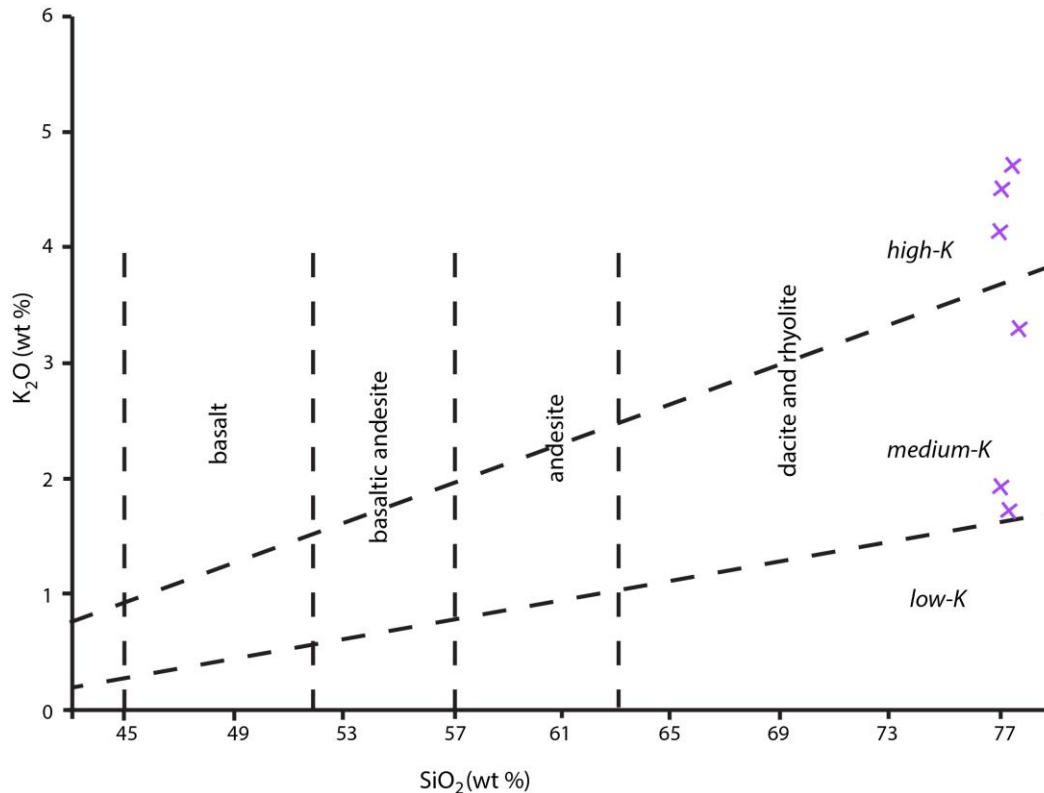


Figure 5.11 Plot of +  $\text{K}_2\text{O}$  vs  $\text{SiO}_2$  wt. % of the Hikurangi Rhyolite (based on Deer *et al.*, 1992).

Na<sub>2</sub>O and K<sub>2</sub>O vs SiO<sub>2</sub> plots are limited when classifying rhyolites. K<sub>2</sub>O vs SiO<sub>2</sub> plots eliminate problems associated with loss/gain of Na<sub>2</sub>O during secondary processes. This plot also classifies rocks into high, medium or low K<sub>2</sub>O. The Hikurangi Rhyolite is medium to high K<sub>2</sub>O (Figure 5.12).



**Figure 5.12 Plot of K<sub>2</sub>O vs. SiO<sub>2</sub> wt. % of the Hikurangi Rhyolite XRF analysis (based on Le Maitre *et al.*, 2002).**

### 5.5.3 Major element chemistry

SiO<sub>2</sub> values have a small range of 77.01 to 77.81 wt. % as rhyolite is classified as silica-rich. Each major element plot shows elements grouped closely with little variation in silica content (Figure 5.13). As this is a spherulitic rhyolite with a low phenocryst content (15-20%) there are no significant overall trends, however looking at different phenocryst types abundances shows variation. Plagioclase (Al<sub>2</sub>O<sub>3</sub> and Na<sub>2</sub>O) and biotite (K<sub>2</sub>O and Fe<sub>2</sub>O<sub>3</sub>) are found throughout this rhyolite with varying abundances (7-10 % and 2-4 % respectively) which is reflected by the varying wt. % shown in these major elements. MgO and CaO show little variation as they are not abundant in the phenocrysts.

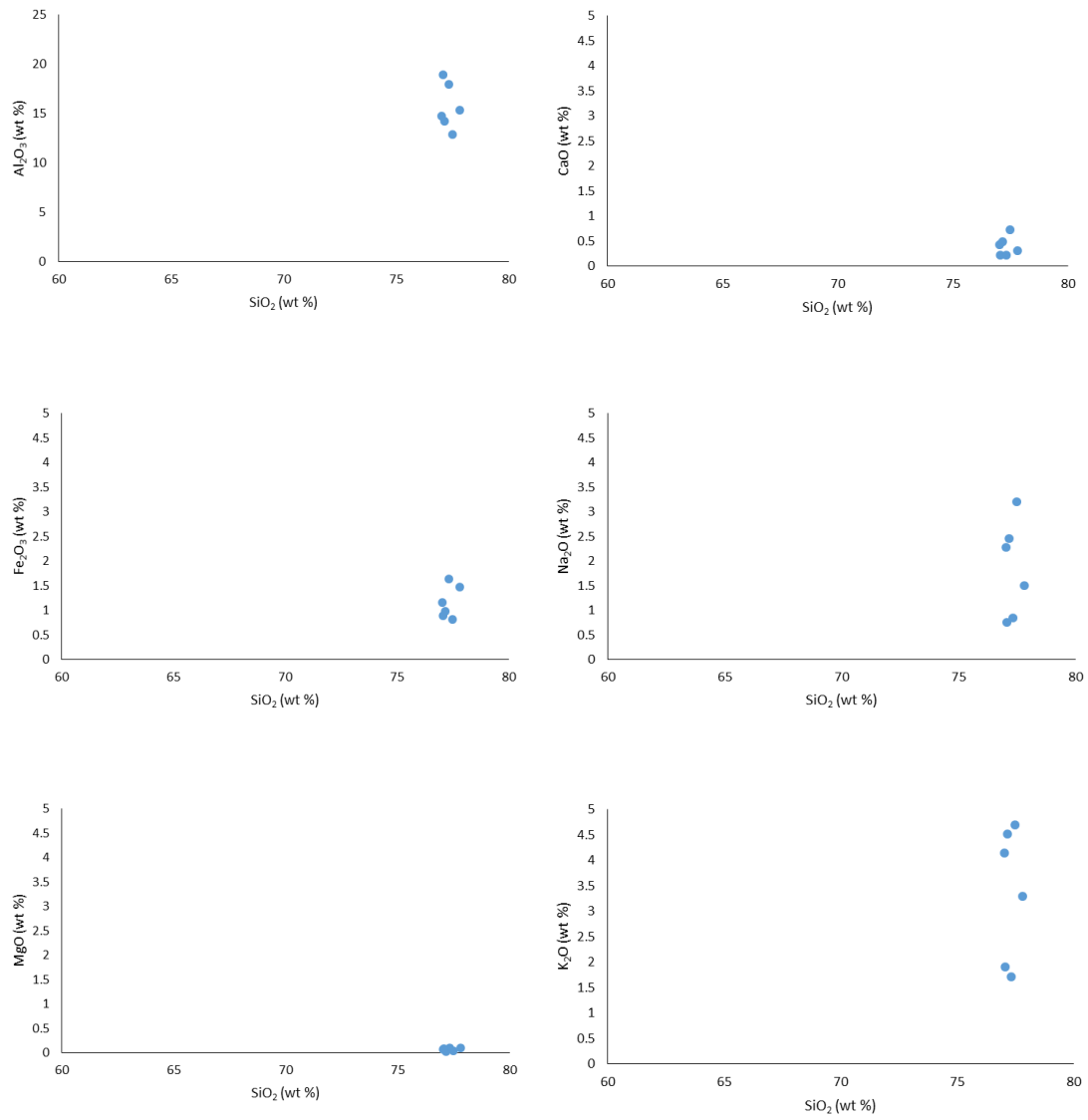


**Figure 5.13 Harker variation diagrams of selected major elements in the Hikurangi Rhyolite.**

#### **5.5.4 Trace element chemistry**

Compositions of trace elements were determined through XRF for six samples (the same as those analysed for major elements). 29 trace elements (in ppm) were analysed (Appendix VI). Trace element Harker plots can be used to help determine the geochemical processes that may have occurred within the chamber. Trace elements were plotted against  $\text{SiO}_2$  to determine any trends as well as incompatible elements (Figure 5.14).

Trends observed in trace elements against  $\text{SiO}_2$  reflect those observed in major elements. This is due to trace elements also being controlled by the crystal content in the melt. Rb and Sr are both elements that are strongly influenced by plagioclase therefore they show similar trends to those observed in major elements  $\text{K}_2\text{O}$  and  $\text{Al}_2\text{O}_3$ . Zr shows a concentrated abundance between 75-110 ppm with a clustered relationship against  $\text{SiO}_2$ . Ba is also clustered with 630-700 ppm. Rb vs Sr shows a positive relationship. The opposite trend is seen in Rb vs Zr where Rb decreases as Zr increases. Ba vs Rb and Ba vs Zr show steady relationships where Ba remains at a relatively constant ppm while Rb and Zr increases.

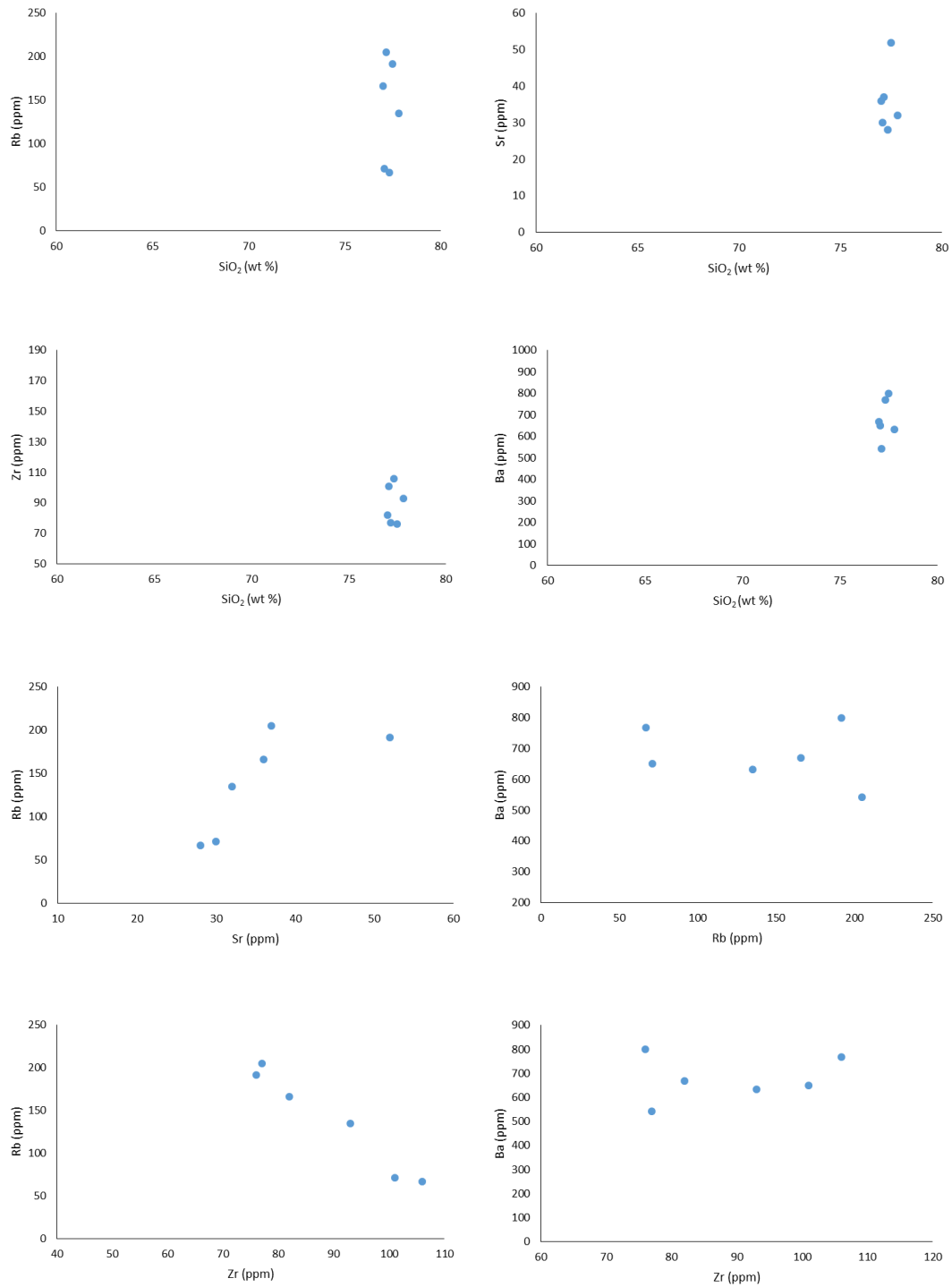


**Figure 5.14 Harker variation plots of trace element geochemistry from XRF results of the Hikurangi Rhyolite.**

## **5.6 Dating**

### **5.6.1 Introduction**

The Homunga Rhyolite is part of the Minden Rhyolite subgroup and includes four lava dome complexes including the Hikurangi Rhyolite. Two other domes belonging to the Homunga Rhyolite have been dated by U-Pb methods by Vincent (2012); Whale Bone Bay Dome with an age of  $5.58 \pm 0.21$  Ma; and Shark Bay Dome with an age of  $4.85 \pm 0.36$  Ma. K-Ar ages of  $5.30 \pm 0.12$  Ma and  $5.28 \pm 0.16$  Ma were determined by Brathwaite and Christie (1996) for the Ruahorehore dome.

### **5.6.2 Zircon age results**

87 spots on zircons were initially analysed, however, 6 spots on zircons that were considerably older than the general cluster were excluded from the age calculation (full list of ages obtained are presented in Appendix VIII). The remaining 50 spots were used to determine the age. The Hikurangi Rhyolite showed a range of zircon ages with an average of approximately 5 Ma (Figure 5.15). Ablation of zircons through LA-ICP-MS provided a maximum eruption age of  $4.53 \pm 0.13$  Ma. This age relates well with the other Homunga Rhyolite domes showing a progression in age of the domes which become younger southwards.

Outliers were determined with the majority being mid to Early Miocene (10.1 Ma, 15.4 Ma, 15.5 Ma, 15.5 Ma, and 16 Ma) and one producing a Mid Eocene age of 46.1 Ma. These zircons are thought to be derived from different sources to those used for calculating the Hikurangi Rhyolite age. The potential origin of these older zircons are assessed in Chapter Six.

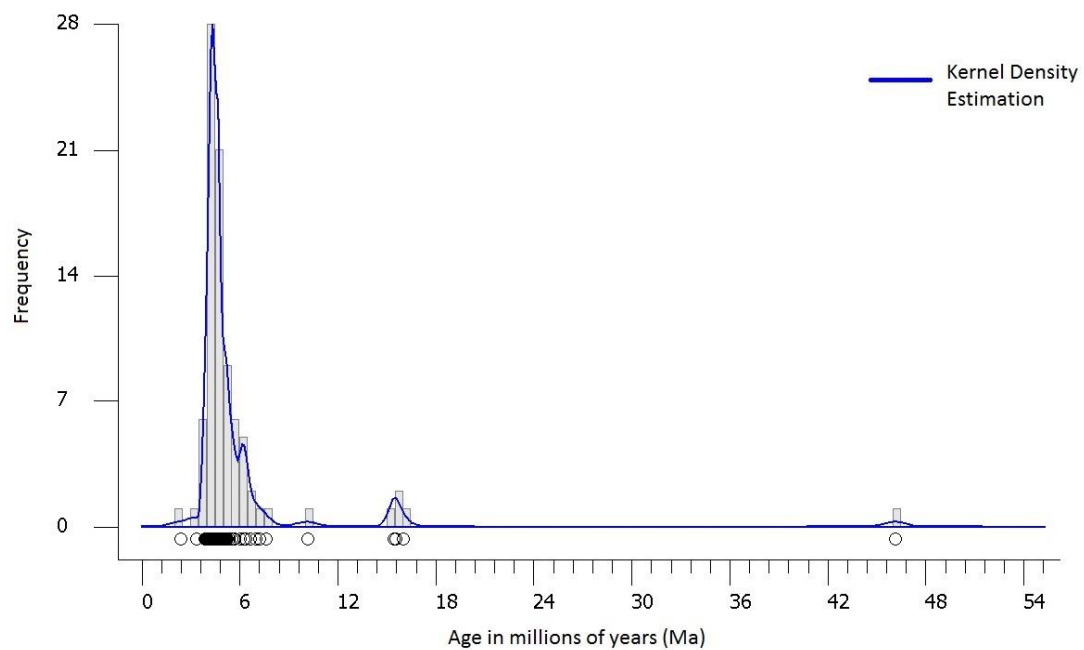


**Figure 5.15** The distribution of ages of Hikurangi Rhyolite zircon crystals that were ablated by LA-ICP-MS.

## 5.7 Discussion

### 5.7.1 Spherulite growth

The Hikurangi Rhyolite has a dark to light brown spherulitic groundmass with spherulites averaging 5 mm in diameter. Spherulites show a single growth layer of radiating feldspar and quartz growth with a granular core of a mixture of quartz and feldspar (Seaman *et al.*, 2009).

As most liquids do not have a long range order of their atoms, where crystals do, the change from liquid to solid is a discontinuous process. Spherulites occur where there is a lower temperature but higher undercooling temperature (Vernon, 2004), as shown in Figure 5.16.

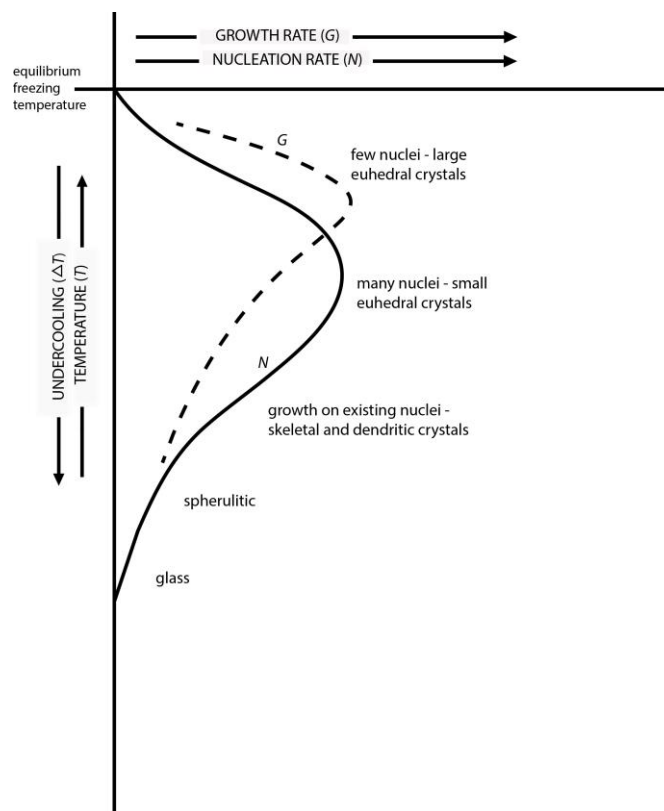


**Figure 5.16 Nucleation (N) and growth rate (G) curves of variation with increasing undercooling showing the general trend in grainsizes and shapes produced at each stage (Vernon, 2004).**

Undercooling refers to crystal-free liquids which have cooled below the temperature required for crystallisation under near-to-equilibrium conditions (Fowler *et al.*, 2002). Under these conditions the growth rate of crystals is rapid

and diffusion in the liquid is slow. This rapid growth causes the low melting constituents that are adjacent to the crystallite-melt boundary to be rejected, increasing the local undercooling. Any protrusions on the crystallite project into the area of undercooling and are grown preferentially causing an array of fibrous crystals (Fowler *et al.*, 2002). Spherulites tend to nucleate on a crystal or alternatively on a vapour bubble (Shelley, 1993).

Spherulites can be formed through either primary magmatic crystallization or secondarily due to devitrification. Primary crystallization is the most common type and shows a progression of morphologies in spherulites as they become further from the cooling contact (spherulites become large away from the cooling contact). If primary crystallisation was the cause of spherulites in the Hikurangi Rhyolite the small scale (averaging 5 mm) of spherulites would indicate they formed close to the cooling contact. Secondary spherulites by devitrification form after primary cooling and show no relationship to cooling contacts (Fowler *et al.*, 2002). Devitrification occurs due to glass being an unstable material which is readily replaced forming a microgranular mass of small grains of feldspar and silica in silicic glassy rocks (Winter, 2014). Unfortunately due to limited samples studied clear relationships between spherulites and cooling surfaces are unable to be determined. The open clusters of widely spaced crystal fibres seen in the Hikurangi Rhyolites spherulites indicates high formation temperatures of approximately 700°C (McPhie *et al.*, 1993).

### **5.7.2 Evidence of deep basement geology**

Two granophyric intergrowth xenocrysts were found within the Hikurangi Rhyolite. These were determined to be granophyric intergrowths based on their distinct texture. These xenocrysts have a bulk composition which is close to the melting minimum in the orthoclase-albite-quartz-H<sub>2</sub>O system, consisting of approximately equal proportions of quartz, K-feldspar and Na-feldspar component (Deer *et al.*, 1992). The results of probing one granophyric intergrowth xenocryst show an intergrowth relationship between an orthoclase (Figure 5.6) and quartz crystal. As the rate of crystallisation affects the size of granophyric intergrowths the 2 mm sized xenocrysts found in the Hikurangi Rhyolite show a slower cooling process (Barker, 1970).

Such intergrowths are common in many types of acid igneous rocks and metamorphic rocks. The closely intergrown relationship of quartz and orthoclase in these granophyric intergrowths are typical of a granophyre origin (Deer *et al.*, 1992). Granophyric intergrowths of quartz-feldspar are reliable indicators of melting and/or remelting in high temperature environments such as contact aureoles or multiphase intrusions.

This is not the first occurrence of a pluton to have been identified within the CVZ, as subvolcanic gabbro, diorite, granodiorite and tonalite plutons are exposed in the northern CVZ (Booden *et al.*, 2012). Great Barrier Island contains volcanic and shallow plutonic intermediate rocks belonging to the Coromandel group (Skinner, 1986). The plutonic rocks which occur as andesite and quartz-porphyry dikes have been dated through K-Ar methods providing ages between  $16.3 \pm 0.3$  and  $18.5 \pm 0.4$  Ma (Adams *et al.*, 1994). However this is the first occurrence of a plutonic body in southern CVZ. Due to the progression in age of volcanism in the CVZ, becoming younger southwards, it is likely the plutonic body below the Hikurangi Rhyolite dome is closer in age to volcanism in the Waihi area. The presence of these crystals showing there is a granite body below this dome helps with the interpretation of the Waihi Basin caldera. No evidence has been previously found for a magma body in surface geology or gravity data (Smith *et al.*, 2006).

### **5.7.3 Mineralogical and geochemical relationship with other related rhyolite domes in the CVZ**

The plagioclase crystals that were found to be of oligoclase and andesine composition are consistent with the microprobe results obtained by Vincent (2012) on the Whale Bay Dome, which also belongs to the Homunga Rhyolite group. The Hikurangi Rhyolite plagioclase crystals which were found to be in this classification were An<sub>27-33</sub> which is similar to the An<sub>19-32</sub> range in the Whale Bay Dome. Sanidine was found in two plagioclase crystals of the Hikurangi Rhyolite. Phenocrysts of sanidine were also found in the Bowentown Rhyolite in this study (Chapter 3). Sanidine has been previously identified in the Hot Water Beach Dome which was confirmed by XRD analysis, and was thought to have occurred either in spherulites, intergrown with cristobalite, or in the groundmass (Moore,

2011). The sanidine that was found in the plagioclase crystals in the Hikurangi Rhyolite may be due to the microprobe hitting the spherulitic groundmass instead of the phenocryst.

XRD analysis of the Hikurangi Rhyolite showed cristobalite resulting from hydrothermal alteration. Vapour phase alteration causes silica to be added due to the crystallisation of quartz inside vesicles causing an increase in silica content. Shark Bay and Whale Bay domes have both been identified as being hydrothermally altered with high  $\text{SiO}_2$  wt. % (Vincent, 2012). The Homunga Rhyolites which have had XRF analysis (Hikurangi, Shark Bay and Whale Bay domes) as well as the Bowentown Rhyolite all have similar  $\text{SiO}_2$  content with varying  $\text{K}_2\text{O}$  (Figure 5.17). Hydrothermally altered rhyolites can also be high in K due to minerals such as plagioclase being altered to sericite or adularia.

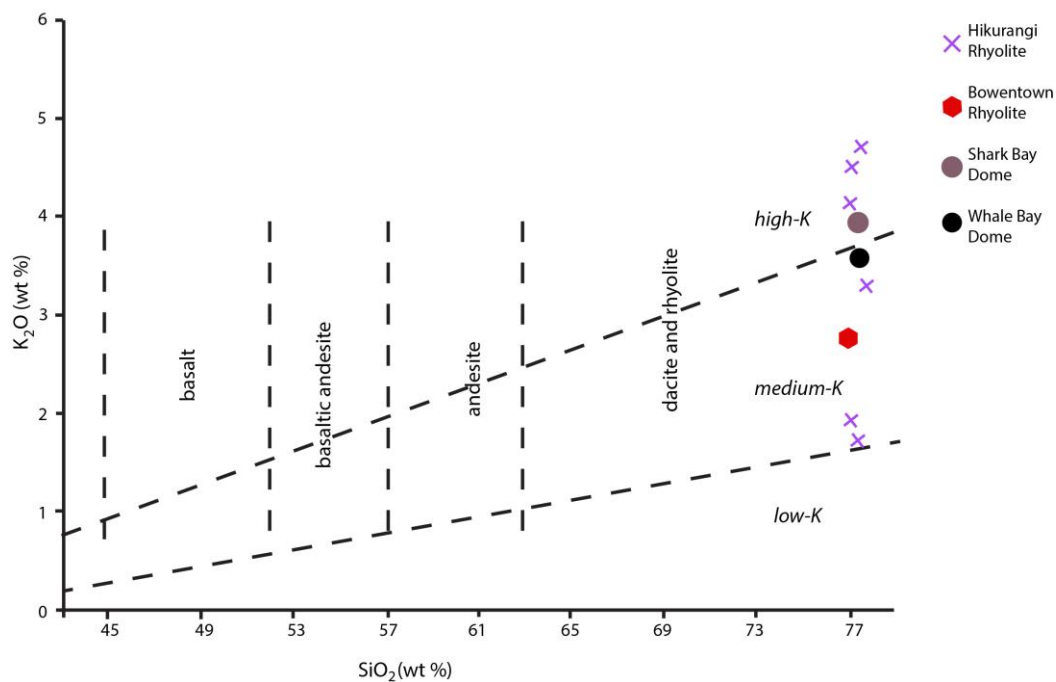


**Figure 5.17** Plot of  $\text{K}_2\text{O}$  vs.  $\text{SiO}_2$  wt. % of the Homunga Rhyolite domes and Bowentown Rhyolite. Data for Shark Bay Dome and Whale Bay Dome from Vincent (2012).

# Chapter Six

## Discussion

---

### 6.1 Introduction

The physical and magmatic processes associated with the Corbett and Ratarua ignimbrites and the Hikurangi Rhyolite have been previously discussed in Chapter 3, 4 and 5 respectively. The purpose of this discussion chapter is to show the relationships between these units. This discussion will present; possible vent locations for the Corbett Ignimbrite, the age of CVZ volcanics and the origin of inherited zircons, and the volcanic geological history of the eastern Waihi area.

### 6.2 Possible vent locations for the Corbett Ignimbrite

The internal stratigraphy and eruption and emplacement processes of the Corbett Ignimbrite have been assessed in Chapter 3, however the vent location for the eruption is still not constrained. Although it is not possible with the present information known for the Corbett Ignimbrite to determine where the vent location is several different possibilities are assessed.

#### 6.2.1 A southern source near the Bowentown Rhyolite

Brathwaite and Christie (1996) suggested that the source for the Corbett Ignimbrite could be in the vicinity of the Bowentown Heads, approximately 16 km south of the type locality. This is due to the ignimbrite outcrop distribution being restricted to the eastern Waihi area and this presence of a rhyolitic centre to the southeast. U-Pb dating of zircons in both the Corbett Ignimbrite and Bowentown Rhyolite show there is no relationship between the ages. The Corbett Ignimbrite has an age of  $6.04 \pm 0.32$  Ma whereas the Bowentown Rhyolite has a considerably younger age of  $2.09 \pm 0.34$  Ma. The significant difference between these two ages shows that the Corbett Ignimbrite could not have been sourced from a volcanic centre associated with the Bowentown Rhyolite.

### 6.2.2 Waihi Caldera

Although the distribution of the Corbett Ignimbrite is constrained to eastern Waihi, it is the oldest ignimbrite within the Ohinemuri group, thus part of the original surface deposit of this ignimbrite may now be buried by younger deposits, including the Owaharoa and Waikino ignimbrites, or eroded. The Corbett Ignimbrite is found predominantly within the proposed boundary of the Waihi Caldera suggesting its vent may be sourced from the caldera. Brathwaite and Christie (1996) inferred that the Corbett Ignimbrite overlies lake sediments of Romanga Formation (Figure 6.1). The presence of this sedimentary lake deposit, below the Ohinemuri Subgroup ignimbrites, suggest that a depression existed prior to the deposition of all three ignimbrites, which then represent later eruptions of material from a local source (Smith *et al.*, 2006).

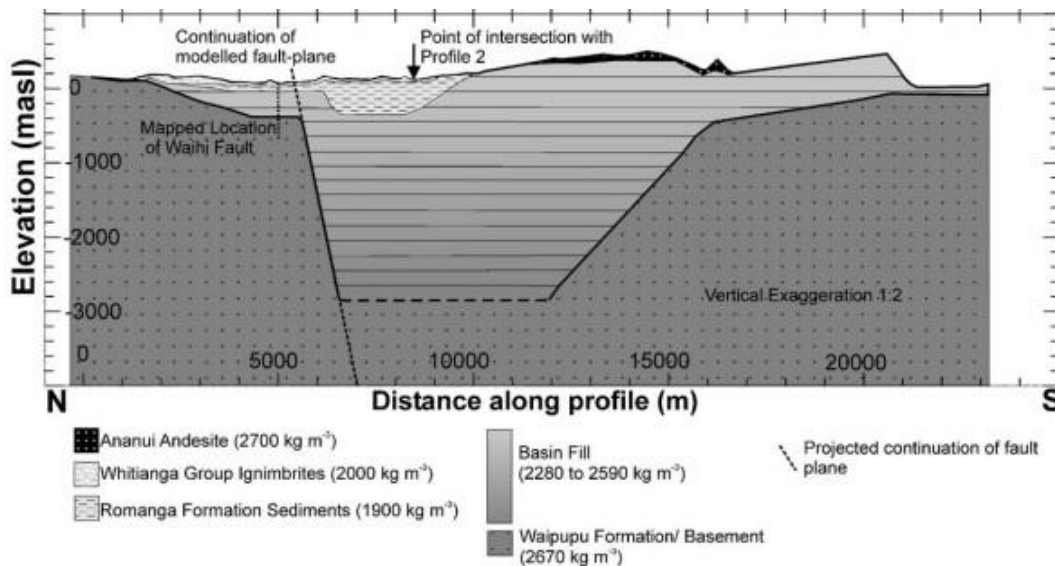


**Figure 6.1** Cross section of the Waihi Caldera showing the relationship between the different units found in the Waihi area (Smith *et al.*, 2006).

The Corbett Ignimbrite was originally attributed to a Late Pliocene age estimated to be between Waipipian to Mangapanian based on a K-Ar age of 4.5 to 4.0 Ma from Ananaui Andesite plugs that intruded underlying lake sediments of the Romanga Formation (Brathwaite & Christie, 1996). However the U-Pb determined age of  $6.04 \pm 0.32$  Ma for the Corbett Ignimbrite implies that the age of the Romanga Formation may be older than suggested above, if indeed Brathwaite and Christie (1996)'s inferred stratigraphic position of the Corbett

Ignimbrite above is correct. Brathwaite and Christie (1996)'s study identifies a hornblende-bearing pumice lapilli that overlies lake and fluvial sediments in a drill core, as well as an ignimbrite overlying lacustrine siltstones along Athenree Gorge. This pumice lapilli was implied to be the Corbett Ignimbrite but was never confirmed. Furthermore the fluvial and lacustrine sediments along Athenree Gorge have not been attributed to the Romanga Formation and may alternatively be older lake sediments predating the Romanga Formation.

The Owharoa Ignimbrite has a U-Pb age of 3.79 Ma (Vincent, 2012) and the younger Waikino Ignimbrite has a U-Pb age of 3.48 Ma (Julian, 2016), showing a large age difference between the ages of these units, relative to the older Corbett Ignimbrite. For the Corbett Ignimbrite to have been sourced from the caldera the caldera would have had to be active for a minimum of 2.61 million years, which is a significant period of time. The currently active TVZ shows calderas with activity spans from 150 to 600 ka (Wilson *et al.*, 1984). This disparity in ages suggests it is likely the Corbett Ignimbrite source is elsewhere.

### **6.2.3 Tunaiti Caldera**

The Late Miocene age of the Corbett Ignimbrite suggests its source may be located to the north, as the CVZ becomes progressively younger towards the south. Approximately 11 km north of the Corbett Ignimbrite type section is the southern edge of the Tunaiti Caldera (Figure 6.2). This caldera contains a Late Miocene volcanic and pyroclastic sequence comprised of; precaldra andesite and dacite lavas; caldera-forming dacitic eruptions and interbedded plinian tuffs; moat deposits of rhyolitic volcanics, lake sediments and postcollapse mesobreccias; intracaldra biotite rhyolite domes and flows; post caldera hornblende rhyolites dikes and lavas; and postcaldra dacite lavas (Briggs & Fulton, 1990).

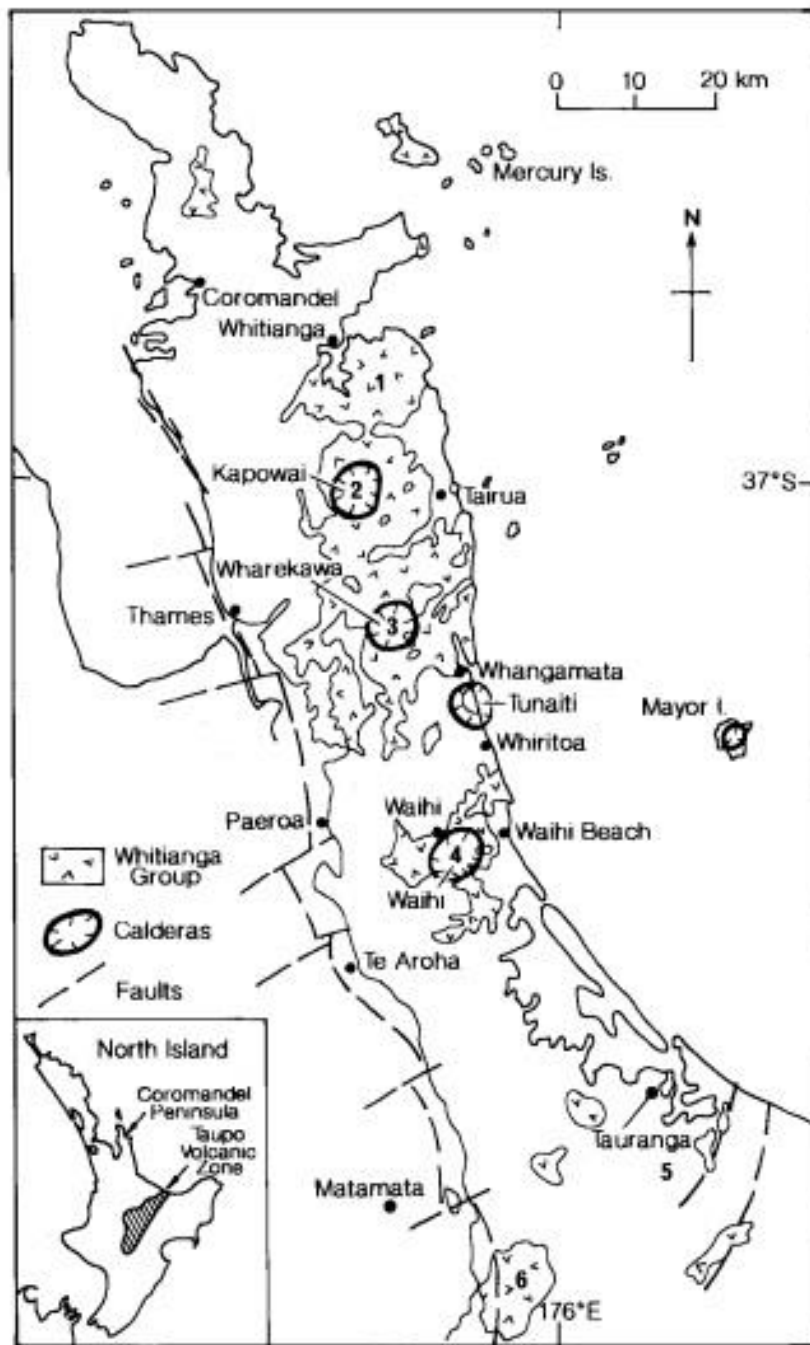


**Figure 6.2 Map of the Coromandel Volcanic Zone showing the Whitianga Group distribution and associate calderas (Briggs & Fulton, 1990).**

Papakura Bay Dome is one of the intracaldera rhyolite lava domes and was originally dated through K-Ar methods by Takagi (1995) with an age of  $5.45 \pm 0.15$  Ma and was later dated by Vincent (2012) with a U-Pb age of 5.51 Ma. These ages, which are in fair agreement with each other, are younger than the Corbett Ignimbrite ( $6.09 \pm 0.34$  Ma). The major outflow sheet of the Tunaiti caldera was identified as the dacitic Waimama Bay lenticulite by Briggs and

Fulton (1990) who described it as being crystal-rich with plagioclase, orthopyroxene, augite, hornblende, biotite, quartz, titanomagnetite, and ilmenite. This shows a similar crystal assemblage as the Corbett Ignimbrite, except that the Corbett Ignimbrite does not contain biotite. Although the Waimama Bay lenticulite was identified as the main caldera-forming eruptive unit for the Tunaiti Caldera its dacitic composition is not consistent with the later intracaldera resurgent rhyolitic dome lavas. The Corbett Ignimbrite shows a transition from andesitic to rhyolitic volcanism and may have formed the transition into rhyolitic volcanism in the Tunaiti Caldera before the formation of the Papakura Bay Dome.

Although the Corbett Ignimbrite is not identified in this region it may be buried by younger deposits, or alternatively due to its predominantly unwelded nature it may have been eroded.

#### **6.2.4 Volcanic source east of Waihi**

The Corbett Ignimbrite is constrained to the eastern Waihi area suggesting it may have a vent source to the east of Waihi. Erosional shoreface retreat occurred during the post-glacial marine transgression, which occurred c. 12.0-6.5 ka (Bradshaw *et al.*, 1994). During this time much of the east coast of the CVZ became inundated forming the shelf. Sea level stabilised to its present day position 6.5 ka. The CVZ has a steep coastline and a narrow (20-30 km) continental shelf dominated by Tertiary volcanic rocks, predominantly ignimbrites, rhyolites and andesites (Skinner, 1986). These deposits are now covered by Quaternary tephra which is predominantly sourced from the TVZ. There are limited studies on volcanic sources in this submerged coast. It is probable that other caldera structures occurred to the east of Waihi with a centre being the possible source for the Corbett Ignimbrite.

### 6.3 Ages of CVZ volcanics

Volcanic activity began in the CVZ during the Early-Mid Miocene approximately 18 Ma and transitioned southwards (Smith *et al.*, 2006) becoming younger (Figure 6.3). The earliest recorded rhyolitic volcanism occurred at 12 Ma and has since dominated the structure of volcanism in the North Island (Booden *et al.*, 2012). Volcanism in the wider CVZ throughout 9-7 Ma was bimodal with basalt to basaltic andesite/rhyolite events as well as major caldera collapse, ignimbrite eruptions and post caldera andesite eruptions (Adams *et al.*, 1994). Volcanism in the CVZ from 7-2 Ma was dominated by rhyolite domes, ignimbrites, pumice breccia and associated breccias which form the subgroups of the Whitianga group within the Waihi area. Waihi is dominated by Late Miocene to Early Pliocene volcanics with the southern extent becoming Late Pliocene to Early Pleistocene. Active volcanism in the CVZ ended approximately 1.5 Ma, with volcanism transitioning into the TVZ (Smith *et al.*, 2006).

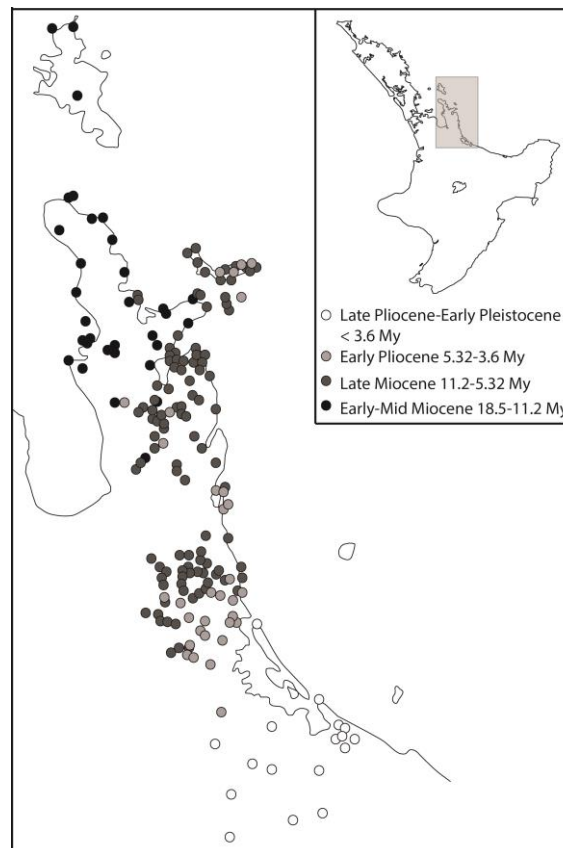


**Figure 6.3** Map of previously dated igneous rocks of the CVZ showing age ranges from Early-Miocene to Late Pliocene-Early Pleistocene (Vincent, 2012).

### 6.3.1 Origin of inherited zircons

As described in Chapters 3 (section 3.7.2), 4 (section 4.7.2) and 5 (section 5.6.2), most samples dated contained zircons that significantly predate the determined age of crystallisation. The U-Pb age determined is the crystallisation age of the zircon, which may occur in the magma chamber several hundred thousand years before the eruption occurs. Averaging the most common ages provides a reliable representation of the maximum eruption age. The Corbett Ignimbrite, Bowentown Rhyolite and Ratarua Ignimbrite all contain antecrysts. These antecrysts are recycled from earlier stages of the magma system. The oldest zircons, which were Jurassic in age, are derived from the underlying basement. However the origins of zircons that have ages older than those possible due to antecrysts but younger than the Jurassic basement also need to be accounted for.

Zircons were identified that were too old to be derived from relatively young magmas associated with volcanism in Waihi, but still within the period of volcanism for the CVZ (i.e. <18 Ma). These zircons may be xenocrysts derived from detrital zircons from sedimentary sediments which originated in northern CVZ, where there are older CVZ volcanics.

Vincent (2012) also found zircons of Late Cretaceous to Early Miocene age when studying zircon ages in a range of rhyolitic lavas and ignimbrites throughout the CVZ. This research suggested these zircons were potentially derived from the Northland Volcanic Arc, provided they were able to be incorporated into the volcanics within the CVZ (Vincent, 2012). The Northland Volcanic Arc was active from 23 – 15 Ma (Cole *et al.*, 1886) and included andesite stratovolcanoes with lesser basalt and rhyolite. The Waitemata Group is found in northern CVZ and contains the Early Miocene Colville Formation. This is a mass flow deposit from northwest of the CVZ with an estimated age of Late Oligocene to Early Miocene based on taxa found in the formation (Grant-Mackie & Moore, 1970) and may be the source for zircons of these ages. The Northland Allochthon is a massive gravity deposit which may be included in the Colville Formation. The Northland Allochthon contains fossils providing evidence of rocks derived from the continental shelf, slope and deep-ocean floor which may be a source for zircons of Late Cretaceous to Early Miocene ages (Vincent, 2012) which have since been reworked and transported to southern CVZ.



### **6.4.1 Volcanic sequence in eastern Waihi**

The formation of the volcanics in Waihi spans from the Early Miocene until the Early Pleistocene, with key volcanic events contributing to the landscape. Throughout this period of volcanism there was a transition from dominantly andesitic to rhyolitic volcanism with the units included in this study showing this transition. There were four key volcanic periods within Waihi; andesite volcanism, explosive volcanism, rhyolite volcanism and the deposition of younger sedimentary deposits (Figure 6.5).

#### **Dominant andesite volcanism**

Overlying the Jurassic basement the oldest geological group within Waihi is the Coromandel Group which is Miocene-Pliocene in age and consists of andesites with lesser dacites and rhyodacite (Skinner, 1986). This group is comprised of the Waiwawa Subgroup (Early-Late Miocene), Omahine Subgroup (Late Miocene-Pliocene) and Kaimai Subgroup (Late Miocene-Pliocene). Throughout the Waihi area the remnants of tuff breccias and lava flows from pre-existing stratovolcanoes form the surrounding hills, however, much of their structure has been eroded and buried by younger deposits. These stratovolcanoes formed similar topography as seen at the currently active TVZ. These hills constrained younger ignimbrites, causing them to infill paleovalleys with many exposures found following streams. The Kaimai Subgroup is the youngest of the Coromandel Group and marks the end of andesite-dominated volcanism in the Waihi area. This consists of four formations including the 6.79 Ma dacitic Ratarua Ignimbrite which forms hills in northeastern Waihi and has been studied in detail in Chapter 4.

The Ratarua Ignimbrite was initially investigated due to its close proximity to the type section of the Corbett Ignimbrite, as it covered the surrounding hills. However, the age of the Corbett Ignimbrite indicates it was deposited during the dominant period of andesitic volcanism (Figure 6.5). The difference in ages suggests that although they are likely to be from different sources they formed in the same volcanic setting.

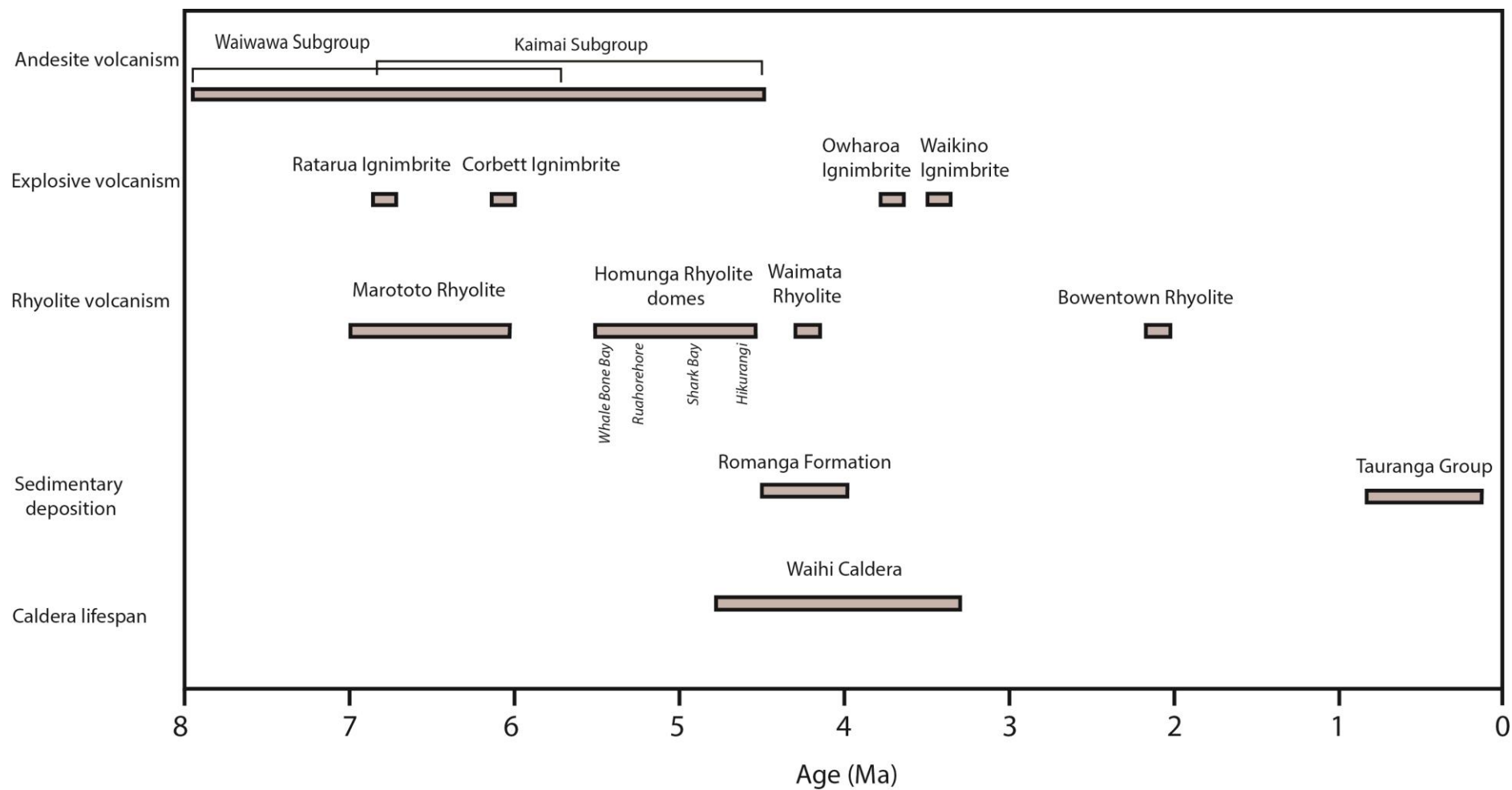


**Figure 6.5 Volcanic stratigraphy of the Waihi area. Based on Smith et al. (2006), Brathwaite and Christie (1996), Vincent (2012) and Julian (2016).**

### **Regional rhyolite domes**

Within the Waihi area there is the Minden Rhyolite subgroup, which contains the Waimata Rhyolite dome (4.06 Ma), the Bowentown Rhyolite dome (2.09) and the Homunga Rhyolite which consists of four rhyolite domes; Whale Bone Bay, Shark Bay, Ruahorehore and Hikurangi domes which are 5.5 Ma, 4.8 Ma, 5.30 Ma and 4.53 Ma respectively (Vincent, 2012; Brathwaite & Christie, 1996). The ages of these domes shows a younging southward progression.

The Ruahorehore and Hikurangi rhyolite domes are respectively situated on the northeastern and southeastern border of the caldera (Figure 6.4) with the Hikurangi Rhyolite being penecontemporaneous with lake sediments of the Romanga Formation (4.5-4.0 Ma). As these domes are on the edge of the caldera they may have formed as a result of radial fracturing (Cole *et al.*, 2005). Lava domes are often useful indicators of calderas with lava domes in the TVZ located within or on the rims of calderas, or else they are situated just outside of caldera rims (Briggs *et al.*, 2005). However, the age of the Ruahorehore Rhyolite predates the expected age of the caldera and may belong to another silicic centre.

The Hikurangi dome is the largest topographical feature in southeastern Waihi, and would have been an obstacle for the flow direction of younger ignimbrites. The Corbett Ignimbrite was deposited before this dome, thus should occur stratigraphically below this rhyolite dome. Granophyric intergrowth crystals show a granite body below the dome. This helps with the interpretation of the caldera in the Waihi area as there needed to have been a shallow magma body during formation. The gravity anomaly from this granite body below this dome may have been too small, or the body is too deep, to detect. A gravity anomaly has been identified 7 km southeast of the centre of the Waihi caldera at 3-4 km depth (Couper & Lawton, 1978), however the Hikurangi Rhyolite dome does not occur this far southwards (although the plutonic body may extend this distance) and the anomaly may instead represent dense Ananui andesites (Smith *et al.*, 2006).

The Hikurangi Rhyolite (4.53 Ma) and the Bowentown Rhyolite (2.09 Ma), are closely related spatially, but occurred approximately 2.44 million years apart. The Bowentown Rhyolite represents the last phase of volcanism in the Waihi area and was penecontemporaneous with the Tauranga Volcanic Centre to the south.

### Formation of the Waihi Caldera and associated ignimbrites

A gravity anomaly in the area has been attributed to a large trapdoor caldera bound by the Waihi and Mangakino faults (Smith *et al.*, 2006). Trapdoor calderas form when collapse leads to an incomplete formation of a ring fault leaving one side 'hinged' where downsag occurs, and is deepest towards the other side (Cole *et al.*, 2005). Gravity decreases from the north showing an asymmetric wedge, with a steep northern boundary and a shallow dipping southern boundary (Figure 6.6) The Ohinemuri and Mangakino faults provided a structural weakness which caused a localised caldera-forming eruption (Cole *et al.*, 2005). The sedimentary Romanga Formation was previously thought to underlie all ignimbrites of the Ohinemuri Subgroup (Figure 6.6) showing that a depression existed prior to the deposition of these ignimbrites (Brathwaite & Christie, 1996).

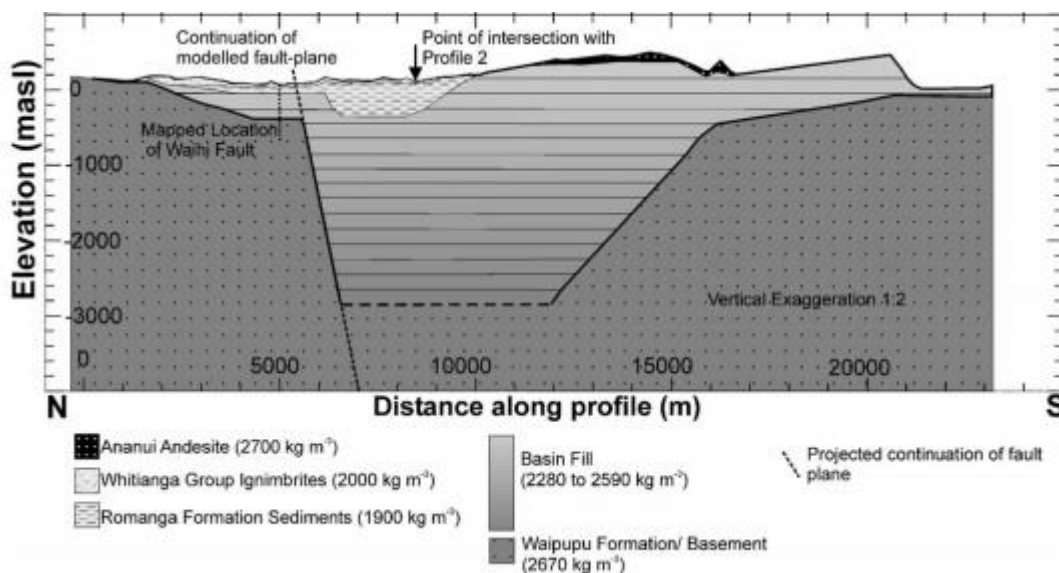


**Figure 6.6 North to south profile of the Waihi Caldera showing the elevation of the different stratigraphic units contained within the caldera**

However, the U-Pb age of the oldest ignimbrite in the Ohinemuri Subgroup, the Corbett Ignimbrite, determined here as 6.09 Ma, predates the age of the Romanga Formation of 4.5–4.0 Ma (Brathwaite & Christie, 1996). The older age of the Corbett Ignimbrite shows that either the previously determined lower age boundary of the Romanga Formation is incorrect, or there are different, older, lake sediments underlying the Corbett Ignimbrite. If the Corbett Ignimbrite is derived from the Waihi Caldera it would have been the first ignimbrite eruptive. However,

for the Corbett Ignimbrite to have been sourced from the caldera the caldera would have had to be active for a minimum of 2.61 million years. This is a significant period of time for a caldera to be active, with calderas in the TVZ (Rotorua, Okataina, Kapenga, Mangakī, Maroa and Taupo) having activity spans from 150 to 600 ka (Wilson *et al.*, 1984). This indicates the Corbett Ignimbrite is likely to be an outflow facies as first suggested by Brathwaite and Christie (1996) with the most probable source being a volcanic centre to the east, which has since been inundated by post-glacial sea level rise.

The Corbett Ignimbrite infills valleys with its flow being constrained by surrounding andesite hills, with the type section 5 km northeast of Waihi township bound by the hills of Ratarua Ignimbrite. The distribution of this ignimbrite is constrained to eastern Waihi, however, as it is significantly older than other widespread ignimbrites from the caldera its full distribution may have been eroded or buried. This ignimbrite shows a transition in composition from andesitic to rhyolitic (being predominantly dacitic). The two overlying Ohinemuri Subgroup ignimbrites, the Owaharoa and Waikino ignimbrites, are 3.76 and 3.48 Ma respectively (Vincent, 2012; Julian, 2016). These younger ignimbrites form thick sheets which are rhyolitic in composition. In drillhole pumice-rich lapilli tuff (inferred to be the Corbett Ignimbrite) is overlain by fine grained welded ignimbrite which is likely to be the Waikino Ignimbrite (Brathwaite & Christie, 1996). The direct contact between the Corbett and Waikino shows a 2.61 Ma age gap where a significant amount of erosion occurred. Due to the large age difference between the Owaharoa and Waikino ignimbrites it is likely that the Corbett Ignimbrite was sourced from another volcanic centre meaning it is an outflow facies with the calderas ignimbrites only being rhyolitic in composition.



# Chapter Seven

## Conclusions

---

The eastern Waihi area has a complex volcanological history with dominant andesite volcanism transitioning into younger rhyolitic volcanism, rhyolite dome complexes and a large, now in-filled, trapdoor caldera encompassing a significant area of this region. The Corbett Ignimbrite, Ratarua Ignimbrite and Hikurangi Rhyolite are exposed within the eastern Waihi area. Facies characteristics, petrographic characteristics and geochemical properties of these units were determined to provide a better understanding of the volcanic history and processes of felsic volcanism in eastern Waihi.

The Corbett Ignimbrite is exposed throughout the eastern Waihi area, infilling valleys which are bound by surrounding hills of andesitic and dacitic volcanic units. Facies variations throughout this ignimbrite show varying eruption processes, with lithic concentration zones suggesting that collapse and erosion of the vent occurred several times during the eruption. The facies distribution at the type section shows rapid depositional pulsing, defined by lithic concentration zones, which becomes a more steady flow in the upper half of the outcrop. Glass shards are not visible under the optical microscope due to their fine scale, however they were observed under SEM analysis. The fine scale of these glass shards, and absence of orientation or alignment, indicate an explosive eruption where larger glass shards were destroyed. Geochemical analysis of these glass shards and pumice samples show a change in composition from andesitic to rhyolitic. The source of this ignimbrite is unknown and four possible locations have been evaluated here; a silicic centre in the vicinity of the Bowentown Rhyolite, the Waihi Caldera, Tunaiti Caldera in the north, or a volcanic centre to the east that has since been inundated due to sea level rise. A U-Pb age of 6.09 Ma determined in this study is significantly older than the 2.09 Ma Bowentown Rhyolite, showing it is not sourced from a silicic centre associated with this dome, and indicating it predates the Waihi Caldera. The age of the Corbett Ignimbrite suggests it was erupted during a period when Waihi was dominated by andesite volcanism (7.9 – 4.5 Ma).

The Ratarua Ignimbrite is confined to northeastern Waihi and is a welded, fiamme-rich, dacitic ignimbrite. This ignimbrite covers the hills surrounding the Corbett Ignimbrites type section, which constrained its flow direction. Abundant fiamme in the Ratarua Ignimbrite shows that welding occurred resulting from high temperatures and loading. Erosion has since removed the partial to non-welded sections of this ignimbrite. U-Pb dating of zircons provides an eruption age of 6.79 Ma showing this dacitic ignimbrite was deposited during dominant andesite volcanism in Waihi, pre-dating the Corbett Ignimbrite.

The Hikurangi Rhyolite is a spherulitic lava dome in southeastern Waihi which belongs to the Homunga Rhyolite. Poor exposure of this rhyolite dome meant only one site was studied. The Hikurangi Rhyolite overlies the Corbett Ignimbrite. Petrographical analysis of this rhyolite determined the presence of granitoid lithics with granophyric and myrmekitic intergrowths, providing evidence for a deep granite body below this dome. No evidence has been previously found for a subsurface magma body in the southern CVZ. U-Pb dating of zircons determined an age of 4.53 Ma which is consistent with ages determined for other rhyolite domes belonging to the Homunga Rhyolite.

Understanding the physical and magmatic processes associated with these three units allows for a better understanding of the volcanic history of eastern Waihi. The ages of the volcanic units in this study are consistent with southward progression of volcanism in the CVZ with deposits becoming younger towards the south. These units reinforce previously determined evolutionary trends within the CVZ, with the older units being andesitic to dacitic in composition transitioning into younger rhyolitic volcanism. However further research is required to better define and understand the volcanic history in the region, with many other units poorly constrained.

## References

---

- Adams, C.J., Graham, I.J., Seward, D., & Skinner, D.N.B. (1994). Geochronological and geochemical evolution of late Cenozoic volcanism in the Coromandel Peninsula, New Zealand. *New Zealand Journal of Geology and Geophysics*, 37. 359-379.
- Ballance, P.F. (1975). Evolution of the Upper Cenozoic Magmatic Arc and Plate Boundary in Northern New Zealand. *Earth and Planetary Science Letters*, 28. 356-370.
- Barker, D.S. (1970). Compositions of Granophyre, Myrmekite, and Graphic Granite. *Geological Society of America Bulletin*, 81. 3339-3350.
- Black, L.P., Kamo, S.L., Allen, C.M., Davis, D.W., Aleinigoff, J.N., Valley, J.W., Mundil, R., Campbell, I.H., Korsch, R.J., Williams, I.S., & Foudoulis, C. (2004). Improved  $^{206}\text{Pb}/^{238}\text{U}$  microprobe geochronology by the monitoring of a trace-element-related matrix effect; SHRIMP, ID-TIMS, ELA-ICP-MS and oxygen isotope documentation for a series of zircon standards. *Chemical Volcanology*, 205. 115-140.
- Booden, M.A., Smith, I.E.M., Mauk, J.L., & Black, P.M. (2012). Geochemical and isotopic development of the Coromandel Volcanic Zone, northern New Zealand, since 18 Ma. *Journal of Volcanology and Geothermal Research*, 219-220. 15-32.
- Bradshaw, B.E., Healy, T.R., Nelson, C.S., Dell, P.M., & de Lange, W.P. (1994). Holocene sediment lithofacies and dispersal systems on a storm-dominated, back-arc shelf margin: the east Coromandel coast, New Zealand. *Marine Geology*, 119. 75-98.
- Branney, M.J., & Kokelaar, P. (2002). *Pyroclastic Density Currents and the Sedimentation of Ignimbrites* (Geological Society Memoir no.27).
- Brathwaite, R.L., & Christie, A.B. (1996). Geology of the Waihi area, scale 1:50,000: Institute of Geological and Nuclear Sciences, Geological map 21. *Institute of Geological and Nuclear Sciences*, 1 sheet. 64.
- Briggs, R.M., & Fulton, B.W.J. (1990). Volcanism, structure, and petrology of the Whiritoa-Whangamata coastal section, Coromandel Volcanic Zone, New Zealand: facies model evidence for the Tunaiti caldera. *New Zealand Journal of Geology and Geophysics*, 33. 623-633.
- Briggs, R.M., Houghton, B.F., McWilliams, M., & Wilson, C.J.N. (2005).  $^{40}\text{Ar}/^{39}\text{Ar}$  ages of silicic volcanic rocks in the Tauranga-Kaimai area, New Zealand: Dating the transition between volcanism in the Coromandel Arc and the Taupo Volcanic Zone. *New Zealand Journal of Geology and Geophysics*, 48. 459-469.

- Brink, M. (2012). *Emplacement processes of ignimbrites in the Ongatiti Valley, southeast Te Kuiti*. (MSc thesis, University of Waikato, Hamilton, New Zealand.)
- Byran, S.E., Cas, R.A.F., & Marti, J. (1998). Lithic breccias in intermediate volume phonolitic ignimbrites, Tenerife (Canary Islands): constraints on pyroclastic flow depositional processes. *Journal of Volcanology and Geothermal Research*, 81. 269-296.
- Bull, K.F., & McPhie, J. (2007). Fiamme textures in volcanic successions: Flaming issues of definition and interpretation. *Journal of Volcanology and Geothermal Research*, 164. 205-216.
- Capaccioni, B., Nappi, G., & Valentini, L. (2001). Directional fabric measurements: an investigative approach to transport and depositional mechanisms in pyroclastic flows. *Journal of Volcanology and Geothermal Research*, 107. 275-292.
- Carter, L., Alloway, B., Shane, P., & Westgate, J. (2004). Deep-ocean record of major late Cenozoic rhyolitic eruptions from New Zealand. *New Zealand Journal of Geology and Geophysics*, 47. 481-500.
- Cas, R.A.F., & Wright, J.V. (1987). *Volcanic Successions Modern and Ancient*. Allen and Unwin Ltd, London.
- Cole, J.W. (1886). Distribution and Tectonic Setting of Late Cenozoic Volcanism in New Zealand in Smith I.E.M. (Ed.), *Late Cenozoic Volcanism in New Zealand*, *Royal Society of New Zealand Bulletin* 23:21-47.
- Cole, J.W., Milner, D.M., & Spinks, K.D. (2005). Calderas and caldera structures: a review. *Earth Science Reviews*, 69. 1-26. In: Smith, I.E.M. ed., *Late Cenozoic Volcanism in New Zealand*. *Royal Society of New Zealand bulletin* 23: 7-20.
- Cooper, G.F. (2014). *The Dynamics of Large-Scale Silicic Magmatic Systems: Case Studies from Mangakino Volcanic Centre*. (PhD thesis, Victoria University of Wellington, Wellington, New Zealand).
- Couper, P.G., & Lawton, D.C. (1978). Final report on exploration licence 33-051, Unpublished open-file company report. *Ministry of Economic Development report MR350*.
- Deer, W.A., Howie R.A., & Zussman, J. (1992). *An Introduction to the Rock Forming Minerals* (2nd ed.), Longman Scientific & Technical, Harlow.
- Efford, J.T., Bylsma, R.J., Clarkson, B.D., Pittari, A., Mauriohooho, K., & Moon, V.G. (2014). Vegetation dieback as a proxy for temperature within a wet pyroclastic density current: A novel experiment and observations from the 6<sup>th</sup> of August 2012 Tongariro eruption. *Journal of Volcanology and Geothermal Research*, 286. 367-372.

- Fisher, R.V., & Schmincke, H.U. (1984). *Pyroclastic Rocks*. New York; Tokyo: Springer-Verlag.
- Fowler, A.D., Berger, B., Shore, M., Jones, M.I., & Ropchan, J. (2002). Supercooled rocks: development and significance of varioles, spherulites, dendrites and spinifex in Archaean volcanic rocks, Abitibi Greenstone belt, Canada. *Precambrian Research*, 15(1-4), 311-328. doi:10.1016/S0301-9268(02)00014-1
- Giordano, Guido. (1998). The effect of paleotopography on lithic distribution and facies associations of small volume ignimbrites: the WTT Cupa (Roccamonfina volcano, Italy). *Journal of Volcanology and Geothermal Research* 87. 255-273.
- Gottsmann, J., & Marti, J. (2008). *Caldera Volcanism: Analysis, Modelling and Response (Vol 10)*. Amsterdam, NLD: Elsevier Science & Technology.
- Grant-Mackie, J.A., & Moore, P.R. (1970). Correlation of the Colville formation. *New Zealand Journal of Geology and Geophysics*, 13:2. 561-563. Doi:10.1080/00288306.1970.10428915
- Haworth, A.V. (1993). *Volcanic Geology and Hydrothermal Alteration of the Lower Waitekauri Valley, Waihi, New Zealand* (MSc thesis, University of Waikato, Hamilton, New Zealand).
- Hildreth, W. (2004). Volcanological perspectives on Long Valley, Mammoth Mountain, and Mono Craters: several contiguous but discrete systems. *Journal of Volcanology and Geothermal Research*, 136. 169-198.
- Hochstein, M.P., & Nixon, I.M. (1979). Geophysical study of the Hauraki depression, North Island, New Zealand. *New Zealand Journal of Geology and Geophysics* 22. 1-19.
- Hunt, P. (1991). *The Volcanic Geology of the Whiritoa Hill Area*. (MSc thesis, University of Waikato, Hamilton, New Zealand).
- Izett, G.A. (1981). Volcanic ash beds: recorders of Upper Cenozoic silicic pyroclastic volcanism in the western United States. *Journal of Geophysics Research*, 86. 10200- 10222.
- Jackson, S.E., Pearson, N.J., Griffin, W.J., & Belousova, E.A. (2004). The application of laser ablation-inductively coupled plasma-mass spectrometry to in situ U-Pb zircon geochronology. *Chemical Geology*, 211. 47-69.
- Julian, H.A. (2016) *Volcanology of the Owaharoa and Waikino ignimbrites, Waihi, Coromandel Volcanic Zone*. (Unpublished Msc thesis, University of Waikato, Hamilton, New Zealand).

- Klimm, K., Holtz, F., Johannes, W., & King, P. (2003). Fractionation of metaluminous A-type granites: an experimental study of the Wangrah Suite, Lachlan Fold Belt, Australia. *Precambrian Research*, 124 (2-4), 327-341.
- Kohn, B.P. (1973). *Some aspects of New Zealand Quaternary pyroclastic rocks*. (Unpublished Ph.D. thesis, Victoria University of Wellington).
- Le Maitre, R.W., Streckeisen, A., Zanettin, B., Le Bas, M.J., Bonin, B., Bateman, P., Bellieni, G., Dudek, A., Efremova, S., Keller, J., Lameyre, J., Sabine, P. A., Schmid, R., Sorensen, H. & Woolley, A. R. (2002). *Igneous rocks: a classification and glossary of terms* (2<sup>nd</sup> ed.), Cambridge University Press, West Nyack, NY.
- Malengreau, B., Skinner, D., Bromley, C., & Black, P. (2000). Geophysical characterisation of large silicic volcanic structures in the Coromandel Peninsula, New Zealand. *New Zealand Journal of Geology and Geophysics*, 43. 171-186.
- McKay, D.F. (1985). Geology of proposed plant and waste disposal sites for PL 31-777, Martha Hill, Waihi: Waihi Gold Company. *Unpublished open-file report, Institute of Geological and Nuclear Sciences, MR780*.
- McPhie, J., Doyle, M., & Allen, R. (1993). *Volcanic textures: A guide to the interpretation of textures in volcanic rocks*. University of Tasmania. Centre for Ore Deposit and Exploration Studies.
- Milner, D.M., Cole, J.W., & Wood, C.P. (2002). Asymmetric, multiple-block collapse at Rotorua Caldera, Taupo Volcanic Zone, New Zealand. *Bulletin of Volcanology*, 64. 134-149.
- Montero-Lopez, C., Guzman, S., & Barrios, F. (2015). Late Miocene ignimbrites at the southern Punaenorthern Sierras Pampeanas border (~27° S): Stratigraphic correlation. *Journal of South American Earth Sciences*, 62. 80-91.
- Moore, P.R. (2011). Rhyolite domes and pyroclastic rocks (Whitianga Group) of the Hahei Area, Coromandel Peninsula. *Journal of the Royal Society of New Zealand* 13. 79-92.
- Murphy, P.J., Briedis, J., & Peck, J.H. (1979). Dating techniques in fault investigations. *Geological Society of America Reviews in Engineering Geology*, 4. 153–157.
- Nicholson, K.N., Black, P.M., Hoskin, P.W.O., & Smith, I.E.M. (2003). Silicic volcanism and back-arc extension related to migration of the Late Cainozoic Australian-Pacific plate boundary. *Journal of Volcanology and Geothermal Research*, 131. 295-306.
- Pittari, A. (2004) *Eruption dynamics and emplacement processes for the climatic Abrigo Member, Tenerife, Canary Islands*. (PhD thesis, Monash University, Clayton).

- Pittari, A., Cas, R.A.F., Wolff, J.A., Nichols, H.J., Larson, P.B., & Marti, J. (2008). The use of Lithic Clast Distributions in Pyroclastic Deposits to Understand Pre- and Syn-Caldera Collapse Processes: A Case Study of the Abrigo Ignimbrite, Tenerife, Canary Islands. In: Gottsman, J. & Marti, J. (Eds.) *Caldera Volcanism Analysis, Modelling and Response*. (pp. 97-136). Developments in Volcanology.
- Pittari, A., Cas, R.A.F., Edgar, C.J., Nichols, H.J., Wolff, J.A., & Marti, J. (2006). The influence of paleotopography on facies architecture and pyroclastic flow processes of a lithic-rich ignimbrite in a high gradient setting: The Abrigo Ignimbrite, Tenerife, Canary Islands. *Journal of Volcanology and Geothermal Research*, 152. 273-315.
- Rabone, S.D.C., & Keall, P. (1985). Progress report: PL 31-758 Waihu, June to December 1984: Amoco Minerals NZ Ltd. *Unpublished open-file mining company report, Institute of Geological and Nuclear Sciences MR810*.
- Rollinson, H. (1993). *Using geochemical data: evaluation, presentation, interpretation*, Longman Scientific & Technical, Harlow, Essex.
- Rutherford, N.F. (1978). Fission-track age and trace element geochemistry of some Minden Rhyolite obsidians. *New Zealand Journal of Geology and Geophysics*, 21. 443-448.
- Seaman, S.J., Darby Dyar, M., & Marinkovic, N. (2009). The effects of heterogeneity in magma water concentration on the development of flow banding and spherulites in rhyolitic lava. *Journal of Volcanology and Geothermal Research*, 183(3-4). 157-169.
- Shcherbakov, V.D., Plechov, P.Y., Izbekov, P.E., & Shipman, J.S. (2011). Plagioclase zoning as an indicator of magma processes at Bezymianny Volcano, Kamchatka. *Contrib Mineral Petrol*, 162. 83-99.
- Scott, A.C., & Glasspool, I.J. (2005). Charcoal reflectance as a proxy for the emplacement temperature of pyroclastic flow deposits. *Geological Society of America: Geology*, 33(7). 589-592.
- Shelley, D. (1993). *Igneous and metamorphic rocks under the microscope: classification, textures, microstructures, and mineral preferred-orientations*. New York, London: Chapman & Hall.
- Skinner, D.N.B., 1986: Neogene volcanism of the Hauraki Volcanic Region, in Smith I.E.M. (Ed.), *Late Cenozoic Volcanism in New Zealand*, *Royal Society of New Zealand Bulletin* 23:21-47.
- Smith, N., Cassidy, J., Locke, C.A., Mauk, J.L., & Christie, A.B. (2005). The role of regional-scale faults in controlling a trapdoor caldera, Coromandel Peninsula, New Zealand. *Journal of Volcanology and Geothermal Research*, 149. 312-328.

- Solari, L.A., Gomez-Tuena, A., Bernal, J.P., Perez-Arvizu, O., & Tanner, M. (2009). U-Pb Zircon Geochronology with an Integrated LA-ICP-MS Microanalytical Workstation: Achievements in Precision and Accuracy. *Geodards and Geoanalytical Research*, 34 (1). 5-18.
- Sparks, R.S.J. (1976). Grain size variations in ignimbrites and implications for the transport of pyroclastic flows. *Sedimentology*, 23 (2). 147-188.
- Sparks, R.S.J., & Pinkerton, H. (1978). Effects of degassing on rheology of basaltic magma. *Nature*, 276. 385-386.
- Spark, R.S.J., Self, S., & Walker, G.P.L. (1973). Products of Ignimbrite Eruptions. *Geology*, 1. 115-118. doi: 10.1130/0091-7613(1973)12.0.CO;2
- Sparks, R.S.J., & Walker, G.P.L. (1977). The significance of vitric-enriched air-fall ashes associated with crystal-enriched ignimbrites. *Journal of Volcanology and Geothermal Research*, 2. 329-341.
- Takagi, M. (1995). *Miocene-Pliocene arc volcanism of the Hauraki region in North Island, New Zealand*. (MSc Thesis, Okayama University of Science).
- Vernon, R.H. (2004). *A Practical Guide to Rock Microstructure*. Department of Earth and Planetary Sciences, Macquarie University, Sydney: Cambridge University Press.
- Vermeesch, P. (2012). On the visualisation of detrital age distributions. *Chemical Geology*, 312-313. 190-194.
- Vincent, K.A. (2012). *U-Pb Dating of Silicic Volcanic Rocks of the Eastern Coromandel Peninsula*. (MSc thesis, University of Waikato, Hamilton, New Zealand).
- Wolff, J.A. (1985). The effect of explosive eruption processes on geochemical patterns within pyroclastic deposits. *Journal of Volcanology and Geothermal Research*, 26. 189-201.
- Willcock, M.A.W., Cas, R.A.F., Giordano, G., & Morelli, C. (2013). The eruption, pyroclastic flow behaviour, and caldera in-filling processes of the extremely large volume (>1290 km<sup>3</sup>), intra- to extra-caldera, Permian Ora (Ignimbrite) Formation, Southern Alps, Italy. *Journal of Volcanology and Geothermal Research*, 265. 102-126.
- Wilson, C.J.N., Rogan, A.M., Smith, I.E.M., Northey, D.J., Nairn, I.A., & Houghton, B.F. (1984). Caldera volcanoes of the Taupo Volcanic Zone, New Zealand. *Journal of Geophysical Research: Solid Earth*, 89. 8463-8484.
- Winter, J.D. (2014). *Principles of Igneous and Metamorphic Petrology* (2nd ed.). Department of Geology, Whitman College.

# **Appendix I**

## **Sample Catalogue**

---

**Table I.1** Samples collected in the field for the Corbett Ignimbrite, Ratarua Ignimbrite, Hikurangi Rhyolite and Bowentown Rhyolite

<b>Sample No.</b>	<b>Rock Name</b>	<b>Grid Reference</b> (New Zealand Map Grid)	<b>Location</b>
<b>University of Waikato No.</b>			
1.1 W150300	Corbett Ignimbrite	6423791.422N, 2765376.243E	Corbett Farm on Waihi Whangamata Road
1.2 W150301	Corbett Ignimbrite	6423791.422N, 2765376.243E	Corbett Farm on Waihi Whangamata Road
1.3 W150302	Corbett Ignimbrite	6423791.422N, 2765376.243E	Corbett Farm on Waihi Whangamata Road
1.4 W150303	Corbett Ignimbrite	6423791.422N, 2765376.243E	Corbett Farm on Waihi Whangamata Road
1.5 W150304	Corbett Ignimbrite	6423791.422N, 2765376.243E	Corbett Farm on Waihi Whangamata Road
2.1 W150305	Hikurangi Rhyolite	6410403.770N, 2763344.656E	Woodlands Road outcrop of rhyolite
2.2 W150306	Hikurangi Rhyolite	6410403.770N, 2763344.656E	Woodlands Road outcrop of rhyolite

Sample No.	Rock Name	Grid Reference (New Zealand Map Grid)	Location
<b>University of Waikato No.</b>			
2.3 W150307	Hikurangi Rhyolite	6410403.770N, 2763344.656E	Woodlands Road outcrop of rhyolite
2.4 W150308	Hikurangi Rhyolite	6410403.770N, 2763344.656E	Woodlands Road outcrop of rhyolite
2.5 W150309	Hikurangi Rhyolite	6410403.770N, 2763344.656E	Woodlands Road outcrop of rhyolite
2.6 W150310	Hikurangi Rhyolite	6410403.770N, 2763344.656E	Woodlands Road outcrop of rhyolite
3.1 W150311	Corbett Ignimbrite	6411287.402N, 2762717.996E	Woodlands Road by Walls Road
3.2 W150312	Corbett Ignimbrite	6411287.402N, 2762717.996E	Woodlands Road by Walls Road
3.3 W150313	Corbett Ignimbrite	6411287.402N, 2762717.996E	Woodlands Road by Walls Road
3.4 W150314	Corbett Ignimbrite	6411287.402N, 2762717.996E	Woodlands Road by Walls Road

Sample No.	Rock Name	Grid Reference (New Zealand Map Grid)	Location
<b>University of Waikato No.</b>			
3.5 W150315	Corbett Ignimbrite	6411287.402N, 2762717.996E	Woodlands Road by Walls Road
5.1 W150317	Ratarua Ignimbrite	6424399.133N, 2765998.709E	Corbett Farm on Waihi Whangamata Road
5.2 W150318	Ratarua Ignimbrite	6424399.133N, 2765998.709E	Corbett Farm on Waihi Whangamata Road
6.1 W150319	Corbett Ignimbrite	6425280.920N, 2767725.794E	Landlyst Road boulders
7.1 W150320	Corbett Ignimbrite	6425269.851N, 2767721.354E	Ngatitangata Road stream outcrop
7.2 W150321	Corbett Ignimbrite	6425269.851N, 2767721.354E	Ngatitangata Road stream outcrop
8.1 W150322	Corbett Ignimbrite	6411970.918N, 2763239.406E	Woodlands Road farm with rock outcrops
9.1 W150323	Corbett Ignimbrite	6407067.339N, 2763432.581E	Woodlands Road Katikati following Ananui Falls track

Sample No.	Rock Name	Grid Reference (New Zealand Map Grid)	Location
<b>University of Waikato No.</b>			
9.2 W150324	Corbett Ignimbrite	6406956.999N, 2762903.859E	Woodlands Road Katikati following Ananui Falls track
9.3 W150325	Corbett Ignimbrite	6407042.340N, 2760636.540E	Woodlands Road Katikati following Ananui Falls track
10.1 W150326	Bowentown Rhyolite	6410592.499N, 2774509.008E	Bowentown Heads rock outcrop
10.2 W150327	Bowentown Rhyolite	6410592.499N, 2774509.008E	Bowentown Heads rock outcrop
11.1 W150328	Corbett Ignimbrite	6421044.942N, 2766805.389E	Golden Valley Road farm quarry outcrop
11.2 W150329	Corbett Ignimbrite	6421044.942N, 2766805.389E	Golden Valley Road farm quarry outcrop
11.3 W150330	Corbett Ignimbrite	6421044.942N, 2766805.389E	Golden Valley Road farm quarry outcrop
11.4 W150331	Corbett Ignimbrite	6421044.942N, 2766805.389E	Golden Valley Road farm quarry outcrop

<b>Sample No.</b>	<b>Rock Name</b>	<b>Grid Reference</b> (New Zealand Map Grid)	<b>Location</b>
<b>University of Waikato No.</b>			
11.5 W150332	Corbett Ignimbrite	6421044.942N, 2766805.389E	Golden Valley Road farm quarry outcrop
12.1 W150333	Corbett Ignimbrite	6411444.356N, 2767872.512E	Athenree Gorge stream cutting
13.1 W150334	Ratarua Ignimbrite	642322.296N, 2766097.472E	Waihi Whangamata Road farm land boulders
13.2 W150335	Ratarua Ignimbrite	642322.296N, 2766097.472E	Waihi Whangamata Road farm land boulders
13.3 W150336	Ratarua Ignimbrite	642322.296N, 2766097.472E	Waihi Whangamata Road farm land boulders
13.4 W150337	Ratarua Ignimbrite	642322.296N, 2766097.472E	Waihi Whangamata Road farm land boulders
13.5 W150338	Ratarua Ignimbrite	642322.296N, 2766097.472E	Waihi Whangamata Road farm land boulders

**Table I.2** Different analysis methods used on different samples

<b>Sample no.</b>  <b>University of Waikato No.</b>	<b>Rock type</b>	<b>SEM</b>	<b>XRF</b>	<b>XRD</b>	<b>EPMA</b>	<b>Thin Section</b>	<b>Thin section type and number</b>	<b>Point counted</b>	<b>Sample for dating</b>
1.1 W150300	Corbett Ignimbrite	X		X	X	X	1.1.1 – matrix	X	X
1.2 W150301	Corbett Ignimbrite	X	X						
1.3 W150302	Corbett Ignimbrite	X	X	X	X	X	1.3.1 - Pumice	X	
1.4 W150303	Corbett Ignimbrite		X	X		X	1.4.1 - lithic 1.4.2 - matrix		
1.5 W150304	Corbett Ignimbrite	X	X	X		X	1.5.1 – matrix 1.5.2 – matrix 1.5.3 – matrix		
2.1 W150305	Hikurangi Rhyolite		X	X	X	X	2.1.1 – matrix	X	X

<b>Sample no.</b>  <b>University of Waikato No.</b>	<b>Rock type</b>	<b>SEM</b>	<b>XRF</b>	<b>XRD</b>	<b>EPMA</b>	<b>Thin Section</b>	<b>Thin section type and number</b>	<b>Point counted</b>	<b>Sample for dating</b>
2.2 W150306	Hikurangi Rhyolite	X	X	X		X	2.2.1 – matrix	X	
2.3 W150307	Hikurangi Rhyolite	X	X	X					
2.4 W150308	Hikurangi Rhyolite		X	X		X	2.4.1 - matrix		
2.5 W150309	Hikurangi Rhyolite		X	X		X	2.5.1 – matrix	X	
2.6 W150310	Hikurangi Rhyolite		X	X		X	2.6.1 – matrix	X	
3.1 W150311	Corbett Ignimbrite					X	3.1.1 – matrix	X	
3.2 W150312	Corbett Ignimbrite								
3.3 W150313	Corbett Ignimbrite								

Sample no.  University of Waikato No.	Rock type	SEM	XRF	XRD	EPMA	Thin Section	Thin section type and number	Point counted	Sample for dating
3.4 W150314	Corbett Ignimbrite								
3.5 W150315	Corbett Ignimbrite		X	X					
5.1 W150317	Ratarua Ignimbrite		X	X		X	5.1.1 – matrix	X	X
5.2 W150318	Ratarua Ignimbrite					X	5.2.1 – lithic 5.2.2 – matrix		
6.1 W150319	Corbett Ignimbrite					X	6.1.1 – lithics 6.1.2 – pumice	X	
7.1 W150320	Corbett Ignimbrite		X	X					
7.2 W150321	Corbett Ignimbrite								

Sample no.  University of Waikato No.	Rock type	SEM	XRF	XRD	EPMA	Thin Section	Thin section type and number	Point counted	Sample for dating
8.1 W150322	Corbett Ignimbrite	X	X	X		X	8.1.1 – lithic 8.1.2 – pumice 8.1.3 – matrix	X	
9.1 W150323	Corbett Ignimbrite					X	9.1.1 – pumice 9.1.2 – clay		
9.2 W150324	Corbett Ignimbrite					X	9.2.1 – matrix 9.2.2 – pumice	X	
9.3 W150325	Corbett Ignimbrite		X	X		X	9.3.1 – lithics 9.3.2 – pumice	X	
10.1 W150326	Bowentown Rhyolite		X	X	X	X	10.1.1 – matrix 10.1.2 – matrix	X X	X
10.2 W150327	Bowentown Rhyolite								

Sample no.  University of Waikato No.	Rock type	SEM	XRF	XRD	EPMA	Thin Section	Thin section type and number	Point counted	Sample for dating
11.1 W150328	Corbett Ignimbrite		X	X					
11.2 W150329	Corbett Ignimbrite					X	11.2.1 – matrix 11.2.2 – matrix		
11.3 W150330	Corbett Ignimbrite		X	X		X	11.3.1 – fiamme 11.3.2 – matrix		
11.4 W150331	Corbett Ignimbrite					X	11.4.1 – matrix 11.4.3 – matrix		
11.5 W150332	Corbett Ignimbrite								
12.1 W150333	Corbett Ignimbrite					X	12.1.1 – matrix		
13.1 W150334	Ratarua Ignimbrite		X	X		X	13.1.1 – matrix 13.1.2 – matrix 13.1.3 – fiamme	X X X	

Sample no.  University of Waikato No.	Rock type	SEM	XRF	XRD	EPMA	Thin Section	Thin section type and number	Point counted	Sample for dating
13.2 W150335	Ratarua Ignimbrite		X	X		X	13.2.1 – fiamme 13.2.2 – matrix 13.2.3 – fiamme	X	
13.3 W150336	Ratarua Ignimbrite		X	X	X	X	13.3.1 – matrix 13.3.2 – fiamme 13.3.3 – lithic	X X	
13.4 W150337	Ratarua Ignimbrite		X	X		X	13.4.1 – matrix 13.4.2 – fiamme 13.4.3 – lithic	X	
13.5 W150338	Ratarua Ignimbrite		X	X		X	13.5.1 – fiamme 13.5.2 - matrix		

## **Appendix II**

### **Stratigraphic logs**

---





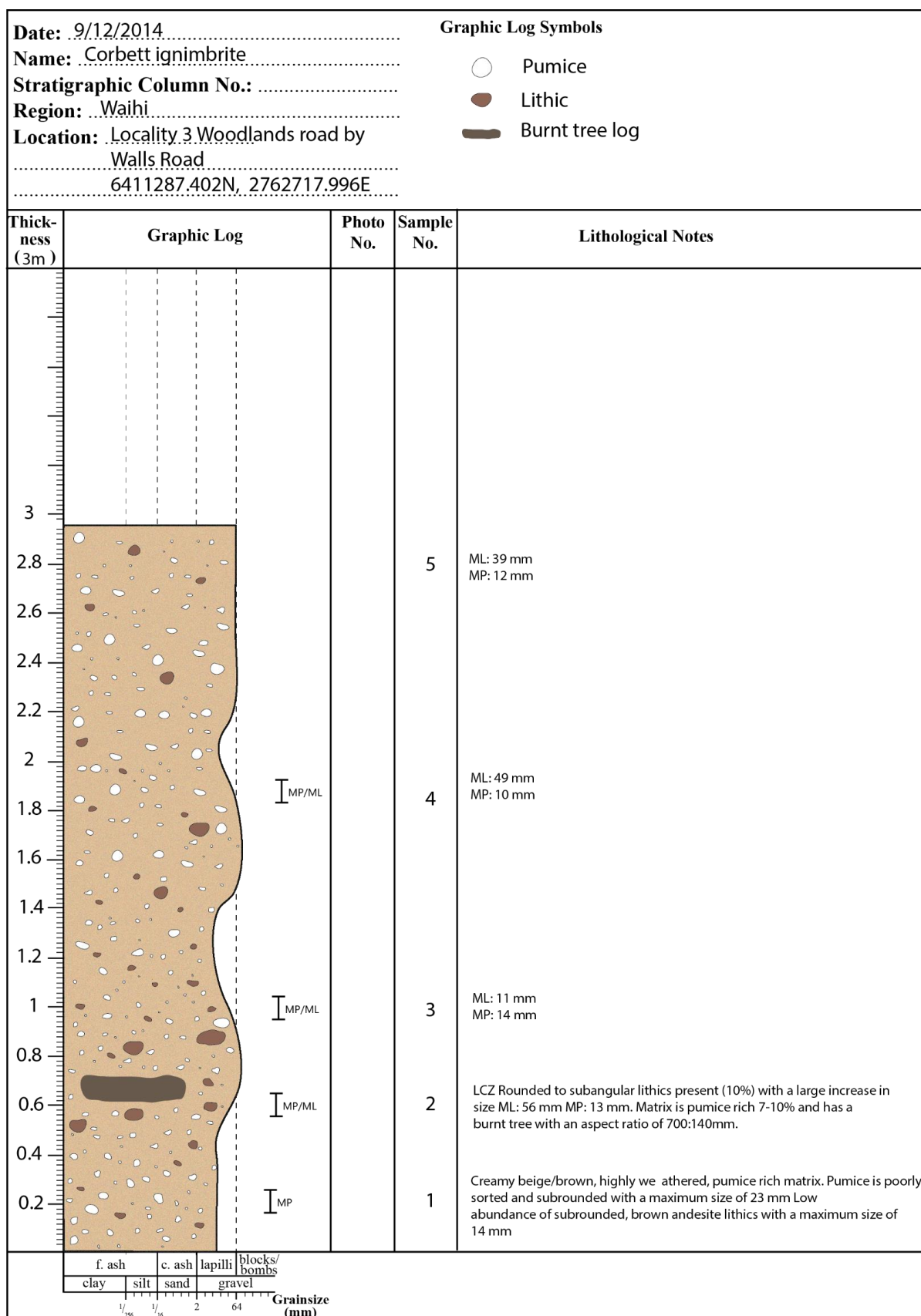
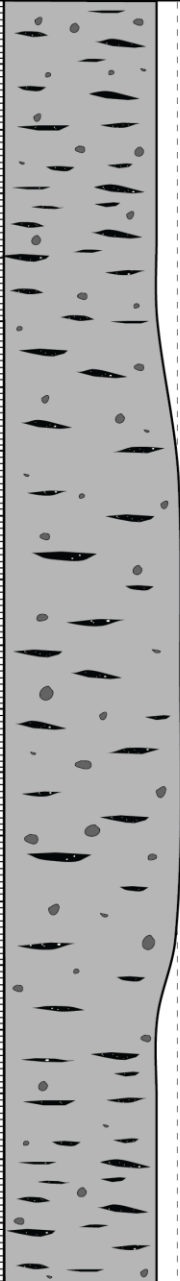









**Figure II.3:** Corbett Ignimbrite Woodlands Road stratigraphic log, locality 3





Date: 19/04/2015		Graphic Log Symbols												
Name: Ratarua Ignimbrite		 Fiamme  Lithic												
Stratigraphic Column No.: .....														
Region: Waihi														
Location: Waihi Whangamata Road														
642322.296N, 2766097.472E														
Thickness (10 m)	Graphic Log	Photo No.	Sample No.	Lithological Notes										
9.5			5	Maximum fiamme size of 28:3.6 mm Maximum lithic size of 9.4 mm										
9				 MF/ML	4	Increase in fiamme (25%) with a maximum size of 23.6:6.4 mm Lithics (10 %) with a maximum size of 9.8 mm.								
8.5						 MF/ML	3	Maximum fiamme size of 30:8 mm. Maximum lithic size of 8.2 mm						
8								 MF/ML	2	Decrease in abundance of fiamme (10%) with a maximum size of 32:6 mm. Lithic increase to 10% with a maximum size of 22 mm. Crystals decrease to 4%				
7.5										 MF/ML	1	Dark grey, crystal rich matrix. Dark grey to black, cusped and elongated, crystal rich fiamme throughout. Fiamme contains dark mafics, white and clear crystals and makes 20% of the matrix with a maximum aspect ratio of 26:7 mm. Grey, subrounded lithics of andesite make up 5% of the matrix with a maximum size of 11 mm. Biotite, angular quartz and plagioclase make 7% of the matrix.		
7												 MF/ML		
6.5														
6														
5.5														
5														
4.5														
4														
3.5														
3														
2.5														
2														
1.5														
1														
0.5														
<div> <div>f. ash</div> <div>c. ash</div> <div>lapilli</div> <div>blocks/ bombs</div> </div> <div> <div>clay</div> <div>silt</div> <div>sand</div> <div>gravel</div> </div> <div> <div>1/32</div> <div>1/16</div> <div>2</div> <div>64</div> </div> <div>Grainsize (mm)</div>														

**Figure II.6:** Ratarua Ignimbrite Waihi Whangamata Road stratigraphic log, locality 13



# **Appendix III**

## **Point counting results**

---

**Table III.1:** Corbett Ignimbrite raw data of four matrix thin sections point counted

Sample no.	Plagioclase	Hornblende	Orthopyroxene	Augite	Quartz	Opaques	Pumice	Interstitial matrix	Lithics	Uncertain counts	Total points counted
1.1.1	163	8	7	14	15	6	42	343	2	12	600
3.1.1	196	19	24	18	22	5	0	461	55	7	800
9.3.1	80	12	16	19	26	4	176	434	33	9	800
9.2.1	114	31	18	8	74	7	52	496	0	12	800

**Table III.2:** Corbett Ignimbrite raw data of seven pumice thin sections point counted

Sample no.	Plagioclase	Hornblende	Orthopyroxene	Augite	Quartz	Opaques	Vesicles	Pumice	Uncertain counts	Total points counted
1.1.1	18	2	5	4	13	3	272	83	4	400
1.3.1	21	0	1	0	8	7	297	66	2	400
1.4.1	18	8	11	7	21	2	209	124	7	400
1.5.2	16	1	4	3	10	7	231	128	16	400
6.1.2	21	1	1	4	13	7	299	61	6	400
8.1.2	15	15	4	3	31	2	239	91	7	400
9.3.2	18	8	11	7	21	2	209	124	7	400

**Table III.3:** Ratarua Ignimbrite raw data of four matrix thin sections point counted

Sample no.	Fiamme	Hornblende	Orthopyroxene	Plagioclase	Opaques	Augite	Lithics	Groundmass	Uncertain counts	Total points counted
13.1.2	23	17	36	260	6	51	14	393	13	800
13.1.1	8	14	23	305	3	26	6	415	9	800
13.3.1	0	11	28	268	0	35	3	455	6	800
5.1.1	11	13	30	281	3	37	11	414	9	800

**Table III.3:** Ratarua Ignimbrite raw data of four fiamme thin sections point counted

Sample no.	Fiamme	Plagioclase	Hornblende	Orthopyroxene	Augite	Opaques	Uncertain counts	Total points counted
13.3.2	253	110	2	8	18	9	4	400
13.2.1	245	103	4	12	22	14	2	400
13.4.2	251	91	2	15	26	15	11	400
13.1.3	223	119	7	16	27	8	13	400

**Table III.4:** Hikurangi Rhyolite raw data of four thin sections point counted

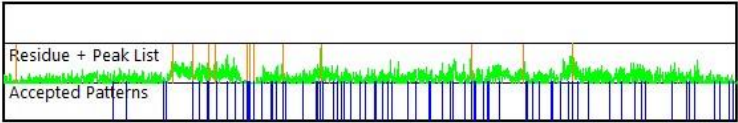
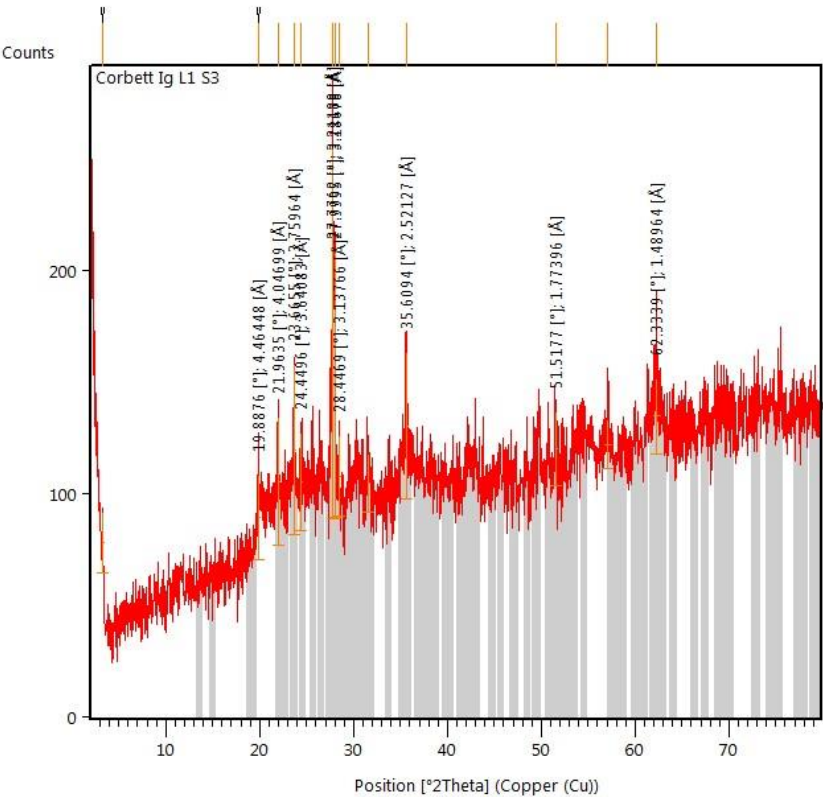
Sample no.	Groundmass	Quartz	Plagioclase	Biotite	Opakes	Uncertain counts	Total points counted
2.11	640	39	86	31	4	3	800
2.21	676	20	68	34	2	8	800
2.5.1	659	47	57	33	4	6	800
2.6.1	663	53	65	18	1	3	800

## **Appendix IV**

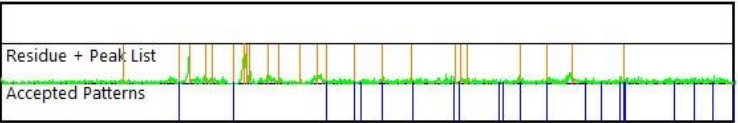
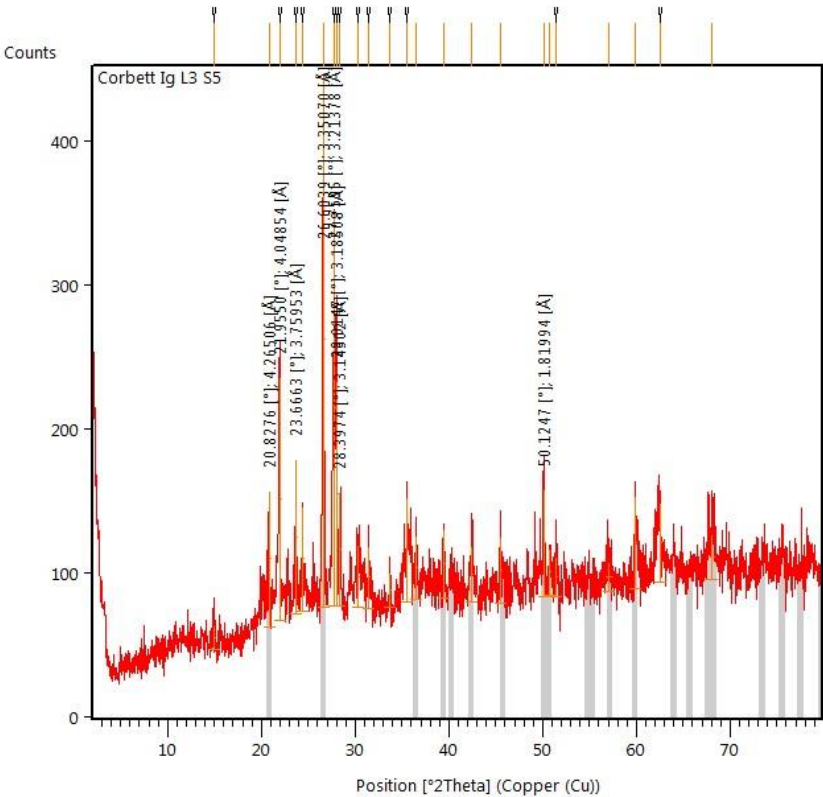
### **XRD results**

---

Corbett Ignimbrite Locality 1 sample 3

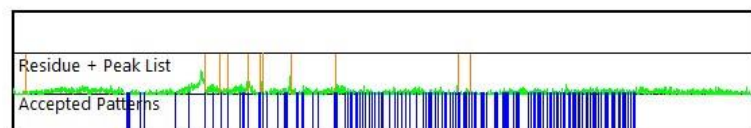
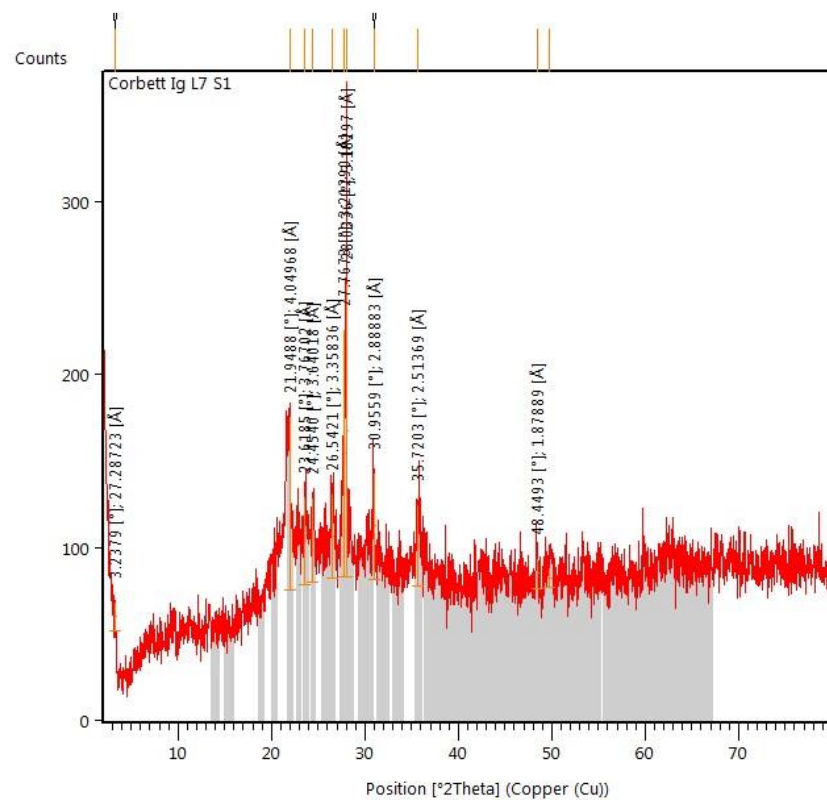


Corbett Ignimbrite Locality 3 sample 5

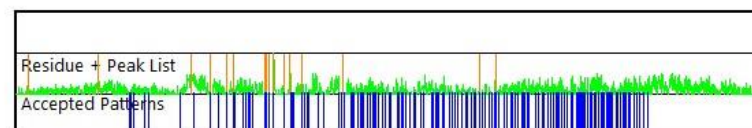
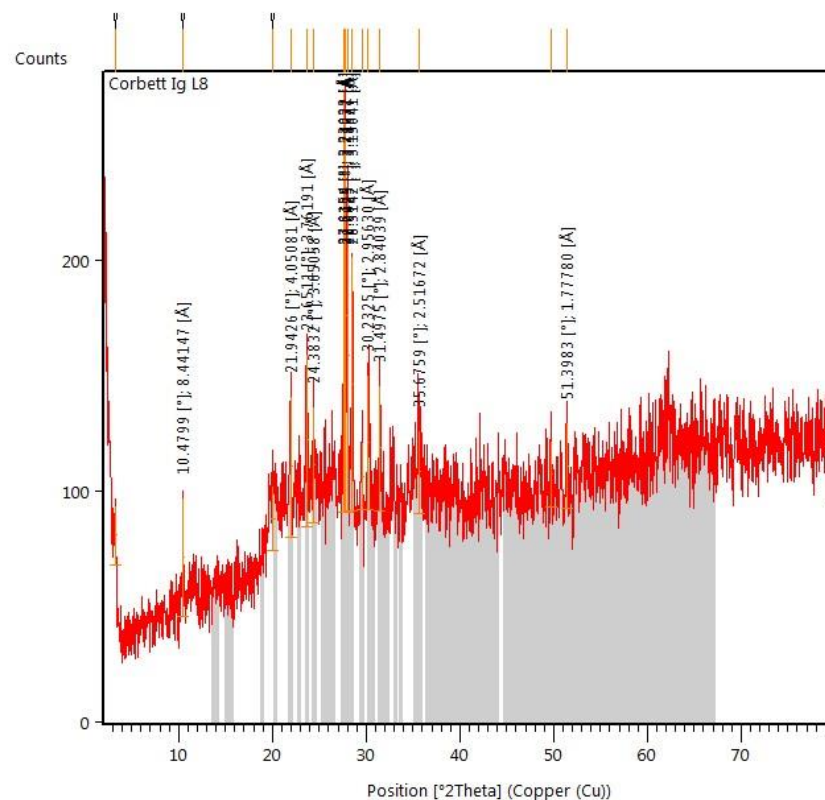


Corbett Ignimbrite locality 7 sample 1

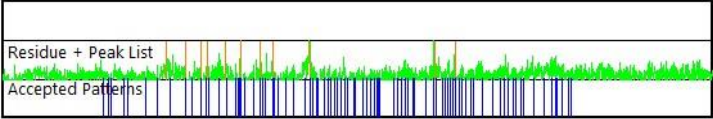
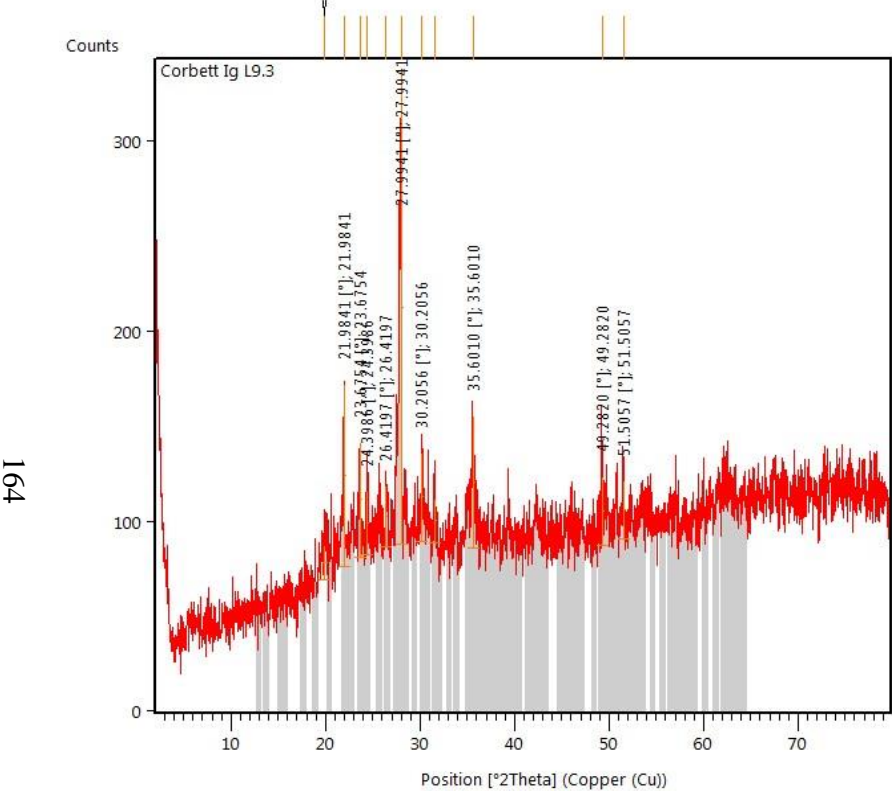
163



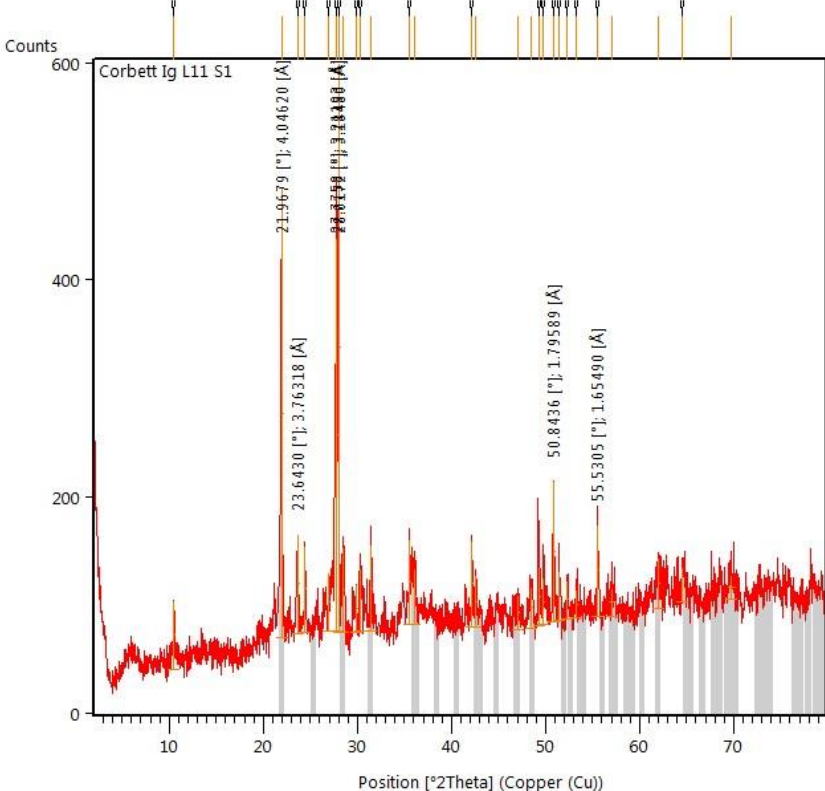
Corbett Ignimbrite locality 8



Corbett Ignimbrite locality 9.3

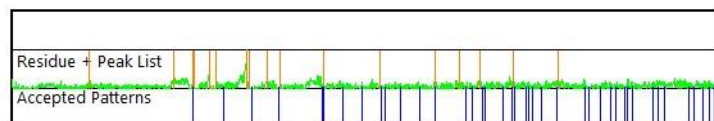
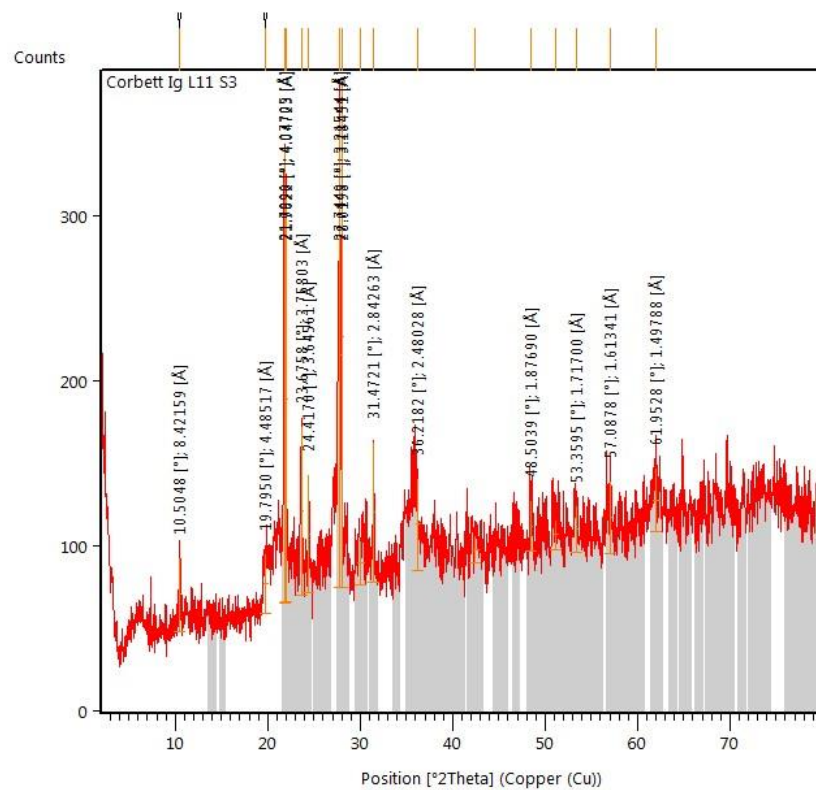


Corbett Ignimbrite locality 11 sample 1

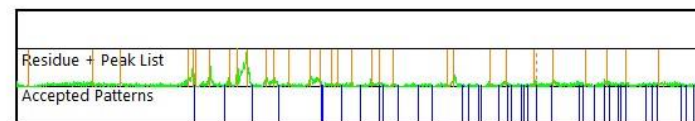
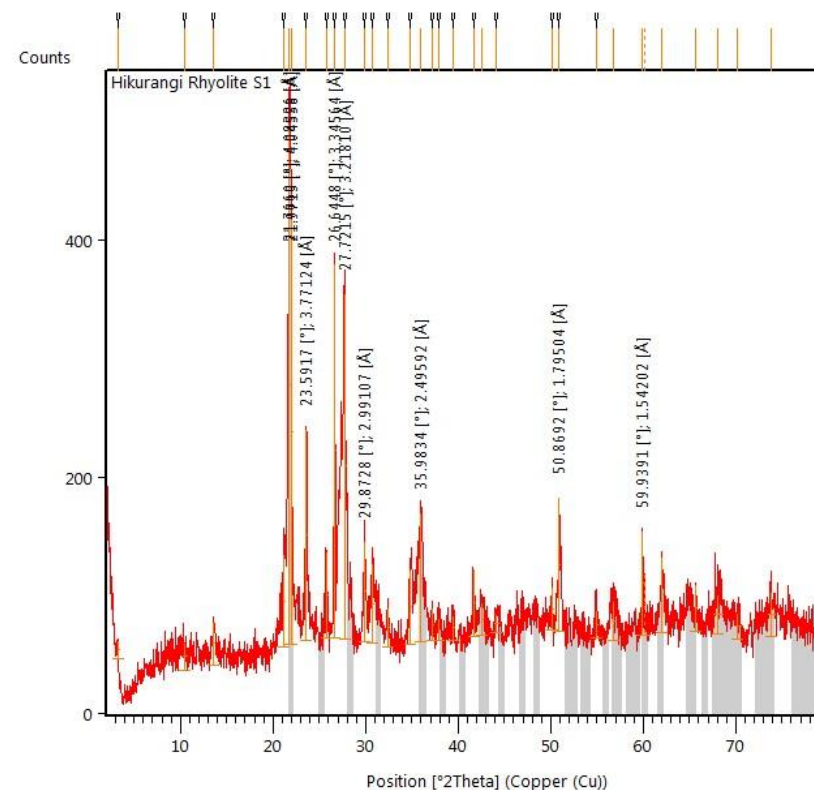


Corbett Ignimbrite locality 11 sample 3

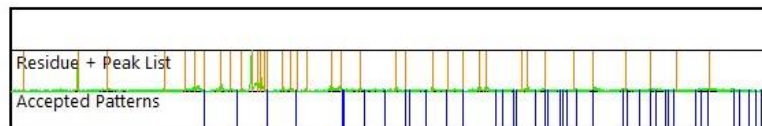
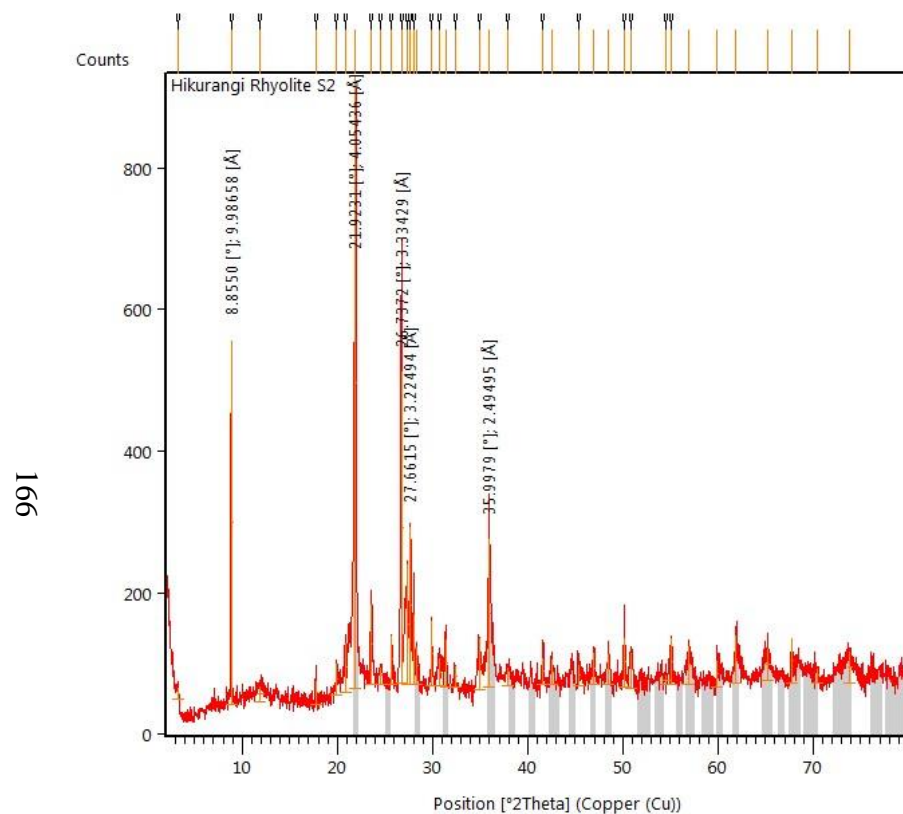
165



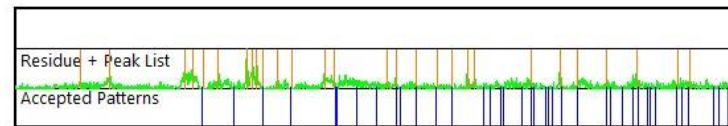
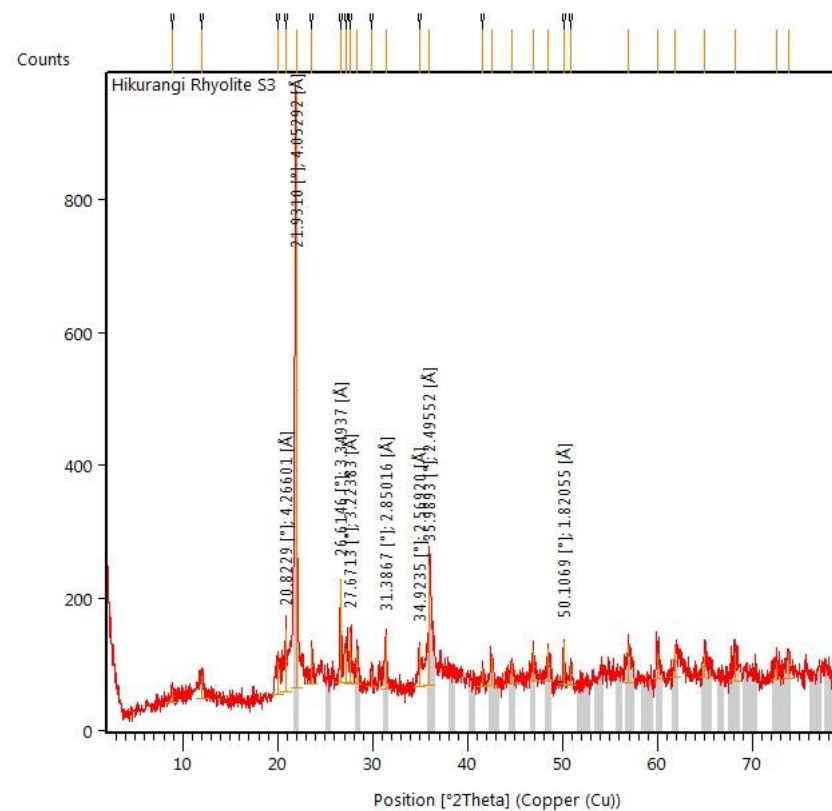
Hikurangi Rhyolite sample 1



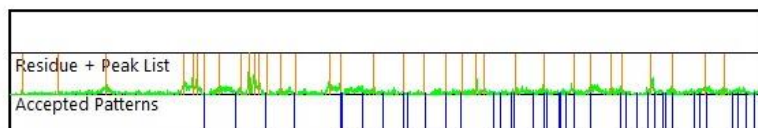
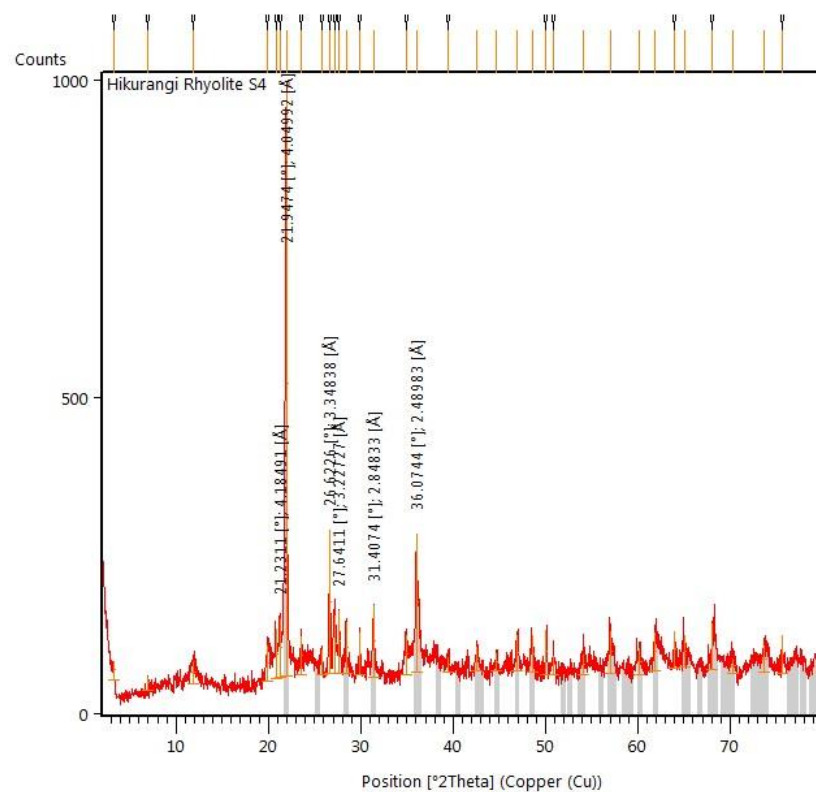
Hikurangi Rhyolite sample 2



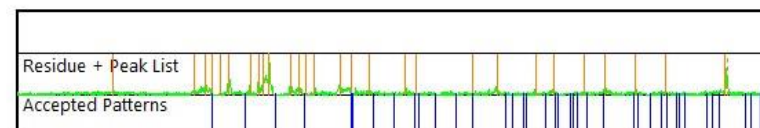
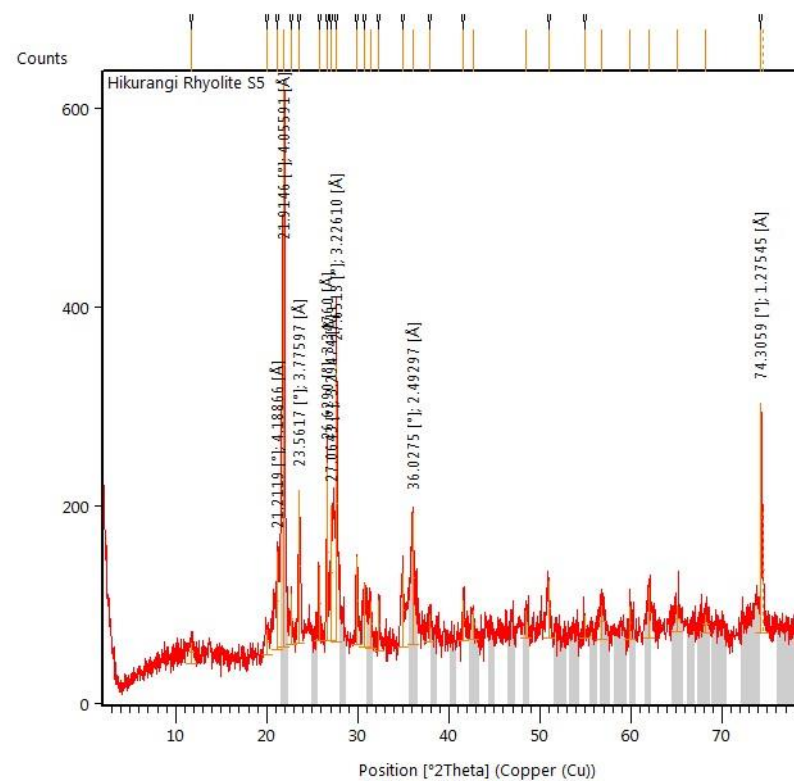
Hikurangi Rhyolite sample 3



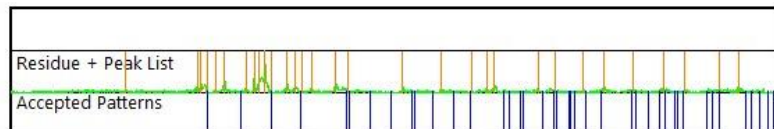
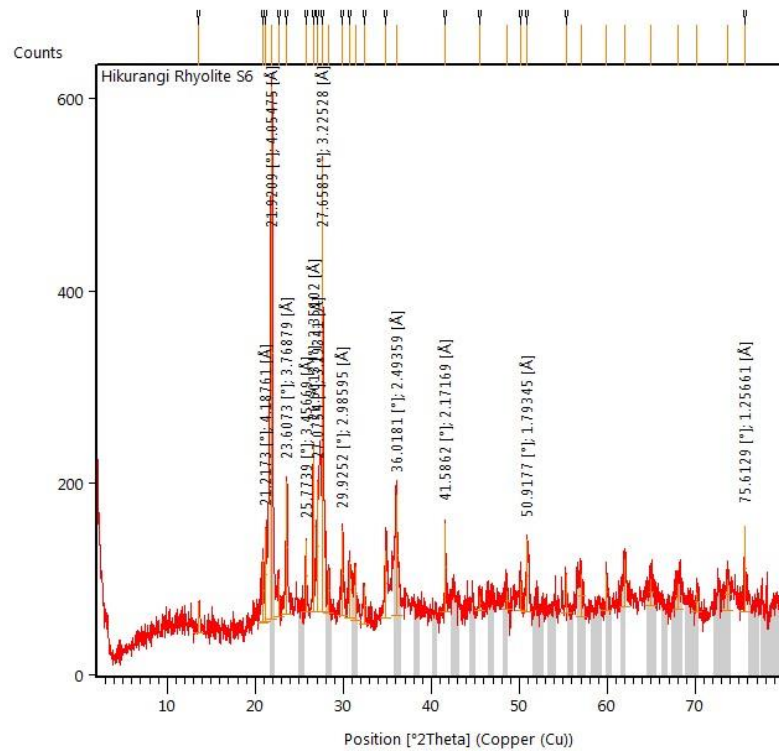
Hikurangi Rhyolite sample 4



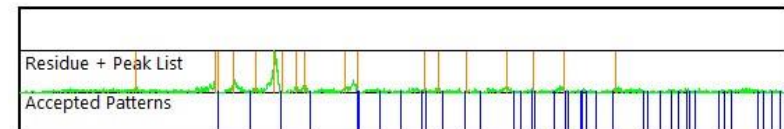
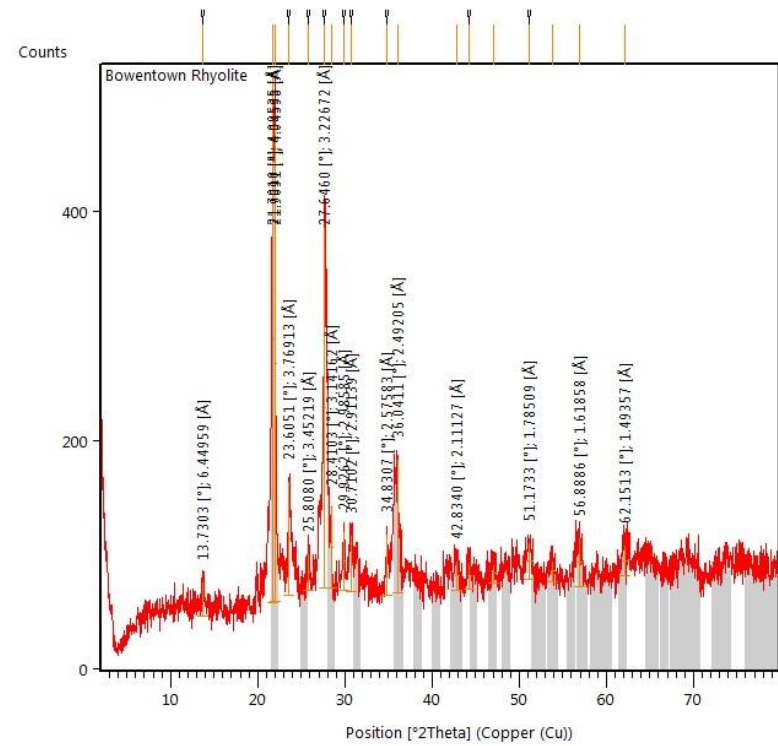
Hikurangi Rhyolite sample 5



Hikurangi Rhyolite sample 6



Bowentown Rhyolite sample 1



## **Appendix V**

### **Electron microprobe results**

---

**Table V.1:** Augite crystals in pumice for the Corbett Ignimbrite (samples 1.1.1p and 1.3.2p) and in fiamme for the Ratarua Ignimbrite (sample 13.3.2p).

UoW (petlab no.) 2015	W150300	W150300	W150302	W150302	W150302	W150302	W150302
Sample no.	1.1.1p	1.1.1p	1.3.2p	1.3.2p	1.3.2p	13.3.2p	13.3.2p
Crystal	1	2	1	2	3	1	2
(wt. %)							
<b>CaO</b>	21.049	15.103	21.323	21.659	21.403	21.411	20.422
<b>TiO<sub>2</sub></b>	0.321	1.182	0.182	0.176	0.158	0.148	0.197
<b>Na<sub>2</sub>O</b>	0.286	0.87	0.29	0.259	0.256	0.24	0.169
<b>MgO</b>	14.203	12.771	14.075	14.322	14.128	14.227	13.793
<b>SiO<sub>2</sub></b>	51.227	49.614	51.903	52.049	51.882	51.77	51.232
<b>Al<sub>2</sub>O<sub>3</sub></b>	1.897	5.568	1.133	0.94	1	0.776	0.872
<b>FeO</b>	8.763	10.78	9.674	8.978	9.906	9.451	10.572
<b>K<sub>2</sub>O</b>	0.003	0.241	0	0.005	0.01	0.02	0.018
<b>MnO</b>	0.283	0.213	0.273	0.285	0.321	0.293	0.405
<b>Cr<sub>2</sub>O<sub>3</sub></b>	0.155	0.091	0.021	0	0	0.006	0.014
TOTAL	98.187	96.433	98.864	98.673	99.064	98.342	97.694
<b>Normalised values</b>							
CaO	44.18	36.59	44.01	44.58	43.87	44.08	42.67
FeO	14.36	20.38	15.58	14.42	15.85	15.19	17.24
MgO	41.46	43.03	40.41	41.00	40.28	40.73	40.09

**Table V.2:** Biotite phenocrysts in the Hikurangi Rhyolite.

<b>UoW (petlab no.) 2015</b>	W150305	W150305	W150305	W150305	W150305	W150305
<b>Sample no.</b>	2.1.1p	2.1.1p	2.1.1p	2.1.1p	2.1.1p	2.1.1p
<b>Crystal</b>	1	2	3	4	5	6
(wt. %)						
<b>CaO</b>	0	0	0.237	0	0.533	0
<b>TiO<sub>2</sub></b>	3.253	3.317	3.27	3.273	3.308	3.244
<b>Na<sub>2</sub>O</b>	1.107	0.995	1.049	0.947	0.986	0.955
<b>MgO</b>	6.822	6.81	6.712	6.491	6.034	6.136
<b>SiO<sub>2</sub></b>	33.858	34.189	33.463	33.801	33.311	33.033
<b>Al<sub>2</sub>O<sub>3</sub></b>	13.638	13.19	13.516	13.213	13.426	13.177
<b>FeO</b>	27.898	28.12	27.911	28.66	29.461	30.38
<b>K<sub>2</sub>O</b>	13.341	13.084	12.951	12.906	12.391	12.81
<b>MnO</b>	0.301	0.272	0.248	0.276	0.274	0.236
<b>Cr<sub>2</sub>O<sub>3</sub></b>	0.007	0	0.016	0.012	0.001	0
<b>TOTAL</b>	<b>100.225</b>	<b>99.977</b>	<b>99.373</b>	<b>99.579</b>	<b>99.725</b>	<b>99.971</b>

**Table V.3:** Orthopyroxene crystals in Corbett Ignimbrite pumice.

<b>UoW (petlab no.) 2015</b>	W150300	W150300	W150300	W150300	W150300	W150302	W150302	W150302	W150302
<b>Sample no.</b>	1.1.1p	1.1.1p	1.1.1p	1.1.1p	1.1.1p	1.3.2p	1.3.2p	1.3.2p	1.3.2p
<b>Crystal</b>	1	2	3	4	5	1	2	3	4
(wt. %)									
<b>CaO</b>	1.236	1.279	1.381	1.211	1.207	1.201	1.382	1.226	1.768
<b>TiO<sub>2</sub></b>	0.144	0.125	0.151	0.114	0.174	0.115	0.11	0.112	0.15
<b>MgO</b>	21.42	21.181	21.745	19.947	22.001	20.869	17.976	21.286	25.507
<b>SiO<sub>2</sub></b>	51.514	51.845	51.872	53.813	51.804	51.589	51.352	52.015	52.905
<b>Al<sub>2</sub>O<sub>3</sub></b>	0.969	0.692	0.813	1.163	0.984	0.755	0.531	0.717	1.117
<b>FeO</b>	23.456	24.251	23.176	21.647	22.708	22.54	27.871	23.58	17.842
<b>MnO</b>	0.657	0.61	0.717	0.571	0.567	0.669	0.923	0.614	0.413
<b>Cr<sub>2</sub>O<sub>3</sub></b>	0.034	0.001	0	0	0	0	0.009	0.014	0
<b>TOTAL</b>	99.43	99.984	99.855	98.466	99.445	97.738	100.154	99.564	99.702
<b>Normalised values</b>									
CaO	2.51	2.58	2.78	2.48	2.44	2.51	2.87	2.49	3.46
FeO	37.11	38.11	36.39	37.10	35.78	36.79	45.19	37.38	27.21
MgO	60.38	59.31	60.83	60.42	61.78	60.70	51.94	60.13	69.33

**Table V.4:** Orthopyroxene crystals in Bowentown Rhyolite (10.1.2p) and Ratarua Ignimbrite (13.3.2p) fiamme.

UoW (petlab no.) 2015	W150326	W150326	W150326	W150326	W150326	W150326	W150326
Sample no.	10.1.2p	10.1.2p	13.3.2p	13.3.2p	13.3.2p	13.3.2p	13.3.2p
Crystal	1	2	1	2	3	4	5
(wt. %)							
<b>CaO</b>	0.0964	0.957	1.226	1.198	1.23	1.306	2.176
<b>TiO<sub>2</sub></b>	0.094	0.074	0.101	0.136	0.142	0.173	0.212
<b>MgO</b>	18.162	16.757	20.576	20.775	20.291	21.653	27.392
<b>SiO<sub>2</sub></b>	50.513	50.257	51.627	51.636	50.996	51.646	52.957
<b>Al<sub>2</sub>O<sub>3</sub></b>	0.67	0.472	0.785	0.78	0.753	1.656	2.395
<b>FeO</b>	27.287	29.599	23.101	23.872	25.58	22.254	13.372
<b>MnO</b>	1.306	1.536	0.644	0.617	0.75	0.538	0.367
<b>Cr<sub>2</sub>O<sub>3</sub></b>	0.012	0	0.004	0	0	0.104	0.079
<b>TOTAL</b>	99.008	99.652	98.064	99.014	99.742	99.33	98.95
<b>Normalised values</b>							
CaO	0.21	2.02	2.56	2.46	2.49	2.68	4.29
FeO	45.65	48.77	37.66	38.24	40.40	35.60	20.58
MgO	54.14	49.21	59.78	59.30	57.11	61.72	75.13

**Table V.5:** Oxide crystals in the Bowentown Rhyolite (10.1.2p) and Hikurangi Rhyolite (2.1.1p).

<b>UoW (petlab no.) 2015</b>	W150326	W150326	W150326	W150326	W150326	W150305	W150305	W150305	W150305	W150305
<b>Sample no.</b>	10.1.2p	10.1.2p	10.1.2p	10.1.2p	10.1.2p	2.1.1p	2.1.1p	2.1.1p	2.1.1p	2.1.1p
<b>Crystal</b>	1	2	3	4	5	1	2	3	4	5
(wt. %)										
<b>TiO<sub>2</sub></b>	10.234	46.92	0.055	47.002	10.21	7.121	1.037	0.783	7.273	0
<b>MgO</b>	0.588	1.138	0.012	1.072	0.34	0.151	0.424	0.585	0.193	0
<b>SiO<sub>2</sub></b>	0.102	0.011	34.931	0.032	0.121	0.252	29.641	29.334	0.223	34.611
<b>Al<sub>2</sub>O<sub>3</sub></b>	1.754	0.208	0	0.172	1.904	1.385	12.322	12.274	1.433	0.001
<b>FeO</b>	78.432	46.507	0.192	47.651	79.17	76.162	16.073	15.683	77.823	0
<b>MnO</b>	0.678	1.062	0.006	1.042	0.765	0.563	0.544	0.485	0.588	0.011
<b>Cr<sub>2</sub>O<sub>3</sub></b>	0	0	0.005	0	0.016	0.009	0	0	0.008	0.028
<b>TOTAL</b>	<b>91.788</b>	<b>95.846</b>	<b>35.201</b>	<b>96.971</b>	<b>92.526</b>	<b>85.643</b>	<b>60.041</b>	<b>59.144</b>	<b>87.541</b>	<b>34.651</b>

**Table V.6:** Oxide crystals in the Corbett Ignimbrite pumice.

UoW (petlab no.)											
2015	W150300	W150300	W150300	W150300	W150300	W150300	W150300	W150300	W150300	W150300	W150300
Sample no.	1.1.1p	1.1.1p	1.1.1p	1.1.1p	1.1.1p	1.1.1p	1.1.1p	1.1.1p	1.1.1p	1.1.1p	1.1.1p
Crystal	1	1	2	3	4	4	5	6	7	8	8
(wt. %)											
TiO2	11.035	11.069	10.829	10.413	10.804	10.614	10.628	10.496	10.862	10.696	10.775
MgO	1.34	1.239	1.149	1.49	1.155	1.203	1.784	1.241	1.517	1.466	0.969
SiO2	0.067	0.751	0.074	0.057	0.059	0.064	0.069	0.061	0.061	0.051	3.618
Al2O3	2.057	2.471	1.869	2.209	1.923	1.985	2.292	1.89	2.216	2.153	2.89
FeO	77.628	74.3	77.711	76.606	76.626	77.167	77.2	78.194	77.822	76.502	70.059
MnO	0.349	0.43	0.351	0.372	0.383	0.42	0.397	0.381	0.401	0.411	0.223
Cr2O3	0.04	0.127	0.115	0.416	0.296	0.32	0.061	0.161	0.178	0.192	0.136
TOTAL	92.516	90.387	92.098	91.563	91.246	91.773	92.431	92.424	93.057	91.471	88.67

**Table V.7:** Oxide crystals in the Corbett Ignimbrite pumice.

<b>UoW (petlab</b>							
<b>no.) 2015</b>	W150302	W150302	W150302	W150302	W150302	W150302	W150302
<b>Sample no.</b>	1.3.2p	1.3.2p	1.3.2p	1.3.2p	1.3.2p	1.3.2p	1.3.2p
<b>Crystal</b>	1	2	3	4	5	5	6
(wt. %)							
<b>TiO2</b>	10.774	10.798	10.987	10.82	10.605	10.764	10.719
<b>MgO</b>	1.71	1.83	1.634	1.66	1.238	1.294	1.34
<b>SiO2</b>	0.075	0.094	0.057	0.084	0.082	0.076	0.076
<b>Al2O3</b>	2.292	2.26	2.275	2.178	2.092	2.057	2.088
<b>FeO</b>	77.164	77.066	77.379	78.375	78.535	78.306	77.539
<b>MnO</b>	0.412	0.412	0.365	0.399	0.413	0.422	0.432
<b>Cr2O3</b>	0.219	0.18	0.16	0.075	0.222	0.217	0.344
<b>TOTAL</b>	<b>92.646</b>	<b>92.64</b>	<b>92.557</b>	<b>93.591</b>	<b>93.187</b>	<b>93.136</b>	<b>92.538</b>

**Table V.8:** Oxide crystals in the Ratarua Ignimbrite fiamme.

UoW (petlab no.) 2015	W150335	W150335	W150335	W150335	W150335	W150335	W150335
Sample no.	13.3.2p	13.3.2p	13.3.2p	13.3.2p	13.3.2p	13.3.2p	13.3.2p
Crystal	1	2	3	4	5	6	6
(wt. %)							
<b>TiO<sub>2</sub></b>	7.673	43.15	9.78	29.257	43.713	9.864	9.624
<b>MgO</b>	0.654	1.083	0.923	1.555	1.611	0.945	0.911
<b>SiO<sub>2</sub></b>	0.257	0	0.057	0.099	0.004	0.229	0.082
<b>Al<sub>2</sub>O<sub>3</sub></b>	2.027	0.109	2.004	1.148	0.209	2.357	2.212
<b>FeO</b>	77.264	49.836	78.257	58.761	48.792	75.184	78.361
<b>MnO</b>	0.367	0.606	0.436	0.631	0.61	0.379	0.435
<b>Cr<sub>2</sub>O<sub>3</sub></b>	0.27	0.025	0.063	0.076	0.001	0.197	0.184
<b>TOTAL</b>	<b>88.512</b>	<b>94.809</b>	<b>91.52</b>	<b>91.527</b>	<b>94.94</b>	<b>89.155</b>	<b>91.809</b>

**Table V.9:** Plagioclase in the Corbett Ignimbrite pumice (samples 1.1.1p and 1.3.2p).

UoW (petlab no.) 2015	W150300	W150300	W150300	W150300	W150300	W150300	W150300
Sample no.	1.1.1p	1.1.1p	1.1.1p	1.1.1p	1.1.1p	1.1.1p	1.1.1p
Crystal	1	1	1	2	2	3	3
Position on crystal	Mid	Core	Rim	Mid	Core	Mid	Rim
(wt. %)							
<b>CaO</b>	11.561	10.202	10.689	9.946	10.321	10.196	8.536
<b>TiO<sub>2</sub></b>	0	0	0	0	0.004	0	0.002
<b>Na<sub>2</sub>O</b>	4.287	4.966	4.749	5.195	5.059	4.617	5.759
<b>MgO</b>	0.021	0.025	0.021	0.032	0.036	0.016	0.011
<b>SiO<sub>2</sub></b>	52.734	54.391	54.211	55.036	54.338	49.378	57.065
<b>Al<sub>2</sub>O<sub>3</sub></b>	29.003	27.593	28.099	27.588	27.643	26.921	26.331
<b>FeO</b>	0.44	0.4	0.4	0.34	0.407	0.4	0.373
<b>K<sub>2</sub>O</b>	0.244	0.324	0.275	0.32	0.287	0.246	0.403
<b>TOTAL</b>	98.29	97.901	98.444	98.457	98.086	91.774	98.48
<b>Normalised values</b>							
An	58.96	52.12	54.19	50.43	52.08	54.12	43.91
Ab	39.55	45.90	43.54	47.64	46.19	44.33	53.61
Or	1.49	1.98	2.27	1.93	1.73	1.55	2.48

<b>UoW (petlab no.) 2015</b>	W150300	W150300	W150300	W150300	W150300	W150300	W150300	W150300
<b>Sample no.</b>	1.1.1p	1.1.1p	1.1.1p	1.1.1p	1.1.1p	1.1.1p	1.1.1p	1.1.1p
<b>Crystal</b>	4	4	4	5	6	6	7	7
<b>Position on crystal</b>	Mid	Rim	Core	Core	Mid	Rim	Mid	Rim
(wt. %)								
<b>CaO</b>	10.132	11.533	11.271	10.195	9.843	10.203	10.345	11.977
<b>TiO<sub>2</sub></b>	0.006	0.011	0.019	0.003	0	0	0.016	0.005
<b>Na<sub>2</sub>O</b>	5.081	4.471	4.539	5.126	5.278	4.963	4.976	4.207
<b>MgO</b>	0.03	0.018	0.028	0.03	0.02	0.009	0.037	0.016
<b>SiO<sub>2</sub></b>	55.094	53.198	53.71	54.868	55.291	54.823	54.441	52.484
<b>Al<sub>2</sub>O<sub>3</sub></b>	27.52	28.781	28.643	27.633	27.238	27.574	57.876	29.217
<b>FeO</b>	0.442	0.404	0.5	0.409	0.34	0.371	0.271	0.209
<b>K<sub>2</sub>O</b>	0.306	0.24	0.262	0.347	0.427	0.371	0.271	0.209
<b>TOTAL</b>	98.611	98.656	98.972	98.611	98.437	98.385	98.342	98.535
<b>Normalised values</b>								
An	51.47	57.93	56.91	51.27	49.45	51.99	52.57	60.37
Ab	46.68	40.63	41.50	46.64	47.99	45.76	45.78	38.39
Or	1.85	1.44	1.59	2.09	2.56	2.25	1.65	1.24

UoW (petlab no.) 2015	W150302	W150302	W150302	W150302	W150302	W150302	W150302	W150302
Sample no.	1.3.2p	1.3.2p	1.3.2p	1.3.2p	1.3.2p	1.3.2p	1.3.2p	1.3.2p
Crystal	1	1	2	2	3	3	4	4
Position on crystal	Mid	Rim	Mid	Rim	Mid	Rim	Mid	Rim
(wt. %)								
<b>CaO</b>	9.623	10.426	11.201	10.544	9.727	10.596	10.369	10.527
<b>TiO2</b>	0.009	0.005	0.001	0.018	0	0.02	0	0.006
<b>Na2O</b>	5.381	5.037	4.652	4.952	5.462	4.827	5.114	4.948
<b>MgO</b>	0.015	0	0.026	0.033	0.025	0.042	0.022	0.019
<b>SiO2</b>	55.852	54.52	53.548	54.584	56.01	53.729	55.049	54.468
<b>Al2O3</b>	27.343	27.743	28.529	28.136	27.462	27.905	27.606	27.843
<b>FeO</b>	0.243	0.335	0.388	0.306	0.431	0.493	0.48	0.506
<b>K2O</b>	0.327	0.28	0.251	0.279	0.326	0.289	0.338	0.317
TOTAL	98.793	98.346	98.596	98.852	99.443	97.901	98.978	98.634
<b>Normalised values</b>								
An	48.87	52.47	56.24	53.15	48.63	53.85	51.77	53.01
Ab	49.45	45.87	42.27	45.18	49.44	44.41	46.21	45.1
Or	1.68	1.66	1.49	1.67	1.93	1.74	2.02	1.89

**Table V.10:** Plagioclase in the Ratarua Ignimbrite fiamme (sample 13.3.2p).

UoW (petlab no.) 2015	W150335	W150335	W150335	W150335	W150335	W150335	W150335	W150335
Sample no.	13.3.2p	13.3.2p	13.3.2p	13.3.2p	13.3.2p	13.3.2p	13.3.2p	13.3.2p
Crystal	1	1	2	3	4	4	5	5
Position on crystal	Core	Rim	Core	Rim	Mid	Rim	Mid	Rim
(wt. %)								
<b>CaO</b>	14.802	9.773	10.459	0.25	13.627	12.646	10.525	10.015
<b>TiO<sub>2</sub></b>	0.031	0.002	0	3.027	0	0.002	0.012	0.007
<b>Na<sub>2</sub>O</b>	2.687	4.617	4.893	0.07	3.267	3.815	4.88	4.907
<b>MgO</b>	0.014	0.02	0.024	2.334	0.0031	0.024	0.026	0.027
<b>SiO<sub>2</sub></b>	48.551	57.715	53.975	49.476	49.905	51.507	53.759	55.081
<b>Al<sub>2</sub>O<sub>3</sub></b>	31.517	27.092	27.758	35.22	30.456	29.507	27.882	28.08
<b>FeO</b>	0.456	0.491	0.391	1.764	0.397	0.482	0.335	0.424
<b>K<sub>2</sub>O</b>	0.105	0.316	0.273	0.188	0.153	0.169	0.314	0.327
TOTAL	98.163	95.026	97.773	92.329	97.836	98.152	97.733	98.868
<b>Normalised values</b>								
An	74.81	51.43	53.26	3.95	69.10	67.79	53.34	51.95
Ab	24.57	46.59	45.08	92.62	29.99	31.68	44.76	46.04
Or	0.62	1.98	1.66	3.43	0.91	0.51	1.90	2.01

**Table V.11:** Plagioclase in the Bowentown Rhyolite (sample 10.1.2p).

UoW (petlab no.)									
<b>2015</b>	W150326	W150326	W150326	W150326	W150326	W150326	W150326	W150326	W150326
<b>Sample no.</b>	10.1.2p	10.1.2p	10.1.2p	10.1.2p	10.1.2p	10.1.2p	10.1.2p	10.1.2p	10.1.2p
<b>Crystal</b>	1	2	2	4	4	5	5	6	6
<b>Position on crystal</b>	Rim	Mid	Rim	Mid	Rim	Mid	Rim	Mid	Rim
(wt. %)									
<b>CaO</b>	0.305	8.037	7.929	8.808	7.786	7.971	7.657	0.427	0.324
<b>TiO<sub>2</sub></b>	0.036	0	0.001	0	0.006	0	0.009	0.045	0.027
<b>Na<sub>2</sub>O</b>	2.844	6.3	6.065	5.794	5.711	6.048	6.475	3.034	2.578
<b>MgO</b>	0.009	0	0.003	0.017	0.009	0.004	0.014	0	0
<b>SiO<sub>2</sub></b>	66.173	57.416	56.997	56.785	58.067	57.789	58.222	71.715	67.614
<b>Al<sub>2</sub>O<sub>3</sub></b>	19.25	26.184	26.043	26.999	26.252	26.107	25.007	16.869	18.342
<b>FeO</b>	0.098	0.216	0.32	0.269	0.349	0.211	0.254	0.078	0.131
<b>K<sub>2</sub>O</b>	8.606	0.319	0.317	0.274	0.329	0.328	0.363	6.241	8.049
<b>TOTAL</b>	97.321	98.472	97.675	98.946	98.509	98.458	99.001	98.409	97.065
<b>Normalised values</b>									
An	1.94	40.55	41.13	44.91	42.06	41.28	38.66	3.19	2.23
Ab	32.79	57.53	56.92	53.43	55.85	56.71	59.16	41.14	32.01
Or	65.27	1.92	1.95	1.66	2.09	2.01	2.18	55.67	65.76

**Table V.12:** Plagioclase in the Hikurangi Rhyolite (sample 2.1.1p).

<b>UoW (petlab no.) 2015</b>	W150300	W150300	W150300	W150300	W150300	W150300	W150300
<b>Sample no.</b>	2.1.1p	2.1.1p	2.1.1p	2.1.1p	2.1.1p	2.1.1p	2.1.1p
<b>Crystal</b>	1	1	2	2	3	4	4
<b>Position on crystal</b>	Mid	Rim	Mid	Rim	Mid	Mid	Rim
(wt. %)							
<b>CaO</b>	5.356	5.525	6.388	5.721	0.147	0.153	0.136
<b>TiO<sub>2</sub></b>	0	0	0.016	0	0.032	0.013	0.018
<b>Na<sub>2</sub>O</b>	7.268	7.211	6.839	7.137	2.815	2.576	2.671
<b>MgO</b>	0	0.01	0.008	0.005	0.038	0.011	0.045
<b>SiO<sub>2</sub></b>	60.785	60.705	59.848	60.639	62.304	62.68	62.941
<b>Al<sub>2</sub>O<sub>3</sub></b>	24.42	24.554	25.183	24.494	19.114	19.712	19.26
<b>FeO</b>	0.182	0.116	0.129	0.207	0.004	0.067	0.091
<b>K<sub>2</sub>O</b>	0.783	0.766	0.657	0.755	11.45	10.303	11.693
<b>TOTAL</b>	98.749	98.887	99.068	98.958	95.904	95.515	96.855
<b>Normalised values</b>							
An	27.55	28.35	32.68	29.29	0.79	0.89	0.71
Ab	67.66	66.96	63.33	66.12	25.27	27.79	25.59
Or	4.79	4.69	3.99	4.59	73.94	71.82	73.70

UoW (petlab no.)							
<b>2015</b>	W150300	W150300	W150300	W150300	W150300	W150300	W150300
<b>Sample no.</b>	2.1.1p	2.1.1p	2.1.1p	2.1.1p	2.1.1p	2.1.1p	2.1.1p
<b>Crystal</b>	8	8	8	8	8	8	8
<b>Position on crystal</b>	Mid	Rim	Rim	Mid	Core	Mid	Core
(wt. %)							
<b>CaO</b>	0.113	0.145	0.212	0.128	0.13	0.142	0.13
<b>TiO<sub>2</sub></b>	0	0	0	0.017	0	0.004	0
<b>Na<sub>2</sub>O</b>	2.747	3.719	3.77	3.005	3.544	0.373	2.933
<b>MgO</b>	0.01	0	0	0	0	0	0
<b>SiO<sub>2</sub></b>	64.026	65.011	65.653	64.396	64.645	64.112	64.081
<b>Al<sub>2</sub>O<sub>3</sub></b>	19.107	18.999	19.905	19.089	19.077	19.111	19.15
<b>FeO</b>	0.082	0.071	0.145	0	0.064	0.064	0.051
<b>K<sub>2</sub>O</b>	11.666	10.506	10.429	11.136	10.818	11.096	11.326
<b>TOTAL</b>	97.751	98.451	98.304	97.771	98.278	97.902	97.671
<b>Normalised values</b>							
An	0.59	0.75	1.10	0.69	0.66	1.01	0.69
Ab	26.19	34.71	35.08	28.87	33.03	4.81	28.05
Or	73.22	64.54	63.82	70.44	66.31	94.18	71.26

**Table V.13:** Glass shards in the Corbett Ignimbrite (samples 1.1.1p and 1.3.2p). All values have been normalised but total has been left as the original figure.

UoW (petlab no.)										
<b>2015</b>	W150300	W150300	W150300	W150300	W150300	W150300	W150300	W150300	W150300	W150300
<b>Sample no.</b>	1.1.1p	1.1.1p	1.1.1p	1.1.1p	1.1.1p	1.1.1p	1.1.1p	1.1.1p	1.1.1p	1.1.1p
<b>Shard</b>	1	2	3	4	5	6	7	8	9	10
<b>CaO</b>	2.10	2.14	2.11	2.14	2.20	2.49	1.64	2.42	2.44	1.95
<b>TiO<sub>2</sub></b>	0.36	0.36	0.41	0.39	0.39	0.44	0.27	0.42	0.42	0.34
<b>Na<sub>2</sub>O</b>	2.88	2.79	2.79	2.96	2.99	2.69	2.93	2.75	2.99	2.28
<b>MgO</b>	0.44	0.43	0.43	0.48	0.49	0.56	0.27	0.52	0.53	0.41
<b>SiO<sub>2</sub></b>	74.81	74.67	74.77	74.38	73.70	73.66	76.18	73.92	73.41	75.49
<b>Al<sub>2</sub>O<sub>3</sub></b>	14.11	14.20	14.19	14.55	14.52	14.82	13.62	14.66	14.77	14.17
<b>FeO</b>	2.22	2.40	2.27	2.41	2.61	2.56	1.91	2.51	2.52	2.38
<b>K<sub>2</sub>O</b>	2.85	2.78	2.81	2.48	2.80	2.55	2.95	2.53	2.71	2.80
<b>MnO</b>	0.07	0.03	0.05	0.03	0.04	0.05	0.04	0.08	0.03	0.01
<b>Cl</b>	0.16	0.20	0.16	0.18	0.27	0.17	0.18	0.19	0.17	0.16
<b>TOTAL</b>	95.71	95.53	95.49	95.43	95.16	91.76	95.12	94.12	95.70	93.84

UoW (petlab no.)	W150302	W150302	W150302	W150302	W150302	W150302	W150302
<b>2015</b>							
<b>Sample no.</b>	1.3.2p	1.3.2p	1.3.2p	1.3.2p	1.3.2p	1.3.2p	1.3.2p
<b>Shard</b>	1	2	3	4	5	6	7
<b>CaO</b>	1.91	1.97	2.01	1.96	1.98	1.92	1.97
<b>TiO2</b>	0.34	0.32	0.34	0.33	0.32	0.33	0.31
<b>Na2O</b>	2.91	2.95	3.03	2.89	3.03	2.95	3.16
<b>MgO</b>	0.41	0.38	0.35	0.35	0.40	0.36	0.37
<b>SiO2</b>	74.61	74.94	75.09	75.10	74.86	74.75	74.93
<b>Al2O3</b>	14.79	14.13	14.05	14.09	13.96	14.48	14.03
<b>FeO</b>	1.94	2.25	1.93	2.08	2.11	2.13	1.95
<b>K2O</b>	2.85	2.83	2.94	2.97	3.10	2.87	3.05
<b>MnO</b>	0.05	0.03	0.06	0.03	0.03	0.02	0.04
<b>Cl</b>	0.21	0.21	0.19	0.19	0.21	0.19	0.18
<b>TOTAL</b>	95.96	96.46	97.08	96.38	93.29	93.00	96.32

<b>UoW (petlab no.)</b>							
<b>2015</b>	W150302	W150302	W150302	W150302	W150302	W150302	W150302
<b>Sample no.</b>	1.3.2p	1.3.2p	1.3.2p	1.3.2p	1.3.2p	1.3.2p	1.3.2p
<b>Shard</b>	8	9	10	11	12	13	14
<b>CaO</b>	1.98	2.00	1.97	1.98	1.95	1.86	1.96
<b>TiO<sub>2</sub></b>	0.34	0.32	0.31	0.34	0.31	0.31	0.31
<b>Na<sub>2</sub>O</b>	2.98	3.24	3.24	3.22	2.84	3.16	2.91
<b>MgO</b>	0.40	0.39	0.33	0.38	0.37	0.36	0.35
<b>SiO<sub>2</sub></b>	75.18	75.05	74.87	74.75	75.36	75.06	75.42
<b>Al<sub>2</sub>O<sub>3</sub></b>	13.94	13.70	13.94	14.10	14.10	13.95	14.01
<b>FeO</b>	2.11	2.13	2.09	2.17	2.13	2.12	2.06
<b>K<sub>2</sub>O</b>	2.83	2.90	2.99	2.80	2.70	2.95	2.76
<b>MnO</b>	0.05	0.09	0.07	0.07	0.04	0.07	0.01
<b>Cl</b>	0.18	0.18	0.19	0.18	0.18	0.15	0.20
<b>TOTAL</b>	96.06	96.34	97.00	97.10	96.16	96.88	95.54



## **Appendix VI**

### **XRF results**

---

**Table VI.1:** Major (normalised to 100 % volatile free) and trace element XRF analysis of 5 pumice samples from the Corbett Ignimbrite type section.

Corbett Ignimbrite – type section locality 1					
<i>Sample no.</i>	CIL1S1	CIL1S2	CIL1S3	CIL1S4	CIL1S5
<i>Major elements (wt. %)</i>					
<b>SiO<sub>2</sub></b>	71.07	77.80	68.26	65.86	69.12
<b>TiO<sub>2</sub></b>	0.50	0.39	0.748	0.70	0.63
<b>Al<sub>2</sub>O<sub>3</sub></b>	16.78	11.73	16.64	19.65	16.97
<b>Fe<sub>2</sub>O<sub>3</sub></b>	5.25	3.54	4.92	6.80	5.57
<b>MnO</b>	0.06	0.06	0.11	0.09	0.06
<b>MgO</b>	0.81	0.47	1.15	0.73	0.67
<b>CaO</b>	2.38	2.37	2.72	2.14	1.97
<b>Na<sub>2</sub>O</b>	1.34	1.56	2.49	1.94	2.23
<b>K<sub>2</sub>O</b>	1.75	1.92	2.88	2.00	2.70
<b>P<sub>2</sub>O<sub>5</sub></b>	0.02	0.12	0.04	0.04	0.04
<b>LOI*</b>	1.00	8.45	11.25	11.43	11.81
<b>Total*</b>	99.68	99.25	100.76	99.52	99.24
<i>Trace elements (ppm)</i>					
<b>F</b>	236	184	279	306	359
<b>S</b>	356	2107	922	161	315
<b>Cl</b>	1169	1938	5418	1364	2596
<b>Sc</b>	18	12	22	16	17
<b>V</b>	87	56	110	99	88
<b>Cr</b>	13	-	26	21	13
<b>Co</b>	30	40	42	47	53
<b>Ni</b>	15	10	18	10	12
<b>Cu</b>	14	12	14	15	10
<b>Zn</b>	59	39	67	63	64
<b>Ga</b>	17	12	19	20	18
<b>As</b>	8	6	7	10	8
<b>Rb</b>	72	64	55	73	86
<b>Sr</b>	160	157	123	122	124
<b>Y</b>	12	13	11	14	16
<b>Zr</b>	130	100	156	145	148
<b>Nb</b>	5	3	4	6	6
<b>Mo</b>	1	4	4	4	4
<b>Sn</b>	4	3	1	6	4
<b>Sb</b>	3	3	-	2	2
<b>Cs</b>	6	4	1	3	7
<b>Ba</b>	686	1136	427	435	478
<b>Tl</b>	-	1	1	1	1
<b>Pb</b>	11	12	12	16	14
<b>La</b>	12	9	4	10	9
<b>Ce</b>	30	23	24	26	27
<b>Nd</b>	12	15	8	14	15
<b>Th</b>	6	6	8	9	9
<b>U</b>	1	3	3	3	3

\* LOI and total are original figures

**Table VI.2:** Major (normalised to 100 % volatile free) and trace element XRF analysis of pumice samples (CIL7S1, CIL8S1, CIL9S3) and two fiamme samples (CIL11S1, CIL11S3) from the Corbett Ignimbrite and one sample from the Bowentown Rhyolite.

Corbett Ignimbrite and Bowentown Rhyolite						
<i>Sample no.</i>	CIL7S1	CIL8S1	CIL9S3	CIL11S1	CIL11S3	BR
<i>Major elements (wt. %)</i>						
<b>SiO<sub>2</sub></b>	71.72	63.08	64.24	59.91	65.72	75.78
<b>TiO<sub>2</sub></b>	0.16	0.53	0.55	0.88	0.51	0.16
<b>Al<sub>2</sub>O<sub>3</sub></b>	17.74	21.51	19.10	22.92	19.68	13.76
<b>Fe<sub>2</sub>O<sub>3</sub></b>	1.69	5.83	4.91	6.25	4.71	1.59
<b>MnO</b>	0.04	0.05	0.11	0.05	0.03	0.04
<b>MgO</b>	0.41	1.19	2.02	1.68	1.15	0.25
<b>CaO</b>	1.48	2.99	4.31	3.30	2.62	1.07
<b>Na<sub>2</sub>O</b>	2.12	2.42	2.37	2.80	2.58	3.15
<b>K<sub>2</sub>O</b>	4.60	2.35	2.27	1.91	2.91	2.72
<b>P<sub>2</sub>O<sub>5</sub></b>	0.00	0.01	0.08	0.25	0.03	-
<b>LOI*</b>	5.68	7.64	7.55	6.13	4.51	1.45
<b>Total*</b>	99.77	99.74	99.76	99.78	99.79	99.706
<i>Trace elements (ppm)</i>						
<b>F</b>	418	401	185	441	362	97
<b>S</b>	40	100	67	38	25	82
<b>Cl</b>	411	881	709	208	191	1383
<b>Sc</b>	6	13	15	27	16	5
<b>V</b>	20	101	148	158	95	4
<b>Cr</b>	1	11	-	15	31	0
<b>Co</b>	47	35	50	38	23	7
<b>Ni</b>	6	11	18	30	15	4
<b>Cu</b>	14	8	10	15	18	5
<b>Zn</b>	27	58	59	95	51	39
<b>Ga</b>	14	17	17	20	17	15
<b>As</b>	14	5	6	5	6	6
<b>Rb</b>	137	76	74	61	109	76
<b>Sr</b>	95	147	190	170	137	106
<b>Y</b>	19	14	16	27	20	18
<b>Zr</b>	131	130	134	119	149	145
<b>Nb</b>	5	5	5	5	6	7
<b>Mo</b>	1	1	1	1	1	1
<b>Sn</b>	5	4	5	5	4	4
<b>Sb</b>	3	4	3	3	3	2
<b>Cs</b>	10	7	6	5	6	2
<b>Ba</b>	735	477	499	577	662	827
<b>Tl</b>	-	-	-	-	-	-
<b>Pb</b>	18	13	14	11	13	18
<b>La</b>	8	5	8	33	15	17
<b>Ce</b>	46	23	37	33	28	46
<b>Nd</b>	16	9	16	31	19	16
<b>Th</b>	13	8	9	6	11	13
<b>U</b>	4	1	1	3	3	3

\* LOI and total are original figures

**Table VI.3:** Major (normalised to 100 % volatile free) and trace element XRF analysis of 6 fiamme samples from the Ratarua Ignimbrite.

Ratarua Ignimbrite						
<i>Sample no.</i>	RIL5S1	RIL13S1	RIL13S2	RIL13S3	RIL1S4	RIL1S5
<i>Major elements (wt. %)</i>						
<b>SiO<sub>2</sub></b>	67.28	65.56	65.93	67.88	63.15	66.12
<b>TiO<sub>2</sub></b>	0.52	0.62	0.54	0.50	0.59	0.52
<b>Al<sub>2</sub>O<sub>3</sub></b>	15.53	15.22	15.74	15.96	19.37	16.79
<b>Fe<sub>2</sub>O<sub>3</sub></b>	4.77	5.60	5.24	4.11	5.30	4.63
<b>MnO</b>	0.07	0.10	0.08	0.09	0.09	0.07
<b>MgO</b>	1.79	2.26	2.14	1.48	1.67	1.30
<b>CaO</b>	3.95	4.34	4.19	3.66	3.40	3.98
<b>Na<sub>2</sub>O</b>	3.42	3.48	3.18	3.80	3.65	3.66
<b>K<sub>2</sub>O</b>	2.52	2.67	2.80	2.39	2.61	2.77
<b>P<sub>2</sub>O<sub>5</sub></b>	0.11	0.11	0.11	0.09	0.11	0.11
<b>LOI*</b>	1.32	1	0.96	2.57	3.11	1.04
<b>Total*</b>	100.59	94.34	100.62	109.52	99.71	99.76
<i>Trace elements (ppm)</i>						
<b>F</b>	229	175	247	236	286	292
<b>S</b>	-	-	-	-	89	-
<b>Cl</b>	802	948	1128	1258	1020	645
<b>Sc</b>	13	15	14	14	16	14
<b>V</b>	92	112	102	99	113	92
<b>Cr</b>	7	14	16	20	14	11
<b>Co</b>	58	108	65	74	64	54
<b>Ni</b>	14	17	14	14	12	11
<b>Cu</b>	15	15	22	14	17	17
<b>Zn</b>	78	74	60	60	68	58
<b>Ga</b>	16	19	17	13	18	17
<b>As</b>	10	10	9	7	8	8
<b>Rb</b>	92	102	92	51	89	96
<b>Sr</b>	188	260	193	99	167	196
<b>Y</b>	58	56	31	22	22	38
<b>Zr</b>	143	138	143	135	145	145
<b>Nb</b>	5	9	5	-	6	6
<b>Mo</b>	4	5	4	4	2	1
<b>Sn</b>	-	12	3	-	3	4
<b>Sb</b>	2	10	-	-	2	2
<b>Cs</b>	3	1	1	1	4	1
<b>Ba</b>	565	626	555	504	635	578
<b>Tl</b>	-	1	1	-	-	-
<b>Pb</b>	10	18	15	6	14	14
<b>La</b>	67	38	28	43	18	33
<b>Ce</b>	47	54	46	49	42	48
<b>Nd</b>	62	33	30	48	17	31
<b>Th</b>	8	11	9	3	11	9
<b>U</b>	3	3	3	3	3	2

\* LOI and total are original figures

**Table VI.4:** Major (normalised to 100 % volatile free) and trace element XRF analysis of 6 matrix samples from the Hikurangi Rhyolite.

Hikurangi Rhyolite							
<i>Sample no.</i>	HRS1	HRS2	HRS3	HRS4	HRS5	HRS6	BR
<i>Major elements (wt. %)</i>							
<b>SiO<sub>2</sub></b>	77.49	77.81	77.32	77.06	77.01	77.15	76.90
<b>TiO<sub>2</sub></b>	0.07	0.09	0.11	0.10	0.08	0.06	0.16
<b>Al<sub>2</sub>O<sub>3</sub></b>	12.87	15.34	17.99	18.92	14.76	14.25	13.96
<b>Fe<sub>2</sub>O<sub>3</sub></b>	0.81	1.47	1.63	0.89	1.16	0.98	1.61
<b>MnO</b>	0.01	0.01	0.01	0.01	0.01	0.01	0.04
<b>MgO</b>	0.04	0.10	0.10	0.08	0.07	0.02	0.25
<b>CaO</b>	0.72	0.31	0.21	0.22	0.42	0.48	1.09
<b>Na<sub>2</sub>O</b>	3.21	1.50	0.85	0.76	2.28	2.46	3.19
<b>K<sub>2</sub>O</b>	4.70	3.29	1.71	1.90	4.14	4.52	2.76
<b>P<sub>2</sub>O<sub>5</sub></b>	0.02	0.02	0.02	0.01	0.01	0.02	0
<b>LOI*</b>	0.96	4.91	6.88	6.97	2.39	1	1.45
<b>Total*</b>	98.83	99.29	99.02	98.81	100.10	97.18	99.70
<i>Trace elements (ppm)</i>							
<b>F</b>	318	216	368	240	141	147	97
<b>S</b>	0	476	355	239	1	0	82
<b>Cl</b>	527	5766	1738	422	413	393	1383
<b>Sc</b>	4	4	4	4	4	4	5
<b>V</b>	2	5	6	7	4	3	4
<b>Cr</b>	-	-	-	-	-	-	-
<b>Co</b>	28	12	15	11	17	15	7
<b>Ni</b>	6	4	5	6	3	4	4
<b>Cu</b>	5	9	8	6	5	6	5
<b>Zn</b>	24	20	27	24	17	22	39
<b>Ga</b>	13	17	18	18	14	16	15
<b>As</b>	14	20	17	7	16	18	6
<b>Rb</b>	192	135	67	71	166	205	76
<b>Sr</b>	52	32	28	30	36	37	106
<b>Y</b>	19	10	8	30	14	18	18
<b>Zr</b>	76	93	106	101	82	77	145
<b>Nb</b>	6	7	8	8	6	8	7
<b>Mo</b>	4	4	4	4	4	4	1
<b>Sn</b>	7	6	7	8	4	9	4
<b>Sb</b>	4	3	4	5	2	6	2
<b>Cs</b>	5	8	1	2	4	8	2
<b>Ba</b>	800	633	769	650	669	543	827
<b>Tl</b>	1	1	1	1	1	1	0
<b>Pb</b>	27	31	34	17	25	25	18
<b>La</b>	31	4	1	66	20	22	17
<b>Ce</b>	67	47	50	13	39	38	46
<b>Nd</b>	29	13	13	24	17	20	16
<b>Th</b>	22	26	27	26	22	25	13
<b>U</b>	6	6	4	5	5	5	3

\* LOI and total are original figures



## **Appendix VII**

### **LA-ICP-MS specifications**

---

**Table VII.1:** LA-ICP-MS operating conditions and data acquisition parameters used for U-Pb dating.

<b>ICP-MS</b>		
Model		Elan 6100 DRCII ICP-MS (Perkin Elmer Sciex)
Gas flows	Plasma (Ar) Auxiliary (Ar) Carrier (He) Nebuliser	15 L.min 1.2 L.min 1.0 L.min 0.6 to 0.7 optimised range
Shield torch		Used for most analyses
Vacuum pressure		$1 \times 10^{-5}$ Torr
Software		Elan 3.4
<b>LASER</b>		
Model		RESolution SE series excimer laser
Wavelength		193 nm
Repetition rate		5 Hz
Pre-ablation laser warm-up	Laser fired continuously	
Spot size		30 $\mu\text{m}$ (60 for NIST)
Incident pulse energy		c. 0.04 mJ
Energy density on sample (fluence)	c. 6 J.cm <sup>2</sup>	
Software		Geostar v8.50
<b>DATA ACQUISITION PARAMETERS</b>		
Data acquisition protocol	Time resolved analyses	
Scanning mode		Peak hopping, 1 point per peak Pulse counting, dead time correction applied
Detector mode		206Pb, 207Pb, 208Pb, 204Pb, 232Th, 235U, 238U, 29Si, 91Zr
Isotopes determined	50, 50, 50, 50, 30, 50, 50, 15,	
Dwell time per isotope	15 ms respectively	
Quadrupole settling time	c. 2 ms	
Data acquisition		85 s (40 s background, 45 s ablation)
Software		Elan v 3.4

## **Appendix VIII**

### **Dating results**

---

**Table VIII.1:** Data obtained from U-Pb dating of zircons through LA-CIP-MS analysis for the Corbett Ignimbrite.

Spot no.	Final Age $^{206}\text{Pb}/^{238}\text{U}$ (My)	Final Age $^{206}\text{Pb}/^{238}\text{U}$ Int 2 S.E. (My)
Corbett Ig - 1	5.5	1.7
Corbett Ig - 2	11.8	3
Corbett Ig - 3	12.5	3.3
Corbett Ig - 5	7.4	2.4
Corbett Ig - 6	9.6	2.5
Corbett Ig - 7	7.2	2
Corbett Ig - 8	24.8	6.3
Corbett Ig - 9	17.2	3.9
Corbett Ig - 11	6.8	1.9
Corbett Ig - 12	6.5	1.6
Corbett Ig - 13	173	33
Corbett Ig - 15	9.3	2.6
Corbett Ig - 16	5.9	1.7
Corbett Ig - 17	5.9	1.2
Corbett Ig - 19	6.7	1.3
Corbett Ig - 20	12.7	2.6
Corbett Ig - 21	7.4	1.7
Corbett Ig - 23	4.9	1.5
Corbett Ig - 24	21.9	4.7
Corbett Ig - 26	9.6	3.7
Corbett Ig - 27	13.1	2.4
Corbett Ig - 29	5.8	1.6
Corbett Ig - 30	14.6	3.7
Corbett Ig - 31	7.1	1.7
Corbett Ig - 32	10.4	2.4
Corbett Ig - 33	16.3	4.4
Corbett Ig - 35	6.1	2.1
Corbett Ig - 37	15.7	3.2
Corbett Ig - 38	8.4	1.8
Corbett Ig - 39	9	2.1
Corbett Ig - 40	4.7	1.7
Corbett Ig - 41	5.8	2.1
Corbett Ig - 43	6.1	1.7
Corbett Ig - 44	38.4	9
Corbett Ig - 46	6.2	2.1
Corbett Ig - 47	11.5	2
Corbett Ig - 48	48.6	7.5
Corbett Ig - 49	5.3	1.2
Corbett Ig - 50	6.04	0.46
Corbett Ig - 51	5.6	1.6
Corbett Ig - 52	6.2	1.6
Corbett Ig - 53	6.7	1.5
Corbett Ig - 54	17.9	4.3
Corbett Ig - 55	119	16
Corbett Ig - 56	7.3	1.5
Corbett Ig - 57	7.5	2.6
Corbett Ig - 58	4.9	1.7
<b>Final age</b>	<b>6.09 ± 0.34 Ma</b>	

\* Shaded areas represent the readings included in the final age calculation

**Table VIII.2:** Data obtained from U-Pb dating of zircons through LA-CIP-MS analysis for the Bowentown Rhyolite

Spot no.	Final Age $^{206}\text{Pb}/^{238}\text{U}$ (My)	Final Age $^{206}\text{Pb}/^{238}\text{U}$ Int 2 S.E. (My)
Bowentown R - 1	3.14	0.78
Bowentown R - 2	2.95	0.35
Bowentown R - 3	6.6	1.3
Bowentown R - 4	103.3	3.9
Bowentown R - 5	2.47	0.72
Bowentown R - 6	64	12
Bowentown R - 7	250.4	7.8
Bowentown R - 8	1.51	0.62
Bowentown R - 9	3.17	0.73
Bowentown R - 10	4.1	1.1
Bowentown R - 11	1.9	0.79
Bowentown R - 13	2.98	0.68
Bowentown R - 14	42.4	7.6
Bowentown R - 15	2.5	0.45
Bowentown R - 16	2.64	0.5
Bowentown R - 17	4.63	0.59
Bowentown R - 18	2.64	0.61
Bowentown R - 19	2.07	0.84
Bowentown R - 20	3.29	0.8
Bowentown R - 21	2.07	0.66
Bowentown R - 22	0.35	0.17
Bowentown R - 23	3.29	0.82
Bowentown R - 24	2.87	0.53
Bowentown R - 25	4.4	1.4
Bowentown R - 26	3.26	0.87
Bowentown R - 27	2.7	0.68
Bowentown R - 28	199	10
Bowentown R - 29	2.72	0.52
Bowentown R - 30	2.9	1.1
Bowentown R - 31	4.7	1
Bowentown R - 32	6.4	1.4
Bowentown R - 33	9.8	1.7
Bowentown R - 34	3.35	0.83
Bowentown R - 35	0.97	0.5
Bowentown R - 36	4.7	1.2
Bowentown R - 37	1.32	0.4
Bowentown R - 38	2.09	0.86
Bowentown R - 39	21.8	3.4
Bowentown R - 40	35.3	6.7
Bowentown R - 41	6.1	1.2
Bowentown R - 42	3.61	0.84
Bowentown R - 43	2.81	0.46
Bowentown R - 44	3.24	0.89
Bowentown R - 45	1.66	0.64
Bowentown R - 46	2.14	0.66
Bowentown R - 46	2.14	0.66
Bowentown R - 47	2.79	0.67
Bowentown R - 48	2.42	0.99
Bowentown R - 49	4	1
Bowentown R - 50	3.1	0.31
Bowentown R - 51	4.7	1.6

Spot no.	Final Age $^{206}\text{Pb}/^{238}\text{U}$ (My)	Final Age $^{206}\text{Pb}/^{238}\text{U}$ Int 2 S.E. (My)
Bowentown R - 52	2.58	0.82
Bowentown R - 53	5.7	2
Bowentown R - 54	181	11
Bowentown R - 55	1.09	0.66
Bowentown R - 56	3.39	0.89
Bowentown R - 57	13	3.8
Bowentown R - 58	3.46	0.92
Bowentown R - 59	0.85	0.62
Bowentown R - 60	9.1	1.8
Bowentown R - 61	1.11	0.53
Bowentown R - 62	10.3	2.3
Bowentown R - 63	3.39	0.72
Bowentown R - 64	149	4.8
Bowentown R - 65	2.96	0.74
Bowentown R - 66	3.3	1.2
Bowentown R - 67	2.66	0.7
Bowentown R - 68	25	12
Bowentown R - 69	3.3	1.2
<b>Final age</b>	<b>2.09 <math>\pm</math> 0.45 Ma</b>	

\* Shaded areas represent the readings included in the final age calculation

**Table VIII.3:** Data obtained from U-Pb dating of zircons through LA-CIP-MS analysis for the Ratarua Ignimbrite

Spot no.	Final Age $^{206}\text{Pb}/^{238}\text{U}$ (My)	Final Age $^{206}\text{Pb}/^{238}\text{U}$ Int 2 S.E. (My)
Ratarua Ig - 1	7.4	2
Ratarua Ig - 2	6.3	1.7
Ratarua Ig - 5	6.8	2
Ratarua Ig - 6	187	8
Ratarua Ig - 7	7.5	1.2
Ratarua Ig - 8	6.4	1.9
Ratarua Ig - 9	35	10
Ratarua Ig - 10	11.7	3.2
Ratarua Ig - 11	7.1	1.4
Ratarua Ig - 13	5.8	1.5
Ratarua Ig - 14	7.9	2.5
Ratarua Ig - 15	6.2	2.2
Ratarua Ig - 16	6.9	2.1
Ratarua Ig - 17	22.9	3.8
Ratarua Ig - 18	6.8	1.8
Ratarua Ig - 20	7.2	2.2
Ratarua Ig - 22	8.4	2.2
Ratarua Ig - 24	10.6	2.9
Ratarua Ig - 25	3.8	1.4
Ratarua Ig - 26	7.6	2.3
Ratarua Ig - 28	210.2	5.7
Ratarua Ig - 30	6.5	1.8
Ratarua Ig - 31	7.1	2.2
Ratarua Ig - 32	9.3	1.7
Ratarua Ig - 33	10.5	2.2
Ratarua Ig - 34	7	1.7
Ratarua Ig - 35	7.5	1.9
Ratarua Ig - 36	7.4	2
Ratarua Ig - 37	118	21
Ratarua Ig - 38	8.7	2.6
Ratarua Ig - 40	6.2	1.8
Ratarua Ig - 41	5.1	1.6
Ratarua Ig - 42	6.8	1.2
Ratarua Ig - 44	5.9	1.9
Ratarua Ig - 45	8.9	2.7
<b>Final age</b>	<b>6.79 <math>\pm</math> 0.42 Ma</b>	

\* Shaded areas represent the readings included in the final age calculation

**Table VIII.3:** Data obtained from U-Pb dating of zircons through LA-CIP-MS analysis for the Hikurangi Rhyolite.

Spot no.	Final Age $^{206}\text{Pb}/^{238}\text{U}$ (My)	Final Age $^{206}\text{Pb}/^{238}\text{U}$ Int 2 S.E. (My)
Hikurangi R - 1	4.41	0.55
Hikurangi R - 2	4.31	0.33
Hikurangi R - 3	4.25	0.38
Hikurangi R - 4	5.46	0.6
Hikurangi R - 5	4.44	0.21
Hikurangi R - 6	4.83	0.4
Hikurangi R - 7	4.26	0.3
Hikurangi R - 8	5.97	0.92
Hikurangi R - 9	4.4	0.42
Hikurangi R - 10	15.4	1.7
Hikurangi R - 11	4.13	0.5
Hikurangi R - 12	4.44	0.25
Hikurangi R - 13	4.48	0.3
Hikurangi R - 14	4.7	1.1
Hikurangi R - 15	4.7	1.1
Hikurangi R - 16	4.74	0.26
Hikurangi R - 17	5.63	0.99
Hikurangi R - 18	4.72	0.94
Hikurangi R - 19	3.9	1.2
Hikurangi R - 20	4.59	0.66
Hikurangi R - 21	4.21	0.43
Hikurangi R - 22	3.94	0.82
Hikurangi R - 23	5.15	0.48
Hikurangi R - 24	6.62	0.97
Hikurangi R - 25	15.5	2
Hikurangi R - 26	4.3	1.5
Hikurangi R - 27	15.5	2.7
Hikurangi R - 28	5.04	0.4
Hikurangi R - 29	46.1	9
Hikurangi R - 30	4.68	0.47
Hikurangi R - 31	4.27	0.31
Hikurangi R - 32	4.7	1
Hikurangi R - 33	5.5	1.1
Hikurangi R - 34	4.21	0.55
Hikurangi R - 35	7.2	1.9
Hikurangi R - 36	4.65	0.77
Hikurangi R - 37	4.15	0.23
Hikurangi R - 38	5.6	1
Hikurangi R - 39	4.32	0.55
Hikurangi R - 40	3.94	0.79
Hikurangi R - 41	5.33	0.87
Hikurangi R - 42	4.53	0.41
Hikurangi R - 43	4.36	0.47
Hikurangi R - 44	2.38	0.93
Hikurangi R - 45	6.3	1.3
Hikurangi R - 46	4.11	0.47
Hikurangi R - 47	4.58	0.59
Hikurangi R - 48	7.6	1.9
Hikurangi R - 49	4.09	0.29
Hikurangi R - 50	6.3	2.4
Hikurangi R - 51	4.3	0.47

Spot no.	Final Age <sup>206</sup> Pb/ <sup>238</sup> U (My)	Final Age <sup>206</sup> Pb/ <sup>238</sup> U Int 2 S.E. (My)
Hikurangi R - 52	4.81	0.63
Hikurangi R - 53	16	3
Hikurangi R - 54	4.81	0.71
Hikurangi R - 55	4.01	0.92
Hikurangi R - 56	4.44	0.32
Hikurangi R - 57	4.26	0.31
Hikurangi R - 58	4.4	1.2
Hikurangi R - 61	5.96	0.94
Hikurangi R - 62	5.2	1.1
Hikurangi R - 63	3.32	0.85
Hikurangi R - 64	4.03	0.57
Hikurangi R - 65	4.6	1.2
Hikurangi R - 66	3.91	0.76
Hikurangi R - 67	5.17	0.76
Hikurangi R - 68	4.2	1.1
Hikurangi R - 69	6.2	2.1
Hikurangi R - 70	4.98	0.66
Hikurangi R - 71	4.2	0.31
Hikurangi R - 72	4.85	0.79
Hikurangi R - 73	6.95	0.36
Hikurangi R - 74	4.7	0.94
Hikurangi R - 75	4.51	0.31
Hikurangi R - 76	4.88	0.93
Hikurangi R - 77	5.5	1.4
Hikurangi R - 78	3.82	0.77
Hikurangi R - 79	5.1	1.3
Hikurangi R - 80	3.83	0.52
Hikurangi R - 81	4.41	0.35
Hikurangi R - 82	6.31	0.5
Hikurangi R - 83	4.12	0.32
Hikurangi R - 84	5.2	1
Hikurangi R - 85	5.11	0.56
Hikurangi R - 87	6.2	1
Hikurangi R - 88	4.6	0.57
Hikurangi R - 89	10.1	1.4
Hikurangi R - 90	4.62	0.75
<b>Final age</b>		<b>4.53 ± 0.13 Ma</b>

\* Shaded areas represent the readings included in the final age calculation